



<https://theses.gla.ac.uk/>

Theses Digitisation:

<https://www.gla.ac.uk/myglasgow/research/enlighten/theses/digitisation/>

This is a digitised version of the original print thesis.

Copyright and moral rights for this work are retained by the author

A copy can be downloaded for personal non-commercial research or study,  
without prior permission or charge

This work cannot be reproduced or quoted extensively from without first  
obtaining permission in writing from the author

The content must not be changed in any way or sold commercially in any  
format or medium without the formal permission of the author

When referring to this work, full bibliographic details including the author,  
title, awarding institution and date of the thesis must be given

Enlighten: Theses

<https://theses.gla.ac.uk/>  
[research-enlighten@glasgow.ac.uk](mailto:research-enlighten@glasgow.ac.uk)

MECHANISTIC STUDIES OF RETINAL SCHIFF BASE FORMATION AND  
HYDROLYSIS IN RELATION TO VISUAL PIGMENT CHEMISTRY.

JENIFER L. ROBB (B.Sc.)

A thesis submitted to the University of Glasgow for the  
degree of Doctor of Philosophy.

Department of Chemistry

July 1987

© JENIFER L. ROBB, 1987.

ProQuest Number: 10997340

All rights reserved

INFORMATION TO ALL USERS

The quality of this reproduction is dependent upon the quality of the copy submitted.

In the unlikely event that the author did not send a complete manuscript and there are missing pages, these will be noted. Also, if material had to be removed, a note will indicate the deletion.



ProQuest 10997340

Published by ProQuest LLC (2018). Copyright of the Dissertation is held by the Author.

All rights reserved.

This work is protected against unauthorized copying under Title 17, United States Code  
Microform Edition © ProQuest LLC.

ProQuest LLC.  
789 East Eisenhower Parkway  
P.O. Box 1346  
Ann Arbor, MI 48106 – 1346

### ACKNOWLEDGEMENTS

I would like to thank my supervisor, Dr. Alan Cooper, for all his advice and encouragement during the course of this work.

I would also like to thank Mrs. Margaret Nutley for her technical advice and Professor Lawrence Barron for the use of his Raman spectrometer.

I acknowledge funding from the Science and Engineering Research Council.

I wish to thank my parents very much for all their support and encouragement over the past years. Finally, I thank John for all his love.

To John and My Parents.

## CONTENTS

	Page
CHAPTER 1 INTRODUCTION	1
A. VISION	1
1.1 The Visual Process.	1
1.2 The Eye.	2
1.3 The Visual Pigments.	3
1.4 The Structures of Retinal and Rhodopsin.	5
1.5 The Nature of the Retinal-Opsin Linkage.	7
1.6 The Intermediates of the Bleaching Sequence.	11
1.7 The Metarhodopsin I - Metarhodopsin II Equilibrium.	14
1.8 The Generation of the Neural Signal.	21
1.9 The Regeneration of Visual Pigments.	23
1.10 Models of Rhodopsin.	25
1.11 Cephalopod Rhodopsin.	28
1.12 Bacteriorhodopsin.	30
B. SCHIFF BASE CHEMISTRY	32
1.13 Schiff Base Formation and Hydrolysis.	32
1.14 Objectives.	40
CHAPTER 2 TECHNIQUES AND APPARATUS	42
2.1 Stopped-Flow Spectrophotometry.	42
2.1.1 Technique.	42
2.1.2 Description of the Stopped-Flow Apparatus.	43
2.1.3 Measurement of Absorbance.	44
2.1.4 Experimental Conditions in the Stopped-Flow Experiments.	46
2.2 Raman Spectroscopy.	47
2.2.1 Raman Spectroscopy.	47
2.2.2 Resonance Raman Spectroscopy.	48
2.2.3 Fluorescence and Phosphorescence.	48
2.2.4 The Raman Spectrometer.	49
2.3 Ultra-Violet/Visible Spectroscopy.	50
2.3.1 Technique.	50
2.3.2 Description of the UV / Vis. Spectrometer.	51

2.4	pH Measurements.	52
2.4.1	The pH meter.	52
2.4.2	pD Standardisation.	52
2.5	General Preparation of Solutions.	52
2.5.1	Schiff Base Preparation.	52
2.5.2	Preparation of Solutions For Formation Reactions.	53
2.5.3	Buffer Preparation.	53
2.5.4	Detergents.	54
2.6	Kinetic Analysis.	56
2.6.1	First Order Analysis on Apple Computer.	56
2.6.2	Kinetic Analysis on Mainframe Computer.	57
CHAPTER 3 SCHIFF BASE FORMATION REACTIONS		59
3.1	Material Preparation.	59
3.2	Ultra-Violet / Visible Spectroscopy.	60
3.3	Stopped-Flow Spectroscopy.	62
3.4	Kinetic Results.	63
CHAPTER 4 SCHIFF BASE HYDROLYSIS REACTIONS		67
4.1	Material Preparation.	67
4.2	Ultra-Violet / Visible Spectroscopy.	70
4.3	Stopped-Flow Spectroscopy.	72
4.4	Kinetic Results.	74
4.5	General Base Catalysis.	77
4.6	Determination of pK <sub>a</sub> Value of Schiff Base.	78
4.7	Low Temperature Ultra-Violet / Visible Spectroscopy.	81
4.8	Effect of Deuterium Oxide on Schiff Base Hydrolysis Rate.	84
CHAPTER 5 CHARACTERISATION OF INTERMEDIATE FORMED DURING SCHIFF BASE HYDROLYSIS		86
5.1	Introduction.	86
5.2	Methods of Characterisation.	86
5.3	Experimental.	88

5.4	Resonance Raman Spectroscopy.	90
5.5	Use of Deuterium Oxide in Schiff Base Hydrolysis.	97
5.6	Resonance Raman Spectrum of the Tetrahedral Carbinolamine Intermediate.	99
CHAPTER 6 EQUILIBRIUM AND RATE EXPRESSIONS FOR THE REACTION MECHANISM		101
6.1	Equilibrium and Rate Expressions.	101
6.2	Calculated Spectrum of the Intermediate Species.	111
6.3	Prediction of the pK <sub>a</sub> Value of the Intermediate Species.	113
CHAPTER 7 DISCUSSION AND CONCLUSIONS		115
APPENDIX 1 Principles of Raman Spectroscopy.		132
APPENDIX 2 Electronic Spectra of Retinal.		136
APPENDIX 3 Copy of Paper.		140
REFERENCES		189

## SUMMARY

The possible mechanism of chromophore hydrolysis during photolysis of visual rhodopsin has been investigated by a study of the formation and hydrolysis of the schiff base N-retinylidene n-butylamine in various aqueous anionic, cationic and neutral detergent micelle systems. The schiff base was used as a model of the visual pigment chromophore and the detergent micelles allowed some degree of control on the environment of the chromophoric group in an attempt to mimic the specific environmental effects within the binding site of rhodopsin.

The classical schiff base reaction mechanism involves the formation of tetrahedral carbinolamine intermediates and transient species consistent with such intermediates have been observed during the hydrolysis reactions of N-retinylidene n-butylamine in the anionic, cationic and neutral detergents using stopped-flow spectroscopy.

It was found that accumulation of the carbinolamine intermediate during hydrolysis is greatest when the pH is near the peak of the pH-rate profile and rapid transients were not observed during hydrolysis away from the pH maxima, nor under any accessible experimental conditions during the formation reactions.

The non-steady-state kinetic data obtained from stopped-flow experiments have been analysed using a mainframe computer program called "Discrete", and these data can be described by a double exponential expression which is typical of biphasic reactions involving the formation and decay of an intermediate species. Analysis of the kinetic data, along with data obtained from steady-state kinetics, has allowed the determination of all the rate constants in the retinal schiff base

reaction mechanism.

The hydrogen ion titration behaviour of N-retinylidene n-butylamine has been studied and the results have shown that there are significant differences in the apparent pK of the schiff base in the various detergents. These differences can be explained by the fact that the micellar environment has an electrostatic effect on the protonation of the schiff base and it is likely that charged groups in the vicinity of the binding site of rhodopsin could affect protonation behaviour in a similar way.

This would explain the anomalously low pK<sub>a</sub> value of the active lysine group in rhodopsin - electrostatic interaction of an adjacent positively charged group would make protonation of the lysine more difficult and so lower its pK<sub>a</sub> value. Similarly the apparent pK<sub>a</sub> of the retinal schiff base in rhodopsin is anomalously high because of the formation of a hydrogen bond with this adjacent group.

The carbinolamine intermediate formed during schiff base hydrolysis has been observed at room temperature using continuous flow, pH - jump resonance Raman spectroscopy. The spectrum of the intermediate is very similar to the published resonance Raman spectrum of the metarhodopsin II intermediate formed during the bleaching of the visual pigment rhodopsin. This would suggest that the metarhodopsin transition represents the start of the hydrolysis of the schiff base linkage in rhodopsin.

A possible mechanism for the hydrolysis step has been suggested and it seems likely that the change of configuration from trigonal to tetrahedral of the carbon atom of the schiff base linkage at the hydrolysis stage may provide the driving force for the activation of the enzyme cascade which results in the generation of the nerve impulse.

CHAPTER 1

INTRODUCTION.

## A. VISION

### 1.1 The Visual Process

Vision is one of the most interesting fundamental biological processes to occur and in order for it to be even partially understood it must be examined from many different perspectives. From a chemist's point of view the interest lies in the molecular reactions and interactions that occur, a study of which may perhaps lead to a greater understanding of the visual process'.

There are certain requirements that need to be fulfilled in order for vision to occur. First of all there must be light in the environment, secondly there must be an optical device of some kind which can form an image on a photoreceptive layer, and finally this layer must be able to transduce the absorbed light into an electrical signal which can then be transmitted to the brain.

The first requirement for available radiation is fulfilled by the sun which provides the light environment for terrestrial animals, including man, and aquatic species that remain close to the water surface. Species living further into the ocean depths depend on bioluminescence emitted by themselves and other organisms or have no vision at all.

The radiation from the sun that reaches the earth's surface has a wavelength range of 300nm to 1000nm with the maximum intensity just below 500nm. Lower wavelengths than this, in the ultra-violet region, are cut out by the ozone layer lying about 15 miles above sea level, and higher wavelengths in the near infra-red region are cut out because of absorption by atmospheric water vapour.

Man's visual range is between approximately 400nm to 800nm and this part of the electromagnetic spectrum that is visible to man is what we refer to as light. Different parts of the spectrum may however be visible to other species<sup>1e</sup>.

## 1.2 The Eye

The second requirement of vision is an optical device which is capable of forming an image on a photoreceptive layer and which may allow the perception of the position, shape and movement of objects present in the environment. In nature there are three different focussing devices found that can form an image and these are the "pin-hole" eye, the compound eye and the refracting eye.

In the pin-hole eye the inverted image of a stationary object is formed at the back of the eye by light passing through a small opening at the front of the eye. This device is not very efficient at forming images because only a small amount of the light radiating from the object can pass through the small hole. Enlarging the hole does not solve the problem as this reduces the definition of the image. This simplistic method of image formation is exemplified by the eye in certain types of molluscs (fig.1.1).

The compound eye is based on the formation of an image by a stack of parallel "ray selectors" where only the light that falls on a certain tube in the direction of its axis can pass along it, and each of these tubes is aimed on a different point in the visual field thus forming an erect image of the object. If the tubes are arranged around the surface of a segment of a sphere, with the axes pointing toward its centre, then the image of different sized objects can be formed and an impression of distance can be conveyed. This type of eye is found in insects, crustacea and some molluscs (fig.1.2).

The third type of eye is the refracting eye that is found in vertebrates and some invertebrates such as the squid. In this case an image is formed by the refraction

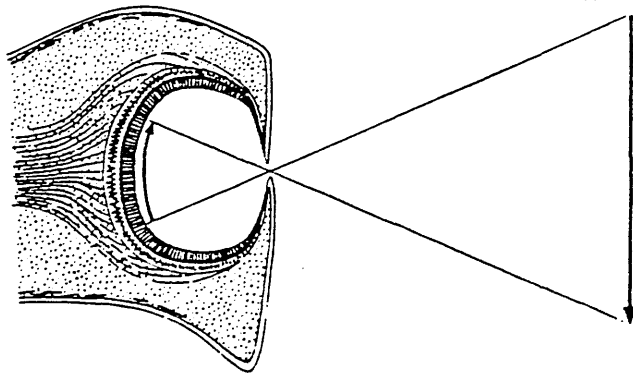


FIGURE 1.1  
A cross-section of the eye of the mollusc.

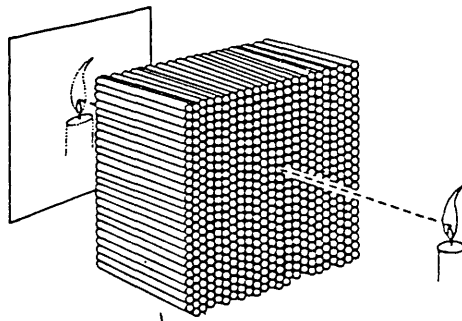


FIGURE 1.2  
Formation of an image by a bundle of parallel  
"ray selectors".

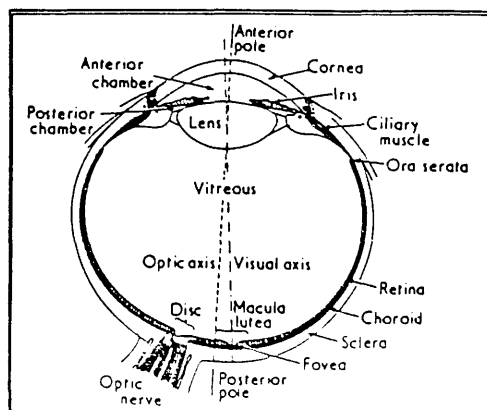


FIGURE 1.3  
Horizontal section of the human eye.

(Figures taken from ref.1e)

of light that occurs at curved surfaces separating media of different refractive index. The light rays that reach the eye from a position on an object are brought to a single point on the photosensitive layer called the retina, and so in this case an arrangement for focussing objects at different distances is required. The cornea, iris and lens provide the necessary optics for focussing this light on the retina and photoreceptors in the retina convert the light signals to electrical pulses which the optic nerve transmits to the brain.

Light enters the eye through the cornea, a transparent layer at the front of the eye, and passes into the anterior chamber which is filled with a liquid called the aqueous humour (fig.1.3). The cornea and aqueous humour together constitute the main refractive surface of the eye. The light then passes through the pupil, which is an orifice in the iris, and reaches the lens. The lens is pliable and can change its curvature by the action of the ciliary muscle to accommodate near or far vision. Finally the light reaches the retina which is a thin sheet of interconnected nerve cells and light sensitive cells or photoreceptors. These photoreceptor cells contain coloured substances that selectively absorb the light and these are called visual pigments.

### 1.3 The Visual Pigments

The third requirement for vision is the presence of a photoreceptive layer which can absorb light energy and convert it into electrical energy so that a signal can be transmitted to the brain. The photoreceptive layer in the refracting eye is the retina and the visual pigments in the retina are the absorbing species.

Vertebrates have two different types of photoreceptor cells called rods and cones and they differ in shape, number and distribution. In the human eye the rods and cones are both about 0.05mm long, but the rods are cylindrical in shape while the cones have a more tapered, conical shape. The rod cells are more abundant accounting for 90% of photoreceptor cells, whereas only 10% are

cones. The rods are more sensitive and operate in dim illumination (scotopic conditions) mediating black and white vision whereas the cones work in bright (photopic) conditions and mediate colour vision. In man there are three cone pigments which are sensitive to blue, green and red light. These three photoreceptors provide a colour discrimination mechanism sensitive enough to distinguish very subtle variations in colour and shade. Rods are not involved in human colour vision and in dim light, when only the rods can function, humans cannot discern colours.

Each photosensitive cell is composed of two segments, an inner cell and an outer segment (fig.1.4). The inner cell contains the nucleus plus a large number of mitochondria and is connected to the outer segment by a narrow cilium. The rod outer segment is composed of discs which are stacked one on top of each other and which are constantly being replenished at the base and disposed of at the top, as shown from studies with radioactive tracers<sup>2</sup>.

Each one of these discs is made up of approximately 60% lipid bilayer membrane and 40% protein, and approximately 90% of this protein component is the visual pigment rhodopsin, a trans-membrane protein which is embedded in the lipid bilayer membrane of the rod discs (fig.1.5).

Research work on this visual pigment began over a hundred years ago when it was referred to as "visual purple" because of its reddish-purple colour. In 1876 Boll discovered that the colour of a pigment that he found in the rod outer segment of a frog retina slowly faded in the light<sup>3</sup>. Shortly after this the pigment was extracted using bile salts, and this is thought to be the first time that a membrane protein had been removed from its membrane and obtained in aqueous solution.

Later it was found that some vertebrates have two types of photoreceptor cells, rods and cones, and the pigments present in rods and cones are not the same as they have their maximum intensities at different wavelengths in the absorption spectra. These spectra

FIGURE 1.4  
A schematic cross-section of  
a mammalian rod cell.

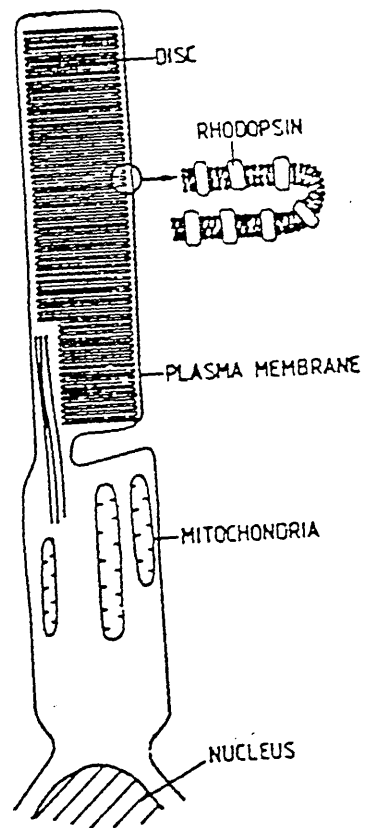
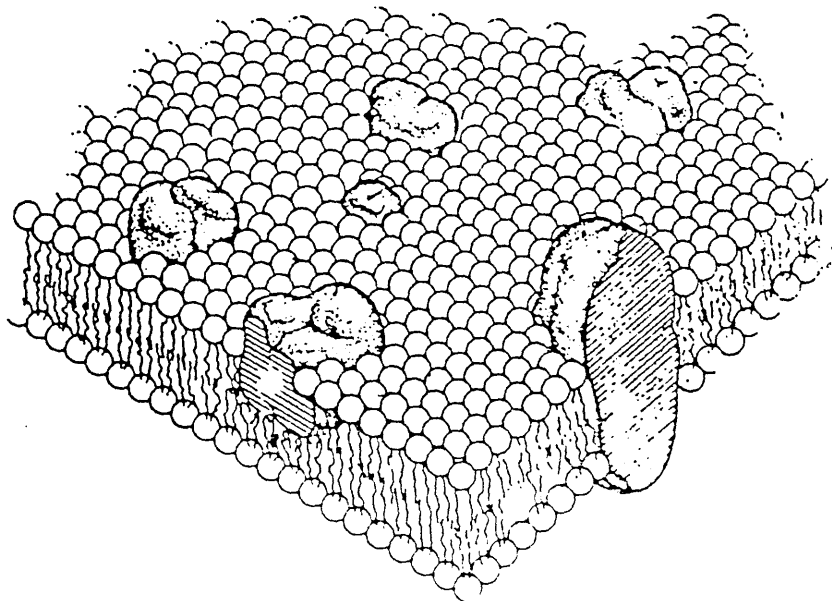


FIGURE 1.5  
A lipid bilayer membrane containing protein molecules in  
various possible modes of association with the membrane.



corresponded to curves obtained from measurements of the visual threshold (the intensity of light required to evoke a sensation) as a function of wavelength in dim and bright conditions respectively. The similarity of the pigment absorption spectra and the threshold curves was evidence that the pigments are of essential importance to vision.

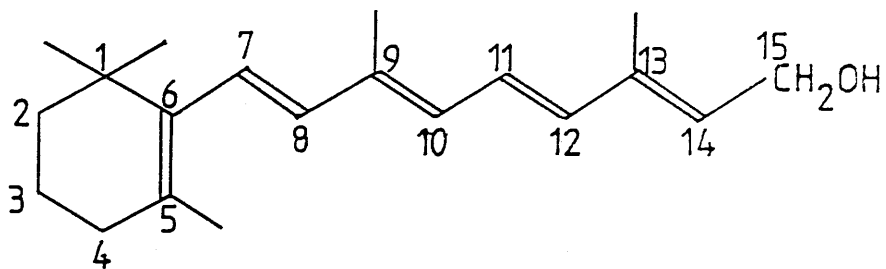
Chemical interest then focussed on elucidating the structure of the pigments. It had been known for many years that vitamin A deficiency caused visual deterioration such as night blindness, and in the 1930's George Wald found that vitamin A is present in the retina<sup>4</sup>. Since then the oxidised form of vitamin A (now called retinal), or an analogue containing an extra double bond in the ring have been found in all visual pigments known.

#### 1.4 The Structures of Retinal and Rhodopsin

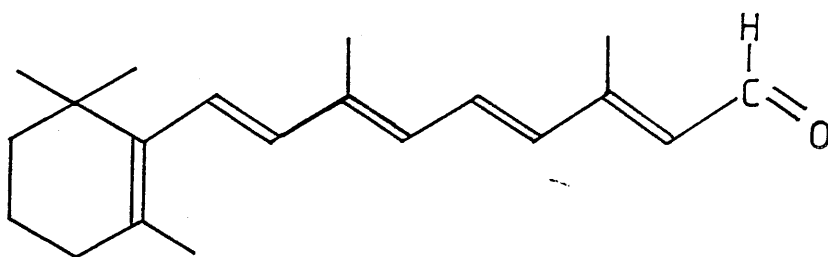
The structures of retinol (vitamin A) and retinal (vitamin A aldehyde) are shown in fig.1.6 . Retinol is oxidised to retinal by enzymes present in the eye called alcohol dehydrogenases. In the visual pigments retinal is the chromophore and is bound to a type of protein called an opsin which is found in the outer segments of vertebrate rods and cones. Retinal bound to rod opsin is called rhodopsin and retinal bound to cone opsin is iodopsin. This work is based on the visual pigment rhodopsin which is responsible for scotopic vision.

The chromophore of rhodopsin, retinal, can exist in many isomeric forms because it contains four carbon-carbon double bonds in the side chain, each of which may potentially exist in the cis or trans configuration. The most stable form is the all-trans form shown in fig.1.6 . The double bonds in the 7,9,11 and 13 positions can all occur as the cis or trans configuration, even though there is steric hindrance between the methyl substituents on the ring and carbon 9 in the 7-cis form, and interactions between the methyl group on carbon 13 and the hydrogen on carbon 10 in the

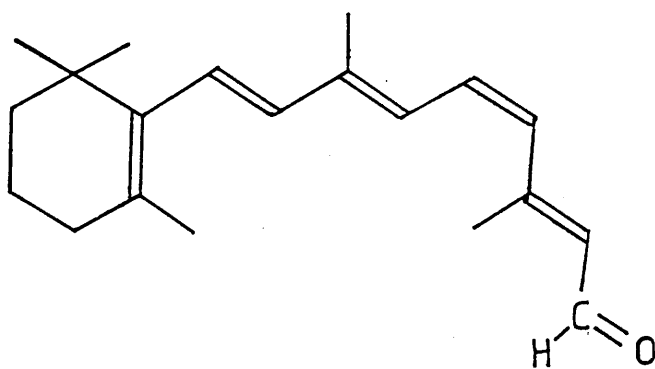
FIGURE 1.6  
The structures of retinol and isomers of retinal.



retinol



all-trans retinal



11-cis retinal

11-cis isomer, which should make the cis-linkages less stable in these isomers.

In 1952 Hubbard and Wald<sup>5</sup> showed that 11-cis retinal is the chromophore in rhodopsin, because only 11-cis and 9-cis retinal will combine with opsin to form pigments and of these only the 11-cis pigment has the absorption spectrum of rhodopsin. 9-cis retinal reacts to form isorhodopsin but there is no evidence to suggest that this pigment which absorbs at 487nm plays any part in the visual process.

It was also found that when rhodopsin has been bleached by light the retinal that emerges is the all-trans isomer which must be isomerised to the 11-cis configuration before it can take part in regenerating the visual pigment. There is therefore a cycle of cis-trans isomerisation occurring with the pigment.

In 1958 Hubbard and Kropf proposed that the action of light in vision is the isomerisation of the chromophore of the visual pigment from the 11-cis to the all-trans configuration and that later reactions in the bleaching sequence can occur in the dark<sup>6</sup>.

The other part of the visual pigment rhodopsin is the protein opsin to which the retinal is attached. Opsin is a membrane bound protein with a molecular weight of about 39000, consisting of 348 amino acid residues<sup>7</sup>. Associated with the protein is a phospholipid component and a carbohydrate component so that a typical visual pigment when extracted from the retina is a complex association of the chromophoric group, protein, phospholipid and carbohydrate.

The most important aspect of rhodopsin's structure that needs to be considered in this thesis is the nature of the binding of the chromophoric group to opsin. This may help to explain why rhodopsin is a red or purple colour absorbing at 500nm, whereas retinal on its own is pale yellow absorbing at 380nm and opsin is colourless, absorbing in the ultra-violet region at 280nm. This colour change must be due to the interactions that occur between retinal and opsin in rhodopsin.

## 1.5 The Nature of the Retinal-Opsin Linkage

The interaction between retinal and opsin is very specific and even minor changes in the chromophoric group prevent its union with opsin, as shown by the fact that only the 11-cis isomer will combine with opsin to regenerate rhodopsin itself, whereas other isomers may combine to form non-physiological pigments.

In 1954 Hubbard determined that the ratio of the two components, retinal and opsin, in the pigment molecule is one to one<sup>8</sup>. The linkage between the retinal and the protein is thought to be covalent rather than non-covalent due to the fact that it is difficult to extract retinal from rhodopsin in the dark.

In 1937 Lythgoe<sup>9</sup> found that a pigment which he named indicator yellow was formed when rhodopsin solutions were exposed to light and that this pigment was sensitive to changes in pH. At high pH the "alkaline" indicator yellow was a very pale yellow colour with a maximum absorbance at a wavelength of 365nm, whereas at low pH the "acid" indicator yellow had a much deeper yellow-orange colour with maximum absorbance at 440nm. He found that between pH 4 and 6 this pigment decomposed to give what was later found to be retinal.

Ball et al<sup>10</sup> found that retinal reacts with many substances containing amino groups, such as amines, amino acids and proteins, to give products that are spectroscopically similar to indicator yellow. They thought that the structure of these products was based on either the interaction of two molecules of retinal with one amino group or the condensation of the carbonyl group of one retinal molecule with one amino group to form a schiff base.

Then in 1955 Pitt et al<sup>11</sup> prepared a schiff base, which they called retinylidenemethylamine, from retinal and methylamine. the absorption spectrum of which was very similar to that of the "alkaline" indicator yellow, with a maximum absorbance at about 365nm. On addition of hydrochloric acid the absorbance peak moves to

approximately 440nm, as with the "acid" indicator yellow. This shift of wavelength in the indicator yellow analogue was accounted for by suggesting the formation of a substituted ammonium salt by addition of a proton to the nitrogen group. In the retinylidenemethylammonium ion this positive charge could formally be localised at many positions along the polyene chain so that at least seven distinct resonance forms can be written compared with one main form for the unprotonated retinylidenemethylamine. This increase in the degree of resonance would contribute to the shift of the absorption maximum towards longer wavelength which is called a bathochromic shift.

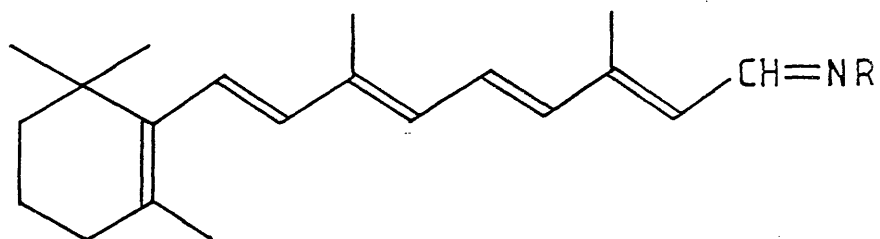
Pitt et al studied other schiff bases to see if this shift was associated with a change of a  $-\text{CH} = \text{N}-$  grouping to  $-\text{CH} = \text{NH}^+$  grouping. On acidification, the solutions of all the schiff bases studied showed a bathochromic shift and they concluded that indicator yellow has an unprotonated schiff base structure in alkali and a protonated schiff base structure in acid (Fig.1.7).

Further studies by Morton and Pitt in 1955<sup>1,2</sup> using the same analogue and studying its stability in aqueous solution over a range of pH values led to the idea that acid and alkaline indicator yellows are actually non-specific schiff base linkages formed between retinal and different amino groups in opsin, the acid form being protonated and the alkaline unprotonated, whereas the retinal-opsin linkage in rhodopsin is a specific schiff base linkage, formed between the aldehyde group of retinal and one specific amino group of opsin.

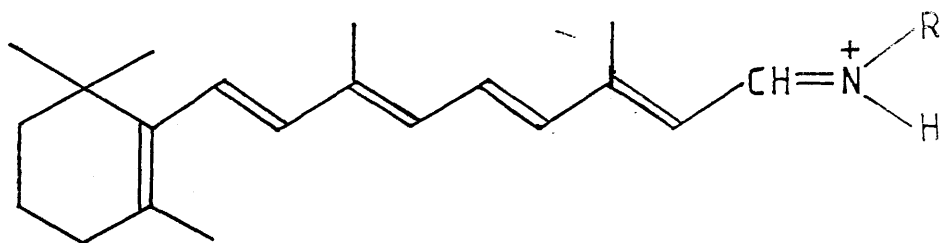
Later Bownds<sup>1,3</sup> and Akhtar, Blossie and Dewhurst<sup>1,4</sup> identified this amino group as the  $\epsilon\text{-NH}_2$  group of a specific lysine residue. This was discovered chemically by borohydride reduction because in a schiff base the  $\text{R-HC=N-R}'$  group can be reduced to  $\text{R-CH}_2\text{-NH-R}'$  using sodium borohydride.

With rhodopsin it was found that an illuminated sample could be reduced and this was hydrolysed, the amino acids isolated and a retinal-lysine complex was present in the hydrolysis products. (This hydrolysis cannot be done with the unreduced schiff base in

FIGURE 1.7  
Schiff base structures.



unprotonated retinal schiff base



protonated retinal schiff base

rhodopsin as the schiff base linkage is unstable to hydrolysis.) These experiments show that at some stage after illumination of rhodopsin a schiff base is formed but does not prove that in rhodopsin itself a schiff base linkage is present.

It is interesting to note that samples of rhodopsin in the dark cannot be reduced by this method. The resistance of rhodopsin before illumination to attack by borohydride suggests that the nature of the attachment between retinal and opsin prevents the C=N group from being reduced, perhaps because the retinal - opsin complex is stabilised by specific non-covalent interactions or simply buried. On exposure to light the cis-trans isomerisation occurs and this will probably be accompanied by protein conformational changes allowing the sodium borohydride to interact with the schiff base linkage.

It was found however that rhodopsin could be reduced in the dark by using sodium cyanoborohydride<sup>15</sup>. These experiments showed that the retinylidene group is bound to lysine in native bovine rhodopsin as well as in illuminated rhodopsin.

Direct evidence that the linkage in rhodopsin is a schiff base is provided by resonance Raman spectroscopy studies and furthermore this suggests that it is a protonated schiff base. By irradiating near the visible absorption bands of the pigment it is possible to enhance the Raman active vibrations of the chromophore and compare the measured frequencies with those of model compounds.

The first attempt at obtaining the resonance Raman spectrum of a visual pigment was reported by Rimai and co-workers in 1970<sup>16</sup>. By cooling a bovine retina to -70°C they were able to detect weak scattering in the 1550cm<sup>-1</sup> region which was assigned to the C=C ethylenic stretch of a protonated schiff base. They used an argon ion laser (488nm) as the exciting light and recognised that the retina contained a photo-stationary mixture of bleaching intermediates.

In 1973 Lewis et al<sup>17</sup> managed to obtain a Raman spectrum without appreciably bleaching the pigment, i.e. without causing significant cis-trans isomerisation of the retinal chromophore, by using an exciting light of longer wavelength. The most interesting feature on the spectrum is the  $1654\text{cm}^{-1}$  C=N vibration which is essentially identical to that of protonated schiff bases of retinal in solution. Unprotonated schiff bases have the C=N frequency at approximately  $1630\text{cm}^{-1}$ .

Further evidence came from Oseroff and Callender<sup>18</sup> who examined the effects of deuteration of the schiff base linkage on the resonance Raman spectra. If the schiff base is protonated, then the proton on the nitrogen can exchange with a deuterium atom which would result in a decrease in the frequency of the stretching mode. They found that in samples of model protonated schiff bases and of rhodopsin in retinal disc membranes that deuteration of the schiff base causes a predictable reduction in the C=N stretching frequency from  $1655\text{cm}^{-1}$  to  $1630\text{cm}^{-1}$  thus giving further evidence of a protonated schiff base linkage in rhodopsin.

These experiments also showed that the chromophore in rhodopsin does not exist as the free aldehyde. Resonance Raman spectra of retinal show a band at  $1660\text{cm}^{-1}$  due to the carbonyl stretch and it could be argued that this is equivalent to the  $1654\text{cm}^{-1}$  band in the rhodopsin spectra - the slight difference in frequency being explained by the environment of retinal in rhodopsin. The deuteration experiments ruled this out because if this were the case then no shift in frequency would be seen on deuteration because replacing water with deuterium oxide would not affect the frequency of a carbonyl vibration.

In 1977 Shriver et al carried out  $^{13}\text{C}$  nuclear magnetic resonance experiments with rhodopsin and model compounds which agreed that the linkage is a schiff base but suggested that this schiff base is unprotonated. They recorded the nmr spectrum of rhodopsin with a  $^{13}\text{C}$  - enriched chromophore at the  $\text{C}_{14}$  position. They compared the spectrum with spectra of  $^{13}\text{C}$  - enriched protonated and unprotonated model schiff bases and concluded that

rhodopsin contains an unprotonated schiff base linkage between retinal and opsin<sup>19</sup>.

These conflicting results from resonance Raman spectroscopy and <sup>13</sup>C-nmr spectroscopy may be explained if the schiff base is protonated via hydrogen bonding to an adjacent group in the binding site such as the  $\epsilon$ -NH<sub>2</sub> of another lysine group nearby or from an arginine residue (fig.1.8). This model for the proposed interactions in the chromophoric binding site in rhodopsin was suggested by Cooper and Converse<sup>20</sup>.

This intramolecular protonation scheme is consistent with Oseroff and Callender's deuteration experiments showing the presence of an exchangeable hydrogen associated with the nitrogen of the schiff base linkage.

## 1.6 The Intermediates of the Bleaching Sequence

Following the absorption of light by rhodopsin two main chemical reactions occur and these are:

1. the photoisomerisation of retinal from the 11-cis isomer to the all-trans isomer,
2. the hydrolysis of the retinal-opsin linkage in rhodopsin releasing the all-trans retinal.

The photoisomerisation of the chromophore has been shown to be the initial process to occur after illumination of rhodopsin and this is followed by a sequence of spontaneous and, in most cases, irreversible steps involving formation of intermediate species. The sequence of intermediates which have been spectrally identified is shown in fig.1.9 and these intermediates were discovered by illuminating rhodopsin at different temperatures.

The processes that occur after metarhodopsin II are relatively slow and can be seen at room temperature, whereas the initial processes are much faster and require low temperature spectroscopy and flash photolysis techniques. This explains why the intermediates later on in the bleaching sequence were discovered first in room temperature experiments in the 1930's and the faster processes were not discovered until later.

FIGURE 1.8

Proposed interactions in the retinal binding site of rhodopsin. A nearby protonated group inhibits titration of the active lysine residue in opsin and provides a source of intramolecular protonation of the aldimine nitrogen in rhodopsin. (Taken from ref.18)

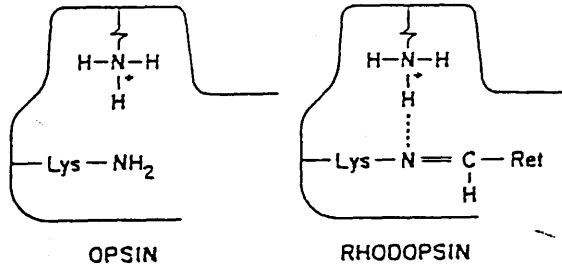
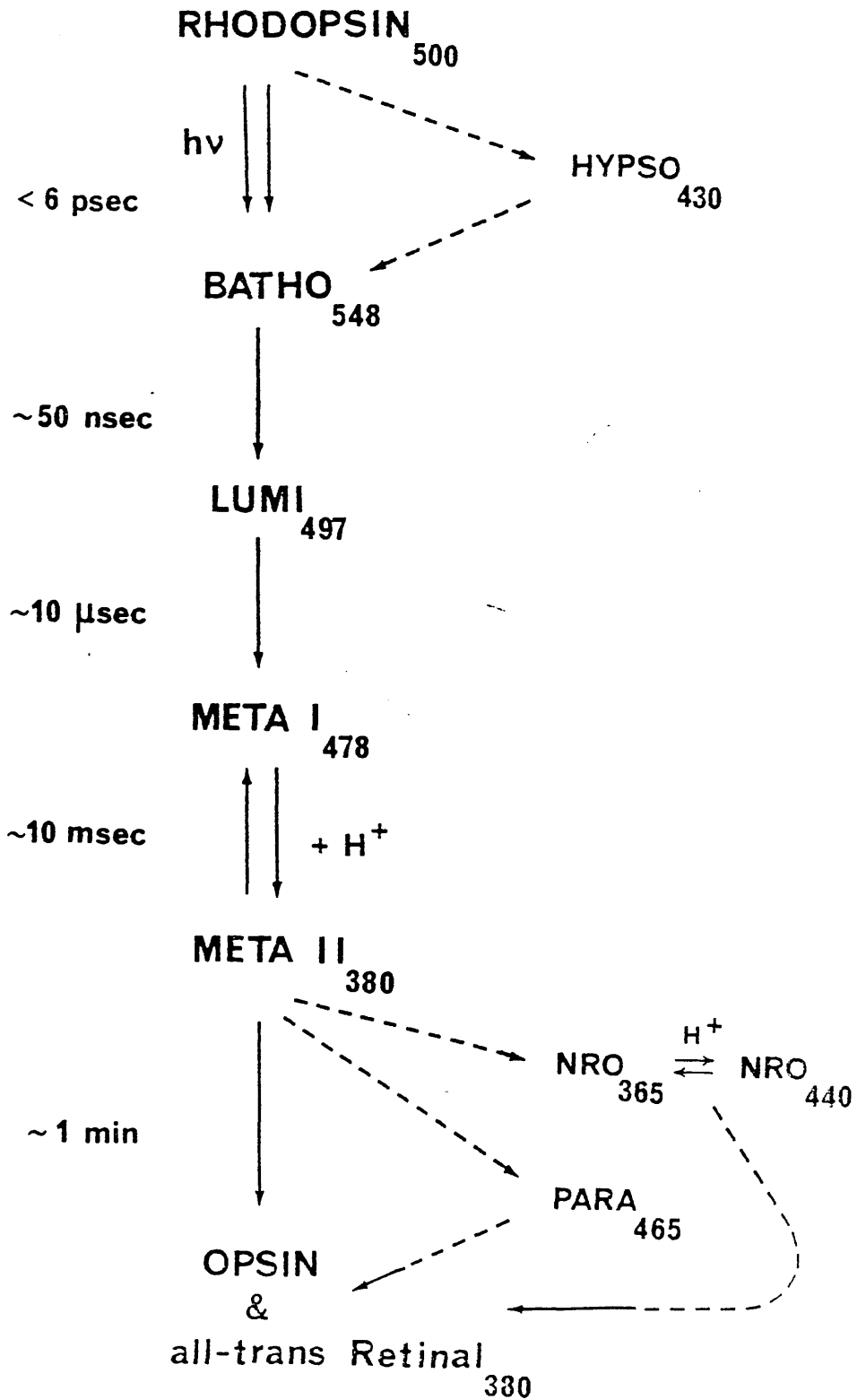


FIGURE 1.9  
The vertebrate rhodopsin bleaching sequence.



Irradiation of rhodopsin at liquid nitrogen temperatures ( $-190^{\circ}\text{C}$ ) generates the first intermediate, bathorhodopsin which has a maximum absorbance at 548nm. The name "batho" is used because the intermediate is red-shifted with respect to rhodopsin, i.e. it has a maximum absorbance at longer wavelength. This first step in the bleaching sequence is the only photochemical step and all other intermediates can be generated from bathorhodopsin in the dark.

When a sample of bathorhodopsin is warmed to approximately  $-140^{\circ}\text{C}$  it is converted to the next intermediate lumirhodopsin, with maximum absorbance at 497nm. Heating this above  $-40^{\circ}\text{C}$  yields metarhodopsin I (absorbance maximum 478nm) which is in equilibrium with metarhodopsin II with absorbance maximum at 380nm. At this stage the wavelength of the maximum absorbance has shifted from 500nm in the rhodopsin to 380nm in the metarhodopsin II and so the pigment has bleached from the original red colour to a yellow colour. The equilibrium between metarhodopsin I and metarhodopsin II is sensitive to temperature and pH. Further heating above  $0^{\circ}\text{C}$  gives pararhodopsin (absorbance maximum 465nm) which decays to give another metastable, pH-sensitive equilibrium between acid indicator yellow and alkali indicator yellow. Finally the products of bleaching are all-trans retinal with an absorbance maximum at 380nm and opsin which absorbs at 280nm in the ultra-violet region.

It is important to consider if these intermediates are formed under physiological conditions at  $37^{\circ}\text{C}$  or whether they are artefacts which only occur at low temperature. The use of kinetic techniques for fast reactions has shown that the intermediates do also exist at physiological temperatures.

Flash photolysis is a technique that involves following the change in the absorbance of a sample as a function of time and is useful for reactions occurring in a time scale of microseconds to seconds. A sample is loaded into a cell in the apparatus and kept in the dark at the appropriate temperature. The photoreactions are initiated by a rapid flash of intense light and the

absorbance of the sample at a particular wavelength is continuously monitored after the flash by means of a low intensity probe lamp, a photomultiplier and an oscilloscope<sup>21</sup>. This technique was used for intermediates occurring after bathorhodopsin, but the first process, which is the conversion of rhodopsin to bathorhodopsin, was too fast to be measured by this apparatus.

The formation and decay of bathorhodopsin was studied by Busch et al in 1972<sup>22</sup> using picosecond flash photolysis. This involves the use of lasers that will deliver intense picosecond pulses for the excitation flash. The probe pulse is directed at a mirror echelon (a stepped mirror surface) and this provides a sequence of pulses which pass through the sample at different times due to the different pathlengths travelled, thus giving a measure of absorbance at these times. Using a spacially separated array of detectors the absorbance is measured as a function of distance enabling the kinetics of the process to be examined.

From these experiments it was found that the conversion of rhodopsin to bathorhodopsin at physiological temperature occurs in approximately one picosecond, bathorhodopsin to lumirhodopsin in approximately fifty nanoseconds, lumirhodopsin to metarhodopsin I in approximately ten microseconds and processes after metarhodopsin II occur in a timescale of seconds to minutes. This suggests that visual excitation must occur at or before the metarhodopsin II stage because beyond meta II the processes are too slow to account for the visual response. These later processes are possibly involved in the regeneration of rhodopsin.

Following the picosecond spectroscopy experiments which showed that bathorhodopsin is formed in approximately one picosecond, there were suggestions that the rhodopsin to bathorhodopsin step may not be a photoisomerisation reaction as was previously believed but rather a proton translocation.

Busch et al thought that the formation of bathorhodopsin was too fast to be due to such a conformational change as cis-trans isomerisation of

retinal, however theoretical calculations predict that an 11-cis to 11-trans photoisomerisation can occur in the opsin binding site in approximately two picoseconds<sup>23</sup> and resonance Raman studies have shown that the state of protonation of the schiff base nitrogen in bathorhodopsin is identical to that in rhodopsin<sup>24</sup>.

Evidence of another intermediate, occurring before bathorhodopsin in the bleaching sequence, has been reported by Yoshizawa from experiments at liquid helium temperatures<sup>25</sup>. He irradiated visual pigments with light of long wavelength - above 520nm - and found a blue-shifted species called hypsorhodopsin with a maximum absorbance at 430nm. However Cooper suggests that hypsorhodopsin is not actually a discrete photoproduct and he provides a numerical model to show that it may be an artefact present at very low temperatures arising from photoselection of existing conformational substates of rhodopsin and bathorhodopsin<sup>24</sup>.

#### 1.7 The Metarhodopsin I - Metarhodopsin II Equilibrium

The equilibrium between metarhodopsin I and metarhodopsin II was first discovered and studied by Matthews et al in 1963<sup>27</sup> who distinguished between meta II and all-trans retinal which had been confused earlier because their maximum absorbances both occur at a wavelength of approximately 380nm. They were distinguished by irradiation with ultra-violet light at 0°C which causes meta II to be rapidly converted into a mixture of rhodopsin, isorhodopsin (which contains 9-cis retinal as the chromophore) and pararhodopsin (maximum absorbance at 465nm). Similar irradiation of the hydrolysis products retinal and opsin results in an extremely slow formation of rhodopsin and isorhodopsin, taking place over many hours.

It was found that metarhodopsins I and II are in thermal equilibrium and this equilibrium is dependent on temperature, pH and solvent. Meta II is favoured by an increase in temperature or acidity and the formation of meta II from meta I involves the uptake of a proton which

binds to a group with a  $pK_a$  value of around 6.4. This conversion is accompanied by an enthalpy increase of approximately 13 kilocalories per mole, i.e. it is an endothermic reaction. Normally most acid groups have positive heats of dissociation so that warming would favour the release of  $H^+$  but in this case the conversion of meta I to meta II involves the addition of a proton on heating and the enthalpy increase is associated with protein conformational changes resulting in an increase in entropy going from meta I to meta II.

By comparing meta I and meta II with model schiff bases Matthews et al proposed that meta I is a protonated schiff base and meta II is an unprotonated schiff base. This would help to explain the blue shift in the spectrum going from meta I to meta II but contradicts the fact that a proton is actually taken up in the conversion. This was explained by the suggestion that two protons are bound by groups in the protein with a simultaneous loss of one proton at the schiff base linkage.

This theory was challenged by Cooper and Converse in 1976<sup>20</sup> who suggested that meta I to meta II is the point during the bleaching sequence where the hydrolysis of the specific retinal-lysine schiff base linkage occurs. They directly measured the relative energies of rhodopsin, meta I, meta II and the hydrolysis products opsin and all-trans retinal in intact rod outer segment membranes at 3°C, using a photocalorimeter which they designed themselves especially for use with visual pigments. They found that all the energy changes that occur are endothermic so that the intermediates have more energy than rhodopsin itself.

They also studied the protonation changes that occur during each step and observed that changing the pH of a rhodopsin solution from 8 to 5.4 has no effect on  $\Delta H$  or protonation whereas the same pH change in an opsin-retinal mixture after hydrolysis was accompanied by an uptake of one proton and an enthalpy change of -12 kilocalories per mole. Retinal itself is unaffected by pH and so a group on the protein opsin must become protonated between pH 8 and 5.4 i.e. the group must have

a pK<sub>a</sub> value lying between 5.4 and 8.

The heat of protonation suggests that this group is a primary amine leading to the theory that it is the amino group of the lysine residue which has been exposed after hydrolysis of the retinal-opsin schiff base. The low pK<sub>a</sub> value of approximately 7 for this lysine group, compared to about 10 for a typical primary amine, can be explained if the lysine group is interacting with a nearby positively charged group situated in the vicinity of the binding site, leading to the intramolecular protonation scheme previously shown in fig.1.8 . The nearby positive charge makes it more difficult to protonate the exposed lysine from the schiff base linkage thus lowering its pK<sub>a</sub> value. Following the hydrolysis reaction the free aldehyde, all-trans retinal, remains non-covalently attached to the active site of opsin. This model led to controversy as to whether meta I to meta II involves the deprotonation of the schiff base or the hydrolysis of the schiff base.

Resonance Raman studies of bovine metarhodopsin I and II and comparison with model protonated and unprotonated retinal schiff bases led Doukas et al in 1978<sup>28</sup> to support the idea that metarhodopsin II is an unprotonated schiff base, despite the absence of a band at approximately 1630cm<sup>-1</sup> which is characteristic of unprotonated model schiff bases of retinal. They disagreed with Cooper and Converse because of the absence of a 1670cm<sup>-1</sup> band due to the carbonyl group which should be present if hydrolysis has occurred and free retinal is present.

However Allan and Cooper<sup>29</sup> later showed that in infra-red and Raman spectra this small band due to the carbonyl stretch is solvent dependent as it can be clearly seen in spectra with organic solvents such as acetonitrile but disappears in the presence of water, possibly due to hydrogen bonding. Therefore the lack of carbonyl band in the resonance Raman experiments of rhodopsin in aqueous buffer solutions which were carried out by Doukas et al may be due to solvent effects and does not provide conclusive evidence that meta II is an

unprotonated schiff base rather than retinal non-covalently bound to opsin.

There is another observation which would imply that meta I to meta II is the hydrolysis step. In 1950 George Wald and co-workers<sup>30</sup> found that dry films of frog or cattle rhodopsin which had been prepared in the dark could be converted, on illumination, to metarhodopsin I and then remain stable for days in the dry state. However on addition of water to the film hydrolysis occurs yielding retinal and opsin, thus indicating that hydrolysis takes place at the meta stage.

The kinetics of the meta I - meta II equilibrium in rhodopsin are complex and suggest that other intermediates may be involved at this important stage.

Baumann and Zeppenfeld studied the kinetics of the metarhodopsin equilibrium in frog rhodopsin over a range of temperatures and pH values using the flash photolysis technique<sup>31-33</sup>. They proposed a model to explain the results of their experiments and this consists of a scheme of two consecutive equilibrium processes involving three species, meta I, meta II' and meta II'', where the latter two are isochromic forms of metarhodopsin II with identical or very similar spectra but different kinetics.

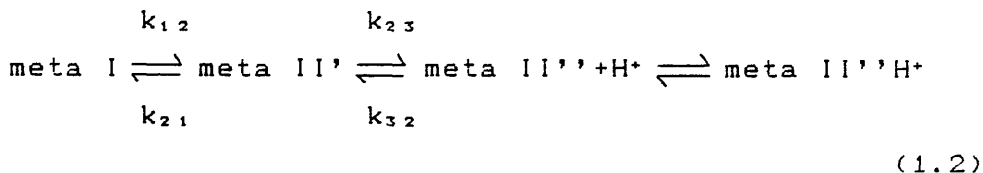
The pH dependence of the equilibrium is explained by the fact that one of the metarhodopsins behaves like a base which can be converted to its conjugate acid on picking up a proton:



where MR is the base and MRH<sup>+</sup> is the acid form. An obvious thought is that meta II' and meta II'' behave as an acid-base pair so that proton uptake occurs at this stage, however if this were so they expected the concentration of the protonated form, meta II'', to decrease at high pH and eventually reach zero as it loses its proton under alkaline conditions. When they found that this was not the case they suggested that meta II'' exists as two forms, meta II'' and meta II''H<sup>+</sup>, which are in equilibrium, with a proton taken up going from meta

II'' to meta II''H<sup>+</sup>.

Their overall reaction scheme for frog rhodopsin is therefore:



Values for the rate constants  $k_{12}$ ,  $k_{21}$ ,  $k_{23}$  and  $k_{32}$  can be obtained, but the rate constants of the reversible proton uptake are unknown. The kinetics of the metarhodopsin equilibrium in cattle rhodopsin were studied by Bennett<sup>34,35</sup> again using flash photolysis at different temperatures and pH values. She studied the pH dependence of the proton uptake between meta I and meta II and of the spectral shift from 480nm to 380nm at 3°C, 20°C and 37°C.

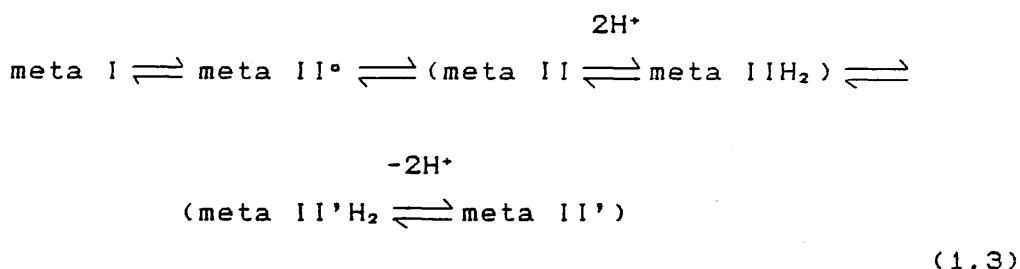
At 3°C she found that two protons are bound per metarhodopsin II molecule formed between pH 6 and pH 8, so that meta II is diprotonated at this temperature. At the higher temperatures the meta II intermediate can exist in two forms depending on pH, the diprotonated form in acid conditions and an unprotonated form in more alkaline conditions. Both these forms of meta II are shown to be in equilibrium with meta I, the equilibrium being pH dependent for the diprotonated form and temperature dependent for the unprotonated form.

The order of the formation of these two forms at higher temperature was studied from experiments on the protonation changes and meta II formation in the presence of a pH indicator dye. The pH variation was measured at a wavelength where the dye absorbs (600nm) and the formation of meta II was monitored at 365nm, the isosbestic point between rhodopsin and meta I.

These experiments showed that rapid protonation was followed by a slower partial deprotonation and that the formation of meta II is biphasic. However the protonation appears to be slightly slower than the initial rapid phase of the meta II formation, although the kinetics of the proton release are similar to the slow phase of meta

II formation. It is not known whether the same groups in the meta II are protonated and then deprotonated or whether there is a proton translocation from one group to another.

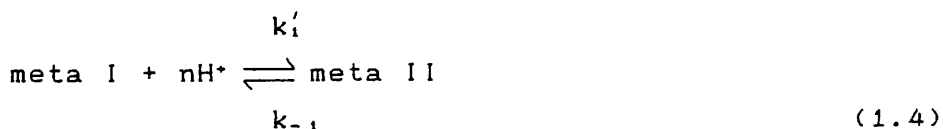
A model for the metarhodopsin was proposed as follows:



where meta II<sup>o</sup> could be another intermediate, the presence of which would explain the delay between the spectral change and the protonation.

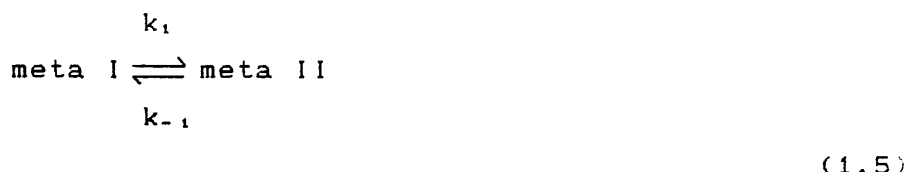
The kinetics of the bovine metarhodopsin equilibrium were also studied by Parkes and Liebman<sup>3,6</sup> over the pH range 5.9-8.1 and temperature range -1°C to 15°C. From their experimental data they obtained the pseudo first-order and true forward rate constants, the reverse and observed rate constants and the equilibrium constant.

The equilibrium between meta I and meta II, involving proton uptake, can be written as:



where  $k'_1$  is the true forward rate constant and  $k_{-1}$  the reverse rate constant. The back reaction is unimolecular and  $k_{-1}$  is a first order rate constant, however  $k'_1$  will be greater than first order unless the proton concentration does not change. If it is assumed that the proton concentration remains constant due to internal buffering then the reaction may be written as

a pseudo first-order reaction:

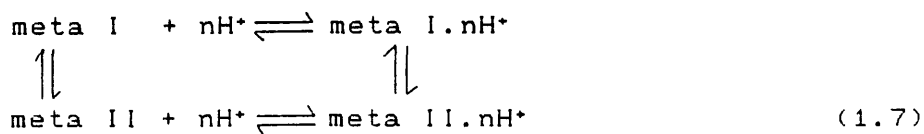


where  $k_1 = [\text{H}^+]^n k'_1$ , is the pseudo first-order forward rate constant. The observed rate constant is  $k_{obs} = k_1 + k_{-1}$ , and the equilibrium constant is:

$$K_{eq} = \frac{[\text{MII}]}{([\text{MI}][\text{H}^+]^n)} \quad (1.6)$$

They also obtained the thermodynamic parameters associated with the meta I to meta II conversion and the value of  $n$ , the apparent net proton uptake. Their results show an increase in entropy during meta II formation which is in agreement with the findings of Matthews et al in 1963<sup>27</sup> suggesting a conformational change occurring at this stage. The fractional value of 0.7 for the number of protons taken up in the reaction (i.e.  $n$ ), although difficult to explain, does agree with observations from Matthews et al that the titration curve of a monoprotic indicator base is not exactly convergent with a plot of the effect of pH on the metarhodopsin equilibrium.

Matthews et al suggested the differences may be due to the ionic strength of their buffer, but this fractional protonation has been observed by many investigators and cannot be easily explained. Parkes and Liebman's experiments do not resolve whether the protonation or the conformational change occurs first but they suggest a general scheme if the protonation occurs in a single step:



Their kinetic analysis suggests that the kinetics of the meta I to meta II equilibrium can be accurately described by a single first order process and they say that a possible explanation of the biphasic response in rod disc membrane preparations could be due to the involvement of meta II in the binding of GTP to G protein which activates the enzyme cascade (Section 1.8). The metarhodopsin equilibrium has been very well studied because it is thought to be an important step in visual transduction but there are many conflicting ideas over:

- (i) what is actually happening at this step - is it the conversion of a protonated schiff base to an unprotonated schiff base or the hydrolysis of the schiff base?
- (ii) how many protons are taken up at this stage and
- (iii) does the reaction involve a single step or is it a biphasic reaction, and are there different forms of the metarhodopsins that are easily inter-convertible.

Some of the dissimilarities in results or interpretation of results may simply be because the rhodopsins of different species do not have exactly the same reaction schemes or perhaps be due to the preparation of samples and different experimental conditions.

### 1.8. The Generation of the Neural Signal

The electrical response of the eye to light can be studied by obtaining an electroretinogram which is a plot of potential versus time. This involves the use of two electrodes, one placed in contact with the cornea, the other elsewhere on the eye or body, and these are connected to a high impedance voltmeter.

It is found that after illuminating the eye with a flash of light there is a delay of a few milliseconds before any change in the potential is observed. It is thought that this latent period before the response corresponds to the time needed to bleach the visual pigment to the critical stage which is believed to be the

metarhodopsin equilibrium. After the time lag the potential changes producing various "waves" on the electroretinogram<sup>37</sup>.

The very small input of energy due to the absorption of a quantum of light in the receptor discs must somehow be amplified and transmitted to the base of the receptor cell in order to generate a nerve impulse. Various mechanisms have been proposed and one possible explanation is that after rhodopsin has absorbed a photon one of the intermediates of the bleaching sequence acts as an enzyme, and this single molecule can initiate changes in a large number of other molecules by activating a cascade of enzymic reactions where each reaction is triggered by the previous one. There is evidence that the intermediate that initiates the cascade could be metarhodopsin II<sup>38</sup>.

Fung et al<sup>39,40</sup> have suggested a possible reaction scheme involving an enzyme cascade of this type based on the knowledge that rod outer segments contain two enzymes that are activated by light. These are a cyclic GMP phosphodiesterase which catalyses the hydrolysis of cyclic GMP to GMP and a GTPase which catalyses the interconversion of GDP and GTP.

They identified a GTP binding protein with GTPase activity which they called transducin (T) or G-protein. In the dark this binding protein has GDP bound to it (T-GDP) but the activated rhodopsin interacts with this to form R\*-T-GDP which is converted to R\*-T-GTP in the presence of GTP (fig.1.10). This form of the binding protein with GTP bound has a lower affinity for the activated rhodopsin which is released and recycled to catalyse the exchange of other GTP molecules for bound GDP. In this way several hundred molecules of T-GTP are formed per rhodopsin molecule and this T-GTP is thought to activate the cyclic GMP phosphodiesterase which catalyses the reaction, T-GTP → T-GDP. The T-GDP can then react with more of the activated rhodopsin.

It is thought that a single photolysed rhodopsin molecule can activate several hundred phosphodiesterase molecules which leads to the hydrolysis of around a

FIGURE 1.10

Proposed scheme for the flow of information in the light-activated cyclic nucleotide cascade of vision. PDE=phosphodiesterase; T=transducin; R\*=photolysed rhodopsin.  
(Taken from ref.40)

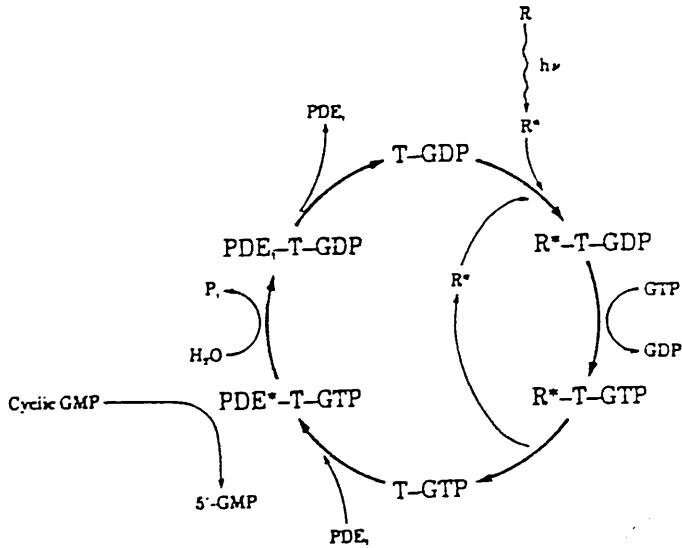
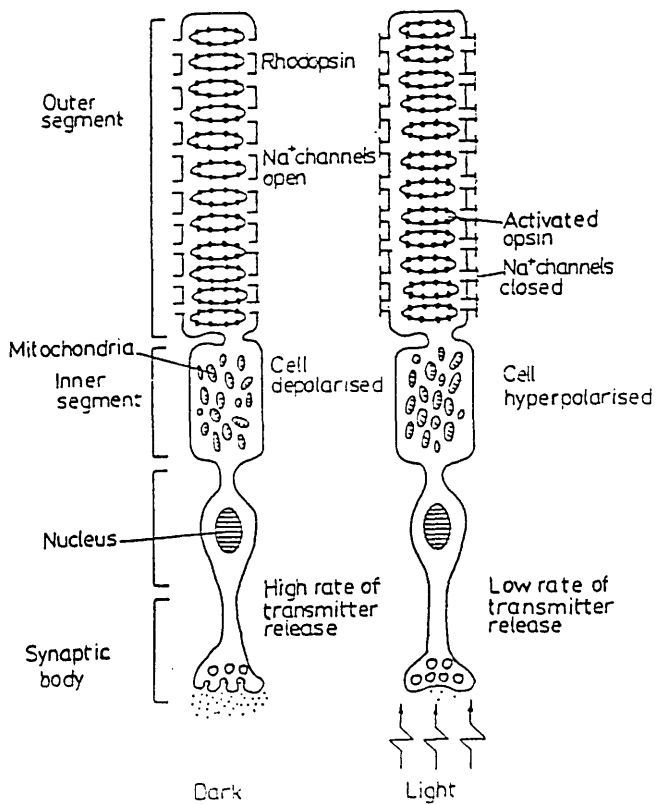


FIGURE 1.11

Schematic representation of the effect of light on the rod outer segments.  
(Taken from ref.42)



thousand cyclic GMP molecules per second by each phosphodiesterase.

Fesenko et al<sup>41</sup> have shown that these cyclic GMP molecules are internal transmitters which act as agonists keeping sodium channels in the plasma membrane in an open state. This means that in the dark, when rhodopsin is in the inactive form, the sodium channels are open, sodium ions can enter the outer segment through these channels due to a concentration gradient and the cell is depolarised (fig.1.11). Inside the cell the ions diffuse to the far end where they are pumped out in a process driven by ATP hydrolysis. In this dark state the cell produces the neurotransmitter at a high rate.

When light interacts with rhodopsin, the dark current is stopped because the activated rhodopsin interacts with the G-protein which leads to activation of the phosphodiesterase and hydrolysis of the cyclic GMP molecules. This leads to closure of the sodium channels in the plasma membrane, stopping the flow of sodium ions into the cell thus causing hyperpolarisation of the cell and a low rate of transmitter release<sup>42</sup>.

Work in this area is continuous as a complete explanation of how the nerve impulse is generated has not yet been found, but it does seem likely that metarhodopsin II is involved in the activation process.

### 1.9 The Regeneration of Visual Pigments

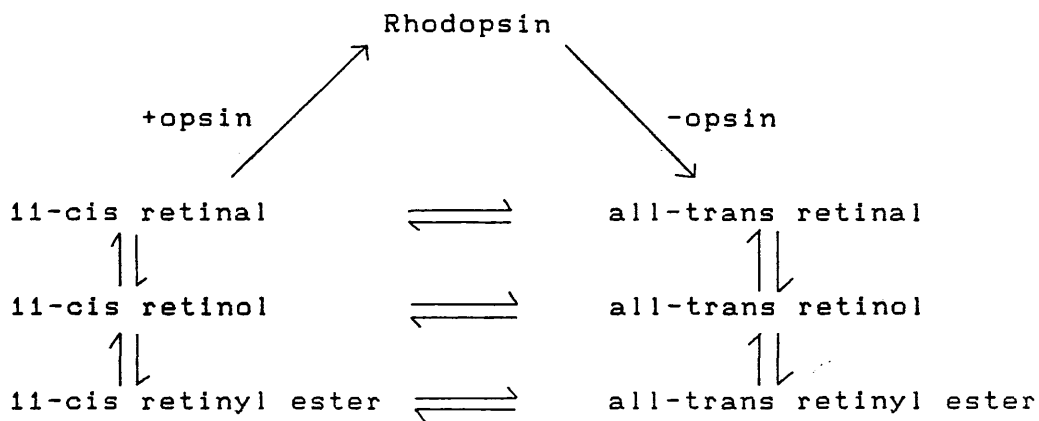
The products of the bleaching of rhodopsin are all-trans retinal and opsin, but for regeneration of rhodopsin the all-trans retinal must be isomerised to the 11-cis isomer which can then react with opsin to form rhodopsin.

The all-trans retinal that is released after hydrolysis is converted to all-trans retinol and this reduction is catalysed by the enzyme retinol dehydrogenase which uses NADPH (reduced form of nicotinamide adenine dinucleotide phosphate) as a coenzyme. The retinol can then react with a fatty acid to form an ester and this ester formation is a means of

storing retinol.

At some stage the chromophore is isomerised and the corresponding 11-cis retinyl esters, 11-cis retinol and 11-cis retinal are all found in the eye. The conversion of retinol to retinal is also catalysed by the dehydrogenase enzyme.

The following scheme contains all the known reactions:



(1.8)

Although all the reactions in this scheme do not occur in every species it would seem likely that most animals use more than one regeneration cycle.

In addition to this "repair" process of previously bleached rhodopsin molecules, new pigment molecules are formed as the discs in the outer segment are continuously renewed in the living eye. As was previously mentioned<sup>2</sup> Young followed the fate of radioactive proteins which were injected into animals and found that the rod discs are constantly renewed. It is also known that a continuous supply of a certain amount of vitamin A (retinol) is needed by the body for normal visual function and in vitamin A deficient animals regeneration is disturbed resulting in night blindness.

## 1.10 Models of Rhodopsin

One area of major interest in rhodopsin chemistry is the bathochromic shift that occurs when the chromophore retinal, which absorbs at 380nm and is yellow coloured, interacts with the protein opsin, which absorbs at 280nm and is colourless, to form rhodopsin which is reddish-purple colour absorbing at 500nm. The mechanism through which the protein shifts the absorption maximum of the chromophore has received much attention and models have been proposed to explain the bathochromic shift.

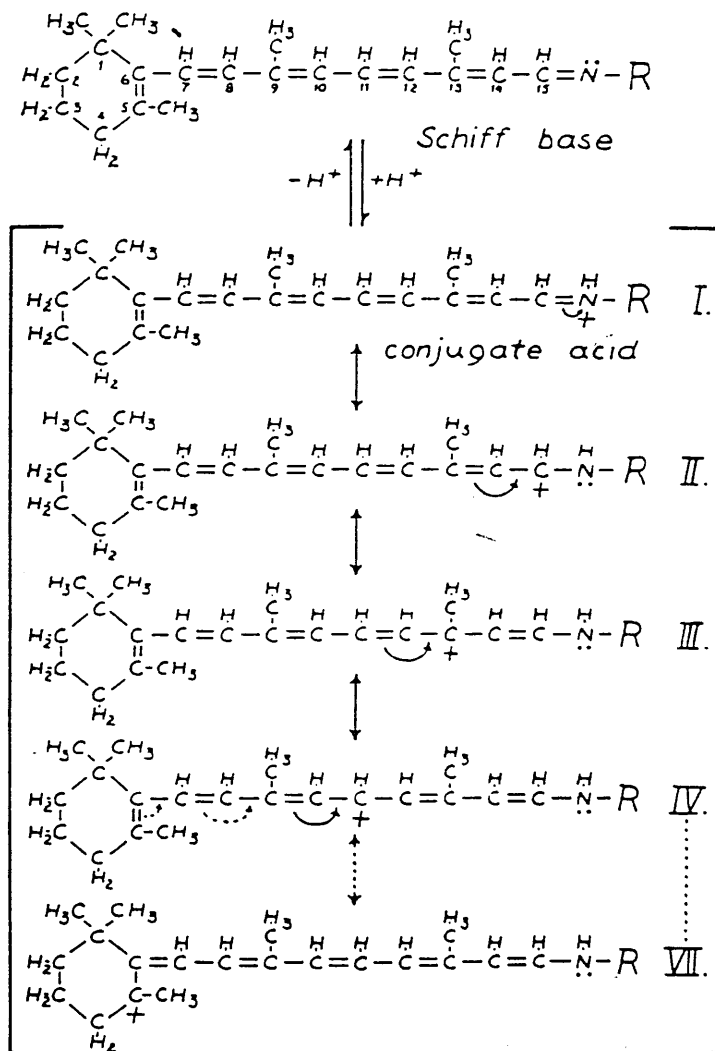
The first models of the interaction between retinal and opsin were the schiff bases prepared from retinal and various amines by Ball et al in 1949<sup>10</sup>, who found that protonated schiff bases absorb around 440nm. Although this partially accounts for the red shift of the chromophore it is still less than in rhodopsin and some other chromophore-protein interactions must occur in order to shift the absorbance maximum to a longer wavelength.

In 1958 Kropf and Hubbard<sup>6</sup> suggested a scheme to try to explain the shift. In order to shift to longer wavelength the energy of the transition from the ground state to the first excited state must be lowered as the wavelength of the light absorbed is dependent on the energy separation of the ground and excited state. This energy separation can be decreased by lowering the energy of the first excited state.

In this case the excited state of the chromophore is a resonance hybrid of structures in which the positive charge of the protonated schiff base is located at different places along the conjugated chain so that in the hybrid the positive charge is distributed over the entire conjugated system, (fig 1.12). The energy of the excited state would be lowered if the positive charge on the chromophore was stabilised by the interaction of negatively charged groups on the opsin. If the protein can stabilise the excited state then the energy of the transition between the ground state and the excited state of the chromophore will be lower and the absorption

FIGURE 1.12

Schiff base of retinal and the most stable limiting states of its conjugate acid. The conjugate acid is not represented accurately by any one of these structures but is a resonance hybrid of structures I to VII. (Taken from ref.6)



spectrum will occur at longer wavelength.

The idea that the red shift of the spectra is a result of secondary interactions between the opsin and polyene chain of retinal is supported by many others and led to the proposal of an external point charge model for wavelength regulation in visual pigments. This model was based on absorbance data obtained from a series of synthetic hydroretinals which were bound to the apoprotein to form hydrohodopsins<sup>43</sup>.

The absorbance maxima of these pigment analogues were compared to those of the respective protonated schiff bases formed between the hydroretinals and n-butylamine, and the difference in the wavelength of the absorbance maximum of the schiff base (in  $\text{cm}^{-1}$ ) and of the pigment (in  $\text{cm}^{-1}$ ) is calculated. The difference in these maxima is regarded as a measure of the influence of the binding site and has been called the "opsin shift".

The data obtained showed that it is the enal moiety rather than the ene moiety that is responsible for the absorbance maxima and with the 11,12-dihydroretinal, in spite of its short chromophore, the difference between the maxima of the n-butylamine schiff base and the rhodopsin is much greater than the other cases examined, including natural rhodopsin. This data made it possible to locate a group on the opsin which is important in the determination of the absorption maximum of bovine rhodopsin, leading to the external point charge model<sup>44</sup>.

In order for external charges to produce a large shift of this nature they must be situated close to the  $\pi$  electron system of the chromophore and so the data suggests that there are significant electrostatic interactions in the vicinity of the chromophoric unit of 11,12-dihydroretinal, which is from carbon 13 to the nitrogen of the schiff base linkage.

Semiempirical  $\pi$  electron calculations of absorption maxima were carried out on model diene protonated schiff bases with external charges located in a variety of positions and it was found necessary to place two negative charges in the chromophoric region. One of the charges is a counterion lying approximately 3Å from the

positively charged nitrogen of the protonated schiff base, the second is located close to both carbon 12 and carbon 14, lying 3Å above carbon 12 and approximately 3Å from carbon 14 (Fig.1.13), and is presumed to be a member of a charge pair in a salt bridge or possibly the negative end of a neutral dipolar group.

This model also provides an explanation of the discrepancy between the resonance Raman spectroscopy results which suggest that the schiff base linkage in rhodopsin is protonated, and the carbon-14  $^{13}\text{C}$  nuclear magnetic resonance experiments which suggest that it is unprotonated. If there is a negative charge located near carbon 14, as proposed by the external point charge model, then it would be expected to reduce the  $\pi$ -electron density at this position because of coulombic repulsion, which could cause a shift in the protonated schiff base peak to a value nearer the unprotonated schiff base peak on the  $^{13}\text{C}$  nmr spectrum. This would explain the Shriver et al<sup>19</sup> proposal that the schiff base linkage is unprotonated.

Experimental evidence which supports the external point charge model was obtained from model compounds related to 11,12 dihydroretinal, containing a quaternary nitrogen with a negative counterion and a second negative charge situated at appropriate distances within the one molecule. It was found that the presence of the second negative charge in the model induces a red shift in the absorbance maximum which supports the point charge model<sup>43</sup>.

A different type of model compound involving cyclodextrin derivatives was reported by Tabushi and Shimokawa<sup>44</sup> to show a remarkable red shift when a retinal schiff base linkage is situated near to a protonated amino group (fig.1.14). This cyclodextrin complex has a maximum absorption at 497nm which is very similar to that of rhodopsin, and the protonated amino group in the model cyclodextrin compound could be equivalent to the  $\epsilon\text{-NH}_2$  of another lysine group in the opsin as previously suggested by Cooper and Converse.

FIGURE 1.13

A model for the electrostatic interactions in the binding site of bovine rhodopsin. The existence of a counterion near the protonated nitrogen is assumed. A second negative charge is located  $\sim 3\text{\AA}$  above carbon 12. (Taken from ref.44)

EXTERNAL POINT-CHARGE MODEL

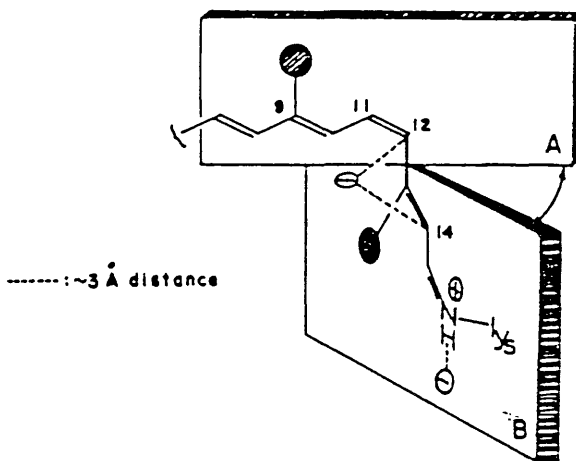
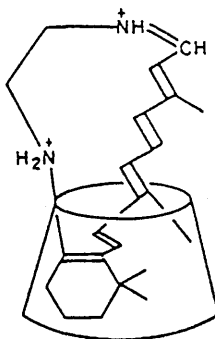


FIGURE 1.14

Model retinal-cyclodextrin complex with a protonated retinal schiff base linkage situated near to a protonated amino group. (Taken from ref.46)



There are other suggestions of possible ways of explaining the bathochromic shift such as effects of solvents on the protonated schiff base linkage<sup>47</sup> or conformational twisting of the chromophore<sup>48</sup>, but the sensitivity of the absorption maxima to these factors is limited and it does not seem likely that these factors alone can account for the bathochromic shift in visual pigments.

### 1.11 Cephalopod Rhodopsin

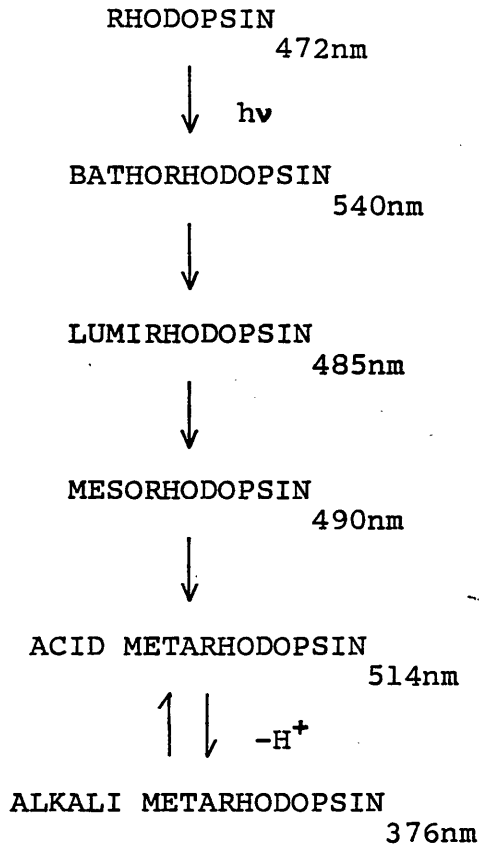
There are certain differences between the visual photoreceptor cells of vertebrates and invertebrates. The vertebrate photoreceptors are the rods and cones which have been described previously, whereas invertebrates have rhabdomeric photoreceptor cells which consist of an inner and outer segment but have no cilium. There is a single internal aqueous compartment along the axis of the outer segment which is surrounded by a tightly packed cluster of finger-like projections of the plasma membrane called microvilli. These microvilli are orientated perpendicular to the axis of the outer segment and the walls of the microvilli contain the visual pigment molecules. Several of these photoreceptor cells are organised into clusters called rhabdomes.

The bleaching sequence of rhodopsin from invertebrate cephalopods such as octopus and squid also differs in certain respects from that of vertebrate rhodopsin (fig.1.15).

The chromophore of the cephalopod rhodopsin, like that of vertebrate rhodopsin, is a protonated schiff base containing 11-cis retinal which on illumination is converted to the all-trans isomer. However, unlike vertebrate rhodopsin, the end product of photolysis is a stable metarhodopsin in which the chromophoric group remains attached to a binding site in the opsin. There is no spontaneous hydrolysis of the schiff base linkage and no release of the retinal chromophore<sup>49</sup>.

The acid and alkaline metarhodopsins (fig.1.15) are in a pH-dependent equilibrium where a proton is released

FIGURE 1.15  
The bleaching sequence of cephalopod rhodopsin.



on the conversion of the red acid form to the yellow alkaline form. This too is different from the analogous metarhodopsin equilibrium in vertebrate rhodopsin where the formation of the blue-shifted species, metarhodopsin II, involves proton uptake rather than release. However, the blue shift in cephalopod rhodopsin is typical of that observed in the conversion of a protonated retinal schiff base to its unprotonated form suggesting that the deprotonation occurring between acid and alkaline metarhodopsin involves the specific schiff base linkage in rhodopsin.

Kitagawa and Tsuda<sup>50</sup> confirmed that the acid and alkaline metarhodopsins correspond to protonated and unprotonated schiff bases respectively in resonance Raman experiments.

The stable photoproduct, acid metarhodopsin, readily reverts to rhodopsin on irradiation. Rhodopsin is therefore regenerated from metarhodopsin in the light.

This bleaching sequence for invertebrates is obviously quite different from vertebrates and leads to the question of how the generation of the nerve impulse is triggered in the case of invertebrates.

The main difference between the vertebrate/invertebrate rhodopsin systems is the stability of the metarhodopsins. In vertebrates the metarhodopsin is unstable and dissociates to all-trans retinal and opsin, whereas for invertebrates it is relatively stable and the main chemical change in the bleaching sequence is the reversible isomerisation of the chromophore.

The fact that the retinal-opsin linkage in vertebrate rhodopsin is susceptible to hydrolysis whereas invertebrate rhodopsin is stable to hydrolysis would suggest that the conformational changes which occur during bleaching do not expose the schiff base linkage to the solvent environment in the case of invertebrate rhodopsin.

The energetics of the octopus rhodopsin bleaching sequence have been studied<sup>51</sup> and have shown that the acid metarhodopsin has a relatively low energy compared to the

parent rhodopsin. This would suggest that the cis-trans isomerisation of the chromophore does not induce very much strain in the molecule and as a consequence there is little driving force for hydrolysis of the schiff base.

In the case of vertebrate rhodopsin the high energies of the metarhodopsin intermediates would suggest that there is a lot of strain in the molecule and this in turn leads to the breakage of the schiff base linkage.

Overall very little is known about the activation of photoreceptors in invertebrates but it has been shown<sup>52</sup> that photoproducts of cephalopod rhodopsins can activate bovine photoreceptor phosphodiesterase and G-protein.

Dixon and Cooper<sup>53</sup> have suggested, from work on the quantum efficiencies of the reversible photoreaction of octopus rhodopsin, that photoreversal in the cephalopod visual cycle has a significant physiological role in that efficient photoreversal of metarhodopsin could result simultaneously in pigment regeneration and photoreceptor deactivation.

If metarhodopsin is the species responsible for the excitation process then it would obviously be more efficient if there is a mechanism for removing the active species because otherwise the photoreceptor response would continue long after the actual photon absorption. Photoreversal of metarhodopsin would fulfil this requirement.

### 1.12 Bacteriorhodopsin

Halobacterium halobium is an organism that lives in environments with high sodium chloride concentrations such as salt lakes where the salt concentration is near saturation. The cell membrane of Halobacteria contains patches of purple membrane and the size of these is controlled by the cell, with a higher abundance in oxygen starved cells. Under these conditions the normal source of metabolic energy in the cell is cut off and the bacteria use light energy to form an electrochemical proton gradient across the cell membrane, and so the purple membrane functions as a light-driven proton pump.

The energy that is stored in the gradient is used by the cells to synthesise ATP and as an energy source for other functions of the cells<sup>54,55</sup>.

The purple membrane pigment is called bacteriorhodopsin because it is very similar to rhodopsin in some respects. For example, it contains retinal as the chromophore and this is covalently attached to a protein of molecular weight 26000 by a protonated schiff base linkage to the  $\epsilon$ -amino group of a lysine residue.

In the dark bacteriorhodopsin exists in two equilibrated forms, one of which contains an all-trans retinal chromophore and has a maximum absorption at 570nm, the other a 13-cis retinal chromophore with a maximum absorbance at 548nm. Under light adapted conditions the form with the all-trans retinal predominates and on illumination bacteriorhodopsin undergoes a photochemical cycle with various intermediates, one of which is a relatively long-lived species with maximum absorbance at 412nm.

Resonance Raman studies of bacteriorhodopsin have shown that the 570nm species contains a protonated retinylidene lysine schiff base linkage whereas the 412nm species contains an unprotonated linkage<sup>56</sup>. This means that bacteriorhodopsin releases protons during this light-induced reaction and binds protons at some stage after this in the photochemical cycle to regenerate the protonated schiff base complex which absorbs at 570nm.

It is interesting to note that bacteriorhodopsin shows a similar bathochromic shift to that of rhodopsin, but even more pronounced. Bacteriorhodopsin with its all-trans retinal protonated schiff base absorbs at 570nm compared to 440nm for an analogous model schiff base. This is also true for the unprotonated 412nm intermediate because an analogous unprotonated schiff base model would absorb at approximately 360nm. As with rhodopsin, this bathochromic shift in the absorbance maximum of the chromophore is thought to be due to interactions in the environment of the protein binding site and an external point charge model was proposed for bacteriorhodopsin<sup>57</sup>.

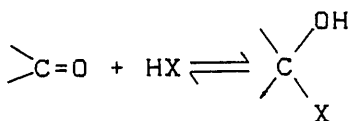
In the case of bacteriorhodopsin, unlike the visual pigments, it was found from using synthetic retinal dihydro chromophores that the largest opsin shift was encountered in the longest enal chromophore. The model proposed has a negative counterion near the protonated nitrogen of the schiff base and another in the vicinity of the  $\beta$ -ionone ring.

This model was recently modified to include an ion-pair protein interaction near the  $\beta$ -ionone moiety along with the previously described negative counterion<sup>58</sup>. The negative charge of the ion-pair is situated above carbon atom 5 while the positive charge is nearer to the 7,8-double bond and there is a planar 6-s trans ring-chain conformation (fig.1.16). This model is in agreement with that proposed by Lugtenburg et al<sup>59</sup> and definitely suggests that protein-chromophore interactions can account for much of the bathochromic shift in bacteriorhodopsin.

## B. SCHIFF BASE CHEMISTRY

### 1.13 Schiff Base Formation and Hydrolysis

The schiff base linkage in rhodopsin is formed between the  $\epsilon$ -amino group of a lysine residue on the opsin and the carbonyl group of the aldehyde retinal. In general carbonyl chemistry, if the compound that is undergoing addition to the carbonyl only contains a single dissociable proton then the reaction would normally proceed as in scheme (1.9).

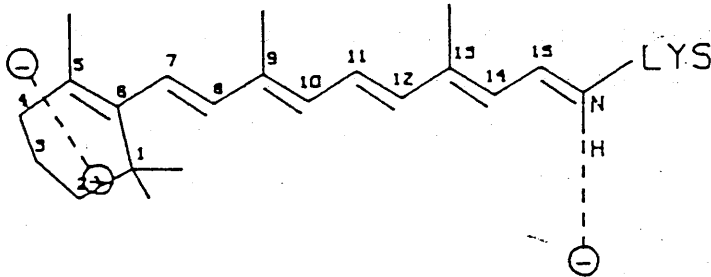


(1.9)

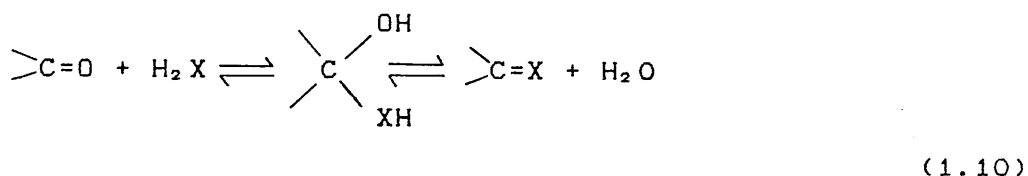
This reaction involves a very fast proton transfer to form a product containing a quaternary carbon atom. If the compound undergoing addition contains two dissociable

FIGURE 1.16

A point charge model for bacteriorhodopsin. The schiff base counter-ion is  $3.9\text{\AA}$  from the schiff base nitrogen. The ring negative charge is  $3.0\text{\AA}$  above C-5. The positive charge by the ring is  $3.0\text{\AA}$  from the negative charge. (Taken from ref.58)



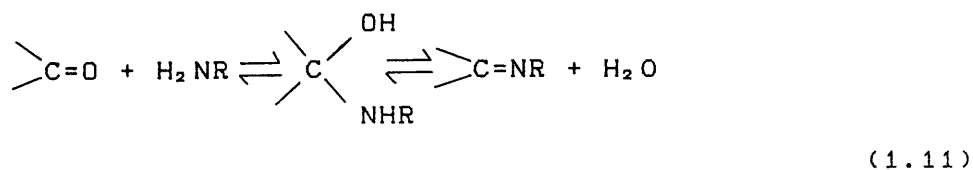
protons then there may be another step involving dehydration of the quaternary carbon-containing species and this would proceed according to reaction (1.10).



These addition reactions at the carbonyl group involve the breaking of a  $\pi$  bond which occurs more readily than the breaking of a  $\sigma$  bond in compounds containing saturated carbon atoms. The carbon atom of the carbonyl group has a partial positive charge due to the strong electronegativity of the oxygen atom which polarises the double bond. This facilitates the attack of the lone pair electrons of a nucleophilic reagent on the carbonyl group so that addition reactions to carbonyl compounds occur frequently in chemistry.

The attacking nucleophilic reagent approaches the carbonyl group perpendicular to the plane of the carbonyl group and the groups attached to it and forms a bond with the orbital which had previously been involved in the  $\pi$  bond to oxygen, with the electron pair of this bond settling on the oxygen atom. In the planar carbonyl group the carbon atom has  $sp^2$  hybridisation with  $120^\circ$  bond angles but as addition of the nucleophile occurs it undergoes a change in hybridisation to  $sp^3$  and becomes tetrahedral.

In the case of schiff bases, the group X in reaction (1.10) is equivalent to N-R, where R is an aliphatic or aromatic group, and the reaction scheme for the formation of schiff bases is shown in scheme (1.11).



The addition of the amine,  $H_2NR$ , to the carbonyl group involves the formation of a tetrahedral carbinolamine intermediate which dehydrates to form a schiff base and water. According to the principle of microscopic reversibility the same mechanism must hold for the reverse reaction under the same experimental conditions, so the hydrolysis of the schiff base should involve the formation of a tetrahedral carbinolamine intermediate prior to the formation of the hydrolysis products which are the amine and the carbonyl compound.

The rate of carbonyl addition reactions can be increased by (i) increasing the charge density and nucleophilic reactivity of the attacking reagent and (ii) increasing the positive charge on the carbonyl group by attaching electron-withdrawing substituents to it.

It is essential that the attacking nucleophilic reagent is in its basic form so that it has an available free electron pair to attack the carbonyl group. In acid conditions the amine  $RNH_2$  can pick up a proton to form the conjugate acid  $RNH_3^+$  which no longer contains the free electrons to attack the carbonyl. This means that the addition reactions are pH dependent and are less likely to occur at low pH when the amine is in the conjugate acid form.

It has been known for a long time that many carbonyl reactions of the type in (1.11) exhibit bell-shaped pH-rate curves where the rate of reaction is very slow at low and high pH and reaches a maximum at some intermediate pH.

A reaction of the type in (1.11) must proceed in two steps, an addition step and a dehydration step, and it is likely that one or other of these steps will be rate determining under certain conditions.

In 1962 Cordes and Jencks<sup>40</sup> studied the formation and hydrolysis reactions of the schiff base N-p-chlorobenzylideneaniline and found that the reactions undergo a transition in the rate determining step as the pH is changed. In the formation reaction at neutral pH the rate determining step is the dehydration of the carbinolamine intermediate whereas at lower pH the attack



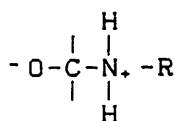
formation and decay of carbinolamines. They have also obtained the equilibrium constants of formation of the carbinolamines along with the rate constants of the dehydration reactions.

After their work on the formation and hydrolysis reactions of benzylideneanilines, Cordes and Jencks went on to study the reactions of schiff bases formed from more basic, aliphatic amines<sup>64</sup>. They found again that in the hydrolysis reactions of these schiff bases there is a change in rate determining step from the attack of water on the schiff base under neutral and basic conditions to decomposition of the tetrahedral intermediate under acidic conditions.

Reactions of this type involving aliphatic amines may be analogous to the schiff base reactions that occur with rhodopsin and so it is interesting to examine the mechanism of hydrolysis and formation of them. It is also useful to note that Morton and Pitt<sup>12</sup> found that the rate of hydrolysis of retinylidenemethylamine is much slower in acid than in neutral solution which can also be interpreted in terms of a change in rate determining step as the pH is changed.

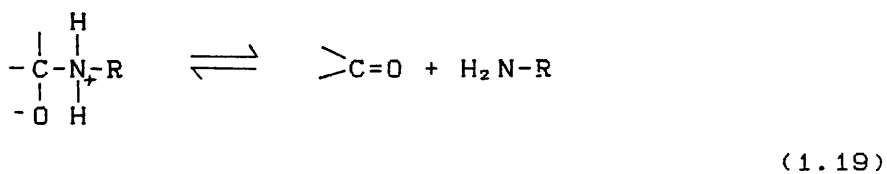
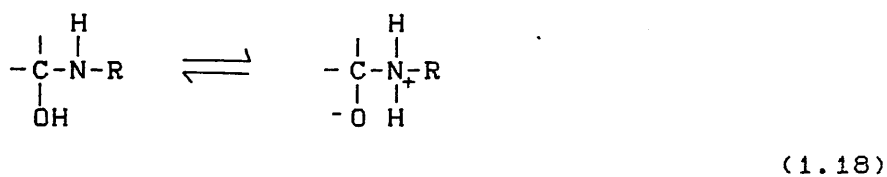
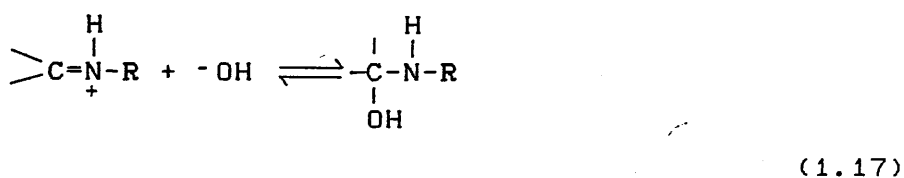
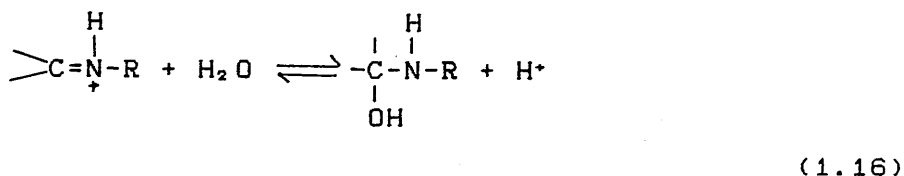
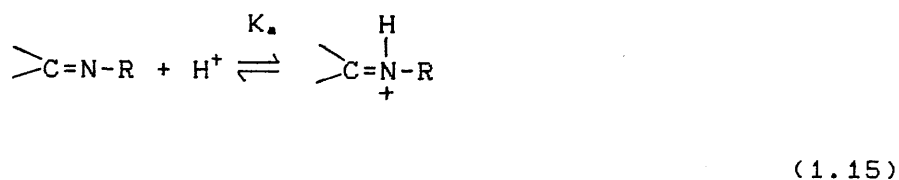
Cordes and Jencks found that the reactive species in hydrolysis is the protonated schiff base and when this schiff base is formed from a strongly basic aliphatic amine there are two possible hydrolysis reactions, one involving the addition of water to the protonated schiff base, the other involving the addition of hydroxide ion to the protonated schiff base which occurs at higher pH.

During the hydrolysis reaction the basic amine is expelled from a dipolar intermediate such as species (1.14).



(1.14)

The reactions that occur during schiff base hydrolysis are therefore:



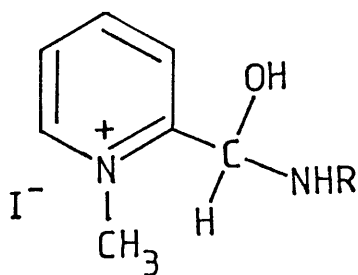
The pH-rate profile of the reactions can be split into different regions. From pH 9 to pH 14 the rate of hydrolysis is independent of pH because of two competing factors - the increase of hydroxide ion concentration which is compensated by a decrease in the protonated schiff base concentration. The rate determining step in this pH range is most likely to be the attack of hydroxide ion on the protonated schiff base because under these conditions only a small amount of the schiff base

exists as the conjugate acid.

Between pH 5 and 9 the hydrolysis rate increases as an appreciable fraction of the schiff base exists as the conjugate acid, and the carbinolamine intermediate is formed by the attack of water on the protonated schiff base. A plateau in the region pH 3 to 5 indicates a transition in the rate determining step from the formation of the carbinolamine to its decomposition.

Below pH 4 the rate decreases because the reverse reaction of equation (1.16) occurs and, as the rate of the acid catalysed dehydration becomes very fast, the rate of decay of the carbinolamine intermediate into the aldehyde and amine can no longer keep up with the rate of its dehydration so that the formation of amine and aldehyde becomes rate determining.

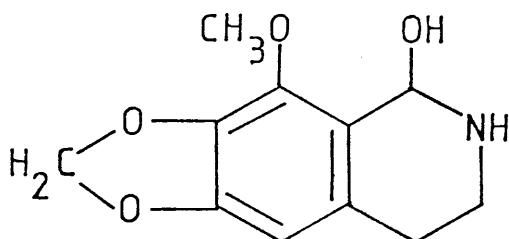
The carbinolamine intermediates in these reactions are normally very unstable but there are cases where they are sufficiently stable to be isolated<sup>45,46</sup>. The carbinolamine (1.20) is formed in the reaction of chloral hydrate with thiosemicarbazides to give chloral hydrate thiosemicarbazones and (1.21) is formed by the



reaction of 2-formyl-1-methylpyridinium iodide with hydroxylamine, hydrazine or phenylhydrazine.

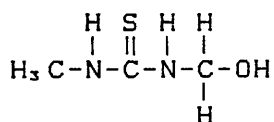
Noncyclic carbinolamines are very unstable; "acetaldehyde ammonia" or 1-aminoethanol is one of the few known to exist and dissociates above 70°C into acetaldehyde and ammonia or forms a trimer<sup>67</sup>.

Cyclic carbinolamines are more stable and a number of naturally occurring substances such as cotarnine (1.22) have such a structure.



(1.22)

The crystal structure of a drug called Noxythioline (N-hydroxymethyl-N'-methyl thiourea) has been reported<sup>68</sup> and is shown to have a carbinolamine structure (1.23).



(1.23)

However, most of the evidence for the presence of carbinolamine addition compounds comes from less direct methods such as following the change in ultra-violet or infra-red absorbance of the carbonyl compound and kinetic studies of the hydrolysis and formation reactions at different pH values.

In an attempt to understand the hydrolysis of the retinal-opsin schiff base linkage of rhodopsin, model studies have been carried out using an analogue of rhodopsin, N-retinylidene n-butylamine, which contains retinal bound to n-butylamine in a schiff base linkage<sup>69</sup>.

It was found that a plot of the steady-state rate constant of hydrolysis versus pH for the hydrolysis reaction of the model compound in aqueous detergent micelle mixtures gives the characteristic bell-shaped pH-rate profile for schiff base hydrolysis (fig.1.17). This suggests that in the model compound at least, the hydrolysis reaction involves the formation and decay of a tetrahedral carbinolamine intermediate.

#### 1.14 Objectives

The aim of this PhD thesis is to investigate one of the main chemical reactions that occur in the visual process, namely the hydrolysis reaction of the retinal-opsin schiff base linkage in the visual pigment rhodopsin, in order to establish a possible mechanism for this reaction and to try to determine the stage during the photolytic bleaching sequence at which it occurs.

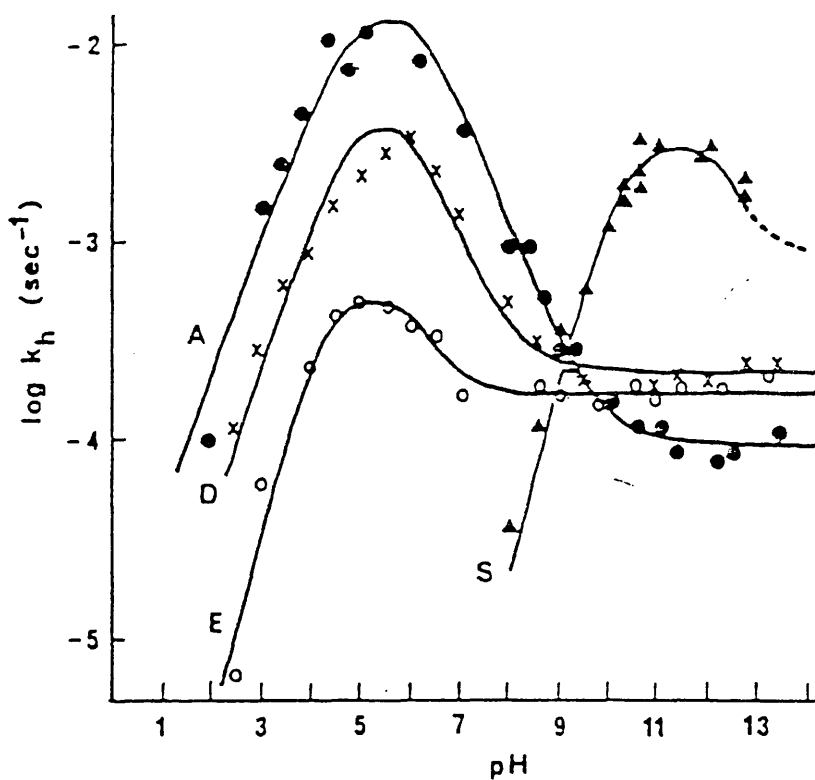
The work involves a comprehensive study of the hydrolysis and formation reactions of a model compound of rhodopsin, N-retinylidene n-butylamine in aqueous detergent micelles, in order to investigate the kinetics and mechanism of the reactions and try to relate these to rhodopsin itself.

In particular it is interesting to see if these reactions show general features that are characteristic of other schiff base reactions, such as the formation of carbinolamine intermediates, and if so to prove the presence of such an intermediate and explain its role in the visual process.

It is intended that kinetic and spectroscopic techniques will be used during this work and these will include UV/visible spectroscopy, stopped-flow kinetics, resonance Raman spectroscopy and infra-red spectroscopy.

The work carried out for this thesis forms part of a major investigation into the mechanism of retinal schiff base formation and hydrolysis. The investigation includes steady-state studies of the formation and hydrolysis of N-retinylidene n-butylamine schiff base<sup>49</sup>, non-steady state studies of the formation and hydrolysis of this

FIGURE 1.17  
Steady-state pH-rate profiles for hydrolysis of  
N-retinylidene n-butylamine in aqueous detergent  
mixtures at 20°C. A=Ammonyx;E=Emulphogene;S=SDS  
and D=DTAB. (Taken from ref.69)



schiff base (this work), resonance Raman spectroscopy of a tetrahedral carbinolamine intermediate (this work) and oxygen-18 labelling of retinal at the metarhodopsin stage in photoreceptor membranes<sup>49</sup>.

The results of these experiments have been used to postulate a possible mechanism for visual pigment photolysis.

CHAPTER 2

TECHNIQUES AND APPARATUS.

## 2.1 Stopped-Flow Spectrophotometry

### 2.1.1 Technique

There are various methods for studying chemical reactions in solution, but the study of fast reactions requires special techniques when the reaction rate exceeds the rate at which solutions can be mixed manually. These techniques can be divided into two main categories:

- (i) rapid mixing techniques where quick, efficient mixing is achieved by mechanical means, eg. continuous flow and stopped-flow,
- (ii) relaxation techniques where a reaction mixture at equilibrium is perturbed by varying an external parameter such as temperature or pressure. This causes a shift to new equilibrium conditions and the determination of the rate of this shift allows the kinetics of the reactions in question to be studied, eg. temperature-jump or pressure-jump.

In this work the stopped-flow technique was used and this falls into the first category as it is a rapid mixing technique. The stopped-flow method was first used by Roughton<sup>70</sup> for reaction times of around 10 seconds. The technique was later developed by Chance<sup>71</sup> to allow the study of reactions in the millisecond time scale.

A typical stopped-flow apparatus is shown in fig.2.1. A detailed diagram of the observation tube arrangement is shown in fig.2.2.

The reagents to be mixed are introduced into 2ml driving syringes, D1 and D2, from the larger reservoir syringes R1 and R2 using the valves V1-V4. The piston drive is pushed against the plungers of the driving syringes so that equal volumes of the reagents are driven together rapidly, under turbulent flow conditions, into a specially designed mixer (M). Turbulent flow is achieved by flowing the solutions along narrow, 2mm diameter, bore tubes and the piston drive ensures the even delivery of the solutions. The reactants flow along the observation tube and enter into a 2ml stopping syringe (SS). The flow

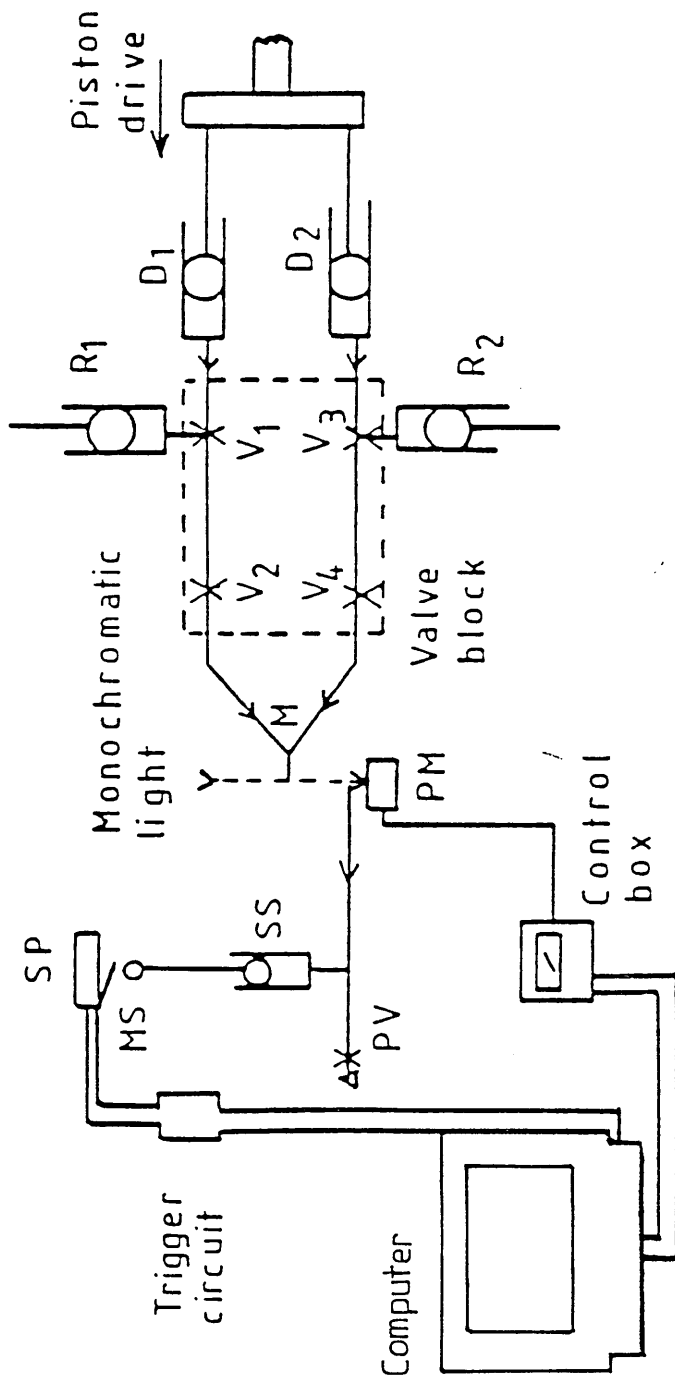


FIGURE 2.1  
Block diagram of stopped-flow apparatus.

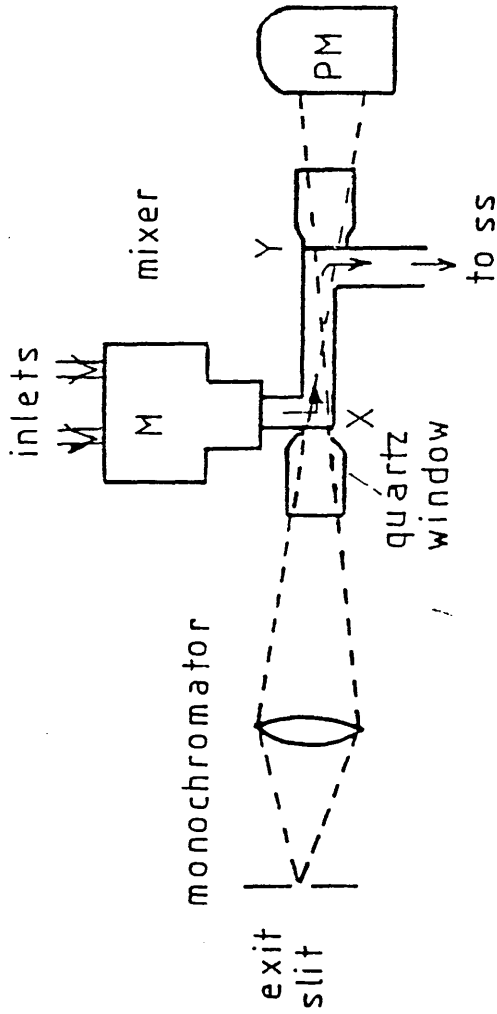


FIGURE 2.2  
Observation tube arrangement.

is abruptly stopped when the plunger of the stopping syringe is forced against a stopping plate (SP), at the same time closing a microswitch (MS) which triggers the recording device.

A monochromatic light beam is focussed through a quartz window into the centre of the observation tube and the transmitted light is detected continuously with a photomultiplier tube. In this way a complete reaction, covering a timescale of a few milliseconds to several minutes, can be followed by spectrophotometry.

### 2.1.2 Description of the Stopped-Flow Apparatus

An Applied Photophysics model number 1705 stopped-flow spectrophotometer was used in this work and was assembled as described above. The stopped-flow apparatus was interfaced to an Apple II microcomputer with a 48 kilobyte internal memory capacity and two Apple Disk II floppy disc subsystems were used for program and data storage. During an experimental run the stopping syringe pushes against the microswitch which is connected via the trigger circuit to the interface controller. The current values from the photomultiplier are converted to voltage readings which are amplified and then collected, digitised using a fast, 12-bit analogue to digital converter and stored in the computer memory.

The drive mechanism is a pneumatic system which is also computer controlled. The gas pressure tube on the stopped-flow apparatus is connected to a nitrogen gas cylinder and the gas pressure used for firing is 15-20 pounds per square inch.

The pathlength of the observation tube (XY) is 2.165cm. This was calculated experimentally using a solution of known absorbance<sup>72</sup>. The part of the reaction which is missed in the mixing process and during the time taken for the mixed solution to reach the stopping syringe and trigger the circuit is called the dead-time. This has also been obtained experimentally for this apparatus<sup>73</sup> and has a value of 8.225 milliseconds.

The monitoring lamp in the stopped-flow apparatus is a tungsten halogen lamp and the power supply is a 15/10 Model, Farnell "S" series, Wetherby.

The temperature is controlled by circulating thermostatted water from an open water bath mounted below the stopped-flow apparatus. The water is pumped in a closed loop through a small steel bath surrounding the driving syringes and around the mixing chamber and observation tube.

### 2.1.3 Measurement of Absorbance

As was previously mentioned, after an experimental run the amplified signals from the photomultiplier are collected and stored in the computer memory. The voltage (V) is directly proportional to the intensity (I) of the light transmitted from the observation tube:

$$V = cI \quad (c = \text{constant}) \quad (2.1)$$

If there is solvent in the observation tube then,

$$V_0 = cI_0 \quad (2.2)$$

where  $V_0$  is the voltage corresponding to light of intensity  $I_0$ , i.e. the voltage corresponding to 100% transmission of light. The optical density or absorbance (A) can be calculated using Beer's Law:

$$A = \log_{10} \frac{I_0}{I} = \log_{10} \frac{V_0}{V} \quad (2.3)$$

Using the Beer-Lambert Law the absorbance can then be related to the concentrations ( $c_i$ , mol l<sup>-1</sup>) and the molar extinction coefficients ( $\epsilon_i$ , l mol<sup>-1</sup> cm<sup>-1</sup>) of all species (i) present in the observation tube with a pathlength of d cm.

$$A = \log_{10} \frac{I_0}{I} = d \sum_i \epsilon_i c_i \quad (2.4)$$

Experimentally  $V_0$  is normally obtained with water or buffer in the observation tube by measuring the difference in voltage readings between 0% and 100% transmission of light, obtained by closing and opening the shutter on the lamp housing unit. Similarly  $V$  is obtained with reaction mixture in the observation tube taking the voltage difference with shutter open and closed. This method of obtaining  $V_0$  and hence  $I_0$  involves flushing the stopped-flow apparatus with water or buffer solution after each run and does not allow consecutive experimental runs to be done. To overcome this problem another method of obtaining  $I_0$  was used.

Calibrations were done with water in the observation tube where the voltage was read over a wavelength range of 280-680nm every 10nm. The slit widths were set at 2nm and 1.25mm as in experimental runs. The voltage readings were normalised by taking the highest reading to be equal to unity with the other values relative to the highest. The calibration was repeated over a range of photomultiplier voltage settings and the results were averaged for each wavelength giving a list of wavelengths and average relative intensities. This was repeated each time the lamp was changed and the values of wavelength and relative intensity were written into the stopped-flow program.

The 100% transmission value ( $I_0$ ) can now be obtained with the sample in the observation tube by using a reference wavelength (usually 600nm) where the sample does not absorb very much. The ratio of the water voltage at the observation wavelength,  $V_w(\text{obs}\lambda)$ , to the water voltage at the reference wavelength,  $V_w(\text{ref}\lambda)$ , (both of which are obtained from the calibration curves) can be multiplied by the sample voltage at the reference wavelength,  $V_s(\text{ref}\lambda)$  to give a  $V_0$  value at the observation wavelength,  $V_0(\text{obs}\lambda)$ .

$$V_0(\text{obs}\lambda) = V_s(\text{ref}\lambda) \times \frac{V_w(\text{obs}\lambda)}{V_w(\text{ref}\lambda)} \quad (2.5)$$

At the start of each experimental run the dark current is obtained by closing the lamphouse shutter giving a value for background voltage which is subtracted from the water and sample voltages.

It can be seen therefore that the absorbance of the sample can be calculated using equation 2.3 .

The absorbance of the sample is followed with respect to time at a fixed wavelength and different timing sequences can be used during the experimental runs, the total reaction time varying between seconds and several minutes, with 256 voltage/absorbance readings being recorded in each case.

Three timing modes have been used during this work, and these are linear, geometric and arithmetic. The linear time scale has equally spaced time intervals (DT) which are multiples of 0.25msec. In the geometric time scale the time interval between consecutive readings doubles after N steps, where  $256/N$  is an integer, starting at a value DT which is a multiple of 0.25msec. In the arithmetic time scale the interval increases by DT at each step where again DT is a multiple of 0.25msec. The advantage of using the geometric and arithmetic sequences is that data in the time range from about 10msec to 10 minutes can be collected during one run. This is obviously an advantage if a reaction is biphasic with a very rapid first step.

After the voltage readings have been converted to absorbances the results of absorbance and time from each run on the stopped-flow apparatus are stored on a data disc in the Apple computer and are analysed at a later stage thus allowing many consecutive runs to be done quickly.

#### 2.1.4 Experimental Conditions in the Stopped-Flow Experiments

All the experiments during this work were done with slit width settings of 2nm and 1.25mm at a temperature of 20°C. The wavelength range used was between 330nm to

540nm with a reference wavelength of 600nm.

## 2.2 Raman Spectroscopy

### 2.2.1 Raman Spectroscopy

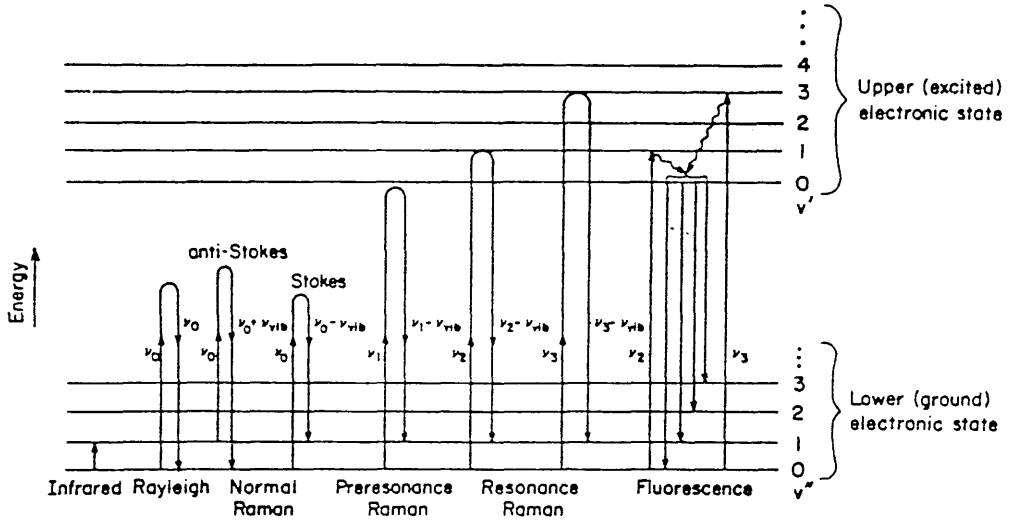
Raman spectroscopy<sup>74</sup> is a technique which explores the vibrational and rotational energy levels of molecules by examining the light scattered by the molecules. The sample is irradiated with monochromatic radiation, normally in the visible region, and the scattered light is usually detected at an angle that is perpendicular to the direction of the incident beam. The light can be scattered elastically (Rayleigh scattering) or inelastically (Raman scattering) by interacting with the sample.

In Raman scattering the emergent light is shifted from its original frequency  $\nu_0$  by a quantum of energy corresponding to a molecular transition of the sample, which is usually a vibrational transition (fig.2.3). If the molecules are excited by the light during the collision then they withdraw energy from the photons and the scattered light emerges with a lower frequency than the incident light,  $\nu_0 - \nu_{10}$ , generating the Stokes lines on the Raman spectrum. If the molecules are already excited before the collision and lose energy to the photons during the collision then the photons emerging will be of higher frequency than the incident light,  $\nu_0 + \nu_{10}$ , giving rise to anti-Stokes lines. These are of lower intensity than Stokes lines due to the fact that most molecules are in the ground vibrational energy level.

The Raman effect is very weak as the transition is forbidden and goes through a "virtual" excited electronic state with most of the light being scattered without change of frequency giving rise to Rayleigh scattering. Raman shifts are measured from the exciting line which is arbitrarily taken as zero on a relative frequency scale. The spectrometer will read out the same shift no matter what the frequency of the laser beam interacting with the

FIGURE 2.3

Some of the possible consequences of a photon-molecule interaction.



(Taken from ref.74)

molecule. The Stokes and anti-Stokes lines are symmetrically placed on either side of the Rayleigh line, the Stokes lines on the low frequency side and the anti-Stokes on the high frequency side.

### 2.2.2 Resonance Raman Spectroscopy

The resonance Raman effect occurs when the exciting laser wavelength lies under an intense electronic absorption band of a chromophore so that excitation leads to an allowed electronic transition from the ground electronic state, which is normally a singlet state, to one of the higher singlet electronic excited states. This leads to selective enhancement of certain Raman bands which correspond to vibrational modes involving motions of the atoms in the chromophore, the part of the molecule in which the electronic transition is localised. This technique is very useful when working with large biological molecules because, as a result of the enhancement, the vibrations of the chromophore can be distinguished from the many vibrational modes of the rest of the molecule.

Resonance Raman spectroscopy is therefore a good technique to use in a study of reactions in which retinal is the chromophore as the frequency of the laser that generates the Raman scattering can be selected to be near the electronic absorption band of the retinal, thus providing resonance enhancement even in dilute aqueous solutions. The resonance Raman bands increase in strength as the exciting frequency approaches the electronic absorption maximum, attaining optimum intensity when the laser frequency co-incides with the absorption maximum.

### 2.2.3 Fluorescence and Phosphorescence

After a molecule has been excited to some vibrational level of an excited electronic state by absorption of a photon it generally loses vibrational energy very rapidly until it reaches the lowest vibrational level of the excited state. Then the predominant path for loss of

excitation energy is via radiationless transitions. This can either be by internal conversion which is the decay to a lower electronic state of the same multiplicity or by intersystem crossing which is a transition to a state of different multiplicity, such as singlet to triplet.

Alternatively the excited singlet state can return to the ground state with the emission of fluorescence, or the triplet state, formed by intersystem crossing, can return to the ground state with the emission of phosphorescence.

Phosphorescence lifetimes are usually considerably longer than fluorescence lifetimes because radiative transitions between states of different multiplicities are forbidden.

Background luminescence from fluorescent or phosphorescent processes may cause problems when acquiring Raman data but the luminescence can often be reduced by changing the excitation wavelength. With resonance Raman spectroscopy a change to shorter wavelength, further into the blue, is recommended and it was found that this greatly reduced luminescence during these experiments.

#### 2.2.4 The Raman Spectrometer

The spectrometer used during these experiments was an Applied Photophysics Multichannel Laser Raman Spectrometer Model 36 and this incorporated a Tracor Northern TN-1223-1 cooled, intensified diode array detector with a TN-1710 mainframe and optical spectrometer module for data display and manipulation. The laser used was a Spectra-Physics Model 171 Argon ion laser with intensity, measured at the sample, of 100mW or less.

Experiments were run using the 488nm, 514.5nm and 457.9nm laser lines for excitation and it was found that there was least sample fluorescence with the 457.9nm line and so this was used for the main Raman experiments. Experiments were carried out at room temperature (20 ± 1°C).

The spectra were obtained using a continuous flow rapid pH-jump set up where the two solutions to be mixed were pumped into a 1cm pathlength quartz cell using two LKB 10200 Perpex peristaltic pumps, each fitted with a variable speed drive unit. The pump head was fitted with 3.0mm internal diameter tubing which is compressed between rollers and the back plate producing a peristaltic action. The two solutions were pumped at a speed of 2.65ml per minute through each channel. These solutions were mixed using a T-piece mixer with a Millipore filter holder fitted to aid mixing. The T-mixing device was constructed of 1mm bore Teflon tubing and the combined flow rate of solutions was about 5-6ml per minute. The dead time from when the two solutions are mixed to when they pass through the laser beam focussed through the quartz cell was approximately 10 seconds. The sample residence time in the laser beam was less than about 0.15 seconds and there was no evidence of sample photoisomerisation under these conditions.

Trial experiments using this experimental set up in a UV-visible spectrometer showed that adequate mixing was achieved. Raman spectra of the appropriate solvent backgrounds were subtracted from the sample spectra in each case (Chapter 5).

All spectra consisted of 400 accumulations with a 0.2 second acquisition time and the instrumental bandwidth was  $7\text{cm}^{-1}$  or less.

## 2.3 Ultra-Violet/Visible Spectroscopy

### 2.3.1 Technique

The ultra-violet and visible spectra of organic compounds are associated with transitions between electronic energy levels. The transitions are between a bonding or lone pair orbital and an unfilled non-bonding or antibonding orbital. The wavelength of the absorption

is a measure of the separation of the energy levels of the orbitals involved:

$$\Delta E = h\nu = hc/\lambda \quad (2.6)$$

The electronic spectrum is taken on a dilute solution normally in a 1cm silica cell. An identical cell containing solvent or water alone is used as a reference in the spectrometer and two equal beams of light are passed, one through the sample solution, the other through the reference. Once again the Beer-Lambert Law holds:

$$\text{Abs} = \log_{10} \frac{I_0}{I} = \epsilon cl \quad (2.7)$$

where  $I_0$  and  $I$  are the intensities of the incident and transmitted light respectively,  $l$  is the pathlength of the cell (cm),  $c$  is the concentration in moles/litre and  $\epsilon$  is the molar extinction coefficient.

The intensities of the transmitted beams from the reference and the sample are compared over the wavelength range of each run giving plots of absorbance versus wavelength for the sample.

### 2.3.2 Description of the UV/Vis Spectrophotometer

The electronic spectra were run on a Pye Unicam SP8-200 UV/Vis. spectrophotometer with a microprocessor incorporated for instrument control and data handling. The instrument has two light sources, a 12 volt quartz halogen lamp for the visible and near infra-red region and a deuterium lamp for the ultra-violet region.

The bandwidth was set at 1nm during these experiments and the spectra were plotted using a scan speed of 2nm per second and chart speed of 10 seconds per centimetre. The wavelength range that was scanned was usually 260-500nm and the temperature was maintained at 20°C by circulating water from a water bath.

## 2.4 pH measurements

### 2.4.1 The pH meter

pH measurements were recorded at the end of experimental runs using a PHM 62 standard pH meter (Radiometer, Copenhagen) with a digital display panel. The electrode is a combined electrode, type GK 2301 C (Radiometer, Copenhagen) which is a glass electrode and calomel reference electrode combined in one body.

### 2.4.2 pD Standardisation

During the resonance Raman spectroscopy experiments some of the solutions were prepared using deuterium oxide in place of water. The "acidity" measured in deuterium oxide is not the activity of hydrogen ion,  $a_H$ , but the activity of deuterium ion,  $a_D$ . Studies of the response of the glass electrode in heavy water give considerable evidence that this electrode, when suitably conditioned, responds to deuterium ions in heavy water as well as to hydrogen ions in ordinary water<sup>75,76</sup>. A glass-calomel pH electrode standardised with a reference solution made up in ordinary water can be used to obtain a pD value if a correction factor of 0.40 is added to the pH meter reading.

$$\text{pD} = \text{pH meter reading} + 0.40 \quad (2.8)$$

In this way pD values were obtained for experiments with deuterium oxide.

## 2.5 General Preparation of Solutions

### 2.5.1 Schiff Base Preparation

All-trans retinal from Fluka, Switzerland was used without further purification as it contained at least 95% of the all-trans isomer and previous analysis using HPLC and mass spectrometry showed that the only impurities present were other geometrical isomers.

Retinal is a yellow solid, molecular weight 284.45, which is sensitive to light, humidity and air. It is stored in a refrigerator, in a sealed container under argon or nitrogen. N-butylamine (Hopkin and Williams) was redistilled before use. The model schiff base, N-retinylidene n-butylamine, was prepared by the addition of all-trans retinal dissolved in a small volume of ethanol, to excess n-butylamine in an aqueous detergent solution made up in distilled water. The schiff base was prepared in a glove box in an inert argon or nitrogen atmosphere. The retinal was removed from the freezer and placed in the glove box for approximately 5-10 minutes to equilibrate to room temperature. After addition of the retinal to the n-butylamine detergent solution, the sample was allowed to sit for at least 20 minutes for the schiff base to form. All samples were wrapped in aluminium foil as light can cause isomerisation of the double bonds in retinal forming other geometric isomers. The solutions were freshly prepared for each experiment.

This method of schiff base preparation was used for all the schiff base hydrolysis reactions.

### 2.5.2 Preparation of Solutions for Formation Reactions

In the experiments studying the formation of the schiff base, the retinal and the n-butylamine were made up separately and were not mixed until the experiment commenced. Once again the retinal was dissolved in a small volume of ethanol but in this case it was added to a buffer and detergent mixture. The n-butylamine was also made in a buffer/detergent solution and mixing of the two solutions started the formation reaction.

### 2.5.3 Buffer Preparation

The buffers were prepared by dissolving the appropriate quantities of the constituents in distilled water to obtain the required concentrations. The constituents were then added together to obtain the correct final pH. A table showing the buffers used in

this work is shown (Table 2.1). pH plays a major role in the formation and hydrolysis of retinal schiff bases because the schiff base is stable to hydrolysis at high and low pH but unstable at neutral pH. The schiff base is therefore formed at high pH and hydrolysed at neutral pH and appropriate buffers must be used.

For the schiff base formation reactions, buffers in the pH range 8-12 were used, usually at a concentration of 0.1M and for the hydrolysis reactions the buffers were in the pH range 4-7 again with a final concentration of 0.1M. When the schiff base was prepared prior to hydrolysis the pH was high due to the excess n-butylamine, so the schiff base was in the unprotonated form and was stable to hydrolysis. The hydrolysis reaction was started by a pH jump which involved 1:1 mixing of the schiff base with a buffer solution in the pH range 4-7.

In the formation reactions the retinal and n-butylamine were both made in buffer solutions in the pH range 8-12 so that when 1:1 mixing occurred the formation reaction took place. In the experiments studying the buffer catalysis, buffers in the pH range 4-6 were used at final concentrations (after 1:1 mixing) of 0.01M, 0.05M, 0.1M and 0.2M.

For the determination of the pK<sub>a</sub> value of the schiff base a pH range of 1-9 was covered and all buffers were 0.1M final concentration.

#### 2.5.4 Detergents

It was necessary to use a detergent in these experiments because all-trans retinal is insoluble in water due to its long hydrocarbon chain and lack of polar groups. The detergent allows the retinal to dissolve in an aqueous solution by forming detergent micelles. It can do this because detergents have distinct hydrophobic and hydrophilic regions. The molecules orient their hydrophobic sites near the non-polar residues of the retinal and their hydrophilic sites beside the polar water molecules and in this way the retinal can be

Table 2.1

Table of Buffers and Their pH Range

BUFFER	CONSTITUENTS	SOURCE	pH RANGE
Hydrochloric Acid	Hydrochloric Acid (HCl)	Hopkin + Williams (Analar)	≤2
Formate	Sodium Formate (NaCHO <sub>2</sub> )	Koch - Light (pure)	2.50-3.75
	Formic Acid (HCOOH)	Hopkin + Williams (G.P.R)	
Acetate	Sodium acetate trihydrate (CH <sub>3</sub> COONa.3H <sub>2</sub> O)	Hopkin + Williams (Analar)	4.00-5.50
	Glacial acetic acid (CH <sub>3</sub> COOH)	Hopkin + Williams (Analar)	
Phosphate	Sodium dihydrogen phosphate (NaH <sub>2</sub> PO <sub>4</sub> .2H <sub>2</sub> O)	May + Baker (Analytical grade)	5.75-8.00
	Disodium hydrogen phosphate (Na <sub>2</sub> HPO <sub>4</sub> )	Hopkin + Williams (Analar)	
Borate	Sodium tetraborate (Na <sub>2</sub> B <sub>4</sub> O <sub>7</sub> .10H <sub>2</sub> O)	May + Baker (Analytical grade)	9.00-10.00
	Sodium hydroxide (NaOH)	Formachem (pure)	

[G.P.R. = general purpose reagent]

brought into aqueous solution. Detergents can be anionic, cationic, zwitterionic or neutral depending on the chemical structure of the polar head group. The hydrocarbon chain can vary in length and may have functional groups incorporated.

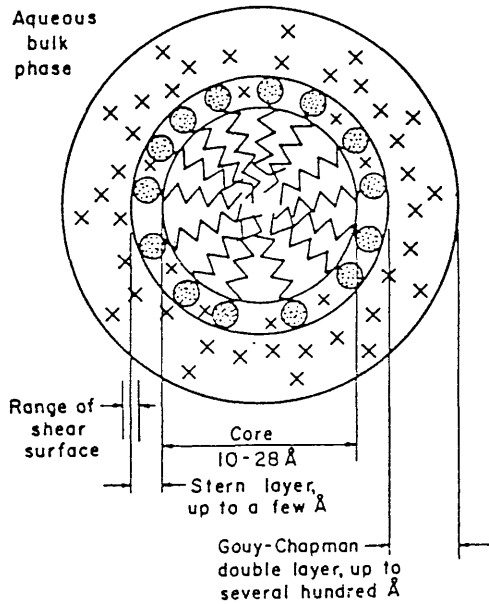
At a certain concentration of a detergent in solution called the critical micelle concentration aggregates are formed and the classical micelle is pictured as a roughly spherical shaped aggregate with a hydrocarbon core and a polar surface. With ionic detergents the charged head group and some of its oppositely charged counter ions are situated in a compact area called the Stern layer. The rest of the counter ions are located in the Gouy-Chapman electrical double layer, are dissociated from the micelle and can exchange with ions in the bulk aqueous phase (fig.2.4).

During the course of this work four detergents were used, namely Emulphogene BC-720, a gift from GAF, Ammonyx-LO from Onyx Chem. Comp., DTAB from Sigma and SDS from Sigma. Emulphogene is polyoxyethylene-10-tridecyl ether and is a liquid, non-ionic detergent. Ammonyx-LO is an aqueous solution of lauryl dimethyl amine oxide and is a neutral detergent at high pH but cationic below about pH5. DTAB is dodecyl (lauryl) trimethyl ammonium bromide which is a solid, cationic detergent. Finally, SDS is sodium dodecyl sulphate which is a solid anionic detergent. Each of these detergents is chemically different and was chosen in order to establish if the micellar environment affects the reactions in any way.

Ammonyx-LO and Emulphogene were both made up as 2% (by volume) solutions which is equivalent to about 25mM solutions, DTAB was also 25mM and SDS was 12.5mM as higher concentrations caused problems with precipitation in the buffer. The concentration of each detergent was slightly higher than the critical micelle concentration which for Ammonyx-LO, DTAB and SDS respectively is  $2.1 \times 10^{-3} \text{M}$ ,  $1.5 \times 10^{-2} \text{M}$  and  $8.1 \times 10^{-3} \text{M}$  and this suggests that the detergents should exist as the classical spherical micelle<sup>77</sup>.

FIGURE 2.4

A schematic representation of the regions of a spherical ionic micelle. The counter-ions (X), the head groups (⊙) and the hydrocarbon chains (∨∨) are indicated to show their relative positions.



(Taken from ref.77)

These critical micelle concentrations are obtained by following the change in some physical property of the solution as a function of surfactant concentration. Some of the physical properties that have been investigated to determine critical micelle concentrations for these detergents are the electrical conductivity, refractive index and turbidity<sup>79,79,80</sup>.

The four detergents that were used during these experiments have also been used to some extent in the extraction of the visual pigment rhodopsin itself. All extractants would appear to modify the structure of the pigment molecule to a certain degree so that in some detergents the rhodopsin denatures or cannot be regenerated once bleached. However Ammonyx-LO and Emulphogene have been shown to yield very pure rhodopsin without bleaching it<sup>81,82</sup>, whereas in DTAB the pigment is less stable and in SDS the rhodopsin denatures sufficiently to bleach spontaneously in the dark<sup>10</sup>.

The effect that the different detergents have on the model compounds will be discussed later.

## 2.6 Kinetic Analysis

### 2.6.1 First Order Analysis on Apple Computer

At the end of each run on the stopped-flow spectrophotometer the values of absorbance and time were stored on a data disc in the Apple computer. The first analysis of these results was a first order analysis using an Apple program for a least squares fit to:

$$A(t) = \alpha_0 + \alpha_1 \exp(-\lambda_1 t) \quad (2.9)$$

where  $A(t)$  is the absorbance at time  $t$ ,  $\alpha_0$  is the absorbance at the end of the reaction when the value of  $t$  is large and  $\lambda_1$  is the rate constant of the reaction.

For a first order reaction  $A \rightarrow B$  the rate equation is:

$$\frac{-d[A]}{dt} = k[A] \quad (2.10)$$

The integrated rate equation:

$$[A] = [A]_0 \exp(-kt) \quad (2.11)$$

is obtained by integration of the rate equation between the time limits  $t_0$ , taken as zero, and time  $t$  and between concentration limits of  $[A]_0$  and  $[A]_t$ , where  $[A]_0$  is the concentration of A at time zero and  $[A]_t$  at time  $t$ .

This analysis is of limited use as the reaction must be first order. In experiments where intermediates are formed, for example in the case  $A \rightarrow B \rightarrow C$  which is a two step reaction referred to as a biphasic process, a more complicated analysis must be undertaken in order to establish the kinetics of the reaction.

#### 2.6.2 Kinetic Analysis on Mainframe Computer

The main kinetic analysis was carried out on an ICL 2976 computer using a program called Discrete which is for the automatic analysis of multicomponent exponential decay data. Discrete was provided by S.W. Provencher (European Molecular Biology Laboratory, Germany)<sup>23</sup> and is a Fortran program for the analysis of data that can be represented by:

$$y_k = \sum_{j=0}^{N_\lambda} \alpha_j \exp(-\lambda_j t_k) \quad (2.12)$$

where  $k = 1, 2, \dots, N$  and  $N_\lambda \leq 9$ .

Only the raw data  $y_k$  and  $t_k$  are input and provision is made for an unknown instrument baseline component  $\alpha_0$  with  $\lambda_0=0$ . The form of the equation that is relevant to the analysis of these results is:

$$A(t) = \alpha_0 + \alpha_1 (\exp-\lambda_1 t) + \alpha_2 (\exp-\lambda_2 t) + \alpha_3 (\exp-\lambda_3 t) + \dots \quad (2.13)$$

where the raw data,  $A(t)$  and  $t$  are the absorbance and time values obtained from the stopped-flow experiments. In this case a biphasic reaction such as  $A \rightarrow B \rightarrow C$  would fit the equation:

$$A(t) = \alpha_0 + \alpha_1 (\exp-\lambda_1 t) + \alpha_2 (\exp-\lambda_2 t) \quad (2.14)$$

The best fit would be one of two components and the analysis would yield values of  $\alpha_0, \alpha_1, \alpha_2, \lambda_1$  and  $\lambda_2$ .

Each experiment that was analysed was at a fixed wavelength and timing sequence yielding 256 absorbance and time readings. In the computer analysis the data is fitted to one, two, three and four components with 5 iterations in each case and the output contains the  $\alpha$  and  $\lambda$  values relevant to that fit. For example a one component fit would give values for  $\alpha_0, \alpha_1$  and  $\lambda_1$  whereas a two component fit would give values for  $\alpha_0, \alpha_1, \alpha_2, \lambda_1$  and  $\lambda_2$  and so on. Finally there is a listing of the number of components in the best fit, second best fit etc. along with parameters for these and the standard deviation of the fit.

CHAPTER 3

SCHIFF BASE FORMATION  
REACTIONS.

### 3.1 Material Preparation

The N-retinylidene n-butylamine schiff base was formed by mixing equal volumes of aqueous detergent solutions of retinal and n-butylamine. The formation reactions were studied in two detergents, Emulphogene and Ammonyx-L0, at pH 8,10 and 12 using 0.04M, 0.5M and 1M butylamine concentrations at pH 8, 0.04M, 0.1M and 1M at pH 10 and 0.04M and 0.1M butylamine concentrations at pH 12. The rate of the formation reaction is first order in butylamine concentration and so the total reaction time could be changed by varying the butylamine concentration until convenient time scales for UV/visible and stopped-flow spectroscopy were found.

The buffers used in this work were prepared following the procedure described previously. At pH 8 a 0.1M phosphate buffer was used to control the pH in the Emulphogene and Ammonyx solutions, and the retinal, dissolved in a small volume of ethanol, was added to the buffer in 2% (by volume) detergent solution. Similarly the appropriate butylamine concentrations were prepared in a 0.1M phosphate / 2% detergent solution and a small volume of concentrated hydrochloric acid was added to re-adjust the solution to pH 8.

At pH 10 a 0.1M borate buffer was used for the reactions with butylamine concentrations of 0.04M and 0.1M, and no buffer was used when the butylamine concentration was 1M. At this high concentration of butylamine the retinal and butylamine were made up in 2% detergent solutions and the pH of the butylamine solution was adjusted to pH 10 by the addition of hydrochloric acid. At this high pH the butylamine itself should provide some buffering action, especially in the more concentrated solutions, as it has a pK<sub>a</sub> value of around 10.7 and so no other buffer was used. Similarly at pH 12 no buffer was used and the 0.04M and 0.1M butylamine solutions were made in 2% detergent with sodium hydroxide added to adjust the pH to 12.

The retinal solutions prepared for use in the

UV/visible and stopped-flow spectroscopy had an absorbance reading of approximately 1 at 380nm and this was diluted after 1:1 mixing with the butylamine solution. Similarly the butylamine concentration is halved on addition of the retinal solution.

At the end of each experiment the pH of the mixed solution was measured and this was taken as the pH of the reaction. The retinal solutions were prepared each day in a glove box under argon or nitrogen and the samples were wrapped in aluminium foil as light causes isomerisation of the retinal.

### 3.2 Ultra-violet/Visible Spectroscopy

The formation reactions were started by pipetting equal volumes of retinal and butylamine in detergent buffer solutions into a 1cm cuvette and mixing the solutions manually. A spectrum was recorded immediately after mixing and that time was taken to be equal to zero seconds. The reaction was followed by recording spectra at certain time intervals after mixing and superimposing each spectrum on the previous spectra.

The absorbance maxima of retinal in Emulphogene and Ammonyx respectively are 384nm and 388nm and that of the schiff base (in the unprotonated form) is 364nm in both detergents. The formation reaction can therefore be easily followed using UV/visible spectroscopy because of the shift in the absorbance maximum as the reaction proceeds. Each spectrum recorded covered a wavelength range of 260nm to 500nm and the temperature remained constant at 20°C during the experiments.

Typical electronic spectra are shown in figs.3.1-3.6. The schiff base formation reaction in figs.3.1-3.3 are in Emulphogene at pH 7.99, 10.04 and 11.75 respectively, and in figs.3.4-3.6 are in Ammonyx at pH 8.05, 10.07 and 11.88 respectively. (These will be referred to as pH 8, 10 and 12 in the text.)

In fig.3.1 it can be seen that the retinal peak at approximately 380nm is present at the start of the reaction and shifts towards 360nm as the schiff base is

FIGURE 3.1  
UV/visible spectrum of schiff base formation reaction  
in phosphate buffer/Emulphogene at pH 7.99, with a  
final butylamine concentration 0.25M.

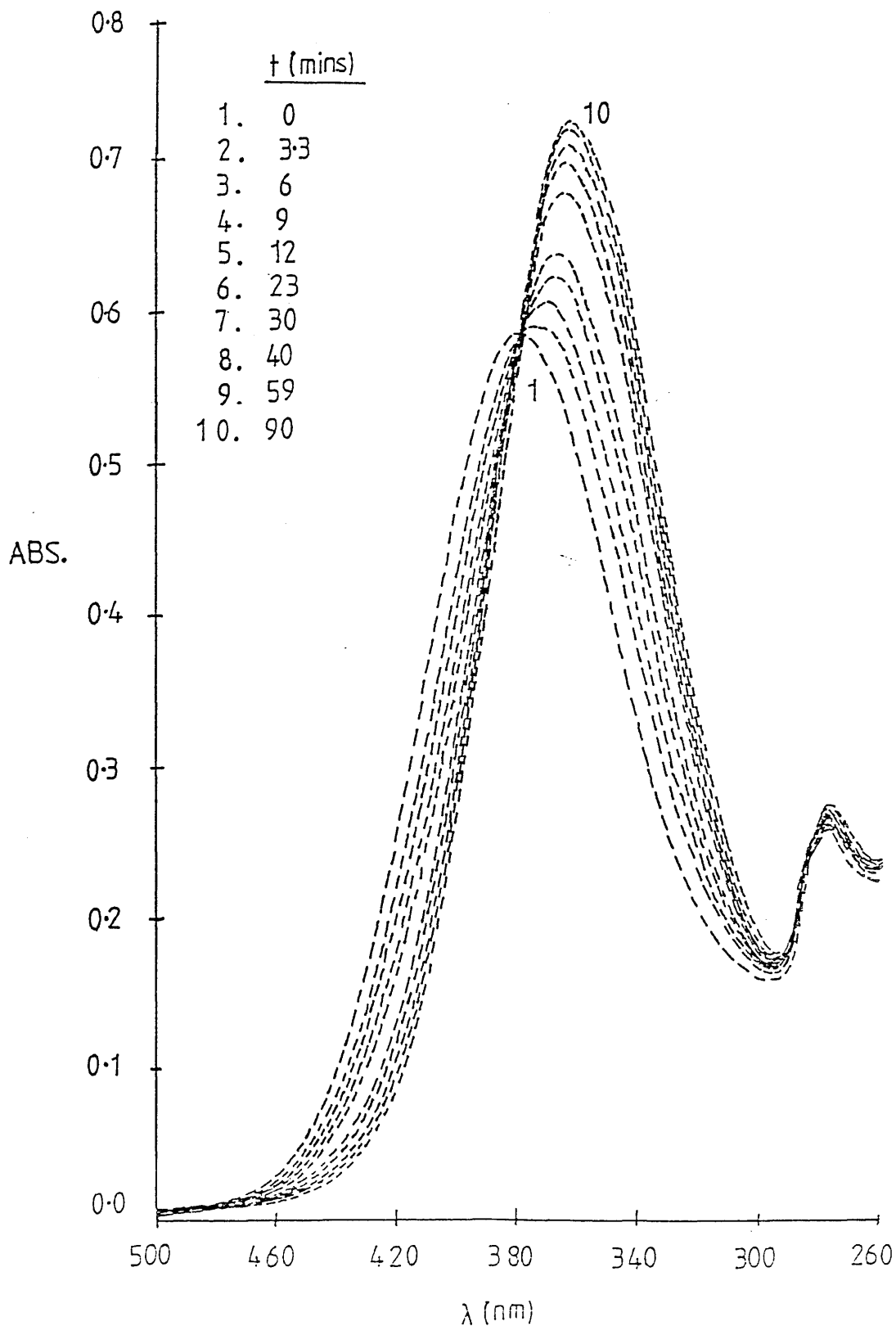


FIGURE 3.2  
UV/visible spectrum of schiff base formation reaction  
in borate buffer/Emulphogene at pH 10.04, final  
butylamine concentration 0.02M.

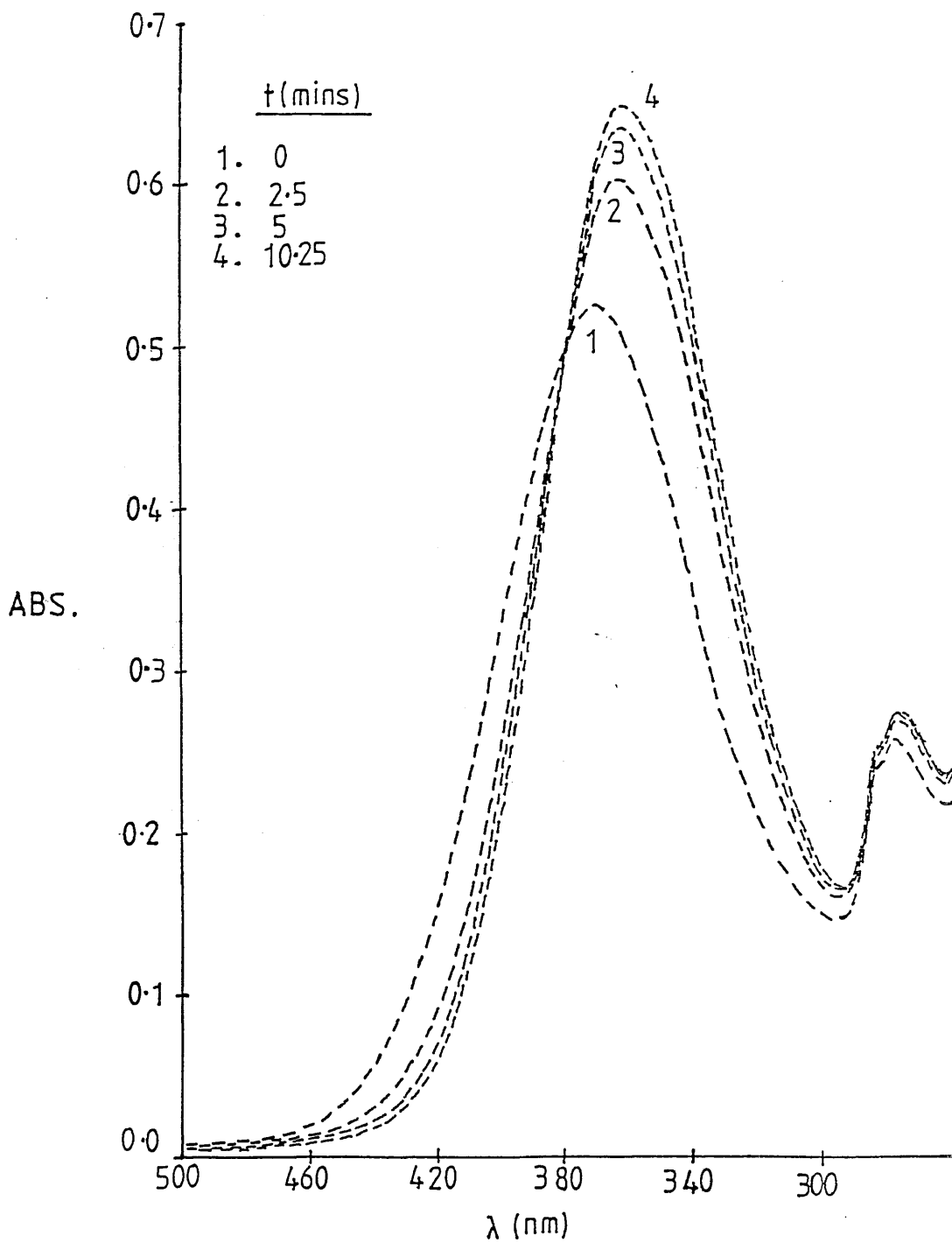


FIGURE 3.3  
UV/visible spectrum of schiff base formation  
reaction in Emulphogene at pH 11.75, final  
butylamine concentration 0.02M.

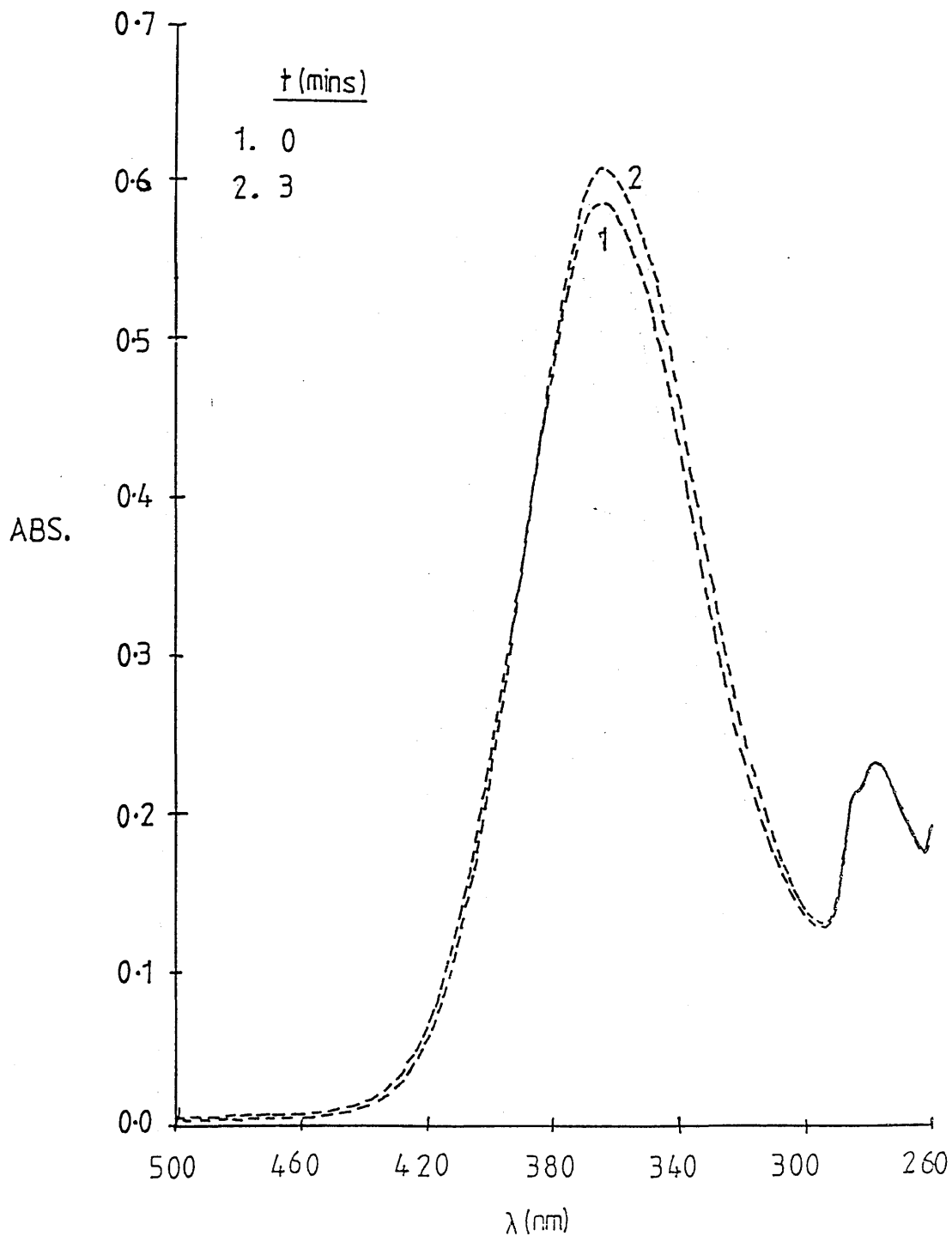


FIGURE 3.4

UV/visible spectrum of schiff base formation reaction in phosphate buffer/Ammonyx at pH 8.05, final butylamine concentration 0.25M.

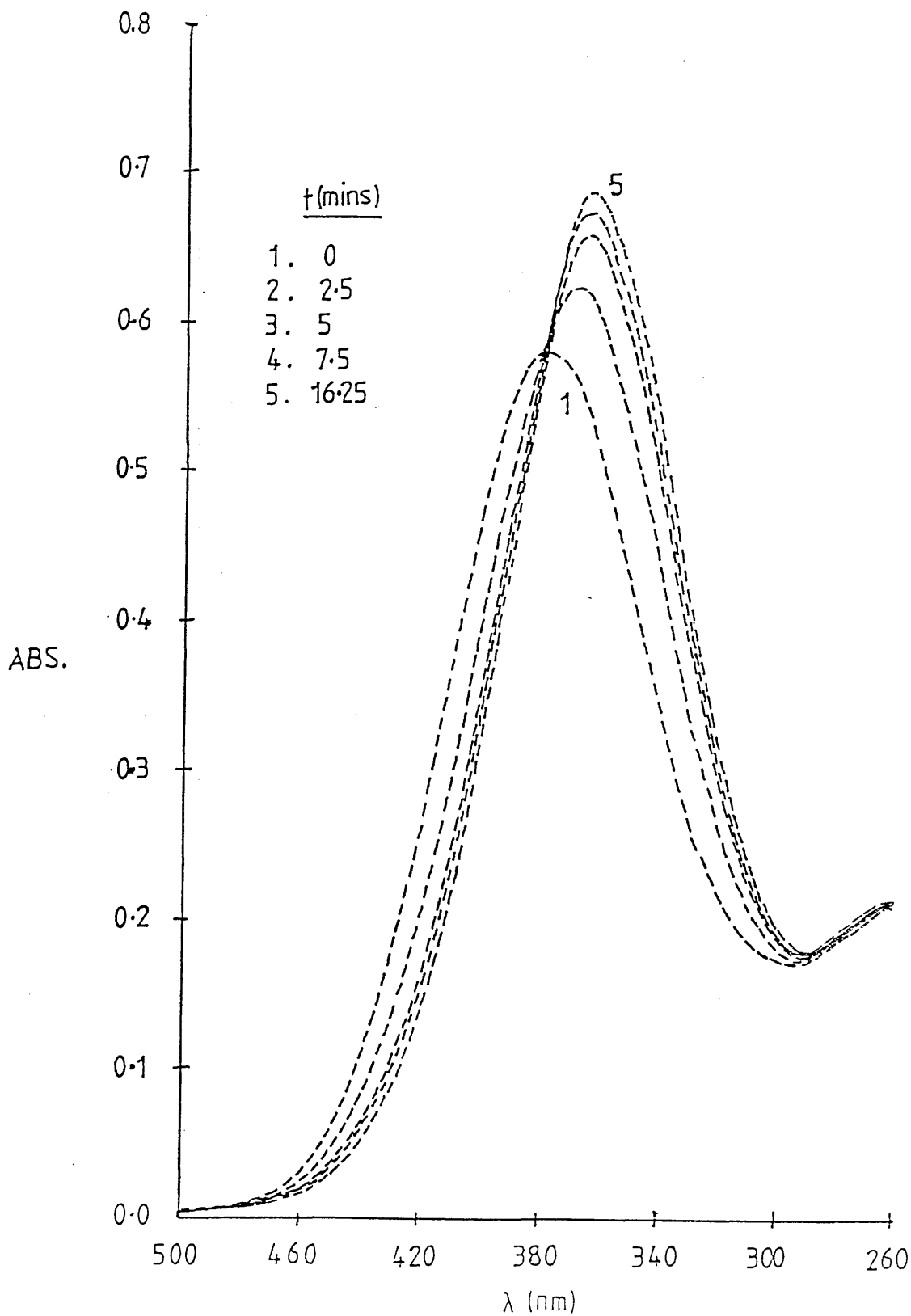


FIGURE 3.5

UV/visible spectrum of schiff base formation reaction in borate buffer/Ammonyx at pH 10.07, final butylamine concentration 0.02M.

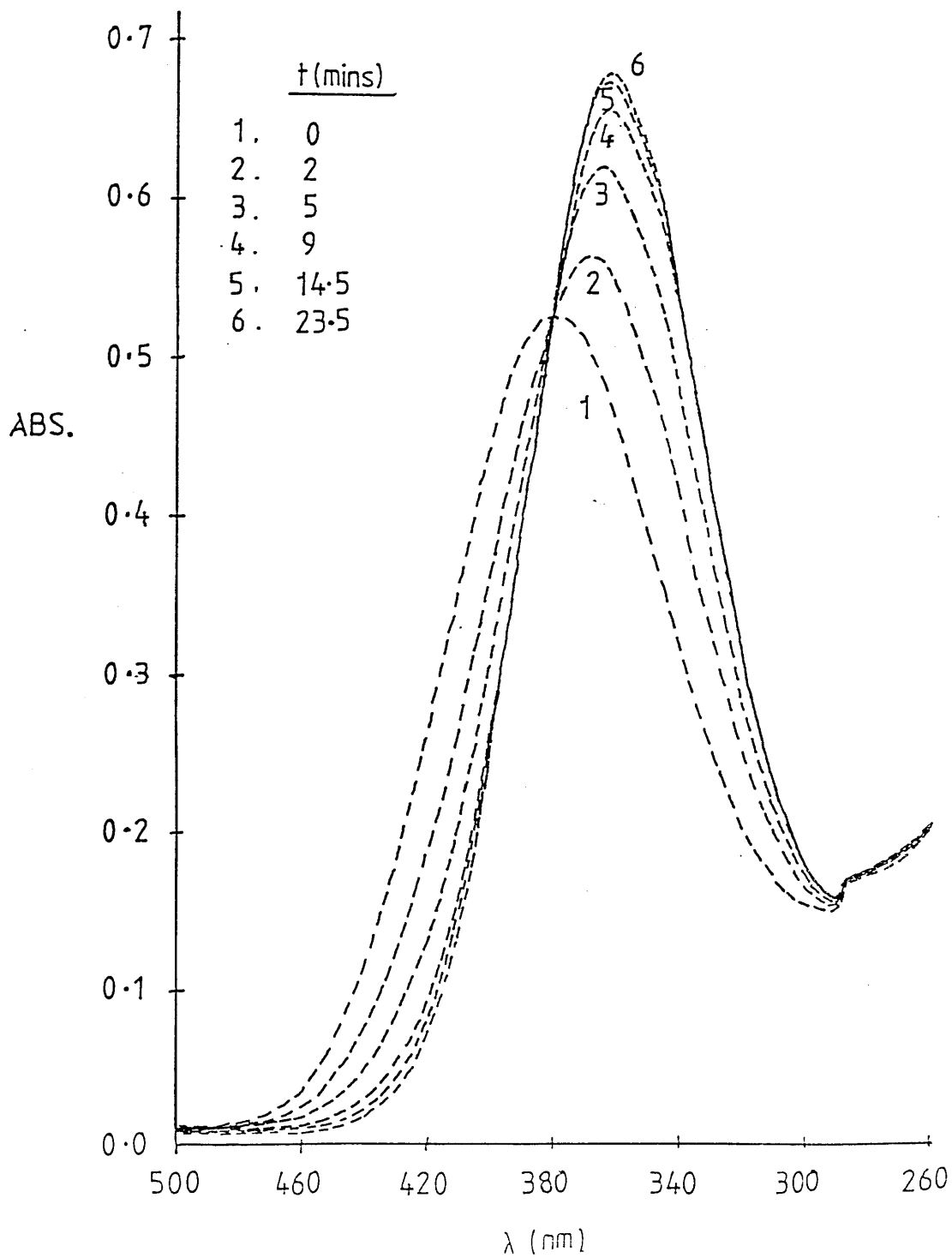
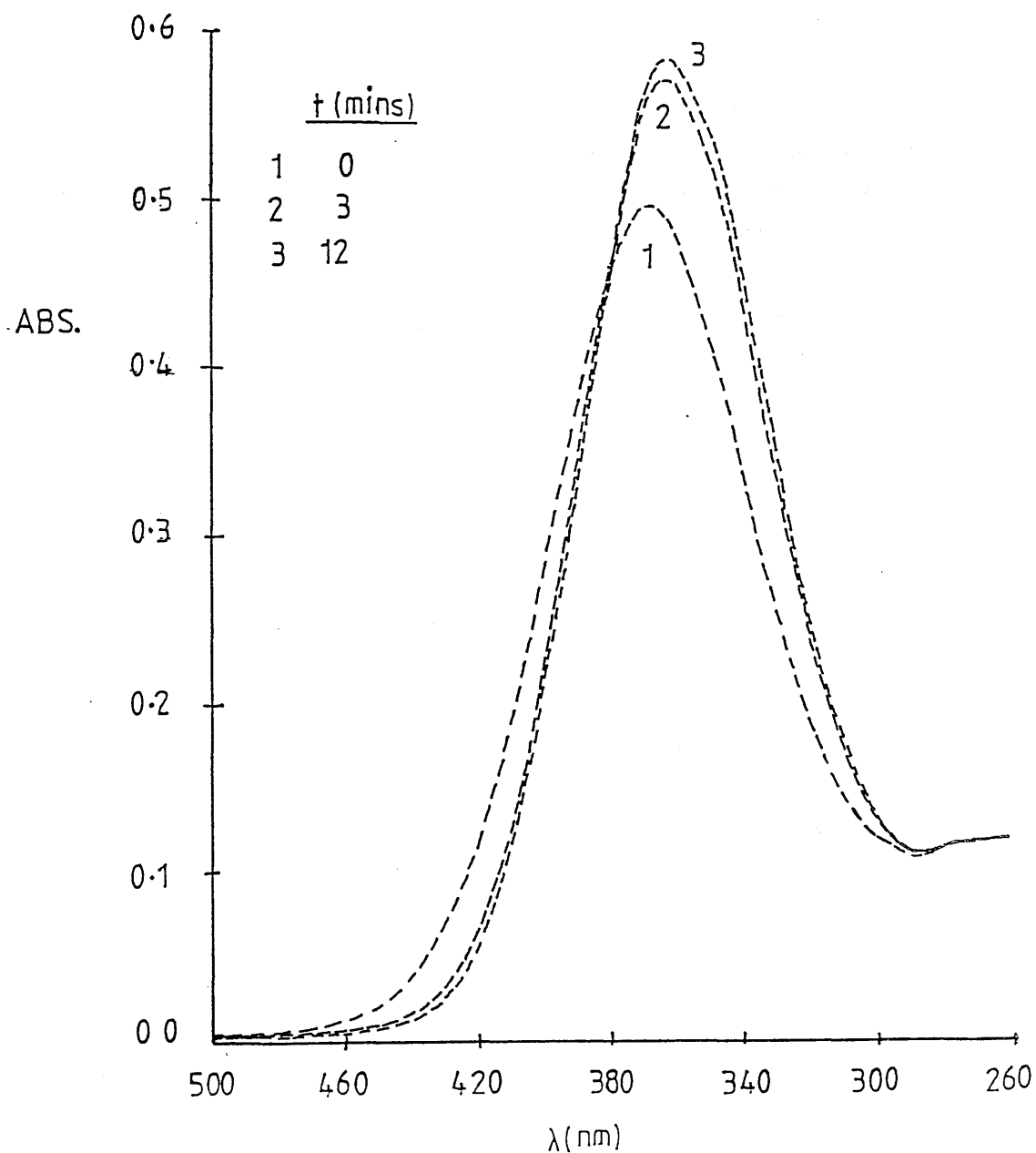


FIGURE 3.6  
UV/visible spectrum of schiff base formation reaction in  
Ammonyx at pH 11.88, final butylamine concentration 0.02M.



formed. The reaction occurs more quickly as the pH is raised between 8 and 12 or as the butylamine concentration is increased. As a result of this, at pH 12 for example, the reaction is almost complete by the time the first spectrum is recorded, even at low butylamine concentrations. This can be seen in fig.3.3 which shows that by the time the solutions are mixed manually and the cuvette is placed in the spectrophotometer, the retinal has already been converted to the schiff base, as shown by the maximum absorbance at 360nm. Similarly at pH 8 and 10 the reaction at high butylamine concentration, for example 0.5M final concentration, is almost complete when the first spectrum is recorded and the spectra obtained are similar to fig.3.3, (spectra not shown).

A major problem with the ultra-violet spectroscopy experiments is that any rapid reactions occurring immediately after mixing will not be detected because of the time taken to mix the solutions manually and place the cuvette in the spectrometer which is approximately 15-20 seconds. This problem is especially bad at high pH and high butylamine concentrations when it is obvious from the spectra that the beginning of the reaction is missed.

The problem is eliminated in the stopped-flow experiments where the mixing is very rapid and for this reason stopped-flow spectroscopy was used as the main technique for studying these reactions. The ultra-violet/visible spectra were recorded to check that the reagents were reacting to form a schiff base (from the shift in absorbance maximum) and to determine the timescales of the reactions for use in the stopped-flow spectroscopy.

It is interesting to note that the spectra in figures 3.1-3.6 all have an isosbestic point which is a point common to the superimposed spectra which were run at different times after mixing. The fact that the spectra all pass through the isosbestic point suggests that the reaction is likely to be a one stage reaction, such as  $A \rightarrow B$ , with no intermediates observable on this time scale. (Transients at the isosbestic point are seen in

stopped-flow hydrolysis experiments.)

### 3.3 Stopped-Flow Spectroscopy

The samples used in the stopped-flow experiments were identical to those used in the UV/visible spectroscopy experiments. The retinal and n-butylamine in detergent buffer solutions were injected into the two driving syringes in the stopped-flow spectrometer and were allowed to equilibrate to 20°C.

Each of the formation reactions was followed for various lengths of time ranging from a few seconds to 10 minutes at a fixed wavelength. These runs were then repeated over a wavelength range of 330nm to 450nm every 10nm to give extensive coverage of the reaction.

The geometric and arithmetic timescales were used in conjunction with linear timescales so that any very fast reactions could be seen by a rapid absorbance change at the start of the run, followed by slower changes as the reaction proceeds.

Control reactions were done where the butylamine solution was replaced by a detergent buffer solution alone, and in these experiments there was no change in the retinal absorbance with time at any wavelength, as would be expected.

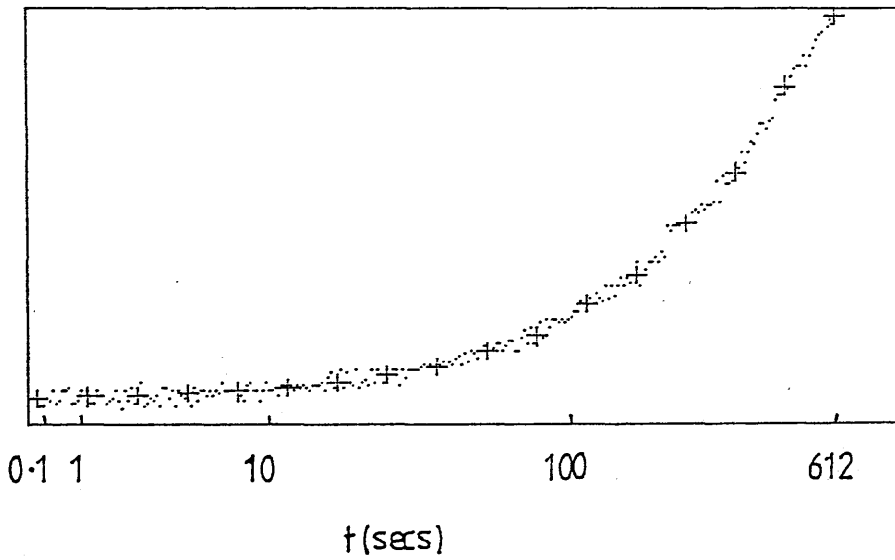
Typical stopped-flow traces can be seen in figs.3.7-3.14. The schiff base formation reactions in figs.3.7-3.10 are in Emulphogene and those in figs.3.11-3.14 are in Ammonyx at pH 8,10 and 12. The first trace in each of these figures is at a fixed wavelength below the isosbestic point at 340nm, 350nm or 360nm. In each of these traces the absorbance increases with time as the retinal is converted to schiff base, as would be expected from the UV/vis. spectra.

The second trace in each figure is at a fixed wavelength above the isosbestic point at 400nm, 410nm or 420nm. In each of these traces the absorbance decreases with time as the schiff base is formed.

The traces shown cover a range of timing sequences such as a 25.6 second, linear run, fig.3.9; 329 second

FIGURE 3.7  
Stopped-flow traces of schiff base formation reaction  
in phosphate buffer pH8/Emulphogene, final butylamine  
concentration 0.5M. Timing sequence is geometric with  
DT=75msec, N=32 and total time=612secs.

a.  $\lambda=340\text{nm}$



b.  $\lambda=410\text{nm}$

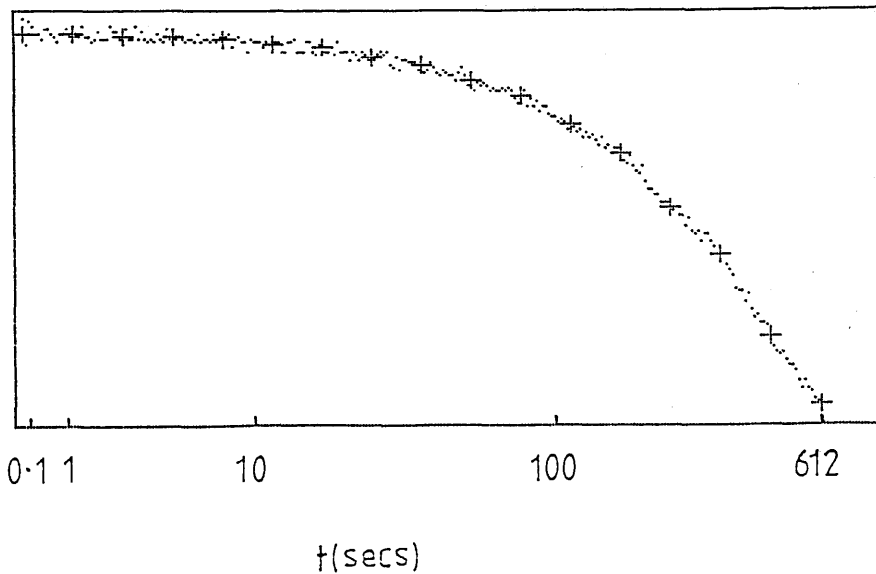
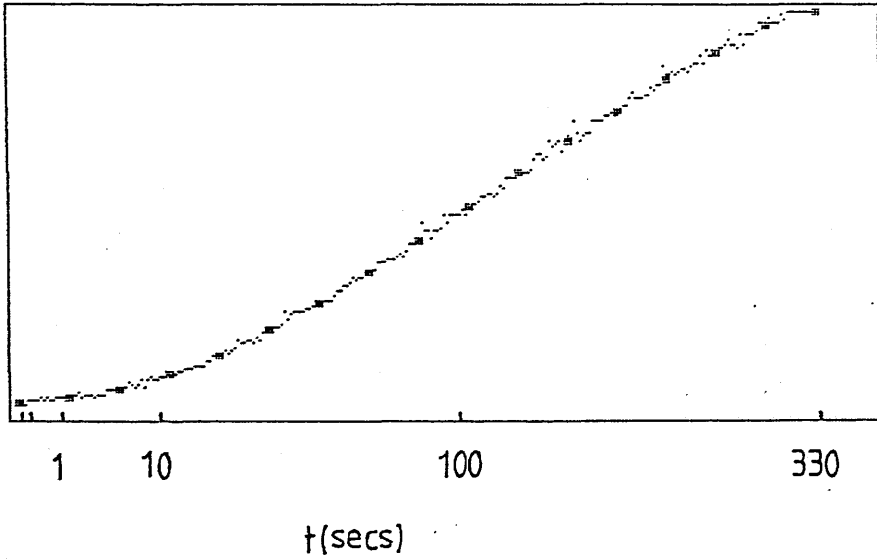


FIGURE 3.8

Stopped-flow traces of schiff base formation reaction in borate buffer pH10/Emulphogene, final butylamine concentration 0.02M. Timing sequence is arithmetic with  $DT=10\text{msec}$  and total time= $329\text{secs}$ .

a.  $\lambda=350\text{nm}$



b.  $\lambda=410\text{nm}$

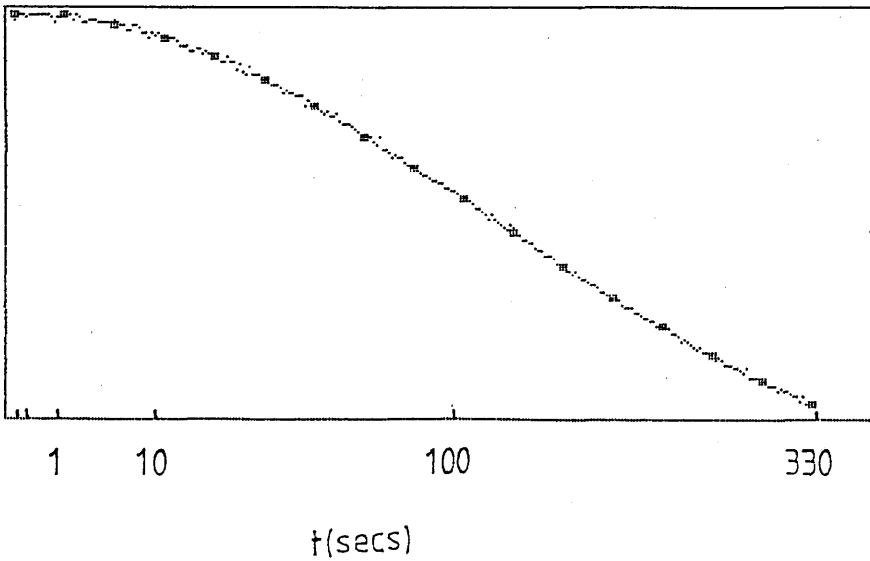
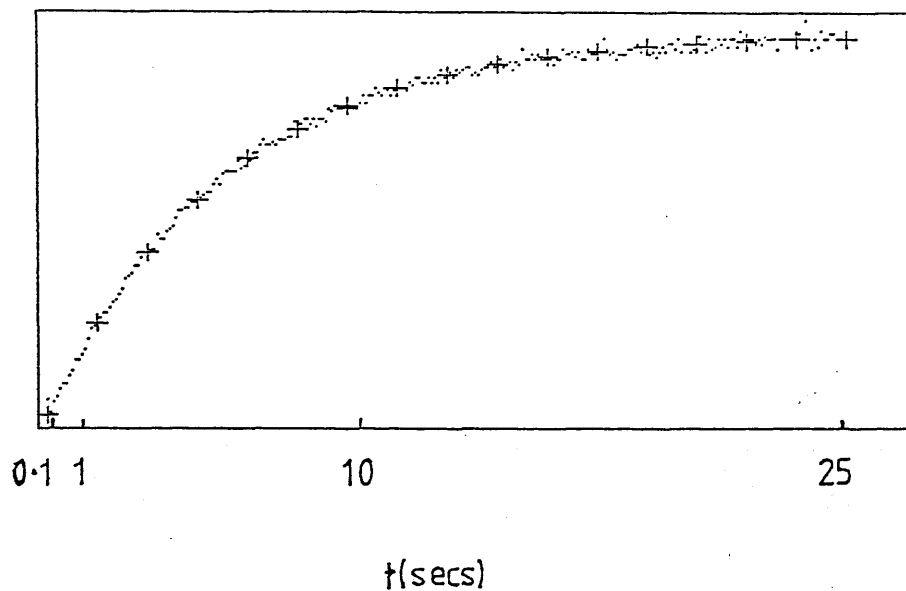


FIGURE 3.9

Stopped-flow traces of schiff base formation reaction in Emulphogene at pH10, final butylamine concentration 0.5M. Timing sequence is linear with DT=100msec and total time=25.6secs.

a.  $\lambda = 340\text{nm}$



b.  $\lambda = 410\text{nm}$

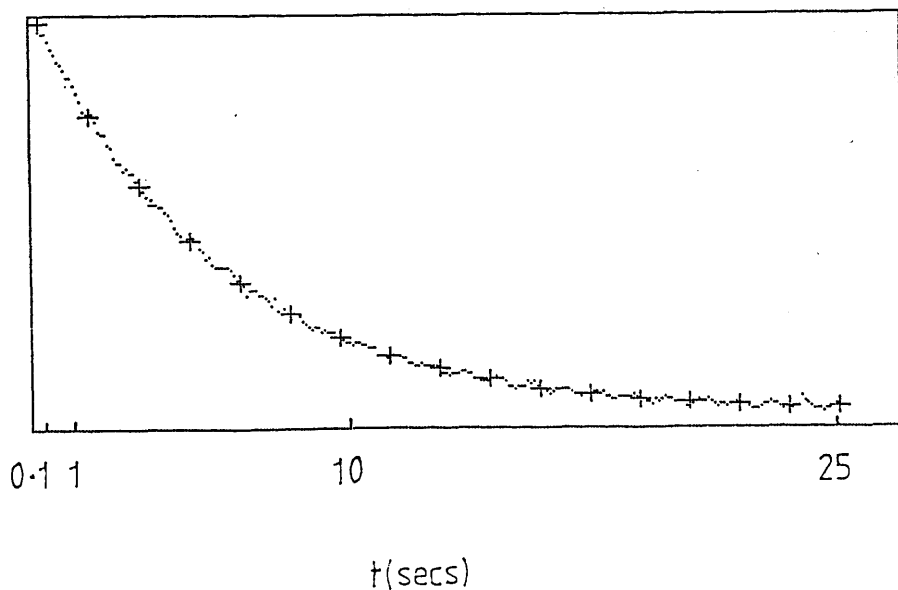
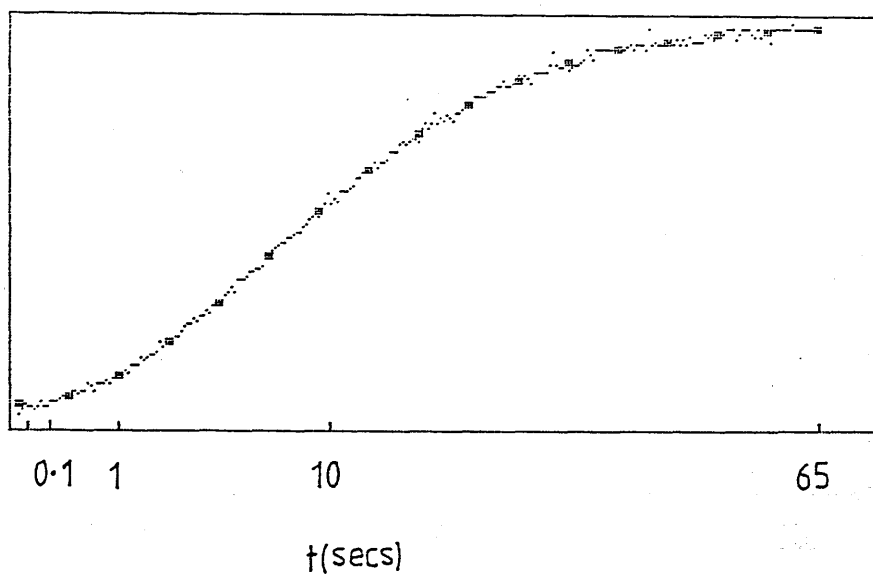


FIGURE 3.10  
Stopped-flow traces of schiff base formation reaction in  
Emulphogene at pH12, final butylamine concentration 0.05M.  
Timing sequence is arithmetic with DT=2msec and total  
time=65.8secs.

a.  $\lambda=340\text{nm}$



b.  $\lambda=400\text{nm}$

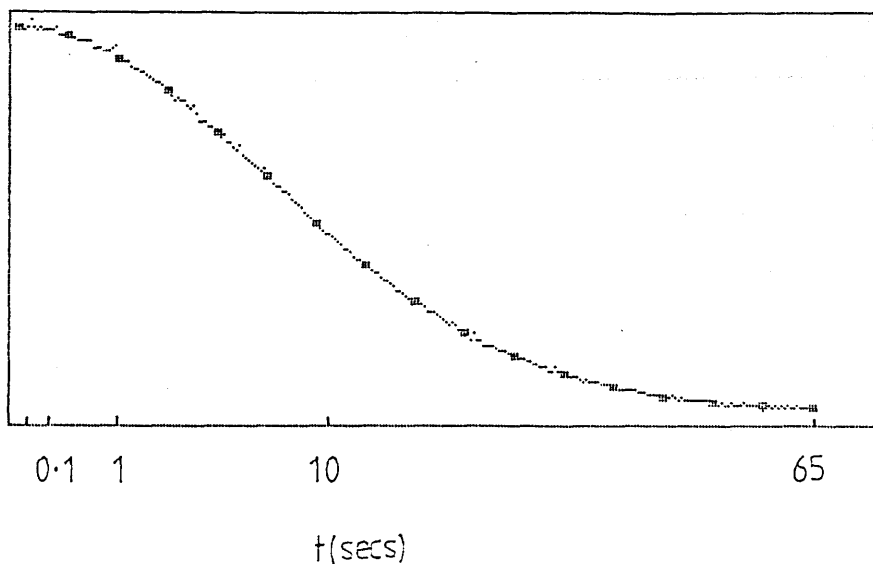
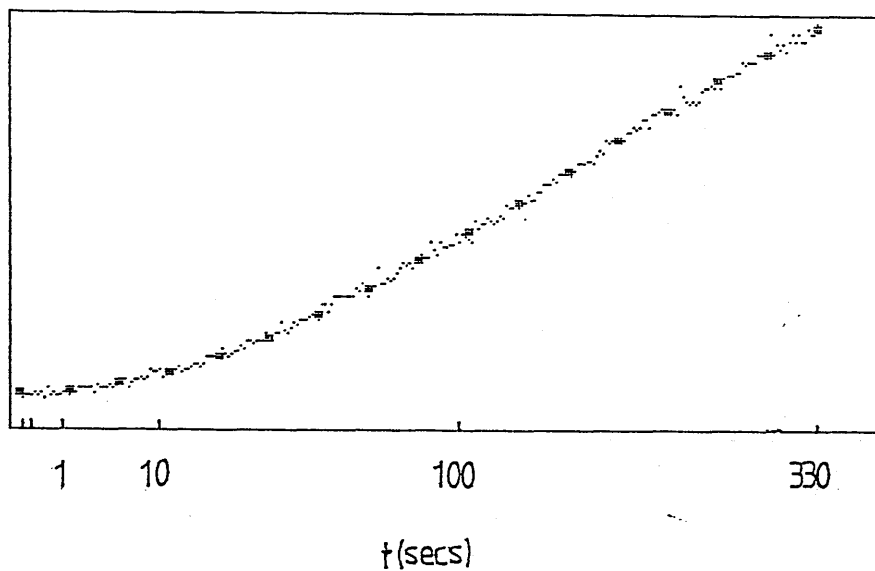


FIGURE 3.11

Stopped-flow traces of schiff base formation reaction in phosphate buffer pH8/Ammonyx, final butylamine concentration 0.25M. Timing sequence is arithmetic with DT=10msec and total time=329secs.

a.  $\lambda = 360 \text{ nm}$



b.  $\lambda = 410 \text{ nm}$

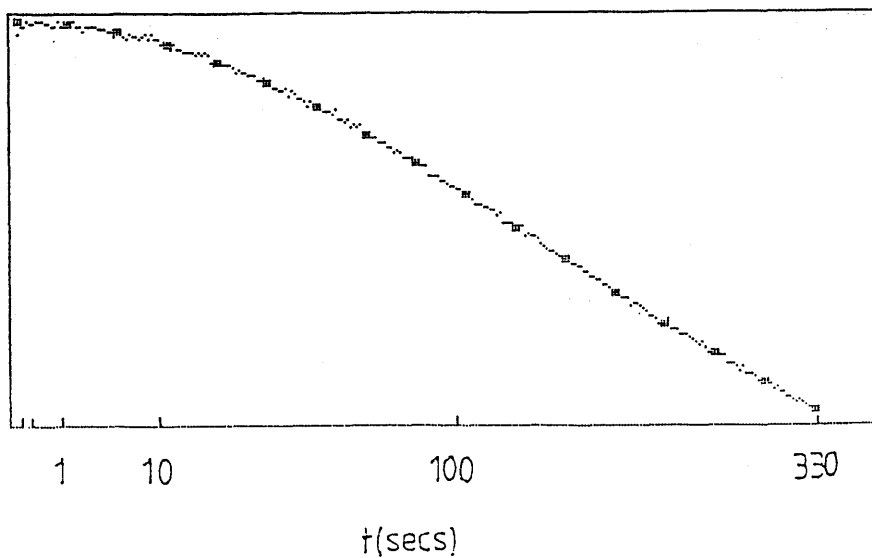
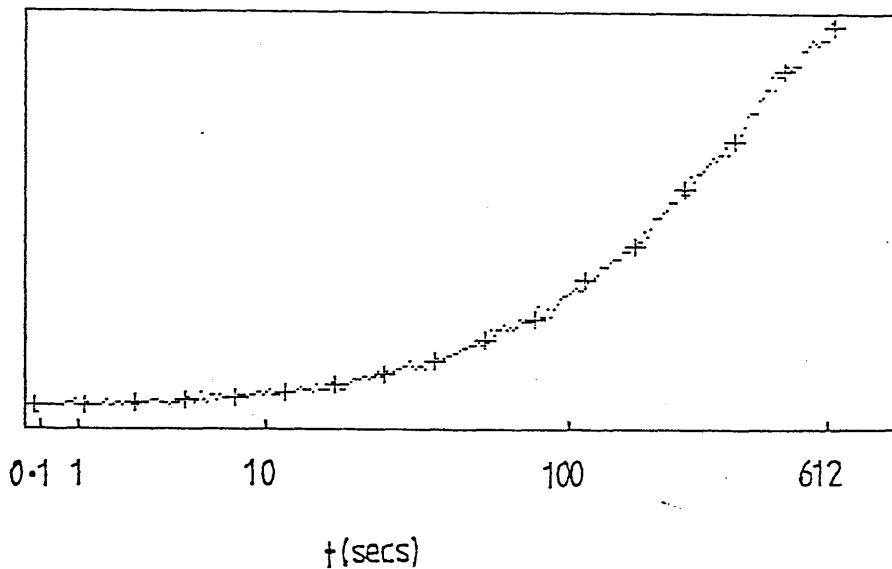


FIGURE 3.12

Stopped-flow traces of schiff base formation reaction in borate buffer pH10/Ammonyx, final butylamine concentration 0.02M. Timing sequence is geometric with  $DT=75\text{msec}$ ,  $N=32$  and total time= $612\text{secs}$ .

a.  $\lambda=360\text{nm}$



b.  $\lambda=420\text{nm}$

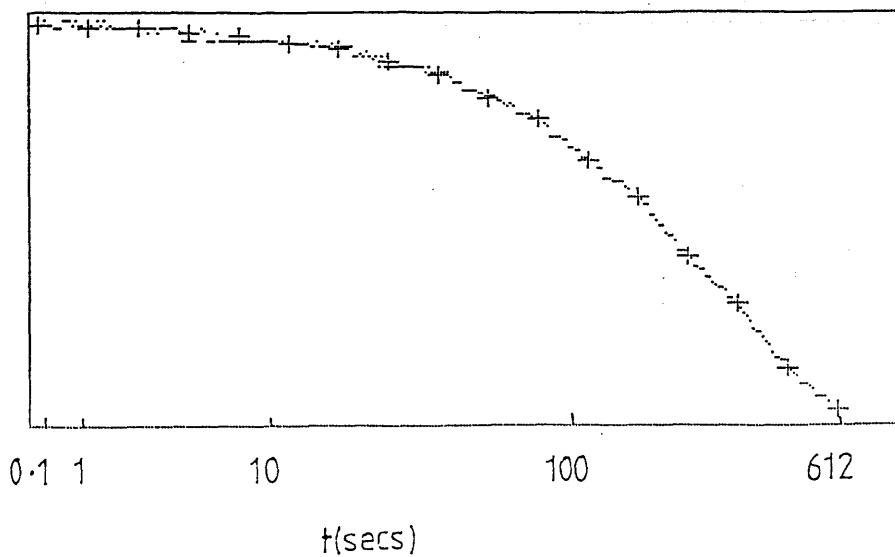
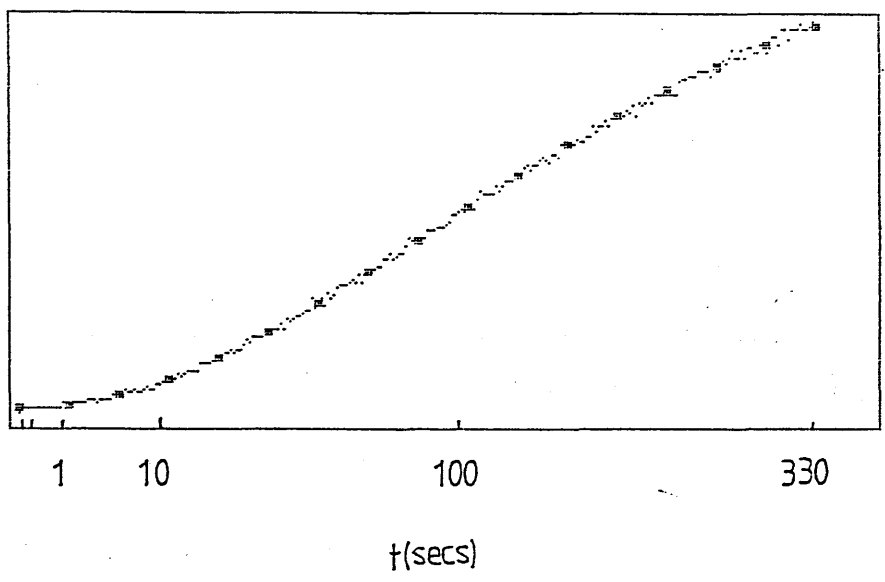


FIGURE 3.13  
Stopped-flow traces of schiff base formation reaction  
in borate buffer pH10/Ammonyx, final butylamine  
concentration 0.05M. Timing sequence is arithmetic with  
DT=10msec and total time=329secs.

a.  $\lambda=340\text{nm}$



b.  $\lambda=410\text{nm}$

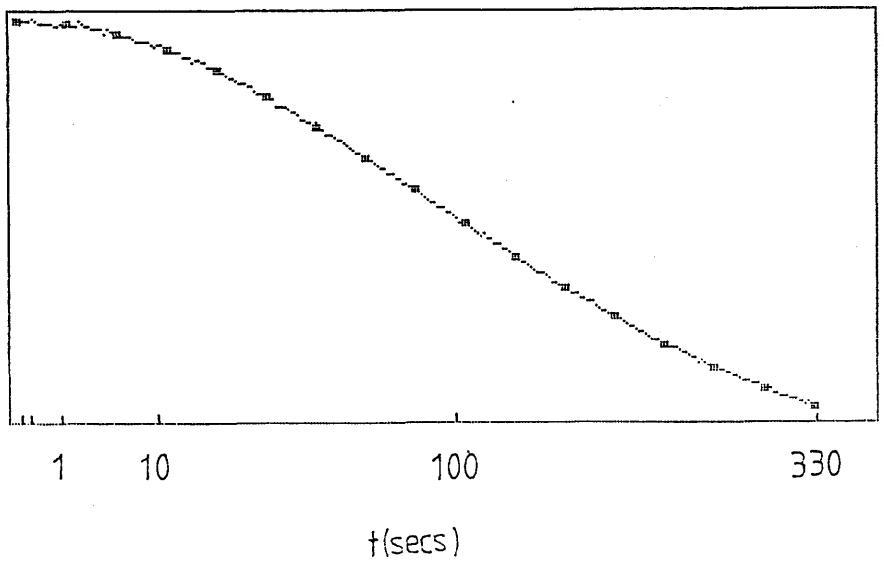
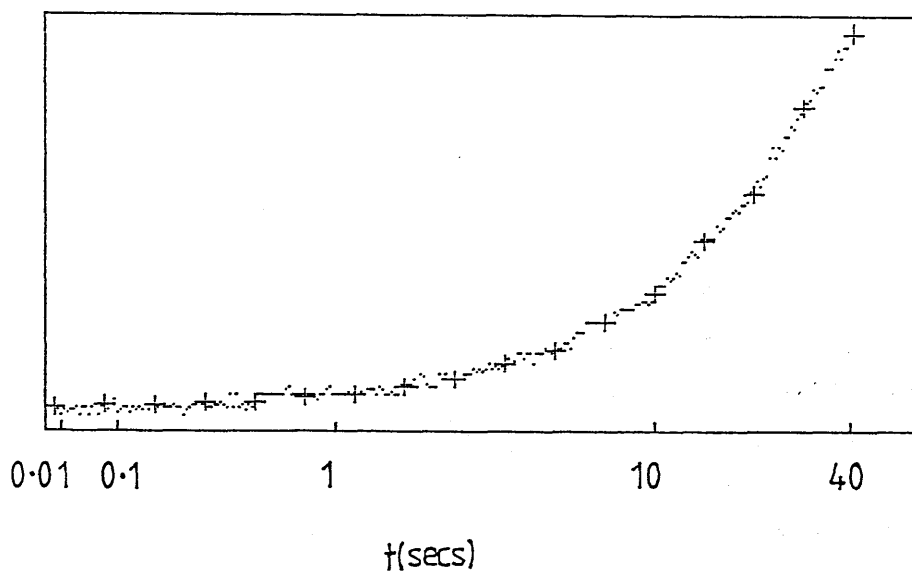


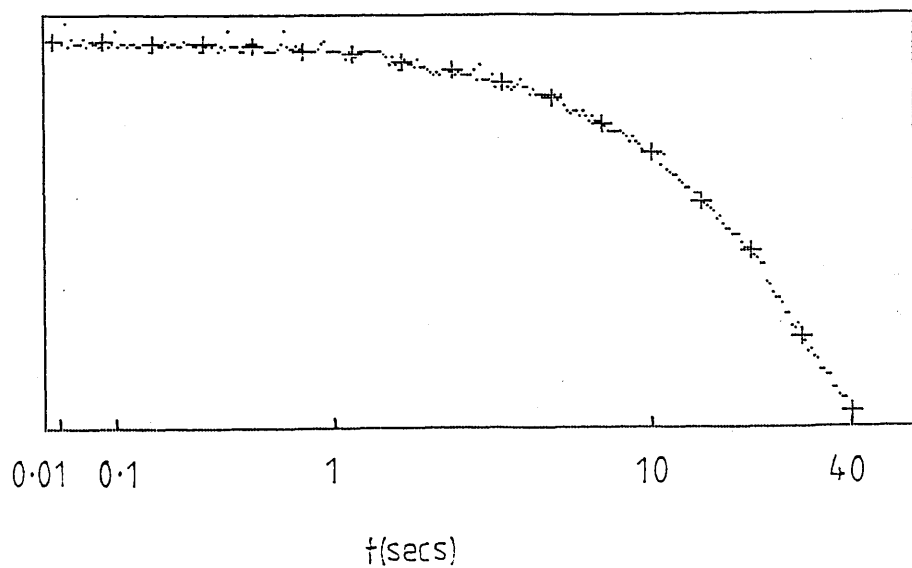
FIGURE 3.14

Stopped-flow traces of schiff base formation reaction in Ammonyx at pH12, final butylamine concentration 0.02M. Timing sequence is geometric with DT=5msec, N=32 and total time=41secs.

a.  $\lambda=350\text{nm}$



b.  $\lambda=410\text{nm}$



arithmetic run, fig.3.8; 65.8 second arithmetic run, fig.3.10; 41 second geometric run, fig.3.14 and 612 second geometric run, fig.3.12. In each trace the best fit is shown from either the Apple computer analysis or the mainframe analysis using the results obtained for a one component fit.

The y-axis in the stopped-flow traces is a measurement of  $\Delta A$  in arbitrary units (the highest and lowest absorbance readings during the experimental run were used to obtain the limits of this axis in each case).

### 3.4 Kinetic Results

Each experimental run on the stopped-flow apparatus yielded 256 absorbance and time readings and these data were analysed using the Apple and mainframe computer programs. This analysis showed that the formation reactions in Ammonyx and Emulphogene, under the conditions of these experiments, are best represented by a one component fit. There is no evidence to suggest that an intermediate is formed during the formation reactions and it would appear that the reaction is a simple one stage,  $A \rightarrow B$  type reaction with a rate constant  $\lambda_1$ .

From the analysis, values of  $\alpha_0, \alpha_1$  and  $\lambda_1$  are obtained for a one component fit as previously shown from eqn. 2.13.

$$A(t) = \alpha_0 + \alpha_1 (\exp - \lambda_1 t) + \alpha_2 (\exp - \lambda_2 t) + \dots$$

(2.13)

A typical example of the values of rate constant obtained in a formation reaction at pH 12, with Ammonyx as detergent, can be seen in table 3.1. The value of rate constant at 380nm was not included in the calculation of the mean as anomalous values are normally obtained at the isosbestic point, which is 380nm. These values can then be averaged, along with data from other runs of the same experiment with different timing sequences, to give a

Table 3.1

Table showing values of rate constants obtained over a wavelength range of 330nm to 440nm during schiff base formation reaction in Ammonyx at pH 12, final butylamine concentration of 0.02M, during a geometric run.

Wavelength (nm)	Rate constant $\lambda_1$ ( $\text{min}^{-1}$ )
330	0.739
340	0.746
350	0.724
360	0.650
370	0.688
380	0.506
390	0.728
400	0.677
410	0.673
420	0.694
430	0.701
440	0.689

Mean = 0.701 (excluding 380nm)

S.D. = 0.030

value of the rate constant for the reaction under those particular conditions. This can be repeated for reactions with different conditions giving average values of the rate constant for the formation reaction in Ammonyx at other pH values (table 3.2).

From these results it can be seen that the rate constant obtained from the analysis increases with increasing butylamine concentration and, as was mentioned previously, the formation reaction is first order in butylamine concentration. The rate constant obtained from the stopped-flow analysis is equal to the true rate constant of formation multiplied by the concentration of butylamine. The true rate constant can therefore be obtained on dividing by butylamine concentration in each case. This is shown in the last column in table 3.2. These results clearly show that the rate of the formation reaction increases as the pH is increased from pH 8 to pH 12 and that there is quite good agreement in the rate constants calculated at different butylamine concentrations.

(The hydrolysis reaction using 0.04M butylamine at pH 8 was not studied using stopped-flow spectroscopy as ultra-violet/visible spectroscopy showed that the reaction was very slow indeed under these conditions - similarly for Emulphogene.)

The results of  $\alpha_0$  and  $\alpha_1$  obtained from the one component fit in the mainframe analysis can be used to construct spectra of retinal and the schiff base. Using equation 2.13 it can be seen that when  $t=0$  (ie at the start of the reaction)  $A=\alpha_0+\alpha_1$ .

If values of A are calculated at each wavelength and plotted versus wavelength, then the spectrum of retinal (which is the absorbing species at the start of reaction) can be obtained. Similarly at the end of reaction, when  $t$  tends towards infinity,  $A=\alpha_0$ , and so a plot of  $\alpha_0$  values versus wavelength should produce a spectrum of the schiff base.

Table 3.3 shows  $\alpha_0$ ,  $\alpha_1$  and calculated A values over a wavelength range of 330nm to 450nm for the schiff base formation reaction in Ammonyx at pH 8. A plot of  $\alpha_0$  and

Table 3.2

Table showing average rate constants for the schiff base formation reactions in Ammonyx at different pH values and final butylamine concentrations.

pH	Final butylamine concentration (molar)	Rate constant ( $\text{min}^{-1}$ ) from analysis	Rate constant corrected for [But] ( $\text{M}^{-1}\text{min}^{-1}$ )
8	0.25	0.215 (0.033)	0.860
8	0.50	0.518 (0.029)	1.036
10	0.02	0.179 (0.013)	8.950
10	0.05	0.341 (0.015)	6.820
10	0.50	3.550 (0.223)	7.100
12	0.02	0.713 (0.041)	35.650
12	0.05	1.652 (0.141)	33.040

(Figures in brackets are standard deviations.)

Table 3.3

Table showing values of  $\alpha_0$  and  $\alpha_1$  from 1 component fit in mainframe analysis of schiff base formation reaction in Ammonyx at pH 8, final butylamine concentration of 0.5M, geometric run.

Wavelength(nm)	$\alpha_0$	$\alpha_1$	$A = \alpha_0 + \alpha_1$
330	0.3176	-0.1270	0.1906
340	0.3874	-0.1664	0.2210
350	0.4569	-0.1817	0.2752
360	0.4822	-0.1615	0.3207
380	0.3980	-0.0073	0.3907
390	0.3102	0.0807	0.3909
400	0.2018	0.1398	0.3416
410	0.1266	0.1568	0.2834
420	0.0774	0.1388	0.2162
430	0.0535	0.1027	0.1562
440	0.0389	0.0653	0.1042
450	0.0267	0.0319	0.0586

$\alpha_0 + \alpha_1$  versus wavelength is shown in figure 3.15 and it can be seen that, from these values, reasonably accurate spectra of retinal and schiff base can be drawn. Similar spectra can be created from the results of the formation reaction at other pH values and butylamine concentrations.

The formation reactions in Emulphogene were followed in addition to those in Ammonyx, and the results obtained from the analysis of the stopped-flow runs can be examined in a similar way.

An example of the values of the rate constant obtained from a schiff base formation reaction in Emulphogene at pH 10, final butylamine concentration of 0.05M, may be seen in table 3.4.

Average values of the rate constants over the pH range 8-12 can be seen in table 3.5.

Once again the values of  $\alpha_0$  and  $\alpha_1$ , obtained from the mainframe analysis of the formation reaction over the wavelength range 330nm to 450nm, may be used to construct spectra of retinal (using  $A = \alpha_0 + \alpha_1$ ) and the schiff base (using  $A = \alpha_0$ ), table 3.6 and fig.3.16. These values allow reasonably accurate spectra of retinal and schiff base to be drawn, and similar spectra can be constructed from other runs.

The average rate constants for the formation reaction in Ammonyx and Emulphogene at pH 8, 10 and 12 can be calculated from the results in tables 3.2 and 3.5 and are shown in table 3.7 along with values of the logarithm of the formation rate constants ( $M^{-1}sec^{-1}$ ). These values can be compared directly with values of  $\log k_f$  obtained from steady-state analysis, the results of which are shown in figure 3.17 (taken from ref.69). The steady-state analysis of the formation reaction yielded values of approximately -2.0, -1.0 and -0.5 for  $\log k_f$  ( $M^{-1}sec^{-1}$ ) in Ammonyx at pH 8, 10 and 12 respectively and values of approximately -2.6, -0.7 and 0 in Emulphogene at pH 8, 10 and 12 respectively. The results obtained from the stopped-flow runs are in good agreement with these values and show that at pH 8 the formation reaction is faster in Ammonyx than in Emulphogene, but at higher pH values of

10 and 12 the formation is faster in Emulphogene.

FIGURE 3.15  
Spectra of retinal and schiff base in Ammonyx constructed  
using  $\alpha_0$  and  $\alpha_1$  values in Table 3.3.

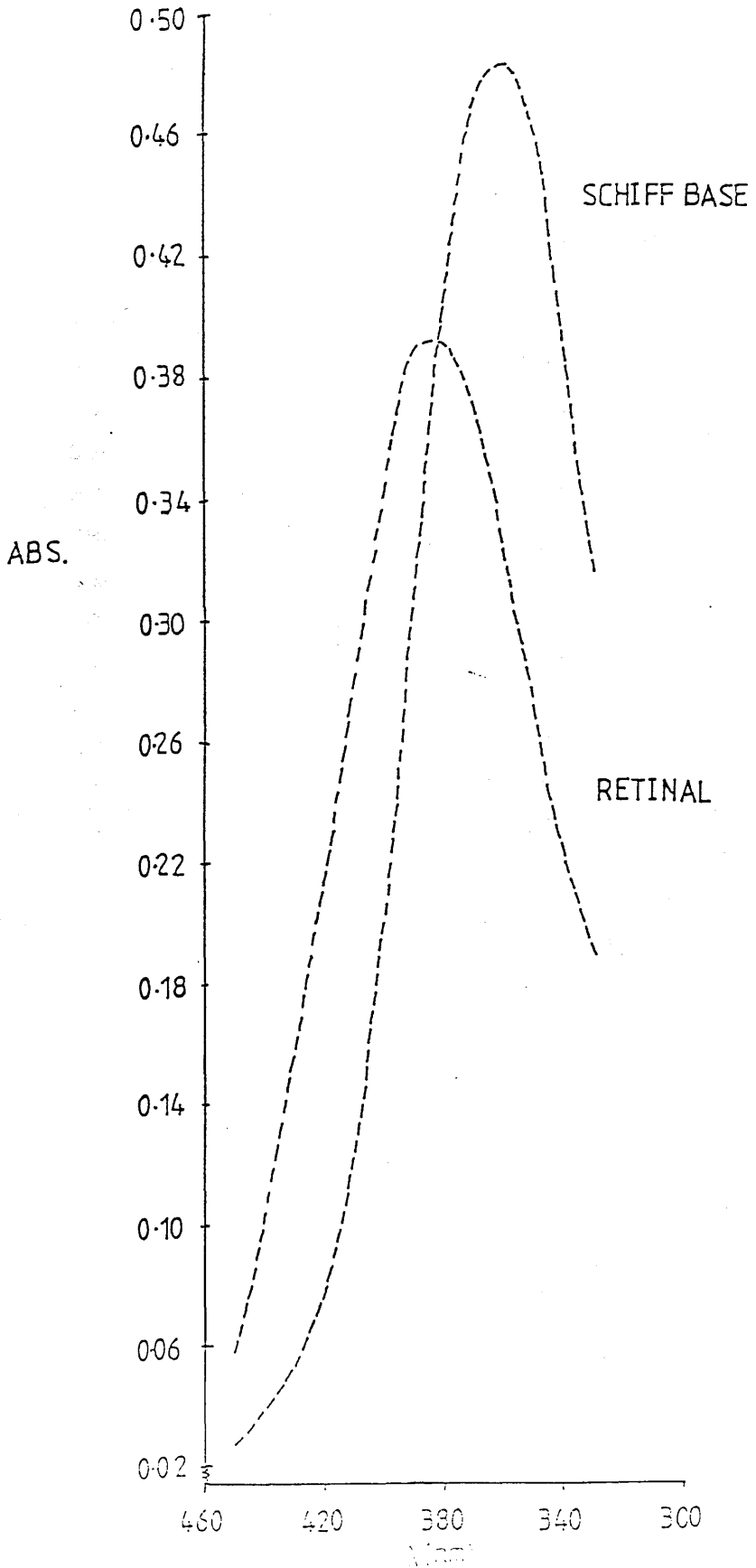


Table 3.4

Table showing values of rate constants obtained over a wavelength range of 330nm to 450nm during schiff base formation reaction in Emulphogene at pH 10, final butylamine concentration of 0.5M, during a run with a linear time-scale.

Wavelength (nm)	rate constant $\lambda_1$ (min <sup>-1</sup> )
330	10.500
340	10.398
350	10.380
360	10.236
370	10.038
380	8.586
390	10.908
400	10.446
410	10.398
420	11.124
430	10.110
440	10.152
450	10.428

Mean = 10.426 (excluding 380nm)

S.D. = 0.315

Table 3.5

Table showing average rate constants for the schiff base formation reactions in Emulphogene at different pH values and final butylamine concentrations.

pH	Final butylamine concentration (molar)	Rate constant (min <sup>-1</sup> ) from analysis	Rate constant corrected for [But] (M <sup>-1</sup> min <sup>-1</sup> )
8	0.25	0.086 (0.043)	0.344
8	0.50	0.126 (0.028)	0.252
10	0.02	0.286 (0.042)	14.300
10	0.05	0.654 (0.023)	13.080
10	0.50	10.360 (0.440)	20.720
12	0.02	1.704 (0.038)	85.200
12	0.05	4.391 (0.109)	87.820

(Figures in brackets are standard deviations.)

Table 3.6

Table showing values of  $\alpha_0$  and  $\alpha_1$  from 1 component fit in mainframe analysis of schiff base formation reaction in Emulphogene at pH 10, final butylamine concentration of 0.5M, linear timescale.

Wavelength(nm)	$\alpha_0$	$\alpha_1$	$A = \alpha_0 + \alpha_1$
330	0.5438	-0.1525	0.3913
340	0.6322	-0.1932	0.4390
350	0.6960	-0.2076	0.4884
360	0.7231	-0.1765	0.5466
370	0.6695	-0.0951	0.5744
380	0.5488	0.0200	0.5688
390	0.4173	0.1172	0.5343
400	0.2700	0.1686	0.4386
410	0.1816	0.1712	0.3528
420	0.1320	0.1627	0.2947
430	0.0984	0.1027	0.2011
440	0.0733	0.0648	0.1381
450	0.0710	0.0356	0.1066

FIGURE 3.16  
Spectra of retinal and schiff base in Emulphogene constructed using  $\alpha_0$  and  $\alpha_1$  values in Table 3.6.

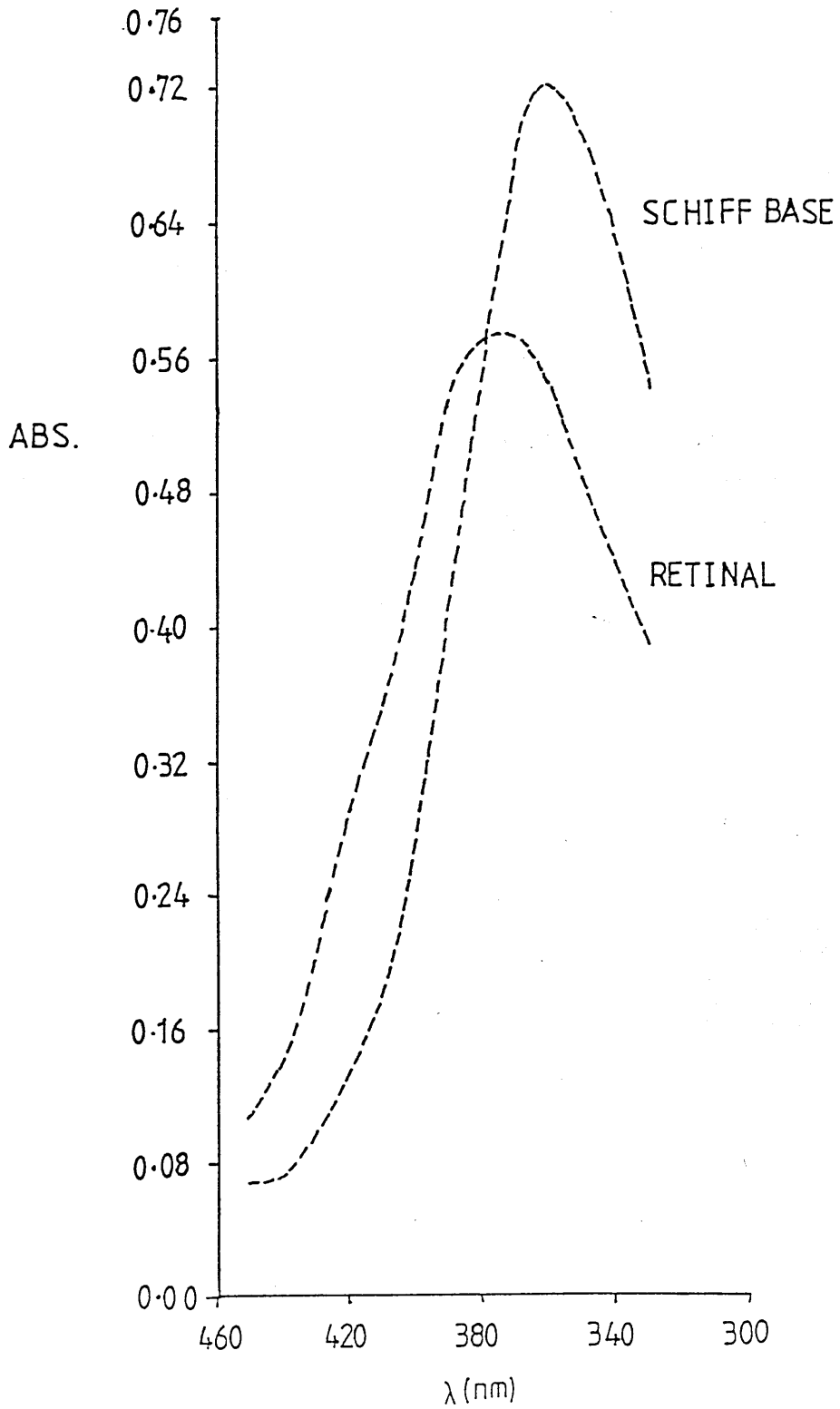
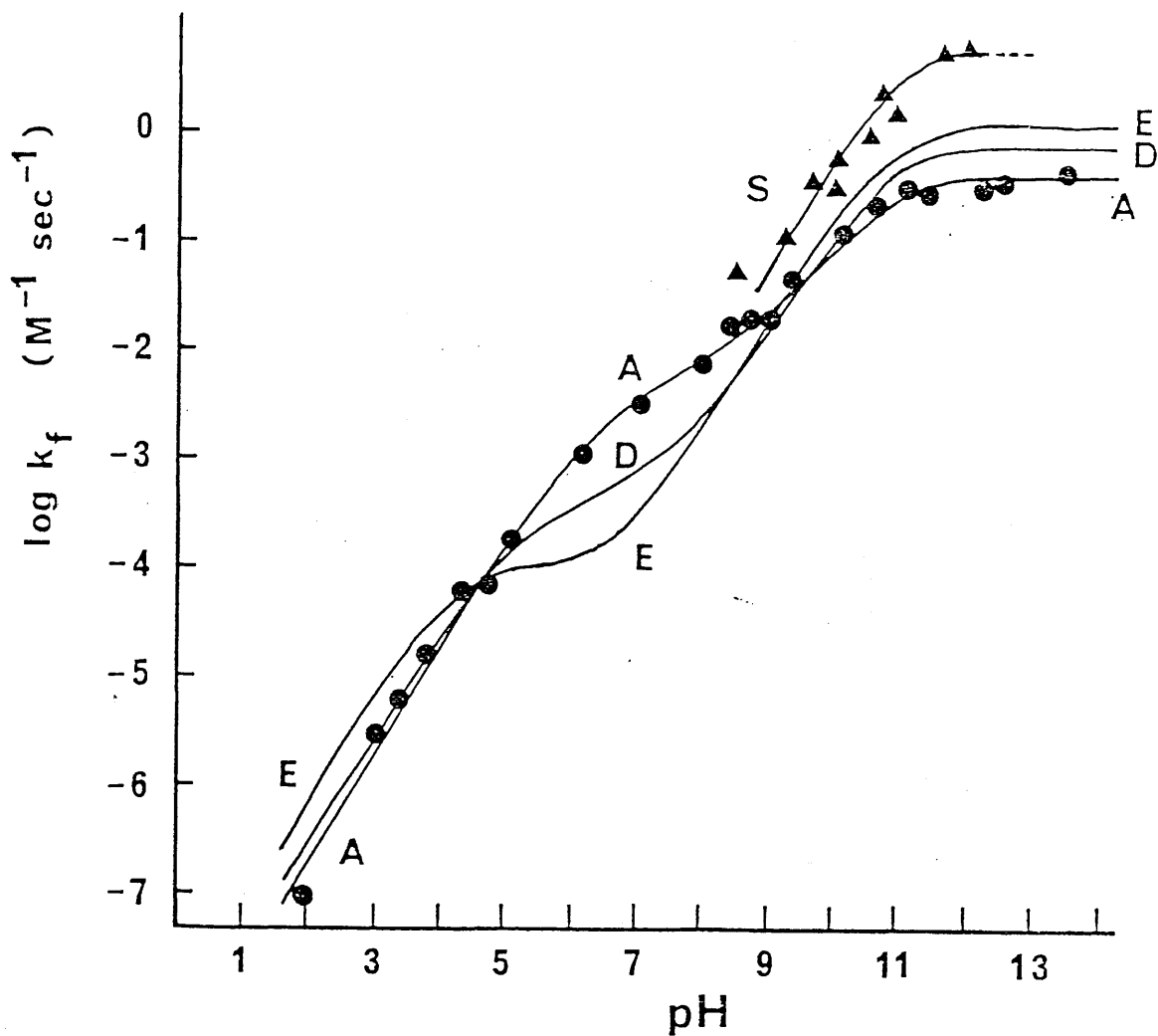


Table 3.7

Table showing average values of the rate constant of schiff base formation in Ammonyx and Emulphogene at pH 8, 10 and 12.

Detergent	pH	average value of	
		rate constant ( $k_f$ ) ( $M^{-1}min^{-1}$ )	$\log k_f$ ( $M^{-1}sec^{-1}$ )
Ammonyx	8	0.948	-1.801
	10	7.623	-0.896
	12	34.345	-0.242
Emulphogene	8	0.298	-2.304
	10	16.033	-0.573
	12	86.510	0.159

FIGURE 3.17  
Steady-state pH-rate profiles for formation of schiff base  
in aqueous detergent mixtures at 20°C. A=Ammonyx;  
E=Emulphogene; D=DTAB and S=SDS.



(Taken from ref.69)

CHAPTER 4

SCHIFF BASE HYDROLYSIS  
REACTIONS.

#### 4.1 Material Preparation

The N-retinylidene n-butylamine schiff base was formed by addition of a small volume of a concentrated retinal in ethanol solution to excess 10mM n-butylamine in an aqueous detergent solution. This mixture was left for at least 20 minutes to allow the schiff base to form and then the hydrolysis reaction was started by mixing equal volumes of this schiff base solution and a buffer/detergent solution.

The hydrolysis reaction was studied in four detergents, namely Emulphogene, Ammonyx, SDS and DTAB. The reactions in Emulphogene and Ammonyx were studied at pH 4,5,6 and 7 using 0.2M acetate buffers at pH 4 and 5, and 0.2M phosphate buffers at pH 6 and 7. These buffers were prepared following the procedure described previously. The schiff base and the buffers were made up in 2% (by volume) Emulphogene or Ammonyx solutions. The hydrolysis reaction in DTAB was studied at pH 5.5 using a 0.2M acetate buffer and in this case the schiff base and buffer were made up in 25mM DTAB solution.

In these three detergents the schiff base prior to mixing with buffer solution is in the unprotonated form as it is prepared at high pH due to the excess butylamine. The hydrolysis reaction is started by mixing the unprotonated schiff base with the detergent/buffer solution in the pH range 4-7. This pH jump causes the formation of the protonated schiff base, which is the reactive species, and so the hydrolysis reaction begins.

The hydrolysis reactions in SDS were studied at pH 9,10 and 11 using 0.04M borate buffer in each case. The schiff base and buffers were made up in 12.5mM SDS solutions (higher concentrations of SDS or of borate buffer caused precipitation problems). In these reactions the pH is much higher than with the other detergents and this is necessary because the entire pH-hydrolysis rate curve is shifted to high pH when SDS is the detergent, fig.1.17. This is because of the pK<sub>a</sub> shift of the schiff base induced by the strongly cationic SDS detergent and will be discussed in more detail later. As a result of

this, hydrolysis will only occur rapidly around pH 9-13 and so the reaction must be studied within this pH range.

This causes problems experimentally because in order for the hydrolysis reaction to occur the schiff base must become protonated. With the other detergents this protonation takes place on 1:1 mixing of the schiff base with the buffer in pH range 4-7 but with SDS a different procedure was used. The unprotonated schiff base was formed by addition of retinal in ethanol to 10mM butylamine in ethanol (not detergent as is usually the case). 1ml of this concentrated unprotonated schiff base solution was then added to 100ml of 10mM hydrochloric acid in 12.5mM SDS to form the protonated schiff base at low pH. The hydrolysis reaction was then started by 1:1 mixing of this protonated schiff base with the 0.04M borate buffer in 12.5mM SDS at pH 9,10 or 11.

With each of the four detergents used in the hydrolysis reactions the schiff base concentration and the buffer concentration are halved when 1:1 mixing occurs. The schiff base was prepared so that before the 1:1 dilution it had an absorbance reading of approximately 1 at 360nm (unprotonated schiff base peak). The protonated schiff base has an absorbance maximum at 430-445 nm (depending on detergent) and so in the SDS experiments the protonated schiff base was prepared with an absorbance of around 1 at 445nm.

It should be noted that in the hydrolysis reactions the rate of the reaction is independent of the butylamine concentration, unlike the formation reactions, but the rate of hydrolysis is dependent on the pH of the reaction. At the end of each experiment the pH of the products of reaction was recorded and this was taken as the pH of the reaction.

General base catalysis of the hydrolysis reaction in Ammonyx was studied at pH 4.5 and 6 using acetate buffers at pH 4 and 5 and phosphate buffer at pH 6. The schiff base was made using the same procedure as before and the buffer concentrations were 0.02M, 0.1M, 0.2M and 0.4M, giving final concentrations of 0.01M, 0.05M, 0.1M and 0.2M after 1:1 mixing. In these experiments it was

essential that for each buffer series at any pH, the final pH after 1:1 mixing with the schiff base must be within about 0.1 pH units to make comparisons between the different concentrations valid. Trial runs showed that the pH of the buffer solution did increase slightly (especially the less concentrated buffers) when mixed with the schiff base solution, due to the excess 10mM butylamine. To compensate for this rise in pH, a calculated (small) amount of 1M hydrochloric acid was added to the buffer before mixing and in this way the final pH of each reaction was carefully controlled and was recorded at the end of reaction.

For the determination of the  $pK_a$  values of the schiff base, the hydrolysis reaction was studied in Emulphogene, Ammonyx and DTAB detergents using buffers in the pH range 1-9. The schiff base was prepared as described previously and the buffer concentration used in all the experiments was 0.2M. Buffers used to control the pH were:- hydrochloric acid pH 1-2, formate buffer pH 2.5-3.75, acetate buffer pH 4-5.5, phosphate buffer pH 5.75-8 and borate buffer at pH 9. These were prepared as described previously.

The schiff base solution for the low temperature ultra-violet/visible spectroscopy was prepared by two slightly different methods. The first method of schiff base preparation was the same as for the ultra-violet/visible spectroscopy at 20°C, where a small volume of retinal in ethanol is added to 10mM butylamine in detergent solution. The hydrolysis is started by mixing equal volumes of this schiff base solution with detergent/buffer solution. The second method involved making a more highly concentrated retinal in ethanol solution and adding this to a 10mM butylamine in ethanol solution. A small volume of this concentrated schiff base in ethanol is then added to a larger volume of buffer/detergent to start the hydrolysis reaction. The low temperature ultra-violet/visible spectra of the hydrolysis reaction were recorded in Ammonyx detergent at pH 4.5 and 6, using 0.2M acetate buffers at pH 4 and 5 and 0.2M phosphate buffer at pH 6.

The effect of deuterium oxide (in place of water) on the schiff base hydrolysis rate was studied by UV/visible and stopped-flow spectroscopy. The hydrolysis reaction was followed in Ammonyx detergent using a 0.2M acetate buffer at pD 4 and the usual 1:1 mixing technique of schiff base and buffer was used in this experiment.

In all these experiments the schiff base solutions were prepared daily, working in an argon or nitrogen atmosphere and the containers were wrapped in aluminium foil to eliminate photoisomerisation problems.

#### 4.2 Ultra-Violet/Visible Spectroscopy

The hydrolysis reactions were started in a similar way to the formation reactions except in this case equal volumes of the schiff base and the buffer in detergent solutions were pipetted into a cuvette and mixed manually. The spectra were recorded in the same way, covering a wavelength range of 260nm to 540nm, in this case, with the temperature remaining constant at 20°C.

The hydrolysis reaction can be monitored by following the shift in the absorbance maximum during the reaction. The unprotonated and protonated schiff bases absorb at around 360nm and 440nm respectively, with the retinal peak at around 380nm. At the start of the reaction the solution contains a mixture of unprotonated and protonated schiff bases with the proportion of each depending on the detergent and the pH of the reaction, and as the reaction proceeds the retinal peak appears at 380nm.

Typical UV/visible spectra can be seen in figs.4.1-4.12. The schiff base hydrolysis reaction in figs.4.1-4.4 are in Emulphogene at pH 4.12, 5.09, 6.26 and 7.23 respectively. (These will be referred to as pH 4,5,6 and 7 in the text.) Figs.4.5-4.8 are in Ammonyx at pH 4.22, 5.04, 6.23 and 7.17 respectively. Fig.4.9 is in DTAB at pH 5.65 and figs.4.10-4.12 are in SDS at pH 9.01, 10.05 and 10.65 respectively.

FIGURE 4.1  
 UV/visible spectrum of schiff base hydrolysis reaction  
 in acetate buffer/Emulphogene at pH 4.12.

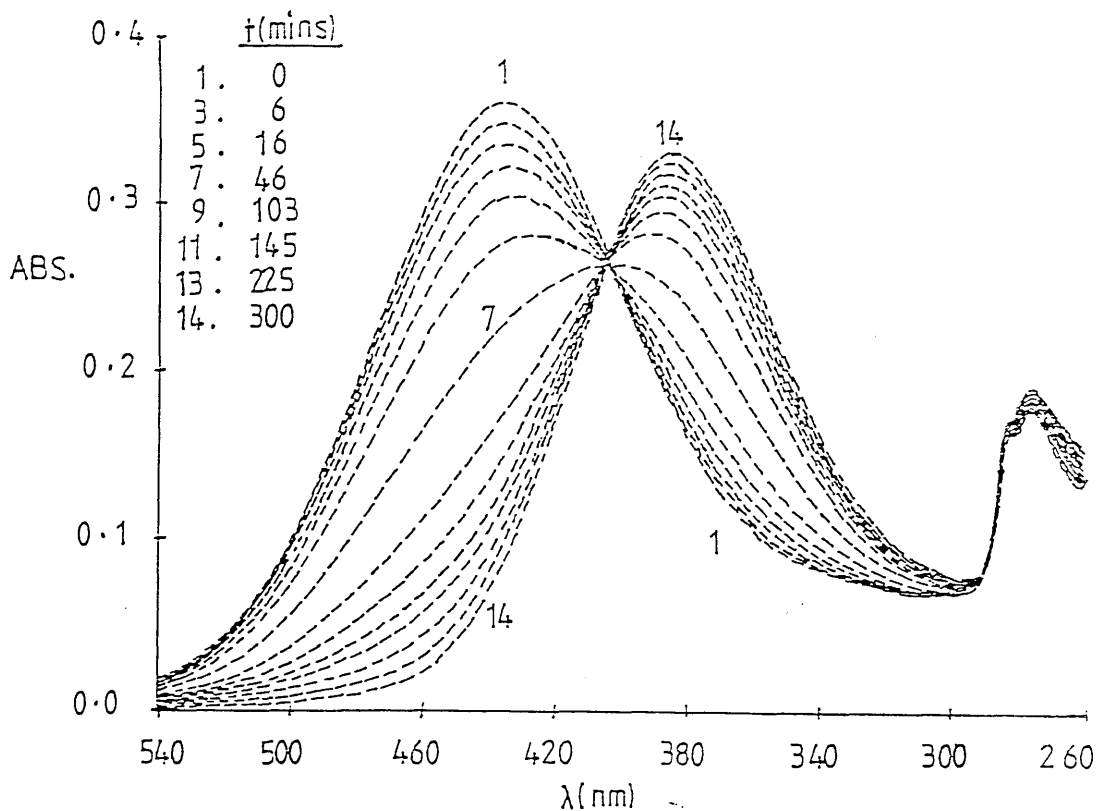


FIGURE 4.2  
 UV/visible spectrum of schiff base hydrolysis reaction  
 in acetate buffer/Emulphogene at pH 5.09.

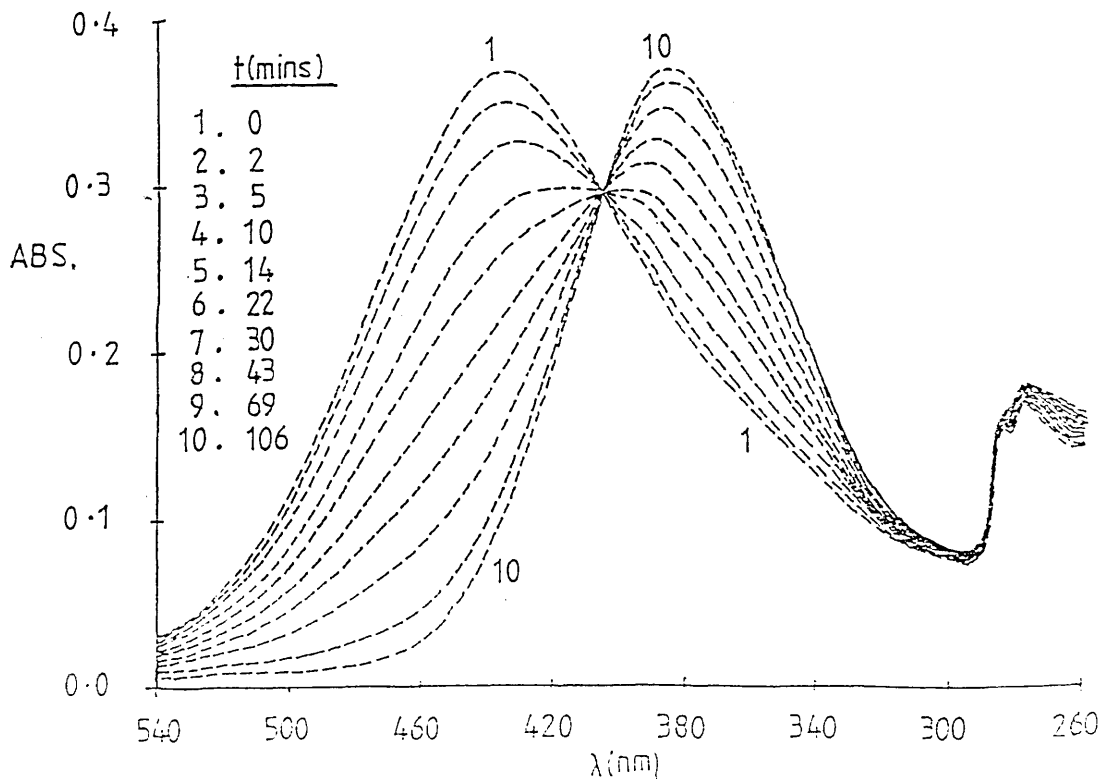


FIGURE 4.3

UV/visible spectrum of schiff base hydrolysis reaction in phosphate buffer/Emulphogene at pH 6.26.

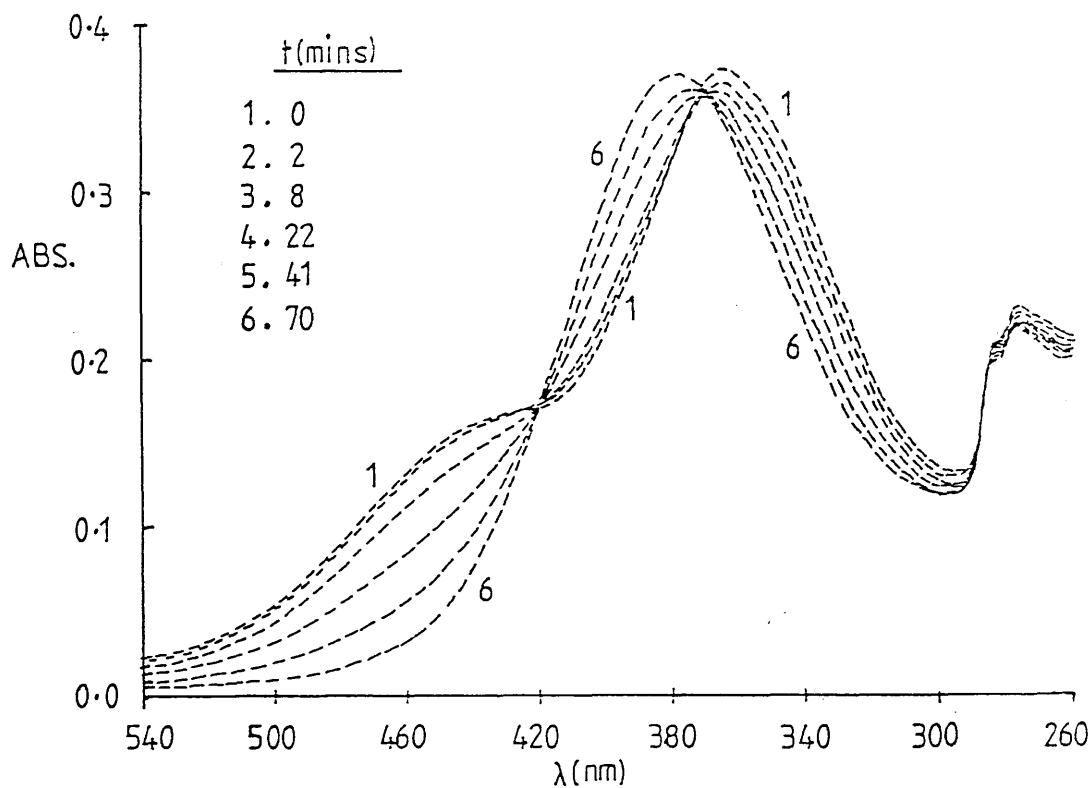


FIGURE 4.4

UV/visible spectrum of schiff base hydrolysis reaction in phosphate buffer/Emulphogene at pH 7.23.

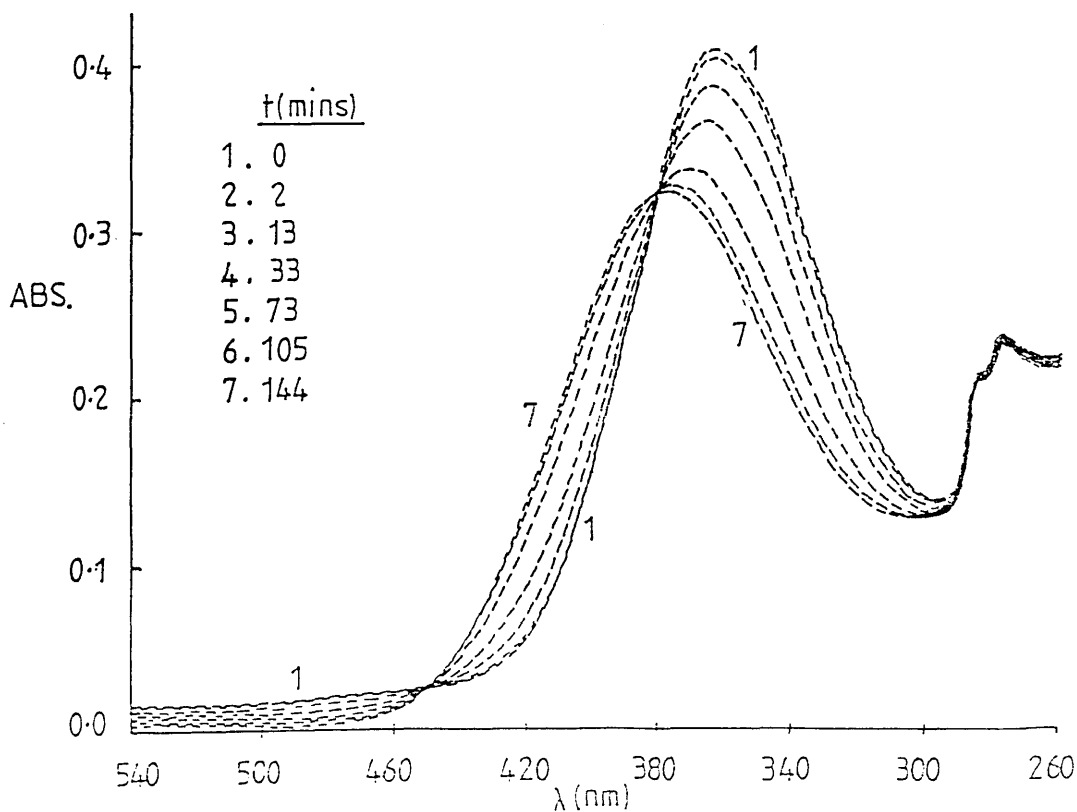


FIGURE 4.5

UV/visible spectrum of schiff base hydrolysis reaction in acetate buffer/Ammonyx at pH 4.22.

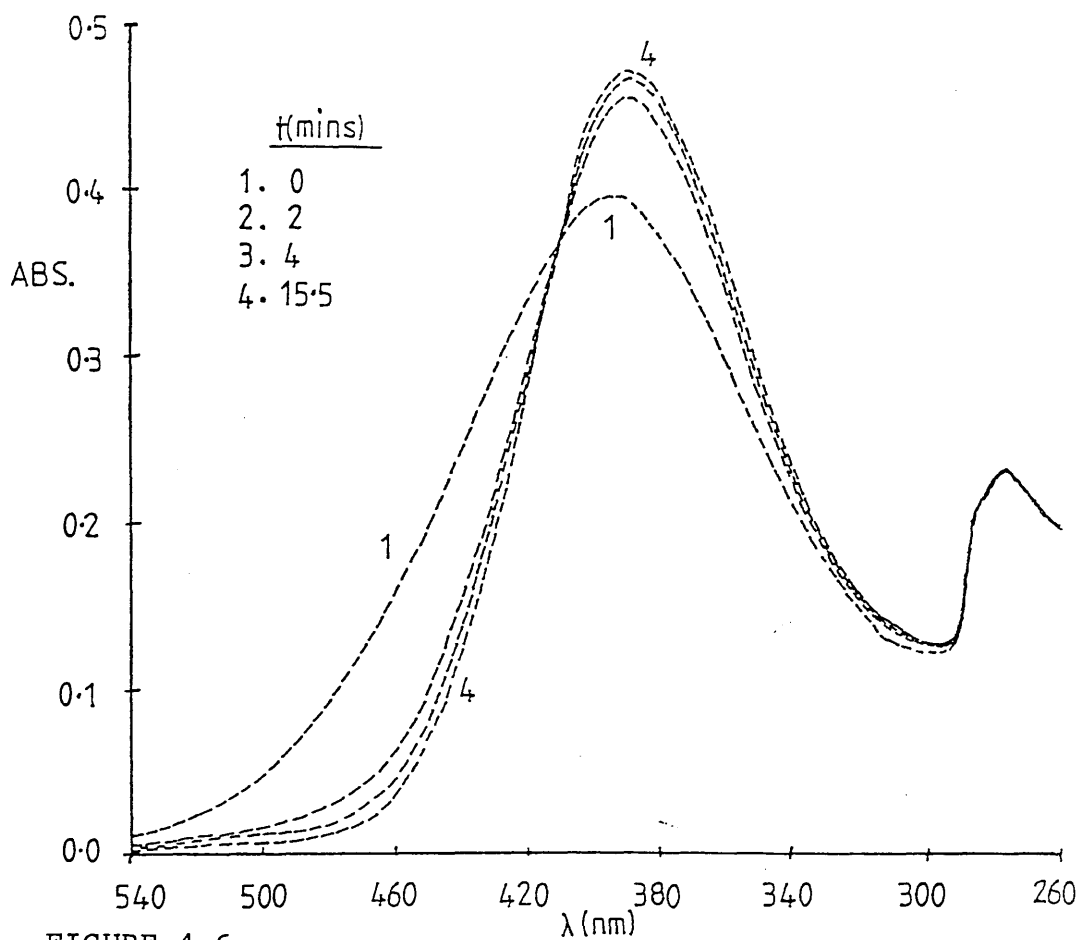


FIGURE 4.6

UV/visible spectrum of schiff base hydrolysis reaction in acetate buffer/Ammonyx at pH 5.04.

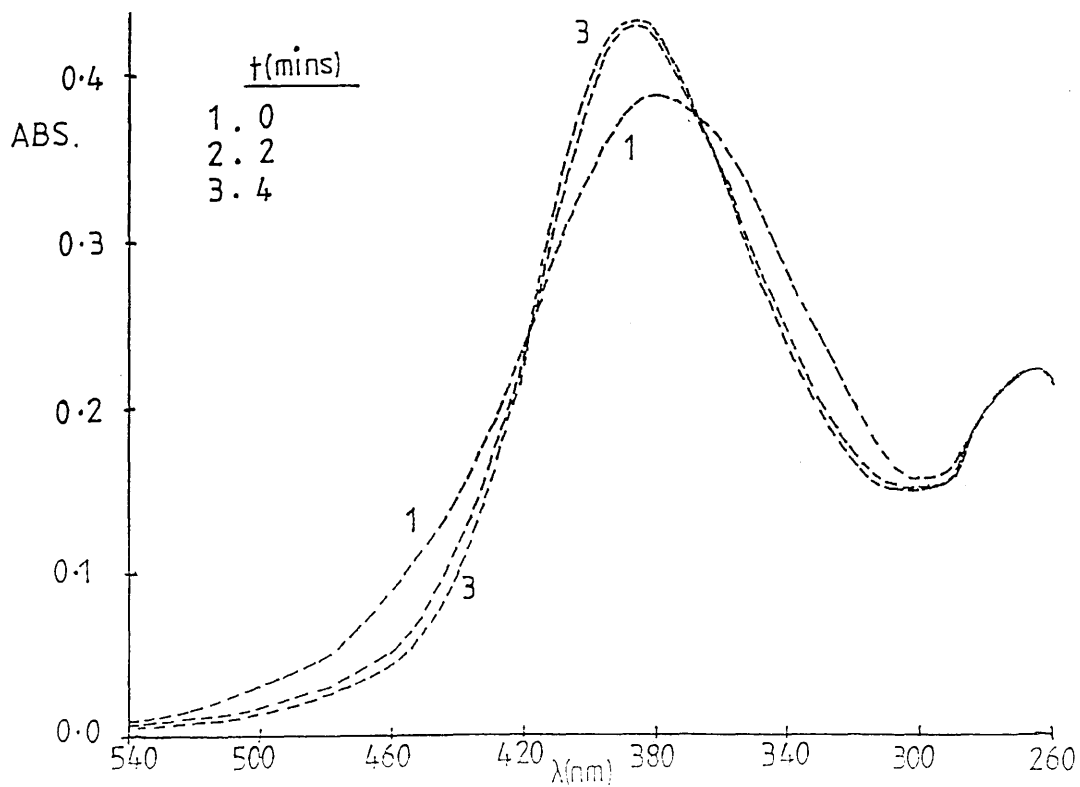


FIGURE 4.7

UV/visible spectrum of schiff base hydrolysis reaction in phosphate buffer/Ammonyx at pH 6.23.

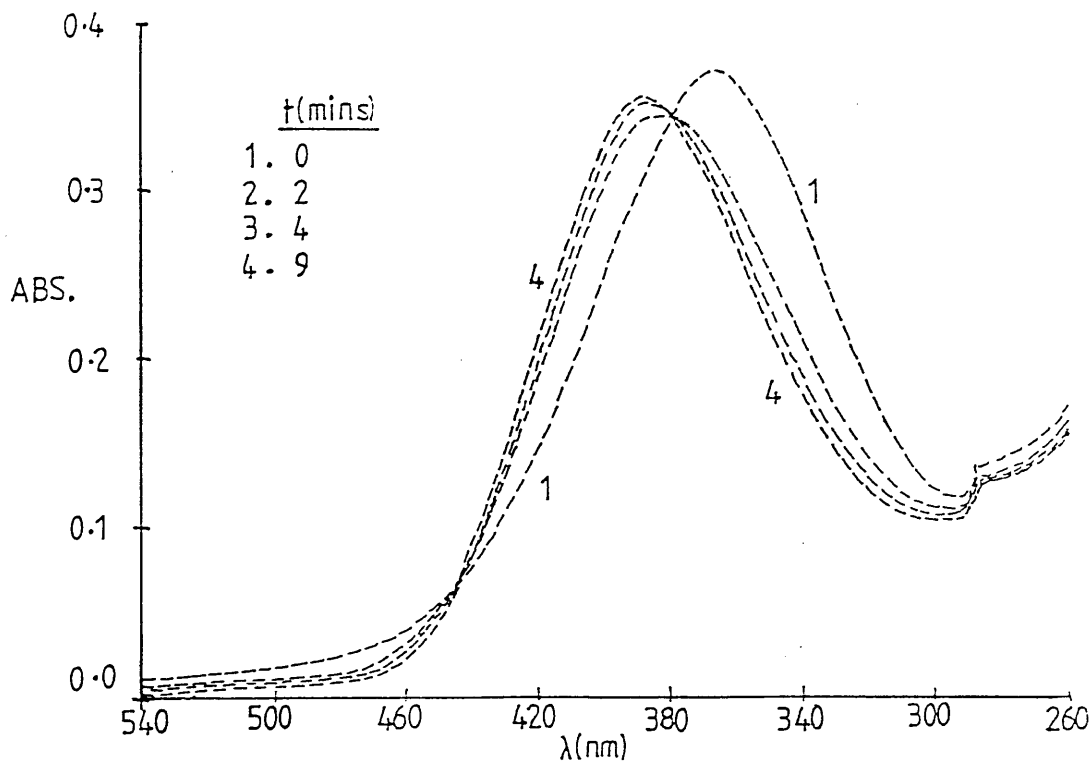


FIGURE 4.8

UV/visible spectrum of schiff base hydrolysis reaction in phosphate buffer/Ammonyx at pH 7.17.

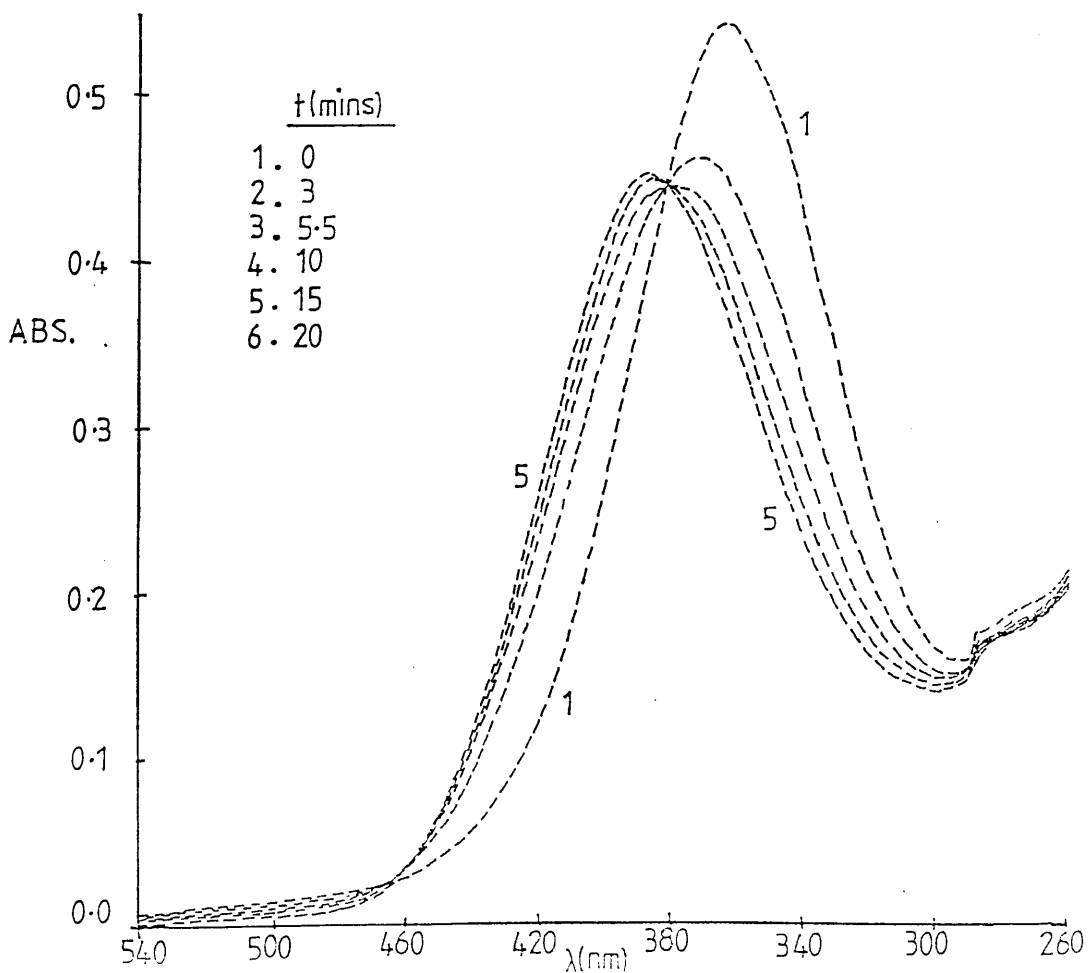


FIGURE 4.9

UV/visible spectrum of schiff base hydrolysis reaction in acetate buffer/DTAB at pH 5.65.

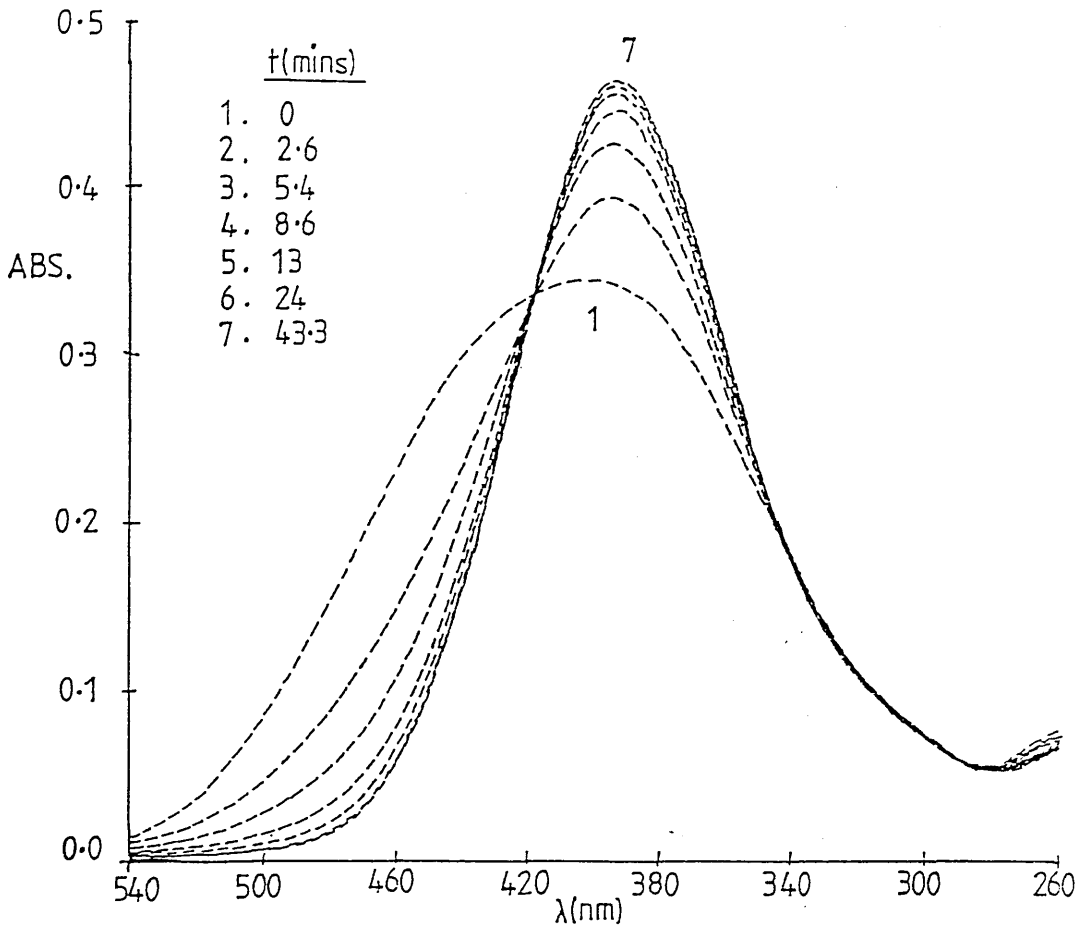


FIGURE 4.10

UV/visible spectrum of schiff base hydrolysis reaction in borate buffer/SDS at pH 9.01.

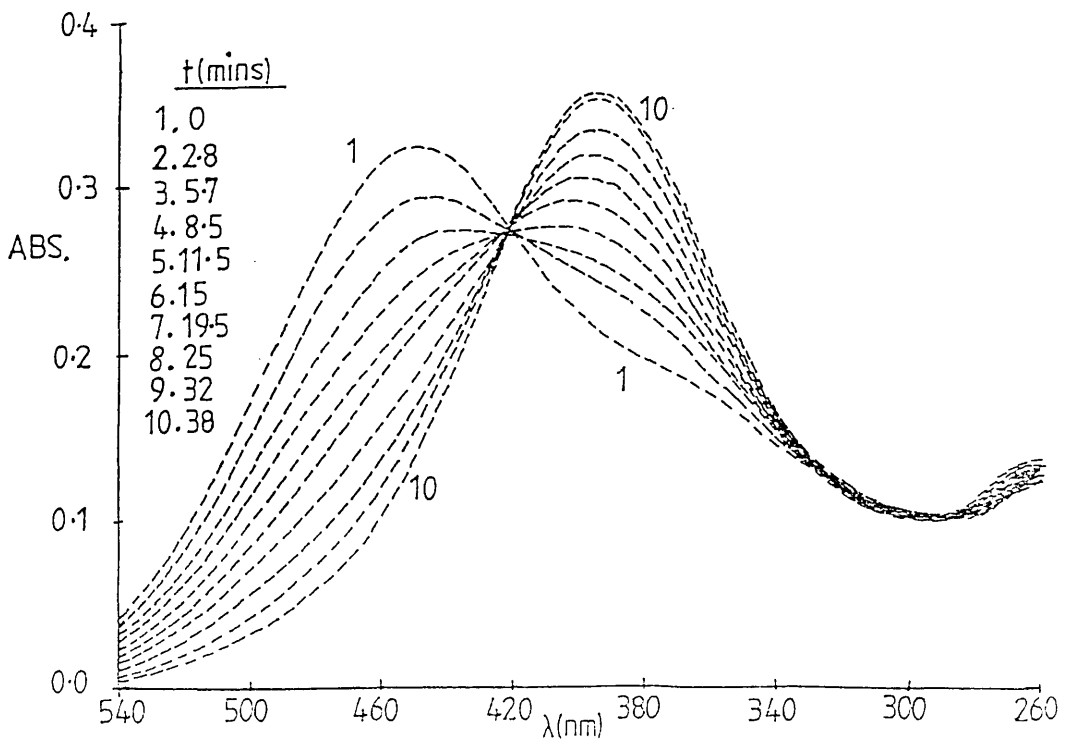


FIGURE 4.11

UV/visible spectrum of schiff base hydrolysis reaction in borate buffer/SDS at pH 10.05.

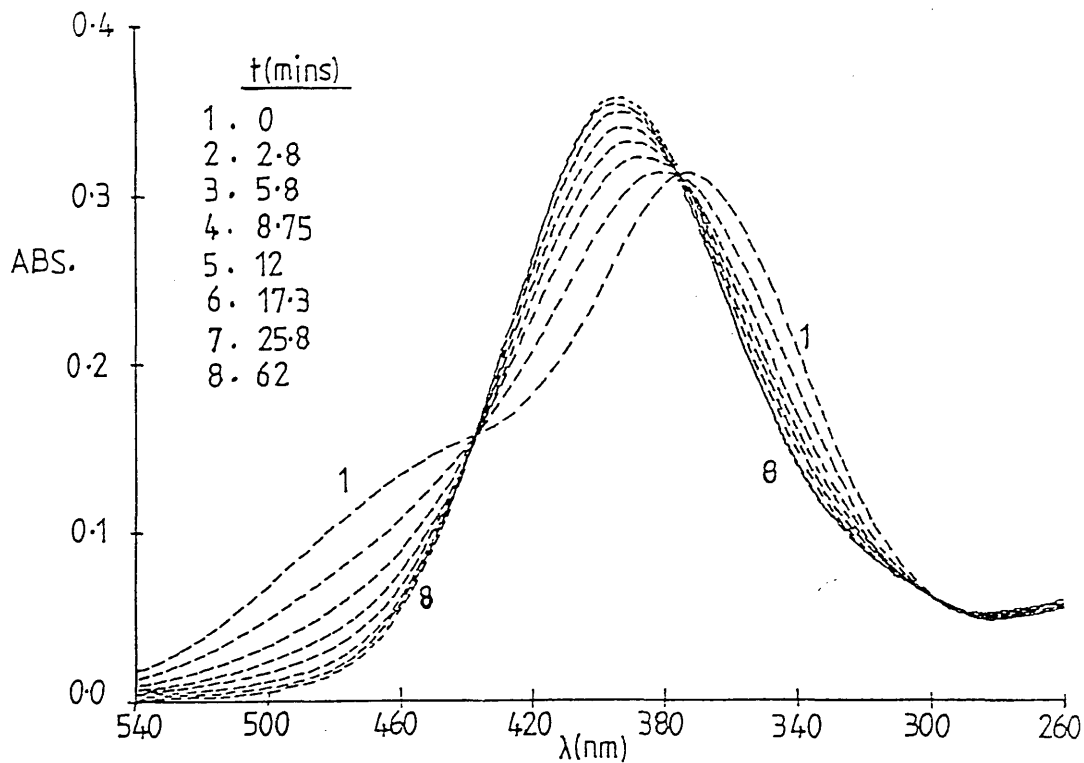
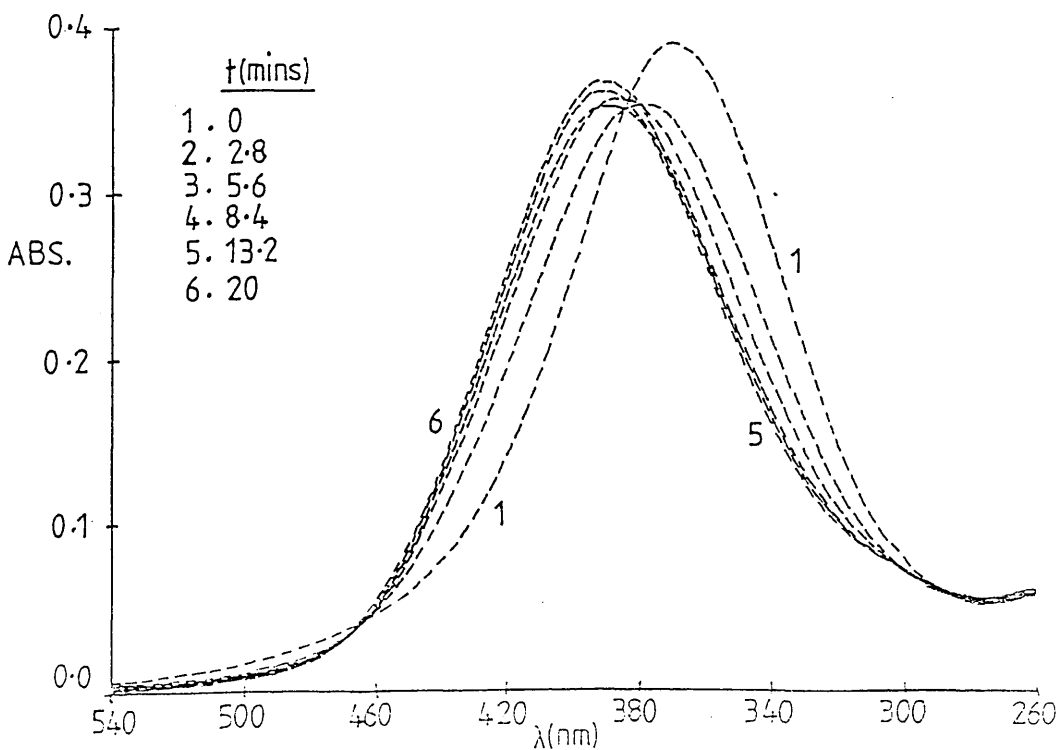


FIGURE 4.12

UV/visible spectrum of schiff base hydrolysis reaction in borate buffer/SDS at pH 10.65.



It can be seen from figs.4.1 and 4.2 that in Emulphogene at pH 4 and 5 the schiff base at the start of the reaction is predominantly in the protonated form (absorbance peak at approximately 440nm) and as the reaction proceeds this is converted to retinal. At pH 6 the schiff base is a mixture of the protonated form and (predominantly) the unprotonated form (absorbance peak at around 360nm) at the start of reaction (fig.4.3). At pH 7 the schiff base is predominantly in the unprotonated form at the start of reaction (fig.4.4). It would appear from these spectra that the reaction occurs more quickly at pH 5 and 6 in Emulphogene and the rate drops off at pH 4 and 7, as would be expected from the bell-shaped pH-rate curves characteristic of schiff base hydrolysis reactions.

Similar observations can be made for the reactions in Ammonyx where at pH 4 (fig.4.5) the schiff base is a mixture of the protonated and the unprotonated form, and as the pH is raised to pH 7 the schiff base is more predominantly in the unprotonated form (figs.4.6-4.8). Again the rate of the hydrolysis reaction in Ammonyx would appear to be faster at pH 5 and 6 and slower at pH 4 and 7. Overall the hydrolysis rate is faster in Ammonyx than in Emulphogene.

The hydrolysis reaction in DTAB was only studied at pH 5.5 which is near the maximum in the pH-rate curve of DTAB. At the start of the reaction the schiff base is a mixture of the unprotonated and protonated forms (fig.4.9).

In SDS at pH 9 the schiff base is predominantly in the protonated form (fig.4.10) and at pH 10 and 11 it is predominantly in the unprotonated form (figs.4.11-4.12).

When the schiff base is mostly in the protonated or unprotonated form then it shows that the pH of the reaction is below or above the  $pK_a$  value of the schiff base, respectively. From these spectra therefore a rough guess of the  $pK_a$  value of the schiff base in Emulphogene, Ammonyx and SDS would be around 5.5, 4.5 and 9.5 respectively.

Close examination of figures 4.1-4.12 shows that in some cases the spectra recorded at certain times during the reaction do not pass through a common isosbestic point. This suggests that the hydrolysis reaction under certain conditions may not be a straight-forward one step reaction after protonation of the schiff base. Once again these reactions were studied in much more detail using stopped-flow spectroscopy which allowed the use of arithmetic and geometric timescales to see if any fast reactions were occurring.

### 4.3 Stopped-Flow Spectroscopy

The samples used for stopped-flow experiments were identical to those in UV/visible spectroscopy experiments. The schiff base and buffer in detergent solutions were injected into the two driving syringes in the stopped-flow apparatus and left to equilibrate to 20°C.

Each hydrolysis reaction was studied at a fixed wavelength using various linear, geometric and arithmetic timing sequences. The runs were repeated over a wavelength range of 330nm to 530nm, at 10nm intervals.

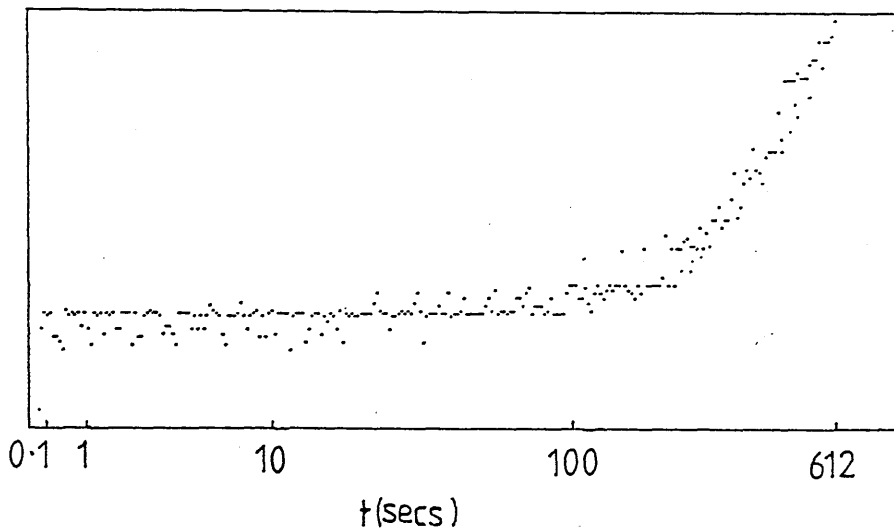
Instrumental controls were done where the buffer/detergent solution was replaced by detergent solution alone and in these experiments no apparent absorbance changes took place at any wavelength.

Typical stopped-flow traces can be seen in figs.4.13-4.24. The schiff base hydrolysis reactions in figures 4.13-4.15 are in Emulphogene detergent at pH 4, 5 and 6 respectively. The timing sequences used for these runs had a long total time as the hydrolysis reaction in Emulphogene is quite slow. The reaction at pH 4 (fig.4.13) appears to have a lag period at the start of the reaction lasting approximately 100 seconds. After this time it can be seen that the absorbance starts to change more as the reaction proceeds. At 360nm (fig.4.13a) the absorbance increases with time and at 440nm (fig.4.13b) the absorbance decreases with time. These changes in absorbance are what would be expected

FIGURE 4.13

Stopped-flow traces of schiff base hydrolysis reaction in acetate buffer pH4/Emulphogene. Timing sequence is geometric with DT=75msec, N=32 and total time=612secs.

a.  $\lambda = 360 \text{ nm}$



b.  $\lambda = 440 \text{ nm}$

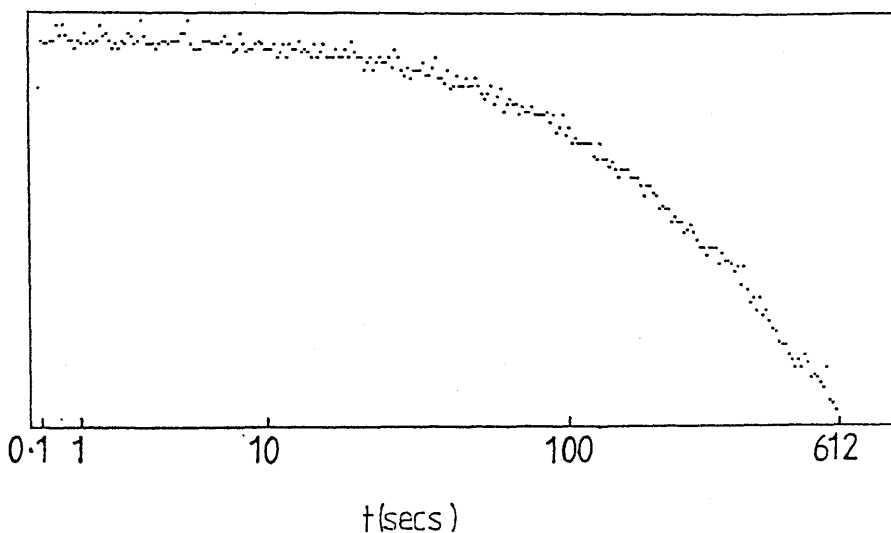
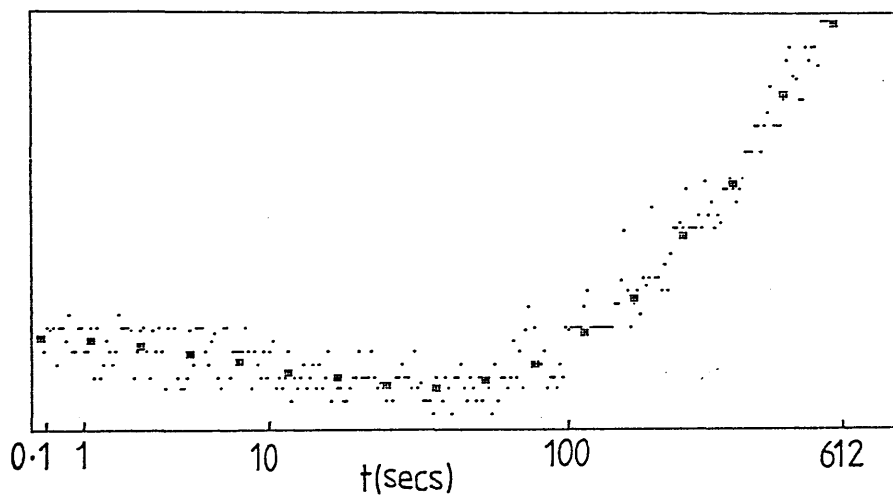


FIGURE 4.14

Stopped-flow traces of schiff base hydrolysis reaction in acetate buffer pH5/Emulphogene. Timing sequence is geometric with DT=75msec, N=32 and total time=612secs.

a.  $\lambda=330\text{nm}$



b.  $\lambda=390\text{nm}$

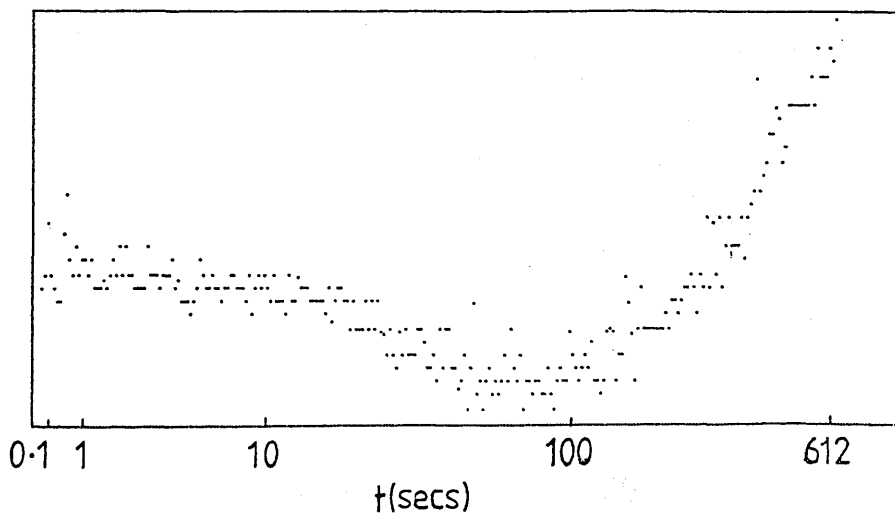
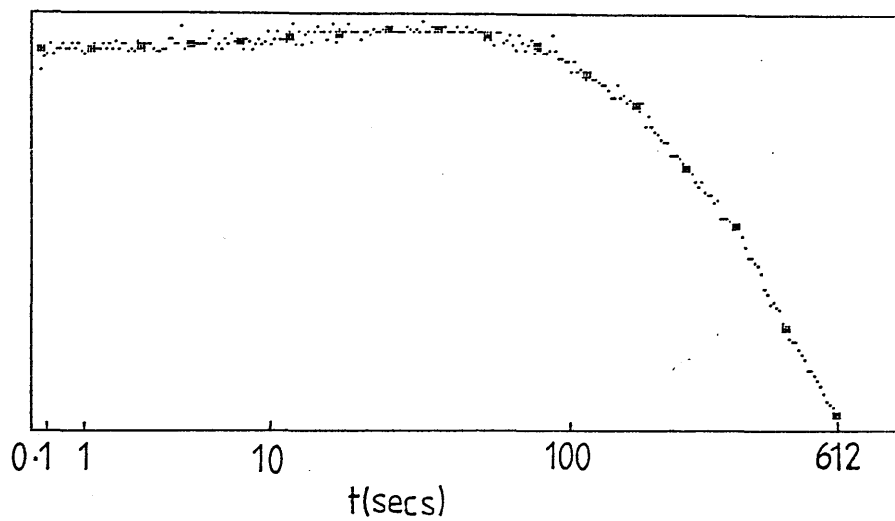


FIGURE 4.14 (cont.)

c.  $\lambda=470\text{ nm}$



d.  $\lambda=510\text{ nm}$

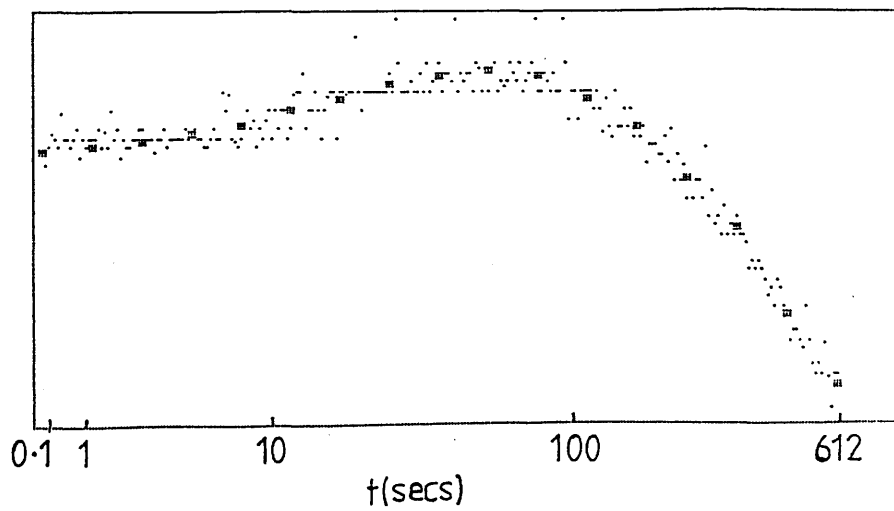
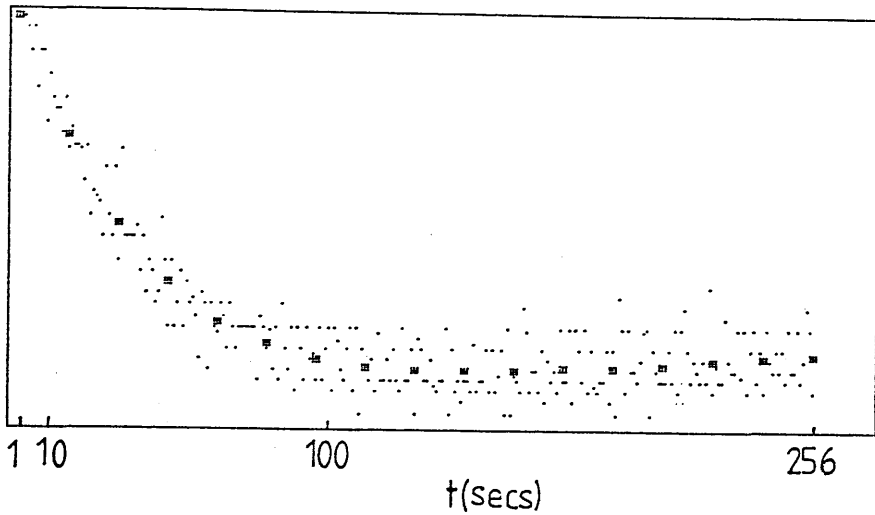


FIGURE 4.15

Stopped-flow traces of schiff base hydrolysis reaction in phosphate buffer pH6/Emulphogene. Timing sequence in (a) and (b) is linear with DT=1sec and total time=256secs and in (c) and (d) is geometric with DT=75msec, N=32 and total time=612secs.

a.  $\lambda=350\text{nm}$



b.  $\lambda=470\text{nm}$

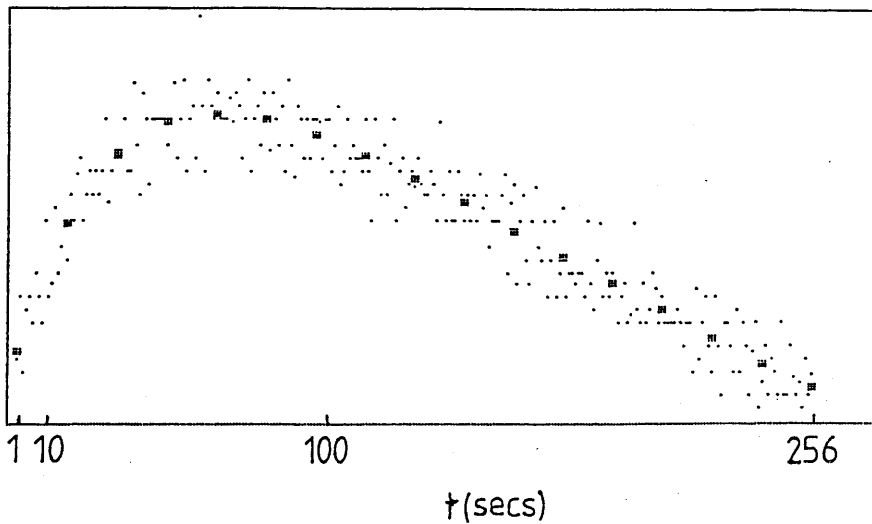
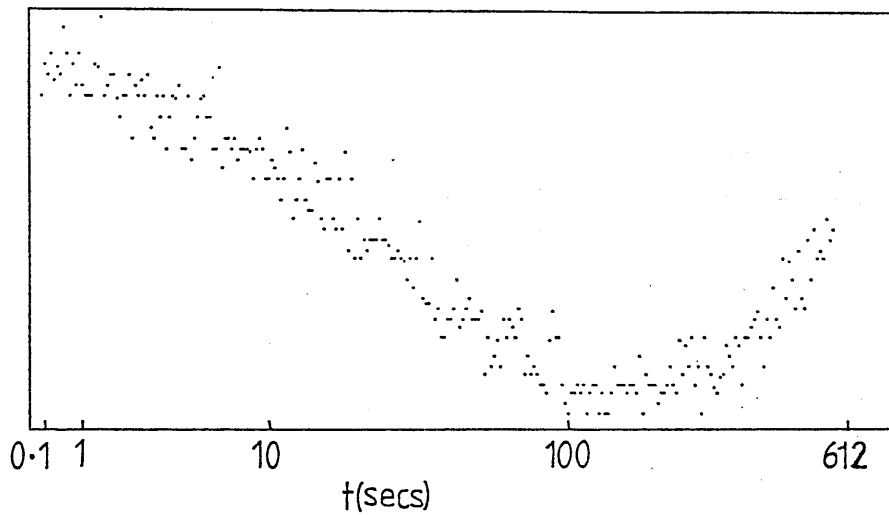
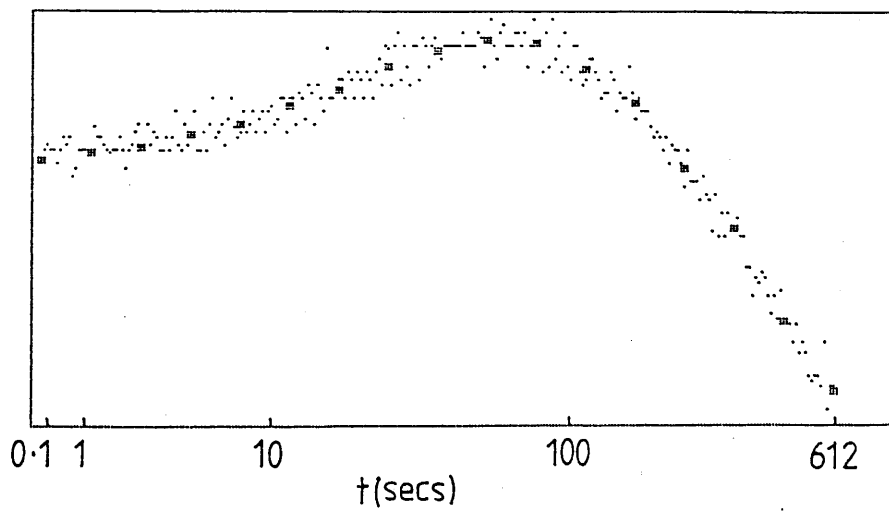


FIGURE 4.15 (cont.)

c.  $\lambda=370\text{nm}$



d.  $\lambda=440\text{nm}$



from examination of the UV/vis. spectrum (fig.4.1).

At pH 5 and 6 the reaction occurs more quickly (figs.4.14-4.15) and it is obvious that there is some reaction taking place within the first 100 seconds. This can also be seen with a shorter, linear timing sequence at pH 6 (fig.4.15 a and b). These traces suggest that the hydrolysis reaction under these conditions is not a single step reaction, but is a two stage reaction involving some transient intermediate species.

At pH 7 the hydrolysis reaction in Emulphogene is very slow and as a result of this the absorbance hardly changed at all during the timescale of the stopped-flow run. Since the absorbance scale on the y-axis represents the difference in absorbance between the maximum and minimum absorbance reading during the time of the run, the plots obtained at pH 7 were very noisy. (Traces not shown.)

In nearly all cases the mainframe analysis yielded a 2 component fit as the best fit and this is shown on the traces. In some cases, especially when the reaction was very slow, no analysis was possible using the Discrete program and in these cases the traces are shown without a best fit.

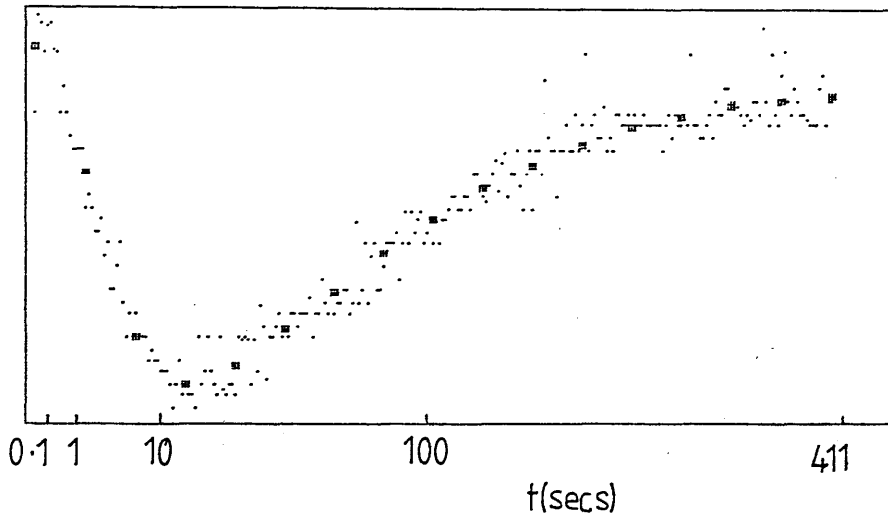
The schiff base hydrolysis reactions in figures 4.16-4.20 are in Ammonyx detergent at pH 4,5,6 and 7. The rapid formation of an intermediate, within the first 10 seconds approximately, can be seen clearly in the traces recorded at pH 4 and 5 (figs.4.16-4.18). This is followed by a slower reaction as the intermediate decays to form the hydrolysis products. Representative traces are shown in the figures, and similar traces were obtained over the wavelength range covered.

The effect is very much less marked at pH 6 when the hydrolysis reaction is slower (fig.4.19), and at pH 7 the intermediate formation is not apparent at all (fig.4.20). These traces are however still very well represented by the 2 component mainframe fit. This suggests that there is again a two stage reaction occurring at high pH, but the intermediate formation is not so obvious on the stopped-flow traces because there is less intermediate

FIGURE 4.16

Stopped-flow traces of schiff base hydrolysis reaction in acetate buffer pH4/Ammonyx. Timing sequence is arithmetic with DT=12.5msec and total time=411secs.

a.  $\lambda=340\text{nm}$



b.  $\lambda=370\text{nm}$

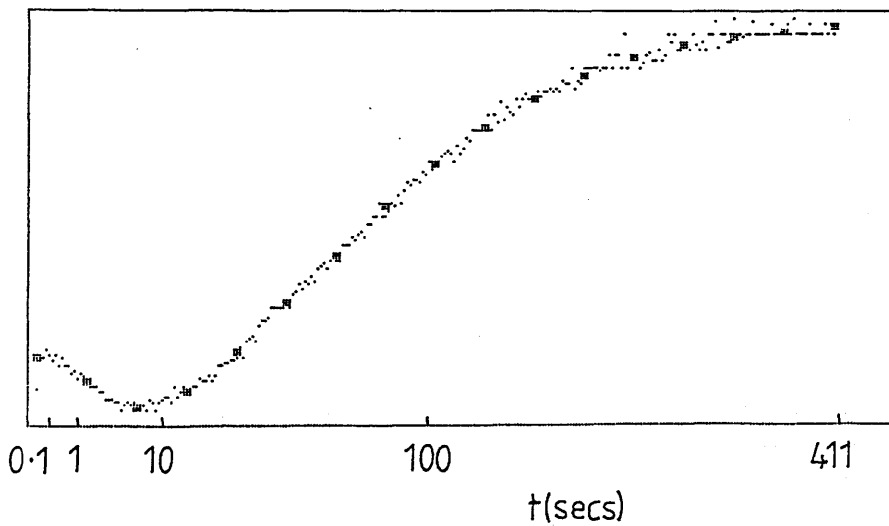
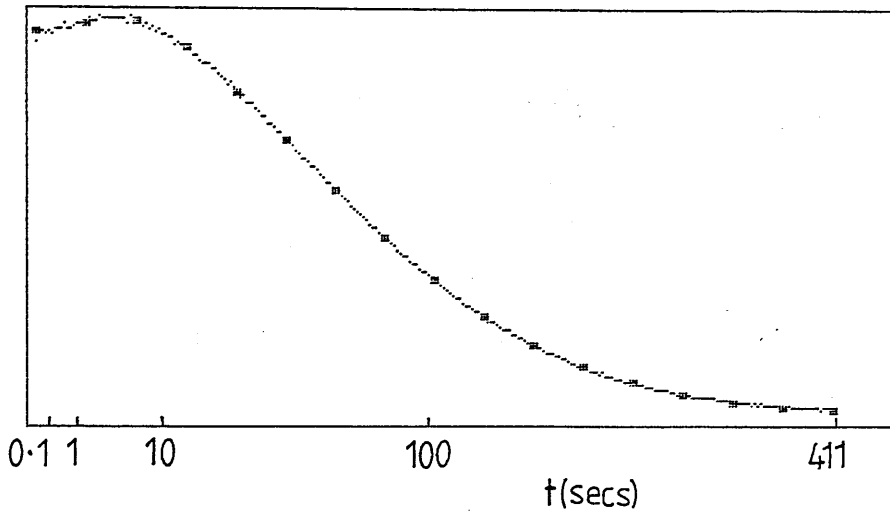


FIGURE 4.16 (cont.)

c.  $\lambda = 460\text{nm}$



d.  $\lambda = 520\text{nm}$

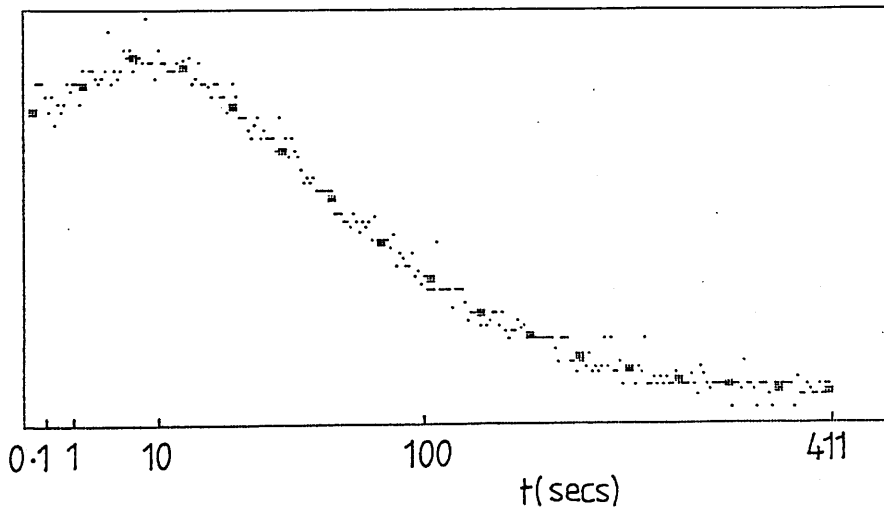
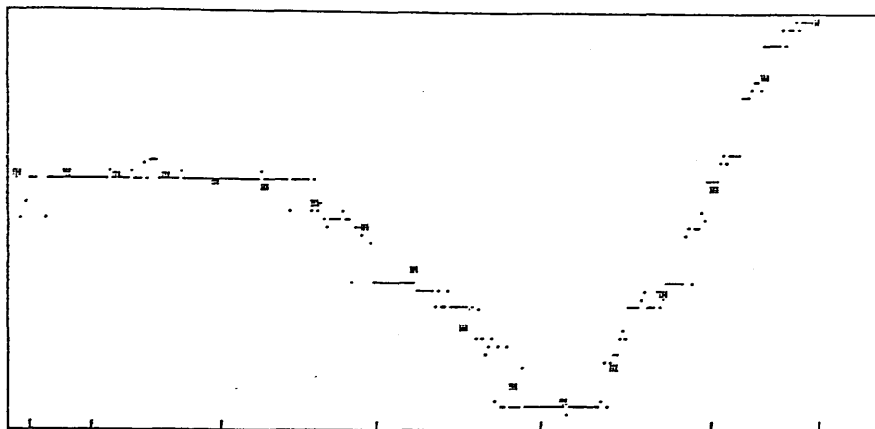


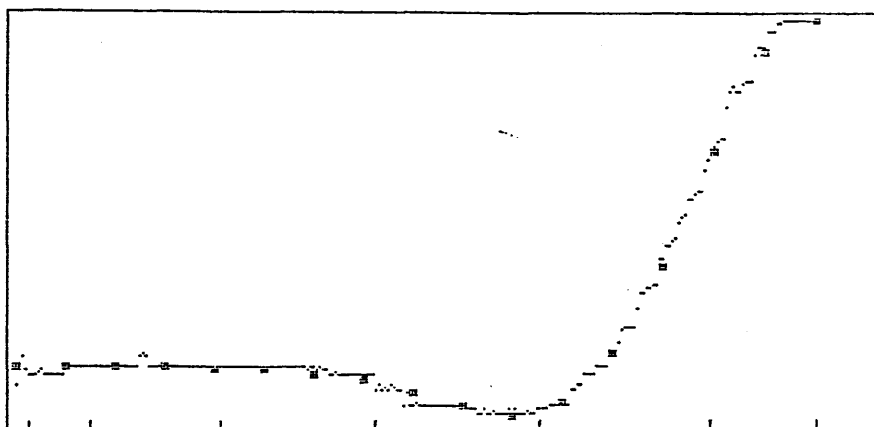
FIGURE 4.17

Stopped-flow traces of schiff base hydrolysis reaction in acetate buffer pH4/Ammonyx. Timing sequence is geometric with  $DT=0.25\text{msec}$ ,  $N=16$  and total time= $420\text{secs}$ .

a.  $\lambda=340\text{nm}$



b.  $\lambda=370\text{nm}$



c.  $\lambda=480\text{nm}$

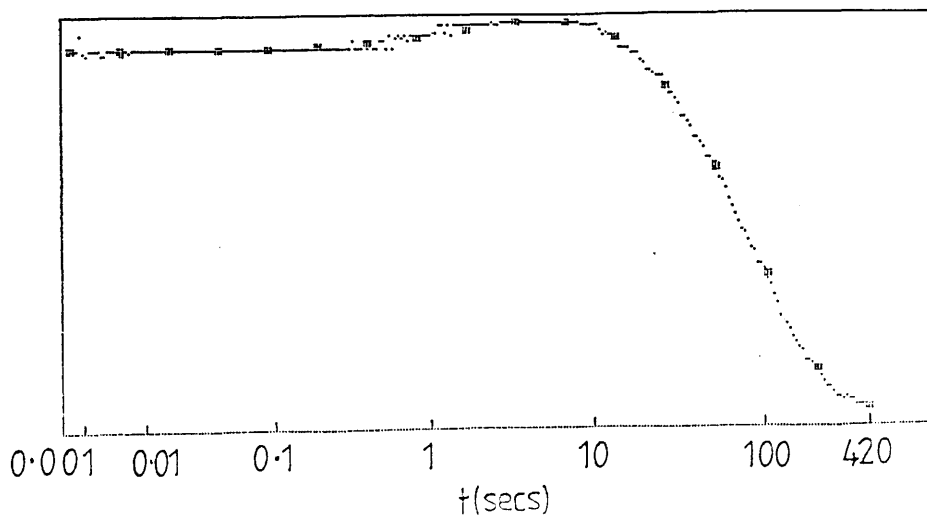
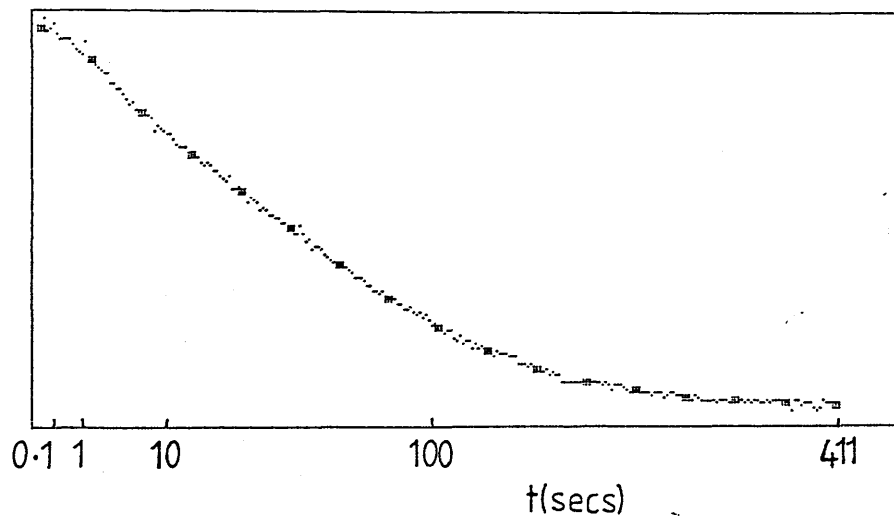


FIGURE 4.18

Stopped-flow traces of schiff base hydrolysis reaction in acetate buffer pH5/Ammonyx. Timing sequence is arithmetic with DT=12.5msec and total time=411secs.

a.  $\lambda=340\text{nm}$



b.  $\lambda=370\text{nm}$

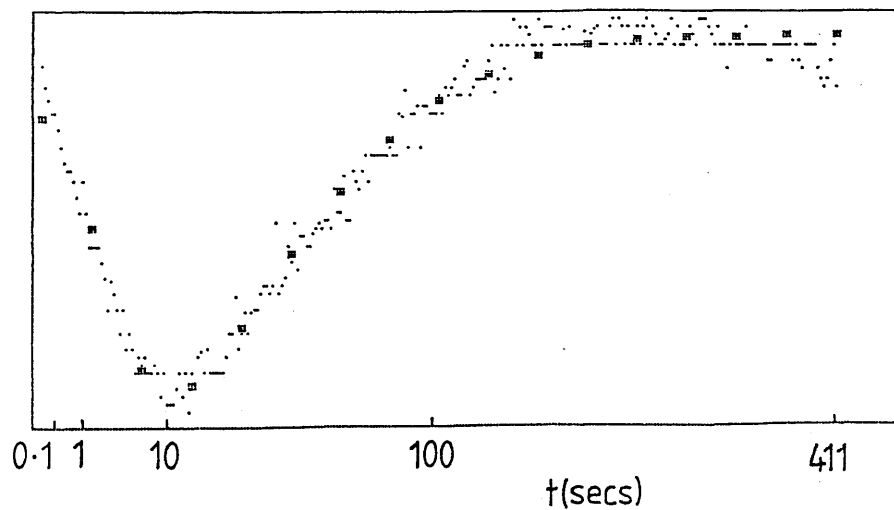
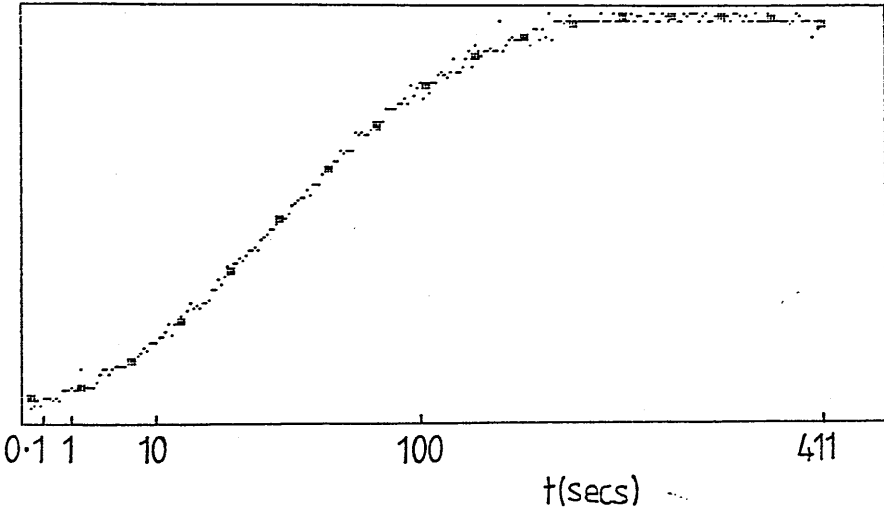


FIGURE 4.18 (cont.)

c.  $\lambda=400\text{nm}$



d.  $\lambda=460\text{ nm}$

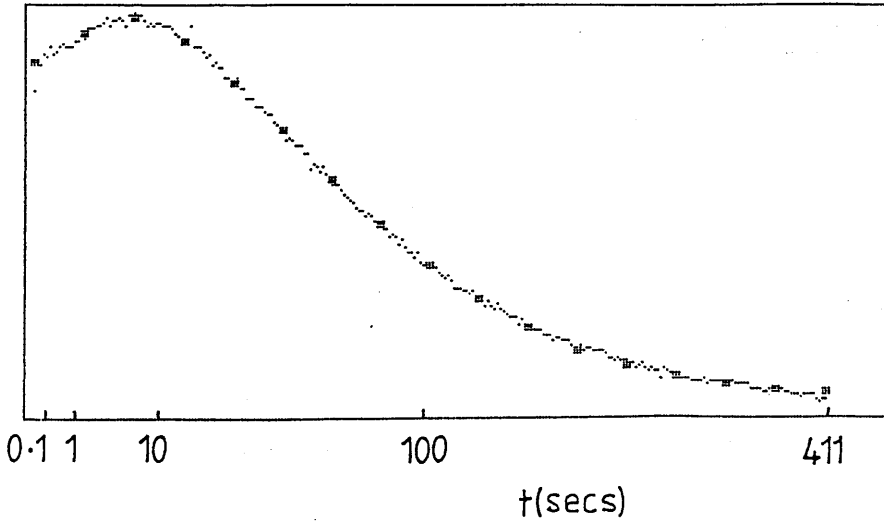
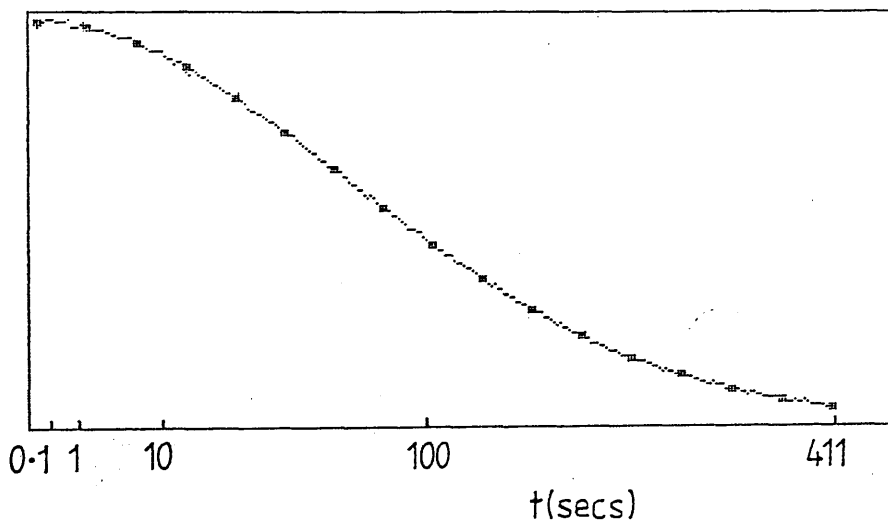


FIGURE 4.19

Stopped-flow traces of schiff base hydrolysis reaction in phosphate buffer pH6/Ammonyx. Timing sequence in (a) and (b) is arithmetic with  $DT=12.5\text{msec}$  and total time=411secs and in (c) and (d) is geometric with  $DT=0.25\text{msec}$ ,  $N=16$  and total time=420secs.

a.  $\lambda=340\text{nm}$



b.  $\lambda=430\text{nm}$

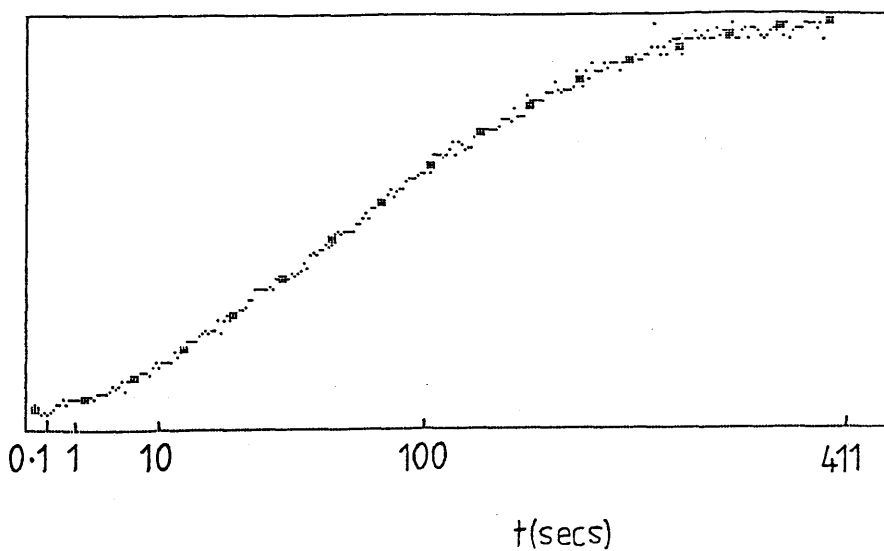
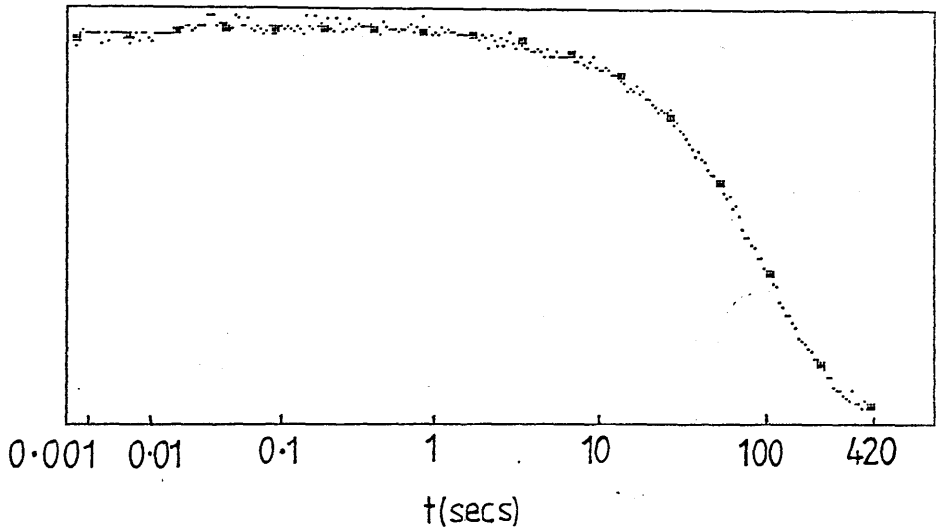


FIGURE 4.19 (cont.)

c.  $\lambda=330\text{nm}$



d.  $\lambda = 410\text{nm}$

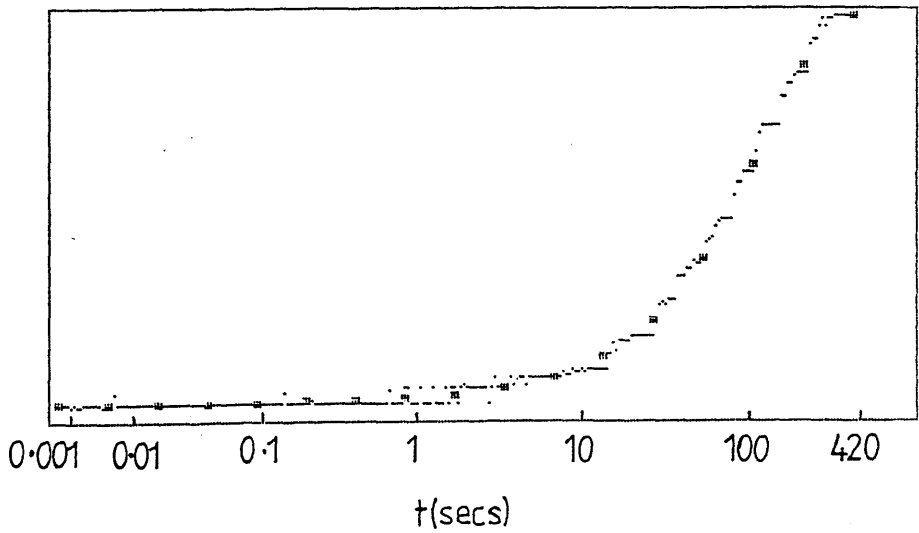
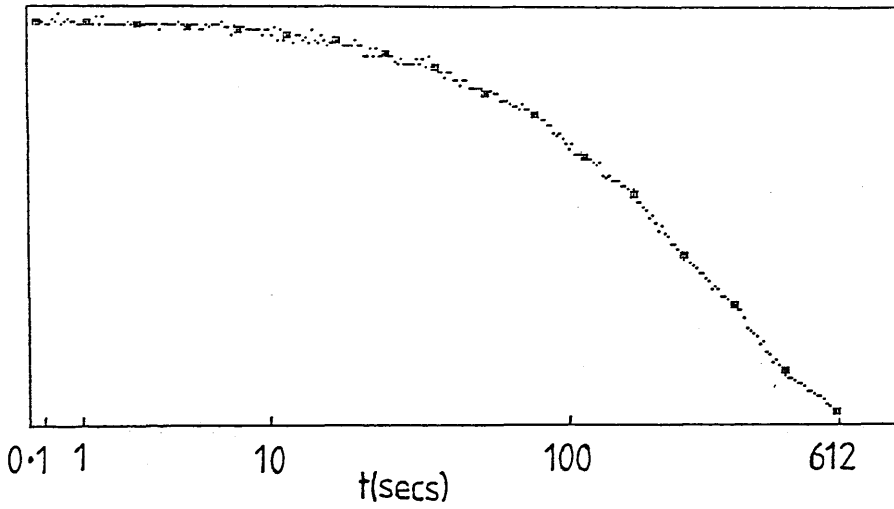


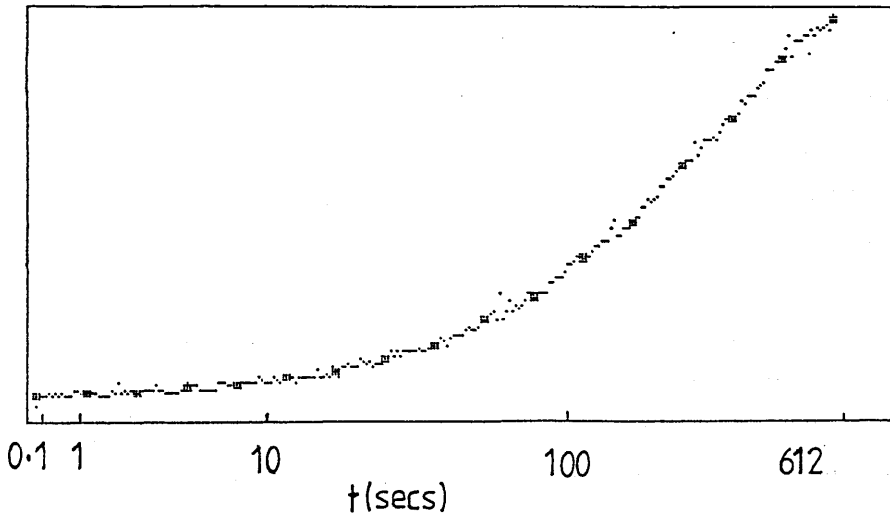
FIGURE 4.20

Stopped-flow traces of schiff base hydrolysis reaction in phosphate buffer pH7/Ammonyx. Timing sequence is geometric with DT=75msec, N=32 and total time=612secs.

a.  $\lambda=350\text{nm}$



b.  $\lambda=420\text{nm}$



present at these pH values.

These experiments in Emulphogene and Ammonyx showed that the intermediate formation is most apparent near the peak in the pH-rate curves i.e. near the pH value where the rate of reaction is greatest. Previous steady-state studies<sup>6,9</sup> have shown that in DTAB the maximum on the pH rate curve is at approximately pH 5.5 and so the hydrolysis reaction was studied at this pH (fig.4.21). Once again the formation and decay of an intermediate species is apparent during the hydrolysis of the schiff base. The intermediate is formed within approximately 50 seconds of mixing when DTAB is the detergent.

The traces in figs.4.22-4.24 show the change in absorbance when the hydrolysis reaction is studied in SDS detergent at pH 9,10 and 11 respectively. The maximum in the pH-rate curve when SDS is the detergent is around pH 11. It can be seen from figs.4.22-4.24 that the intermediate formation occurs within approximately 50 seconds at pH 10 and 11 and is less apparent at pH 9. Again the best fits obtained for a 2 component reaction are shown where possible and in all cases the results suggest that an intermediate is formed during schiff base hydrolysis.

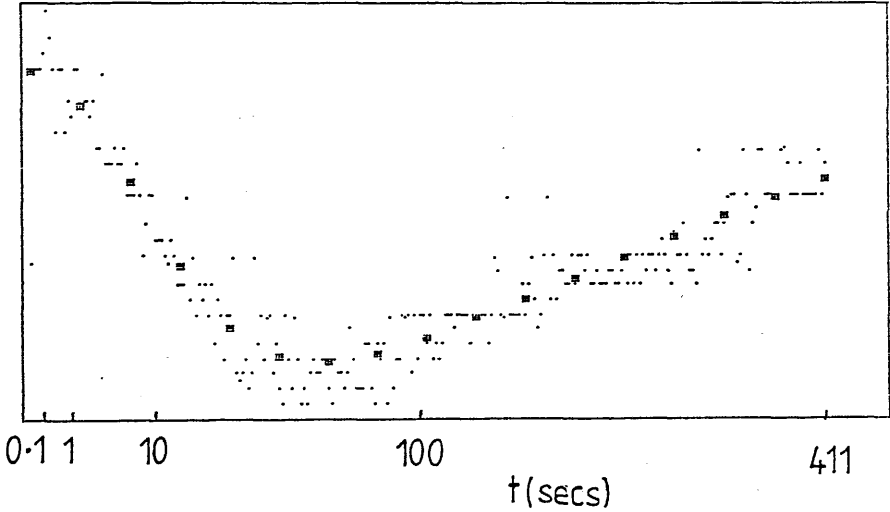
#### 4.4 Kinetic Results

The data obtained from the schiff base hydrolysis reactions studied using the stopped-flow apparatus were analysed on the mainframe computer using the Discrete program. The results obtained in most cases gave a best fit as two components, regardless of whether the detergent was Emulphogene, Ammonyx, DTAB or SDS. This analysis provides evidence that an intermediate species is formed during the hydrolysis reaction, so that the forward reaction is a two stage  $A \rightarrow B \rightarrow C$  type reaction with rate constants  $\lambda_1$  and  $\lambda_2$ .

FIGURE 4.21

Stopped-flow traces of schiff base hydrolysis reaction in acetate buffer pH5.5/DTAB. Timing sequence is arithmetic with DT=12.5msec and total time=411secs.

a.  $\lambda = 350\text{nm}$



b.  $\lambda = 360\text{nm}$

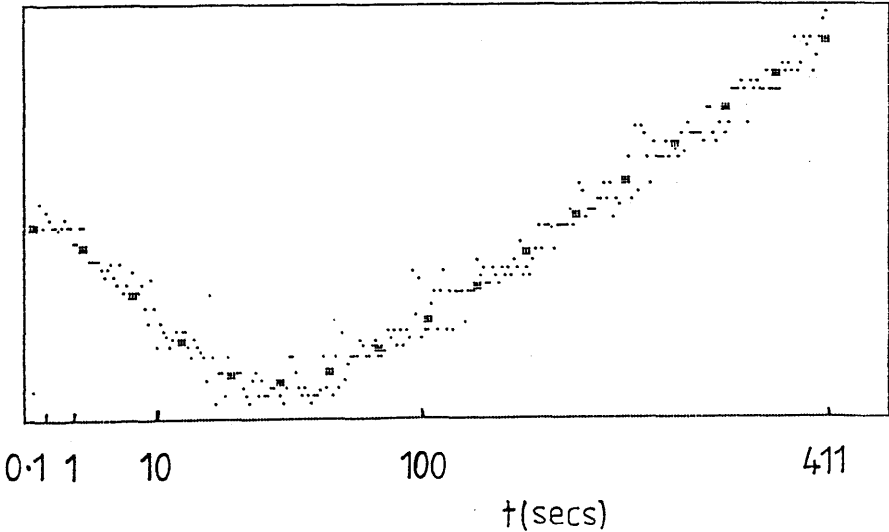
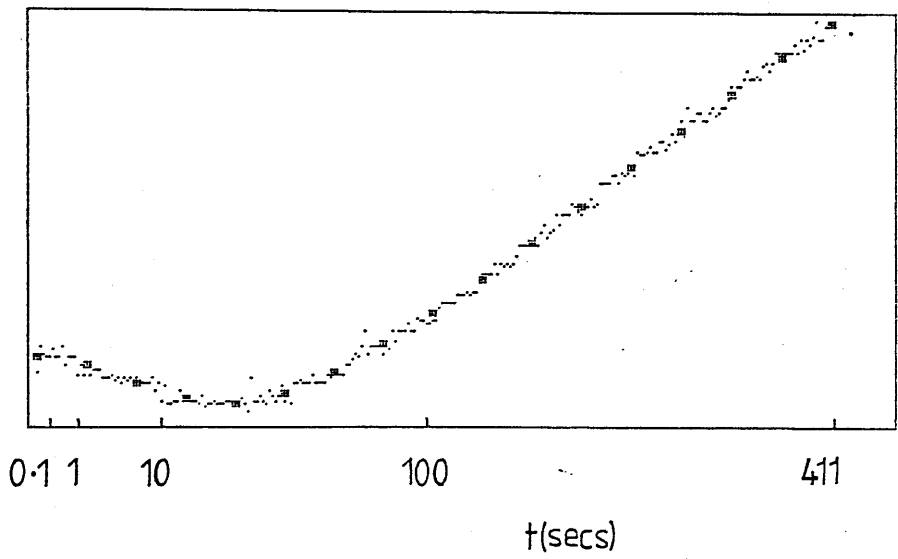


FIGURE 4.21 (cont.)

c.  $\lambda=380\text{nm}$



d.  $\lambda=410\text{nm}$

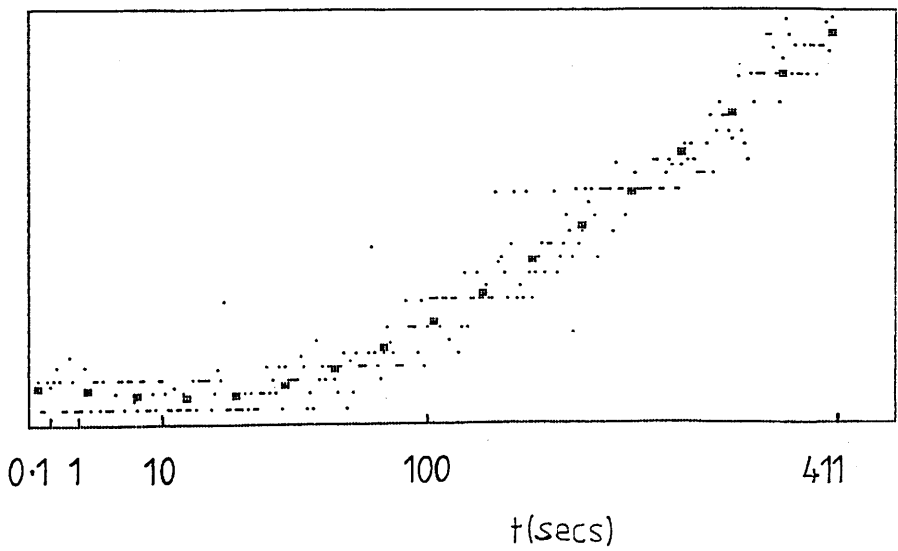
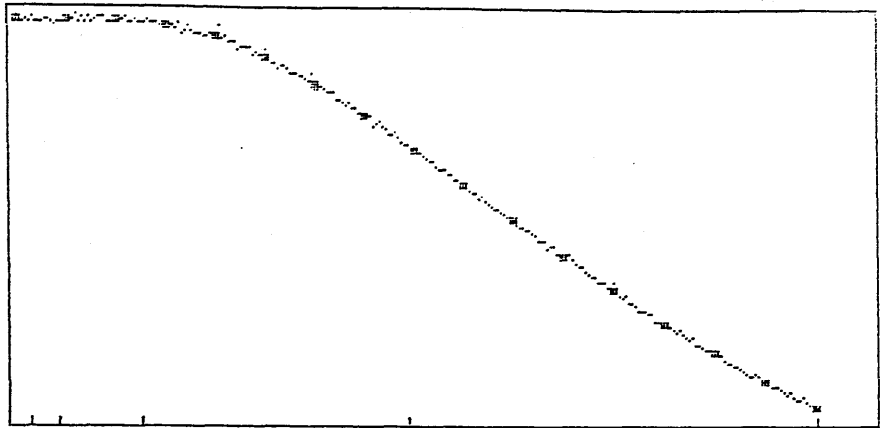
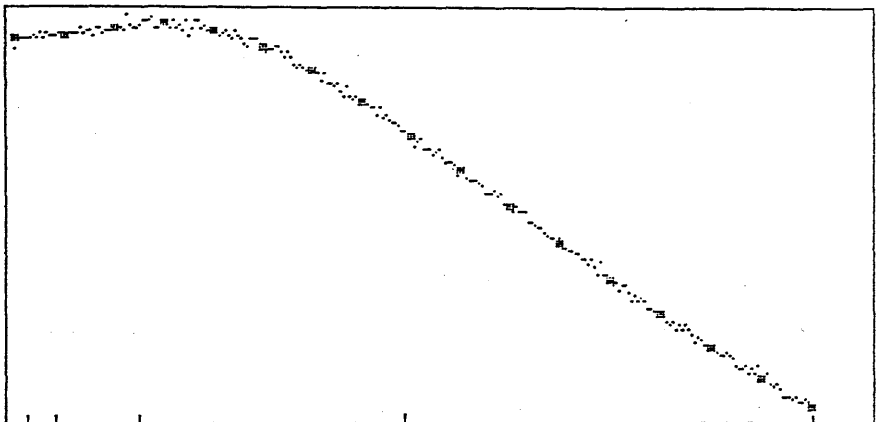


FIGURE 4.21 (cont.)

e.  $\lambda=450\text{nm}$



f.  $\lambda=480\text{nm}$



g.  $\lambda=530\text{nm}$

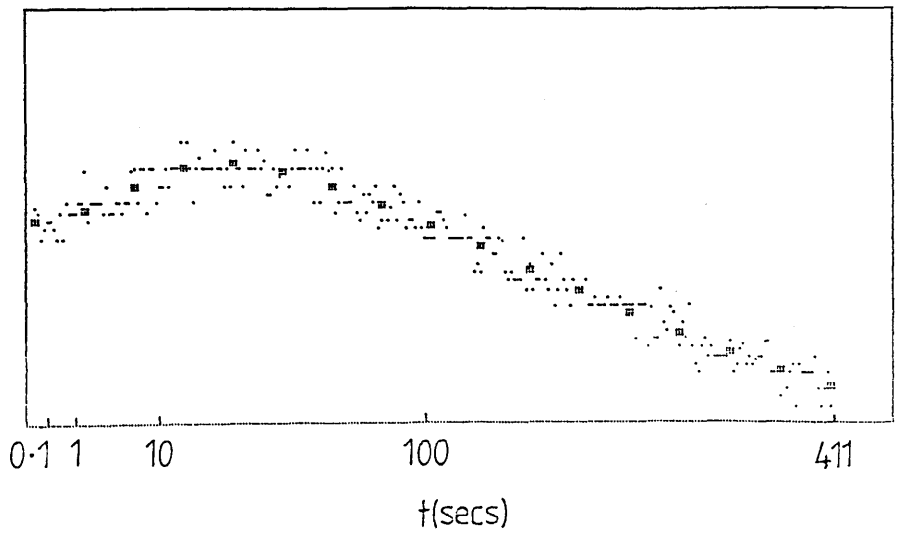
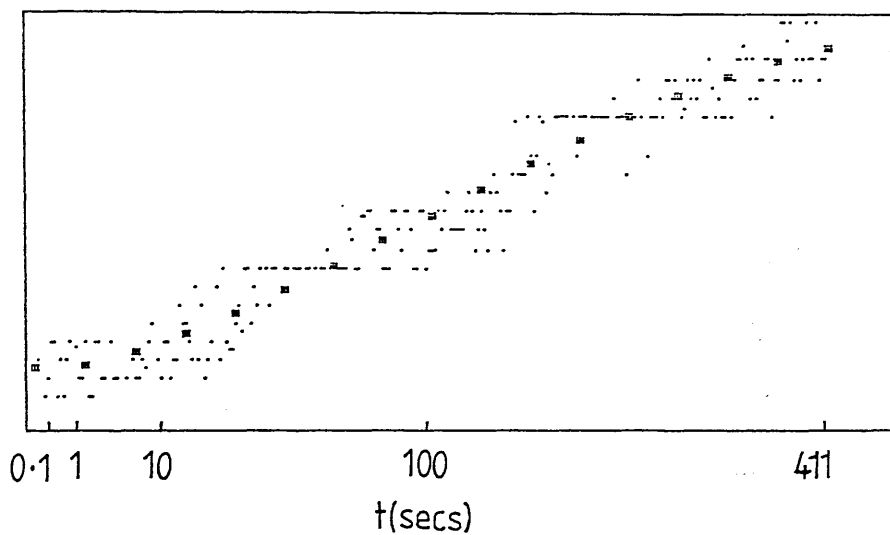


FIGURE 4.22

Stopped-flow traces of schiff base hydrolysis reaction in borate buffer pH9/SDS. Timing sequence is arithmetic with DT=12.5msec and total time=411secs.

a.  $\lambda=370\text{nm}$



b.  $\lambda=460\text{nm}$

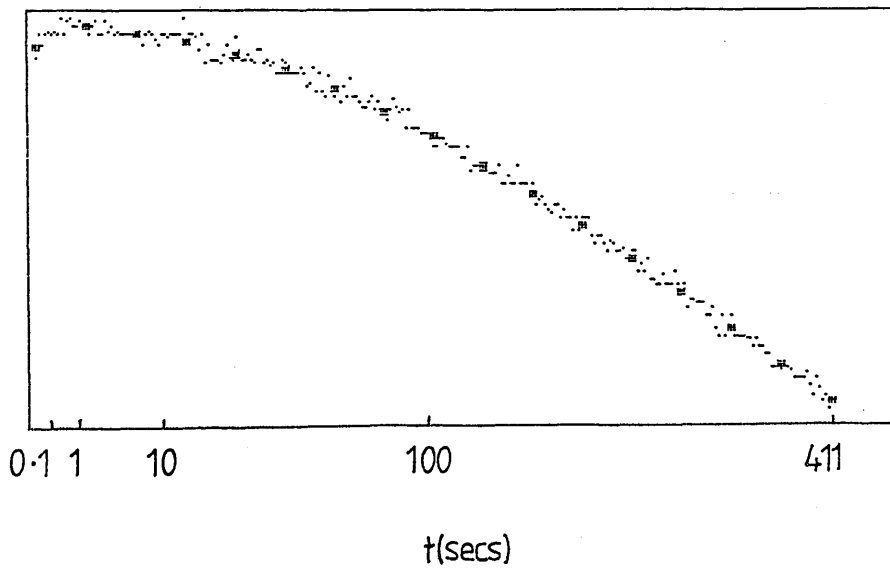
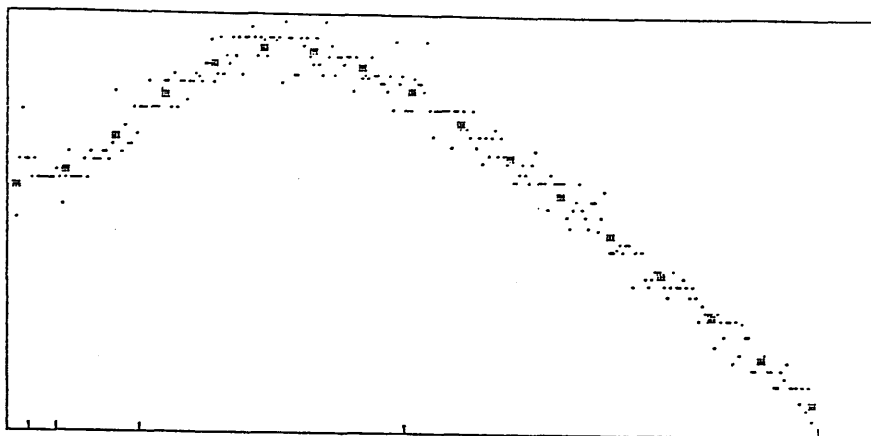


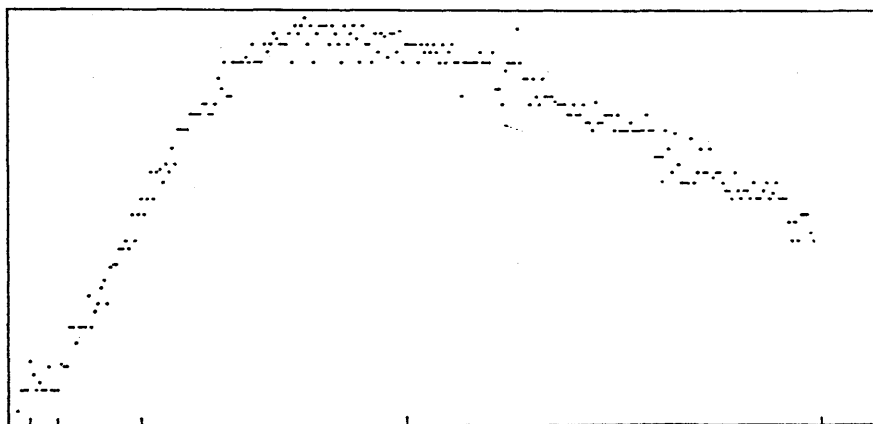
FIGURE 4.23

Stopped-flow traces of schiff base hydrolysis reaction in borate buffer pH10/SDS. Timing sequence is arithmetic with DT=12.5msec and total time=411secs.

a.  $\lambda=340\text{nm}$



b.  $\lambda=360\text{nm}$



c.  $\lambda=370\text{nm}$

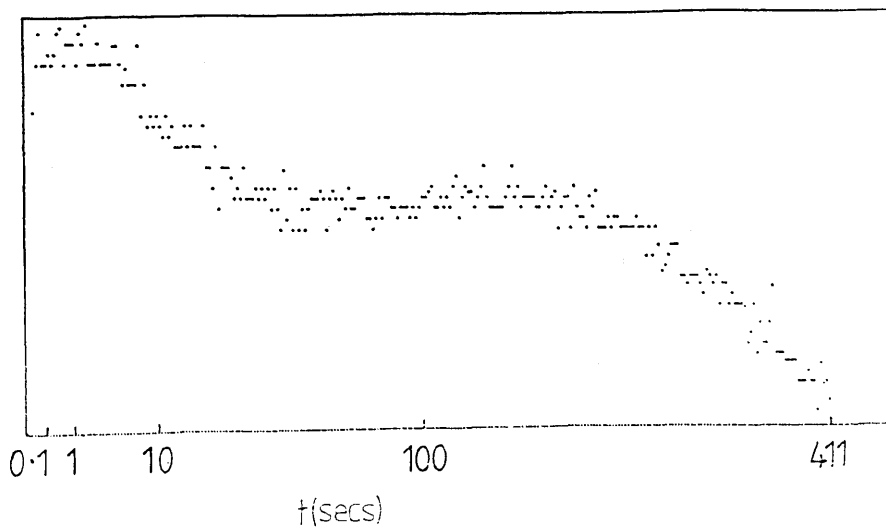
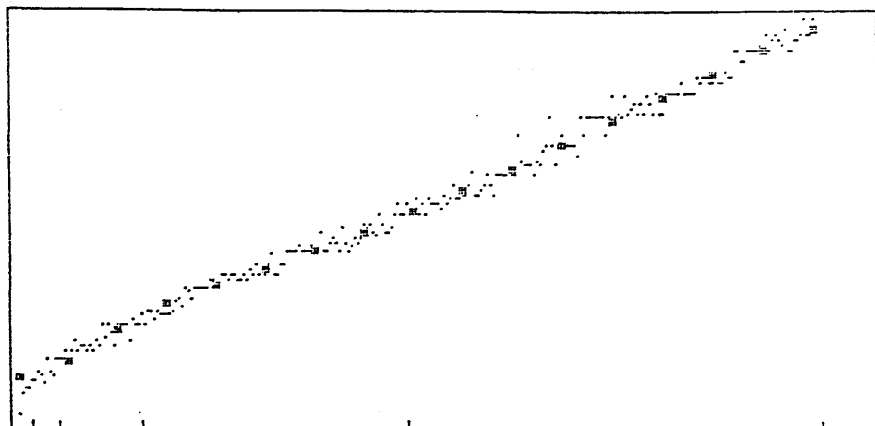
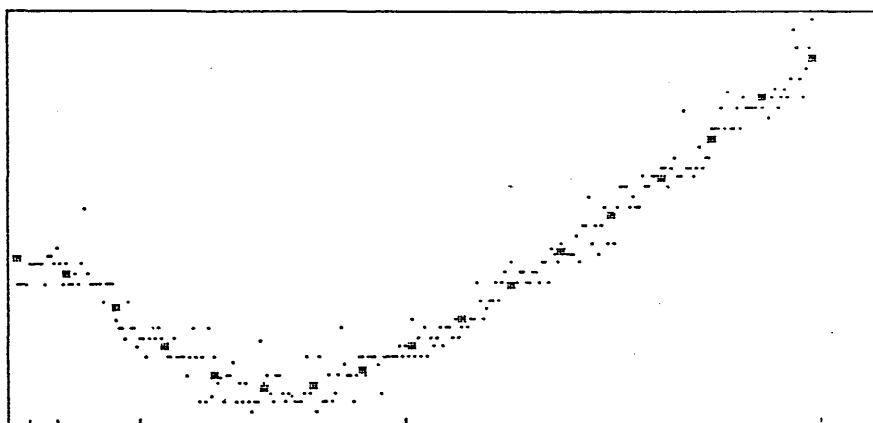


FIGURE 4.23 (cont.)

d.  $\lambda=390\text{nm}$



e.  $\lambda=420\text{nm}$



f.  $\lambda=460\text{nm}$

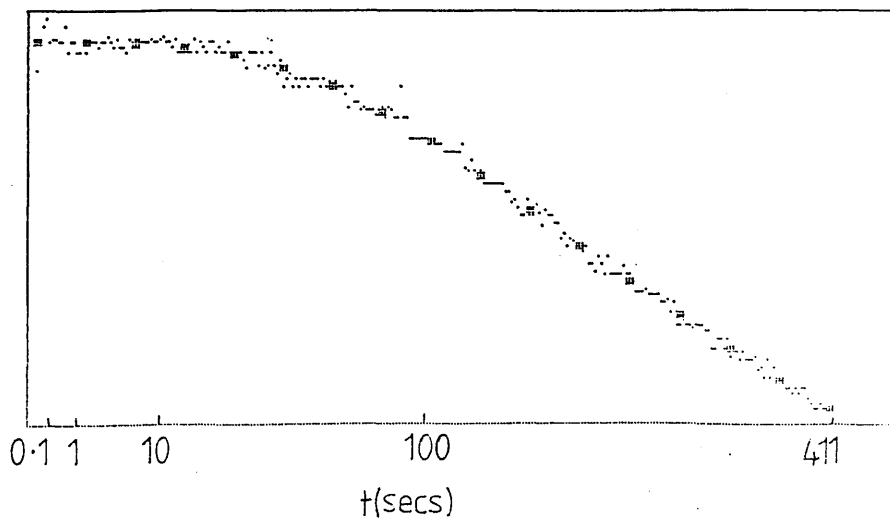
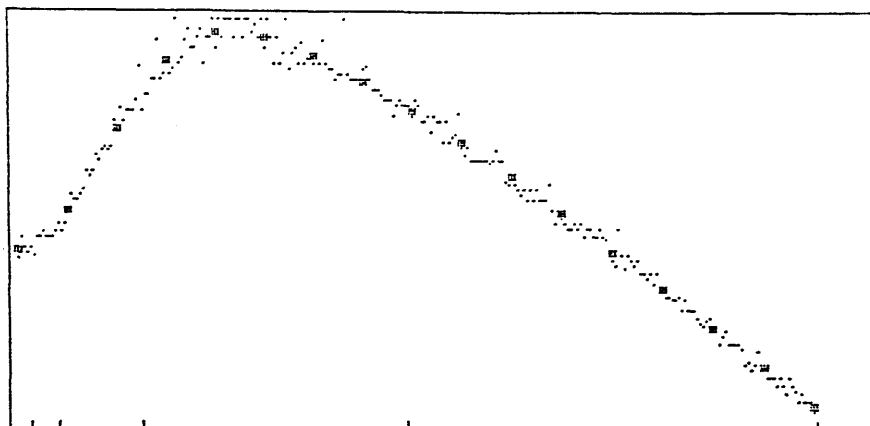


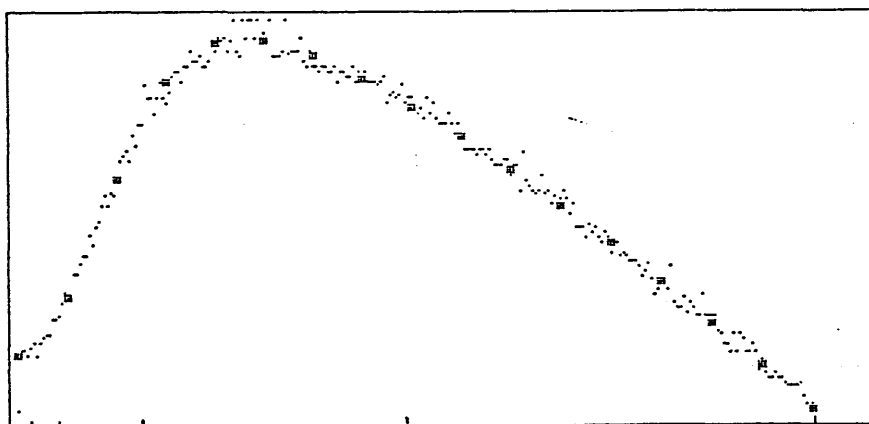
FIGURE 4.24

Stopped-flow traces of schiff base hydrolysis reaction in borate buffer pH11/SDS. Timing sequence is arithmetic with  $DT=12.5\text{msec}$  and total time= $411\text{secs}$ .

a.  $\lambda=340\text{nm}$



b.  $\lambda=360\text{nm}$



c.  $\lambda=380\text{nm}$

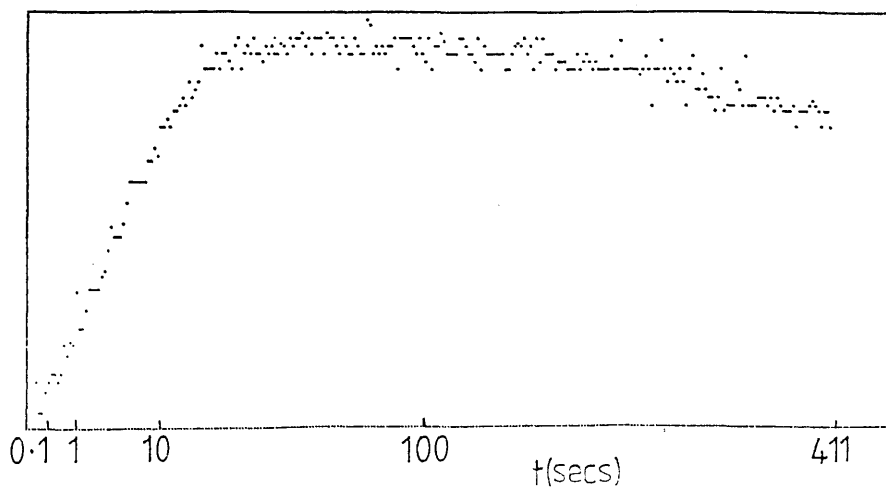
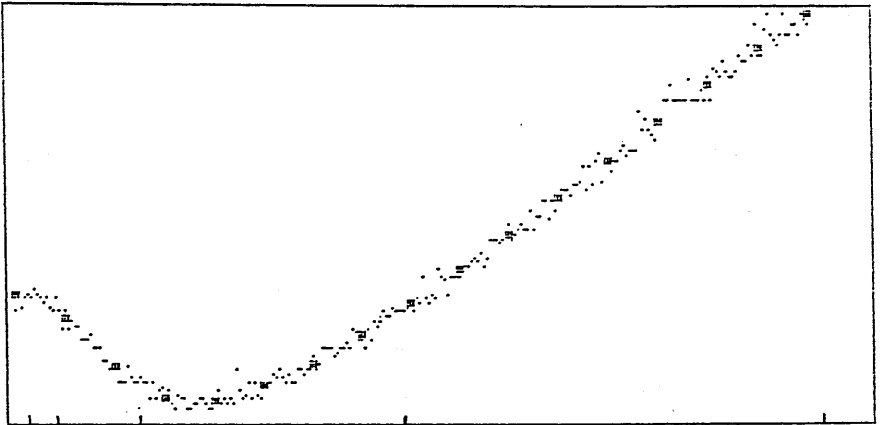
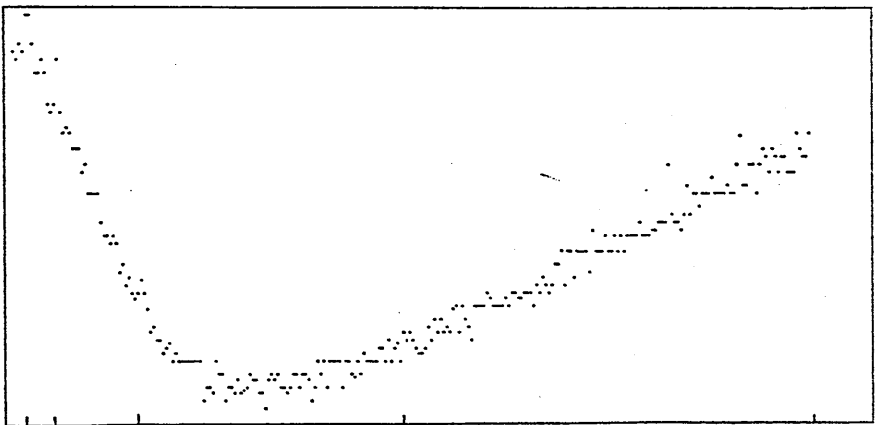


FIGURE 4.24 (cont.)

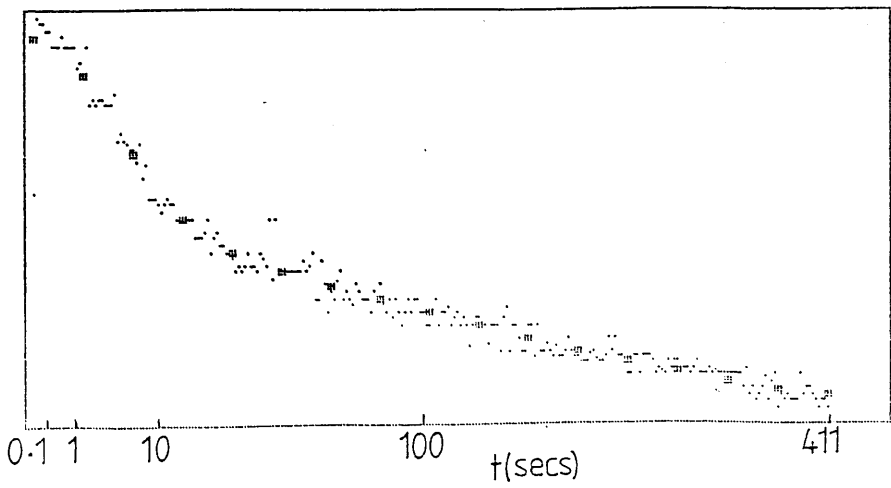
d.  $\lambda=420\text{nm}$



e.  $\lambda=440\text{nm}$



f.  $\lambda=500\text{nm}$



From the mainframe analysis, values of  $\alpha_0$ ,  $\alpha_1$ ,  $\alpha_2$ ,  $\lambda_1$  and  $\lambda_2$  are obtained for a two component fit, as discussed previously from equation 2.13.

$$A(t) = \alpha_0 + \alpha_1 (\exp - \lambda_1 t) + \alpha_2 (\exp - \lambda_2 t) + \dots \quad (2.13)$$

Tables 4.1-4.4 show typical examples of the rate constants obtained in the hydrolysis reactions in Emulphogene, Ammonyx, DTAB and SDS respectively, and similar results were obtained at other pH values.

In table 4.1 it can be seen that there is a wide variation in values of  $\lambda_2$ , especially at high and low wavelengths. This is probably due to the fact that the hydrolysis reaction in Emulphogene is slow and this will result in small absorbance changes during the reaction in the timescale covered. The results for  $\lambda_2$  obtained from the stopped-flow experiments in Emulphogene are probably too high because the reaction does not go to completion in the time-scale of the experiments. Steady-state rate constants for the hydrolysis reaction in Emulphogene will be more accurate than  $\lambda_2$  values. As with the formation reactions, values of rate constants obtained at wavelengths which are near to the isosbestic point(s) are sometimes anomalous.

Table 4.5 lists the average rate constants for the schiff base hydrolysis reactions at different pH values in the various detergents. These values were obtained by averaging the results of rate constants  $\lambda_1$  and  $\lambda_2$  for each reaction over every wavelength and different timing sequences.

Examination of results in tables 4.1-4.4 illustrates that in each of the detergents the value of rate constant  $\lambda_1$  is much larger than that of  $\lambda_2$  and the value of  $\lambda_1$  with Ammonyx as detergent is much larger than with the other detergents.

In table 4.5  $\lambda_1$  and  $\lambda_2$  values for Emulphogene at pH 4 and  $\lambda_1$  value at pH 7 are omitted. At pH 4 the mainframe Discrete program would not analyse the data because, even when using a timescale with a long total time of 612

Table 4.1

Table showing values of rate constants obtained during schiff base hydrolysis reaction in Emulphogene at pH 6 during a geometric run.

Wavelength(nm)	Rate constant $\lambda_1$ ( $\text{min}^{-1}$ )	Rate constant $\lambda_2$ ( $\text{min}^{-1}$ )
340	1.894	0.882
350	1.690	0.554
370	1.455	0.264
380	1.630	0.101
390	0.814	0.291
420	1.331	0.265
430	1.687	0.122
440	1.843	0.117
450	1.697	0.118
460	1.993	0.110
470	1.715	0.106
480	1.500	0.106
490	1.786	0.089
	Mean = 1.685	Mean = 0.140
	S.D. = 0.188	S.D. = 0.066

(excluding 390nm in each case, and also 340nm and 350nm for  $\lambda_2$  - see text)

Table 4.2

Table showing rate constants obtained during schiff base hydrolysis reaction in Ammonyx at pH 4 during a geometric run.

Wavelength(nm)	Rate constant $\lambda_1$ (min <sup>-1</sup> )	Rate constant $\lambda_2$ (min <sup>-1</sup> )
330	15.312	0.580
340	16.128	0.501
350	18.324	0.513
360	16.998	0.627
370	14.766	0.658
380	10.008	0.737
390	13.692	0.713
400	10.452	0.895
410	24.030	0.281
420	19.908	0.550
430	18.042	0.628
440	20.016	0.650
450	11.940	0.728
460	13.980	0.682
470	11.844	0.680
480	16.146	0.668
490	14.544	0.670
500	17.976	0.642
510	11.814	0.664
520	14.100	0.715
530	12.588	0.724

Mean = 14.929      Mean = 0.661  
S.D. = 2.988      S.D. = 0.087

(excluding 410nm)

Table 4.3

Table showing rate constants obtained during schiff base hydrolysis reaction in DTAB at pH 5.5 during an arithmetic run.

Wavelength(nm)	Rate constant $\lambda_1$ (min <sup>-1</sup> )	Rate constant $\lambda_2$ (min <sup>-1</sup> )
330	4.270	0.238
350	3.618	0.145
360	3.518	0.134
370	3.547	0.126
380	3.847	0.135
390	3.924	0.138
400	4.675	0.106
410	2.830	0.060
420	4.033	0.287
430	7.068	0.210
440	5.414	0.206
450	3.721	0.201
460	4.271	0.201
470	3.725	0.196
480	3.822	0.179
490	3.085	0.184
530	4.781	0.201

Mean = 4.207      Mean = 0.180  
S.D. = 0.951      S.D. = 0.047

(excluding 410nm)

Table 4.4

Table showing rate constants obtained during schiff base hydrolysis reaction in SDS at pH 10 during an arithmetic run.

Wavelength(nm)	Rate constant $\lambda_1$ ( $\text{min}^{-1}$ )	Rate constant $\lambda_2$ ( $\text{min}^{-1}$ )
340	2.661	0.066
350	3.035	0.037
360	0.691	0.122
390	7.824	0.134
400	5.122	0.121
410	1.711	0.079
420	2.792	0.063
430	3.092	0.052
450	0.884	0.213
460	1.427	0.182
470	0.344	0.171
480	2.704	0.160
	Mean = 2.691	Mean = 0.117
	S.D. = 2.086	S.D. = 0.057

Table 4.5

Table showing average rate constants for the schiff base hydrolysis reaction in Ammonyx, Emulphogene, DTAB and SDS detergents at different pH values.

	pH	$\lambda_1$ (min <sup>-1</sup> )	$\lambda_2$ (min <sup>-1</sup> )
Ammonyx	4	14.598 (3.180)	0.651 (0.082)
	5	17.277 (6.828)	0.890 (0.063)
	6	13.412 (4.642)	0.497 (0.047)
	7	1.129 (0.573)	0.197 (0.042)
Emulphogene	4	-	-
	5	1.797 (0.576)	0.094 (0.038)
	6	1.593 (0.202)	0.147 (0.071)
	7	-	0.176 (0.066)
DTAB	5.5	4.126 (0.955)	0.173 (0.045)
SDS	9	11.862 (1.882)	0.134 (0.089)
	10	2.691 (2.086)	0.117 (0.057)
	11	6.540 (0.438)	0.130 (0.083)

(Figures in brackets are standard deviations.)

seconds, the reaction has hardly progressed during the data acquisition time. At pH 7, again the reaction is slow and although mainframe analysis was possible, the values of  $\lambda_1$  obtained over the wavelength range were not very consistent.

Comparison of the results in table 4.5 with those in table 4.6 shows that there is quite good agreement in the values of  $\lambda_2$  obtained from the non-steady-state analysis and values of  $k_n$  obtained from steady-state analysis. The values in table 4.6 were obtained from figure 1.17. As was previously mentioned, the steady-state values will be more accurate for Emulphogene because the complete reaction is not followed in the stopped-flow experiments. Values of  $\lambda_1$  cannot be obtained by the steady-state method.

The values of  $\alpha$  and  $\lambda$  obtained from the mainframe analysis of the hydrolysis reactions can be used to construct spectra of retinal and the schiff base in a similar way to the formation reactions. In the hydrolysis reactions when  $t=0$ ,  $A=\alpha_0+\alpha_1+\alpha_2$  from equation 2.13. In this case it is the schiff base that is present at the start of reaction (when  $t=0$ ) and so a plot of  $A$  versus wavelength will give the schiff base spectrum. At the end of reaction  $A=\alpha_0$  and a plot of  $\alpha_0$  values versus wavelength should produce a spectrum of retinal which is the absorbing species present after hydrolysis has occurred.

Table 4.7 shows  $\alpha_0$ ,  $\alpha_1$ ,  $\alpha_2$ ,  $\lambda_1$  and  $\lambda_2$  values for the hydrolysis reaction in Ammonyx at pH 4, along with the calculated values of  $A=\alpha_0+\alpha_1+\alpha_2$ . Figure 4.25 shows the spectra of retinal and schiff base obtained using these values. It can be seen that immediately after mixing with the buffer solution at pH 4, the majority of schiff base is in the protonated form with maximum absorbance around 440nm.

Tables 4.8 and 4.9 show  $\alpha$  and  $\lambda$  values for the hydrolysis reaction in Ammonyx at pH 5 and pH 6 respectively, and figures 4.26, 4.27 the spectra of retinal and schiff base created from these values. At pH 5 the schiff base is mostly in the unprotonated form with

Table 4.6

Table showing steady-state rate constants for the schiff base hydrolysis reaction in Ammonyx, Emulphogene, DTAB and SDS detergents at different pH values.

Detergent	pH	$\log k_h (\text{sec}^{-1})$	
		from steady-state anal. (approx values)	$k_h (\text{min}^{-1})$ from steady-state analysis
Ammonyx	4.22	-2.2	0.379
	5.04	-1.9	0.755
	6.23	-2.1	0.477
	7.17	-2.5	0.190
Emulphogene	4.12	-3.5	0.019
	5.09	-3.3	0.030
	6.26	-3.5	0.019
	7.23	-3.7	0.012
DTAB	5.65	-2.4	0.239
SDS	9.01	-3.6	0.015
	10.05	-2.8	0.095
	10.65	-2.7	0.120

Table 4.7

Values of  $\alpha_0$ ,  $\alpha_1$  and  $\alpha_2$  from 2 component fit in mainframe analysis of schiff base hydrolysis reaction in Ammonyx at pH 4.

Wavelength(nm)	$\alpha_0$	$\alpha_1$	$\alpha_2$	$A = \alpha_0 + \alpha_1 + \alpha_2$
330	0.1955	0.0175	-0.0189	0.1941
340	0.2230	0.0239	-0.0392	0.2077
350	0.2768	0.0270	-0.0559	0.2479
360	0.3338	0.0312	-0.0896	0.2754
370	0.3929	0.0290	-0.1315	0.2904
380	0.4208	0.0267	-0.1509	0.2966
390	0.4170	0.0137	-0.1293	0.3014
410	0.3145	-0.0104	0.0410	0.3451
420	0.2400	-0.0096	0.1350	0.3654
430	0.1673	-0.0165	0.2160	0.3668
440	0.1122	-0.0251	0.2732	0.3603
450	0.0726	-0.0337	0.2906	0.3295
460	0.0419	-0.0336	0.2818	0.2901
470	0.0243	-0.0340	0.2533	0.2436
480	0.0206	-0.0335	0.2007	0.1878
490	0.0148	-0.0112	0.1395	0.1431
500	0.0184	-0.0220	0.1026	0.0990
510	0.0176	-0.0184	0.0723	0.0715
520	0.0197	-0.0150	0.0447	0.0494
530	0.0161	-0.0090	0.0304	0.0375

FIGURE 4.25  
Reconstructed spectra of retinal and schiff base using  $\alpha_0$ ,  $\alpha_1$ , and  $\alpha_2$  values in Table 4.7.

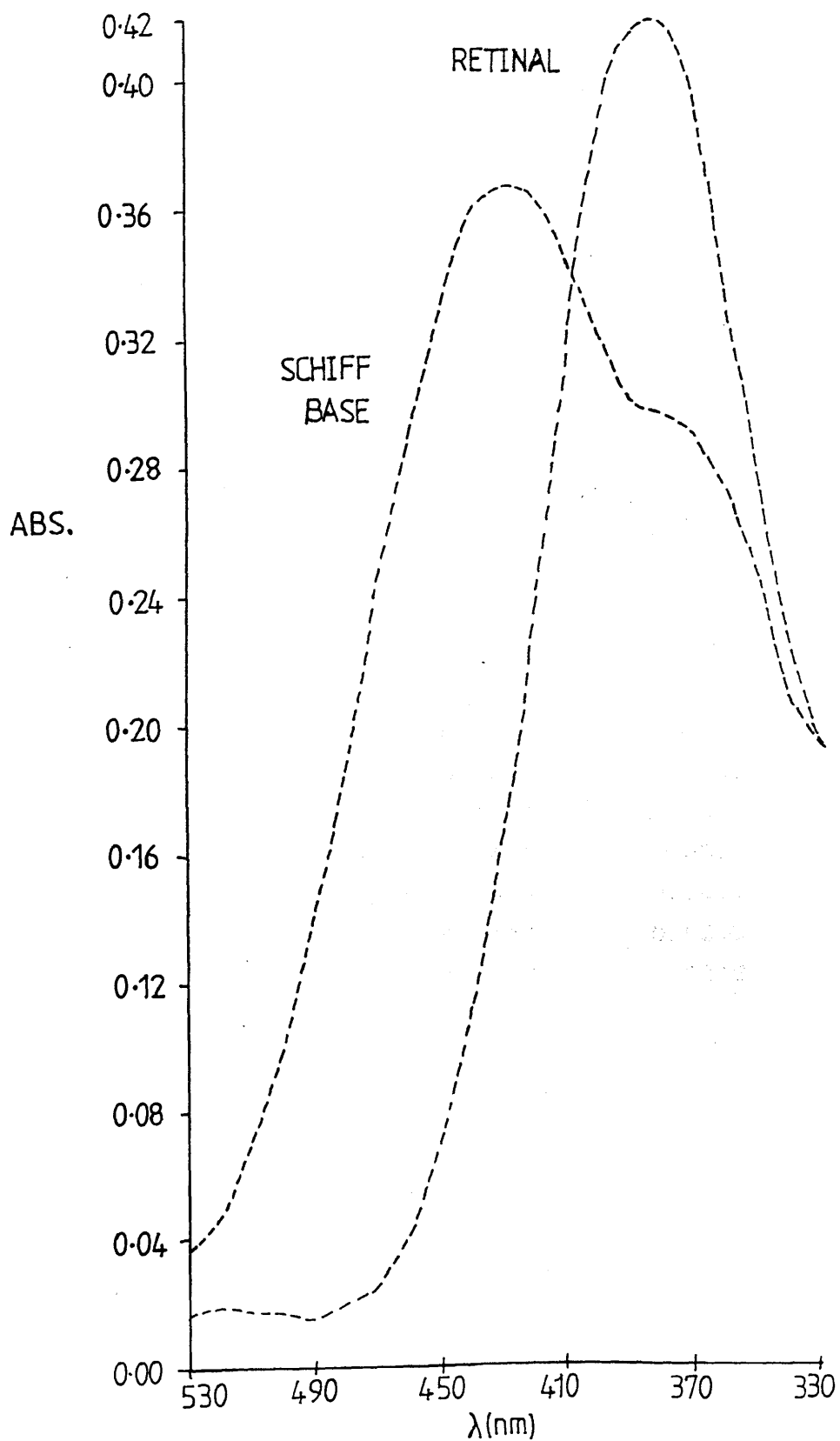


Table 4.8

Values of  $\alpha_0$ ,  $\alpha_1$  and  $\alpha_2$  from 2 component fit in mainframe analysis of schiff base hydrolysis reaction in Ammonyx at pH 5.

Wavelength(nm)	$\alpha_0$	$\alpha_1$	$\alpha_2$	$A = \alpha_0 + \alpha_1 + \alpha_2$
330	0.1839	0.0063	0.0615	0.2517
340	0.2123	0.0128	0.0765	0.3016
350	0.2595	0.0152	0.0777	0.3524
360	0.3130	0.0136	0.0461	0.3727
380	0.3804	0.0108	-0.0661	0.3251
390	0.3885	-0.0084	-0.1096	0.2705
400	0.3497	-0.0051	-0.1171	0.2275
410	0.2822	-0.0074	-0.0804	0.1944
420	0.2029	-0.0089	-0.0152	0.1788
430	0.1487	-0.0130	0.0460	0.1817
440	0.0989	-0.0174	0.0903	0.1718
450	0.0577	-0.0171	0.1092	0.1498
460	0.0351	-0.0177	0.1145	0.1319
470	0.0293	-0.0160	0.1042	0.1175
480	0.0235	-0.0165	0.0834	0.0904
490	0.0174	-0.0118	0.0608	0.0664
500	0.0203	-0.0116	0.0438	0.0525
510	0.0181	-0.0078	0.0308	0.0411
520	0.0117	-0.0079	0.0197	0.0235
530	0.0159	-0.0064	0.0117	0.0212

Table 4.9

Values of  $\alpha_0$ ,  $\alpha_1$  and  $\alpha_2$  from 2 component fit in mainframe analysis of schiff base hydrolysis reaction in Ammonyx at pH 6.

Wavelength(nm)	$\alpha_0$	$\alpha_1$	$\alpha_2$	$A = \alpha_0 + \alpha_1 + \alpha_2$
330	0.1544	-0.0033	0.1090	0.2601
340	0.1823	0.0043	0.1484	0.3350
350	0.2281	0.0044	0.1534	0.3859
360	0.2697	-0.0060	0.1258	0.3895
370	0.3171	-0.0055	0.0747	0.3863
380	0.3465	0.0264	-0.0464	0.3265
390	0.3280	0.0188	-0.1188	0.2280
400	0.2944	0.0077	-0.1426	0.1595
410	0.2452	-0.0014	-0.1342	0.1096
420	0.1852	-0.0040	-0.1029	0.0783
430	0.1250	-0.0057	-0.0571	0.0622
440	0.0842	-0.0045	-0.0237	0.0559
450	0.0572	-0.0053	-0.0050	0.0469
460	0.0247	-0.0030	0.0150	0.0367
470	0.0222	-0.0027	0.0157	0.0352
490	0.0212	-0.0025	0.0115	0.0302

FIGURE 4.26  
Reconstructed spectra of retinal and schiff base using  $\alpha_0$ ,  $\alpha_1$ , and  $\alpha_2$  values in Table 4.8.

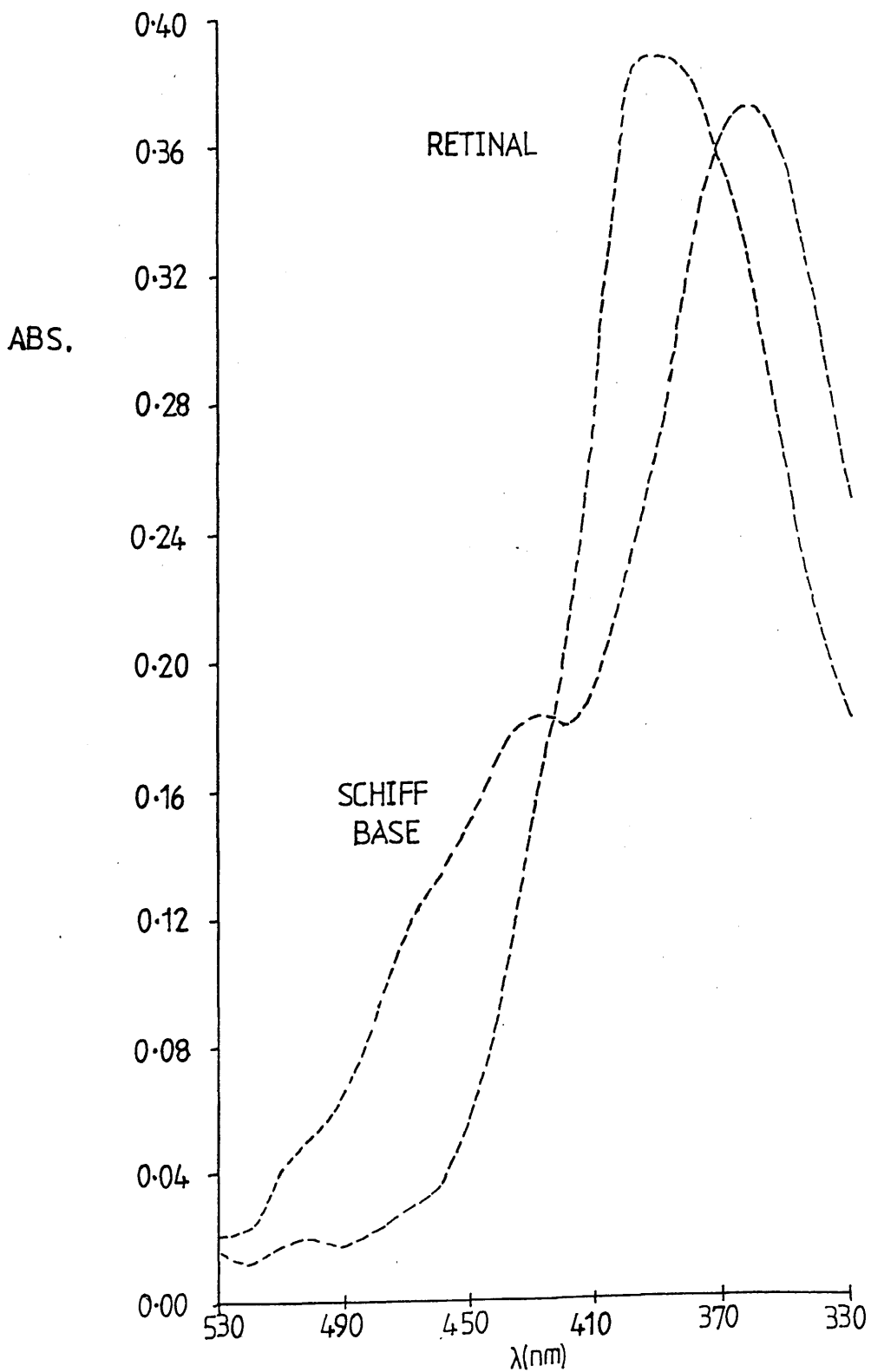
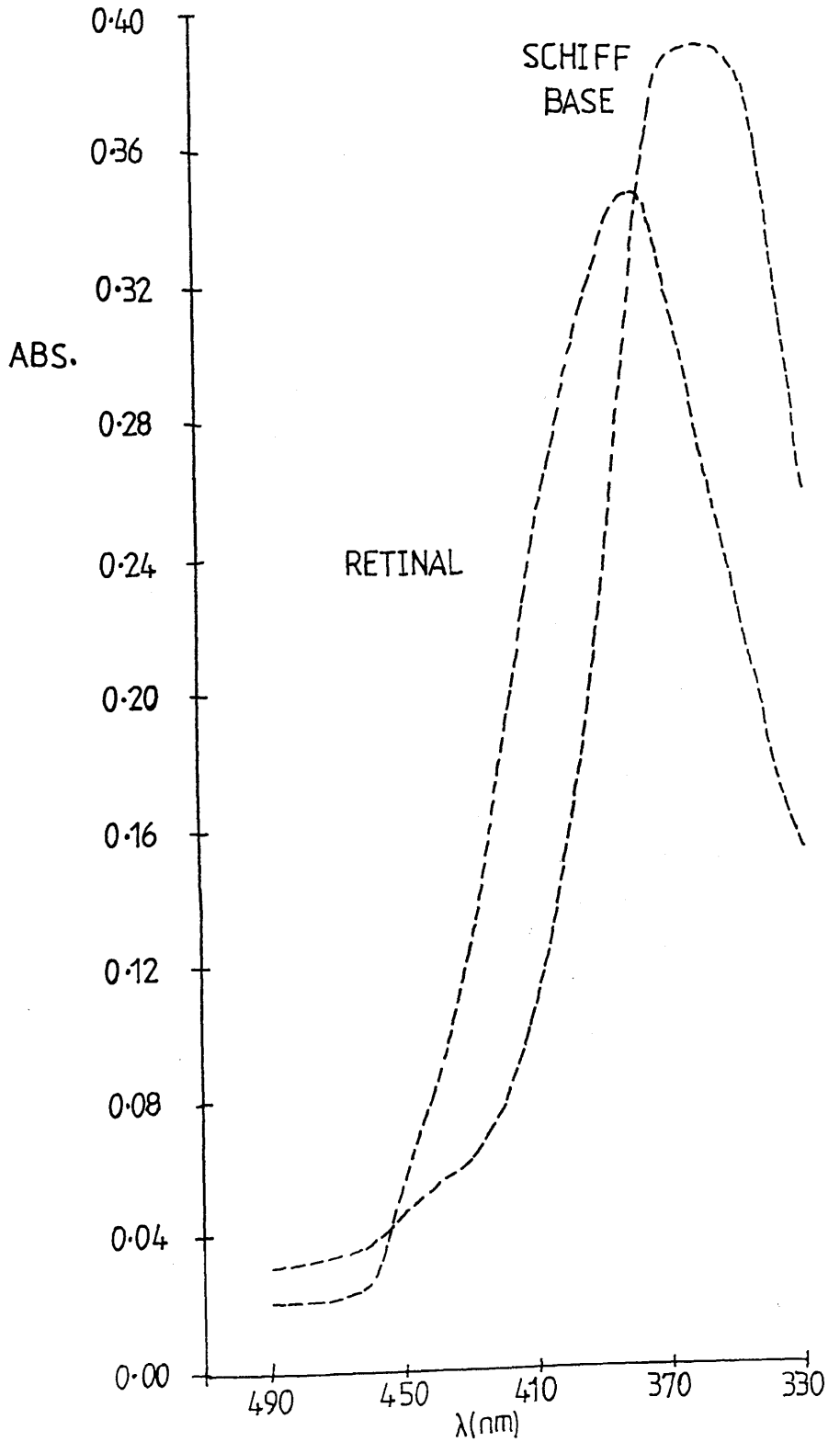


FIGURE 4.27  
Reconstructed spectra of retinal and schiff base using  $\alpha_0$ ,  $\alpha_1$ , and  $\alpha_2$  values in Table 4.9.



maximum absorbance at around 360nm, with a smaller proportion in the protonated form (fig.4.26). At pH 6 the schiff base immediately after mixing is in the unprotonated form (fig.4.27) and results from the hydrolysis reaction at pH 7 give very similar spectra to those at pH 6 (spectra not shown).

The spectra of the schiff base constructed in figs. 4.25-4.27 are from data where  $t$  is very small indeed (i.e. immediately after mixing) and from these spectra it is obvious that the protonation of the schiff base has already occurred and is an extremely fast reaction compared to the hydrolysis reaction. Once again, from these constructed spectra, it can be estimated that the  $pK_a$  value of the schiff base in Ammonyx is between values of 4 and 5.

Similar retinal and schiff base spectra can be constructed using the results in Emulphogene, DTAB or SDS detergents.

#### 4.5 General Base Catalysis of the Hydrolysis Reaction

General base catalysis of the hydrolysis reaction in Ammonyx detergent was studied at pH 4,5 and 6 using final buffer concentrations (after 1:1 mixing with the schiff base) of 0.01M, 0.05M, 0.1M and 0.2M (see section 4.1). Higher buffer concentrations could not be used because of solubility problems with the detergents. The base catalysis was studied on the stopped-flow apparatus and results were confirmed using the UV spectrometer. The pH was recorded at the end of each run and was within 0.1 pH units for each buffer series at any pH. The temperature during the experiments remained constant at 20°C.

At pH 4 and 5 stopped-flow traces were recorded in duplicate at 380nm, 440nm and 460nm and for pH 6 at 340nm, 360nm and 400nm in duplicate, for all buffer concentrations. In each case the timing sequence used was geometric with  $DT=75msec$ ,  $N=32$  and total time = 612secs. The results were analysed using the Discrete program and for nearly all the experiments the best fit was one of 2

components.

The average value of  $\lambda_1$  and  $\lambda_2$  at 380nm, 440nm and 460nm at each of the buffer concentrations at pH 4 are shown in table 4.10, and at pH 5 in table 4.11. The average values of  $\lambda_1$  and  $\lambda_2$  at 340nm, 360nm and 400nm at each buffer concentration at pH 6 are shown in table 4.12. (Some results at pH 6 were not very reproducible and have therefore been omitted.)

Table 4.13 shows the average values of  $\lambda_1$  and  $\lambda_2$  for the reactions in Ammonyx at pH 4, 5 and 6 for each of the buffer concentrations.

Figures 4.28 and 4.29 show the results in table 4.13 in graphical form. Figure 4.28 is a plot of  $\lambda_1$  ( $\text{min}^{-1}$ ) versus buffer concentration at pH 4, 5 and 6 and figure 4.29 is a plot of  $\lambda_2$  ( $\text{min}^{-1}$ ) versus buffer concentration at the same pH values. These results would suggest that there is very little general base catalysis in Ammonyx, compared to the previously determined effect in Emulphogene<sup>®</sup>. The value of  $\lambda_1$  increases to some extent at pH 4 and 5 and less so at pH 6, as the buffer concentration is increased. The value of  $\lambda_2$  increases at pH 5 and 6 and decreases at pH 4 as the buffer concentration increases, but there is not really a marked change in the value of  $\lambda_2$  rate constant and so buffer catalysis was considered negligible when Ammonyx was used as detergent.

#### 4.6 Determination of pK<sub>a</sub> Value of Schiff Base in Aqueous Detergent Micelles

The pK<sub>a</sub> value of the schiff base was determined in three detergent solutions namely Emulphogene, Ammonyx and DTAB by pH-jump experiments of the schiff base over the pH range 1-9. Schiff base protonation, prior to hydrolysis, was studied using the stopped-flow apparatus with a linear timing sequence where DT = 40msec and total time = 10.2sec. The actual absorbance values from the linear run were printed out and the average absorbance over the first four to six readings was calculated to give a value of absorbance at time zero. (The first four

Table 4.10

Table showing rate constants obtained for schiff base hydrolysis reaction in Ammonyx at pH 4 with different buffer concentrations.

Buffer concentration (molar)	Wavelength (nm)	$\lambda_1$ ( $\text{min}^{-1}$ )	$\lambda_2$ ( $\text{min}^{-2}$ )
0.01	380	7.674 (1.452)	0.623 (0.032)
	440	7.305 (0.894)	0.619 (0.018)
	460	2.008 (0.417)	0.997 (0.136)
0.05	380	8.544 (0.252)	0.667 (0.007)
	440	9.120 (0.690)	0.729 (0.121)
	460	5.247 (0.191)	0.817 (0.125)
0.10	380	12.618 (1.128)	0.604 (0.007)
	440	10.281 (1.336)	0.628 (0.015)
	460	10.728 (0.162)	0.641 (0.003)
0.20	380	14.796 (1.548)	0.597 (0.022)
	440	12.381 (1.428)	0.551 (0.007)
	460	15.012 (1.968)	0.569 (0.004)

(Standard deviations are given in brackets.)

Table 4.11

Table showing rate constants obtained for schiff base hydrolysis reaction in Ammonyx at pH 5 with different buffer concentrations.

Buffer concentration (molar)	Wavelength (nm)	$\lambda_1$ (min <sup>-1</sup> )	$\lambda_2$ (min <sup>-2</sup> )
0.01	380	7.092 (0.288)	0.680 (0.017)
	440	14.202 (0.498)	0.408 (0.065)
	460	7.971 (0.162)	0.655 (0.026)
0.05	380	10.143 (0.666)	0.764 (0.031)
	440	12.915 (0.264)	0.697 (0.007)
	460	11.079 (1.104)	0.755 (0.000)
0.10	380	11.859 (0.156)	0.834 (0.015)
	440	15.729 (0.606)	0.723 (0.001)
	460	14.226 (0.042)	0.761 (0.004)
0.20	380	18.738 (3.408)	0.794 (0.022)
	440	20.439 (0.066)	0.721 (0.003)
	460	17.946 (1.014)	0.761 (0.002)

(Standard deviations are given in brackets.)

Table 4.12

Table showing rate constants obtained for schiff base hydrolysis reaction in Ammonyx at pH 6 with different buffer concentrations.

Buffer concentration (molar)	Wavelength (nm)	$\lambda_1$ ( $\text{min}^{-1}$ )	$\lambda_2$ ( $\text{min}^{-2}$ )
0.01	340	-	-
	360	5.781 (1.167)	0.373 (0.009)
	400	-	0.458 (0.028)
0.05	340	6.636 (0.906)	0.475 (0.006)
	360	8.172 (2.394)	0.462 (0.032)
	400	10.476 (1.242)	0.576 (0.021)
0.10	340	7.800 (2.106)	0.523 (0.001)
	360	6.492 (0.138)	0.543 (0.001)
	400	7.938 (0.282)	0.655 (0.003)
0.20	340	8.406 (2.454)	0.590 (0.007)
	360	9.834 (1.530)	0.571 (0.004)
	400	9.762 (1.542)	0.689 (0.026)

(Standard deviations are given in brackets.)

Table 4.13

Table showing average rate constants obtained for schiff base hydrolysis reaction in Ammonyx at pH 4, 5 and 6 with different buffer concentrations.

Final pH reading	Buffer concentration (molar)	$\lambda_1$ (min <sup>-1</sup> )	$\lambda_2$ (min <sup>-1</sup> )
4.30	0.01	5.664 (2.940)	0.746 (0.204)
4.36	0.05	7.638 (1.908)	0.737 (0.103)
4.33	0.10	11.208 (1.356)	0.625 (0.019)
4.33	0.20	14.064 (1.836)	0.572 (0.023)
5.13	0.01	9.756 (3.474)	0.580 (0.140)
5.07	0.05	11.376 (1.392)	0.738 (0.035)
5.04	0.10	13.938 (1.764)	0.773 (0.051)
5.04	0.20	19.038 (1.956)	0.758 (0.034)
6.14	0.01	5.781 (1.167)	0.416 (0.052)
6.16	0.05	8.430 (2.148)	0.504 (0.058)
6.18	0.10	7.404 (1.194)	0.574 (0.063)
6.20	0.20	9.336 (1.632)	0.617 (0.058)

(Standard deviations are given in brackets.)

FIGURE 4.28  
Graph of  $\lambda$ , ( $\text{min.}^{-1}$ ) versus buffer concentration (M) for schiff base hydrolysis reaction in Ammonyx at pH 4,5 and 6.

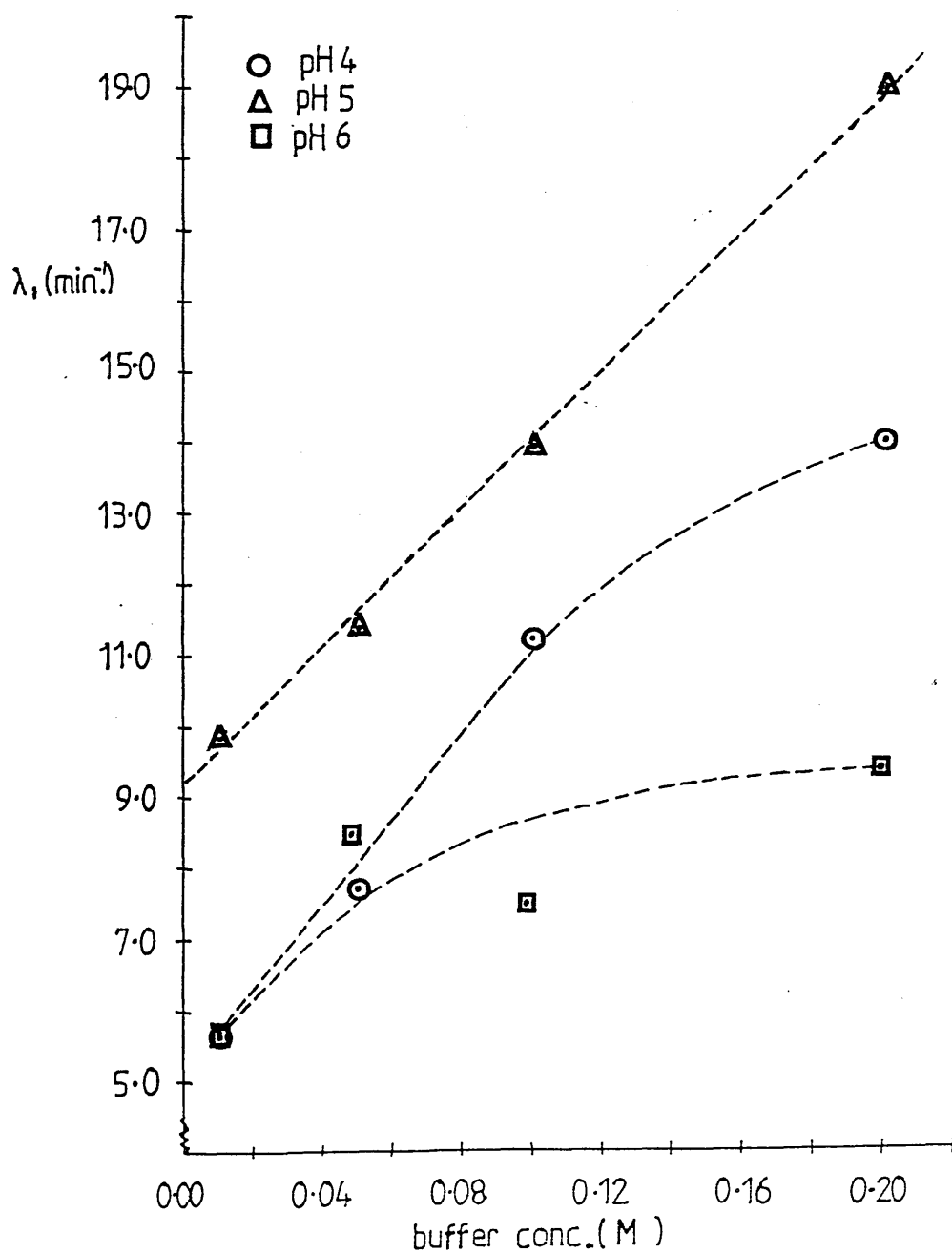
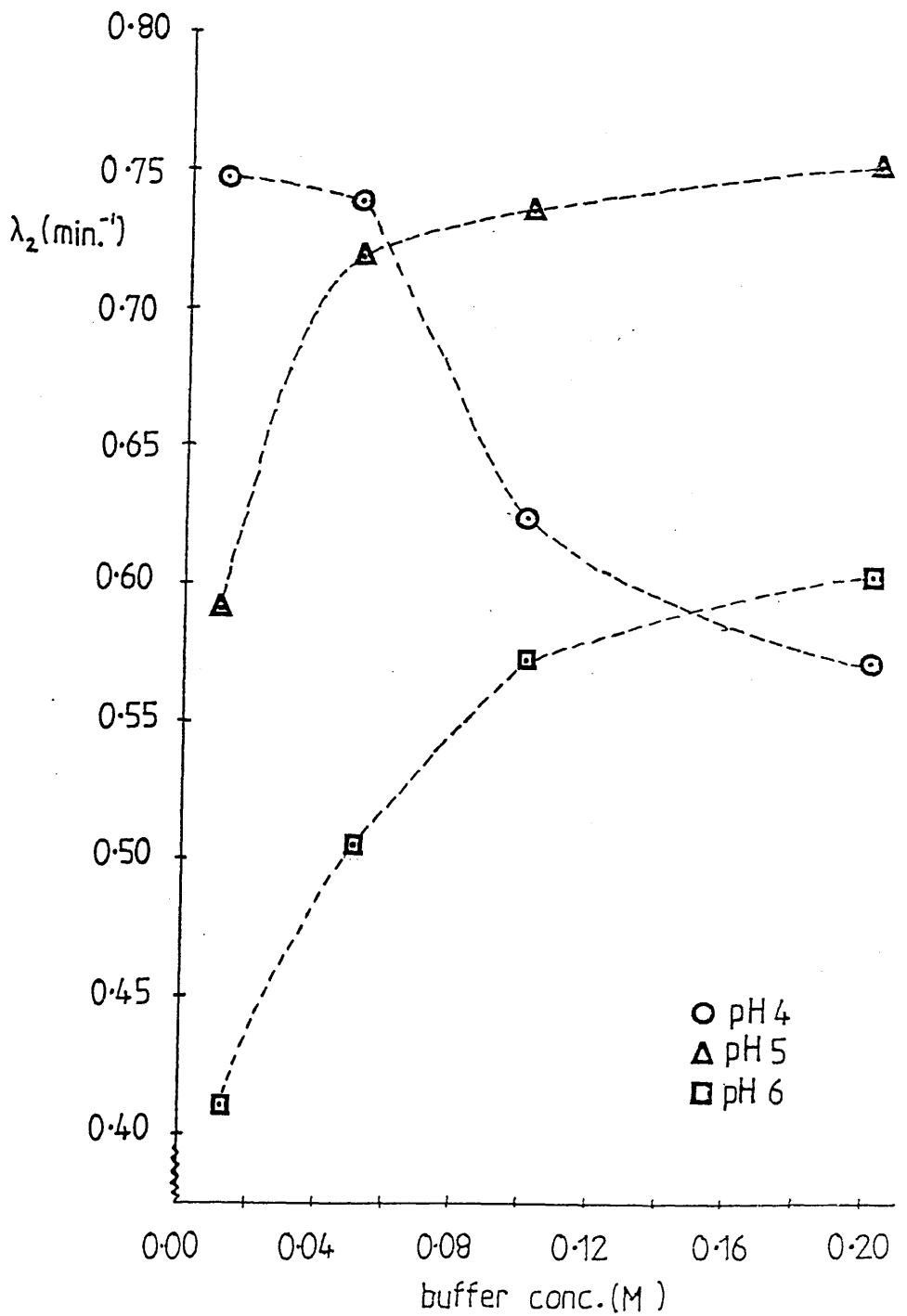


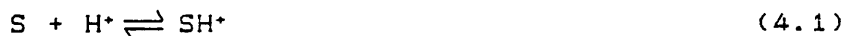
FIGURE 4.29  
Graph of  $\lambda_2$  (min.<sup>-1</sup>) versus buffer concentration (M) for  
schiff base hydrolysis reaction in Ammonyx at pH 4,5 and 6.



to six readings at this timing sequence cover a time of 0.1-0.2 seconds.) The traces were recorded at every pH in duplicate at 360nm and 440nm for each detergent. A range of buffers covering pH values of 1 to 9 were used at 0.2M in each case, and the pH was recorded at the end of the reaction after the 1:1 mixing of the schiff base with detergent buffer solution. The traces were recorded at 360nm and 440nm as these are the peaks in the absorbance spectra of the unprotonated and protonated schiff bases respectively.

Table 4.14 lists the average absorbance values ( $t=0$ ) at 360nm and 440nm over the pH range 1-9, calculated from the results of the pH-jump in Emulphogene. Figure 4.30 shows a plot of the average absorbance values at time = 0 secs for 360nm and 440nm versus pH of reaction for the pH-jump in Emulphogene. Examination of figure 4.30 shows that the  $pK_a$  value is approximately equal to 6 when Emulphogene is detergent. However the  $pK_a$  value can be calculated more accurately than this, as shown below.

The protonation of the schiff base can be represented by equation 4.1 where S = the unprotonated schiff base and  $SH^+$  the protonated schiff base.



The situation is however complicated by the fact that the reaction is occurring in detergent micelle solution. If the acid dissociation constant of the schiff base is defined as:

$$K_{sH} = [S]a_H / SH^+ \quad (4.2)$$

where  $a_H$  is the hydrogen ion activity in the micelle, then by taking logarithms it can be shown that:

$$\begin{aligned} \log [S]/[SH^+] &= \log K_{sH} - \log a_H \\ &= -pK_{sH} + p_{aH} \end{aligned} \quad (4.3)$$

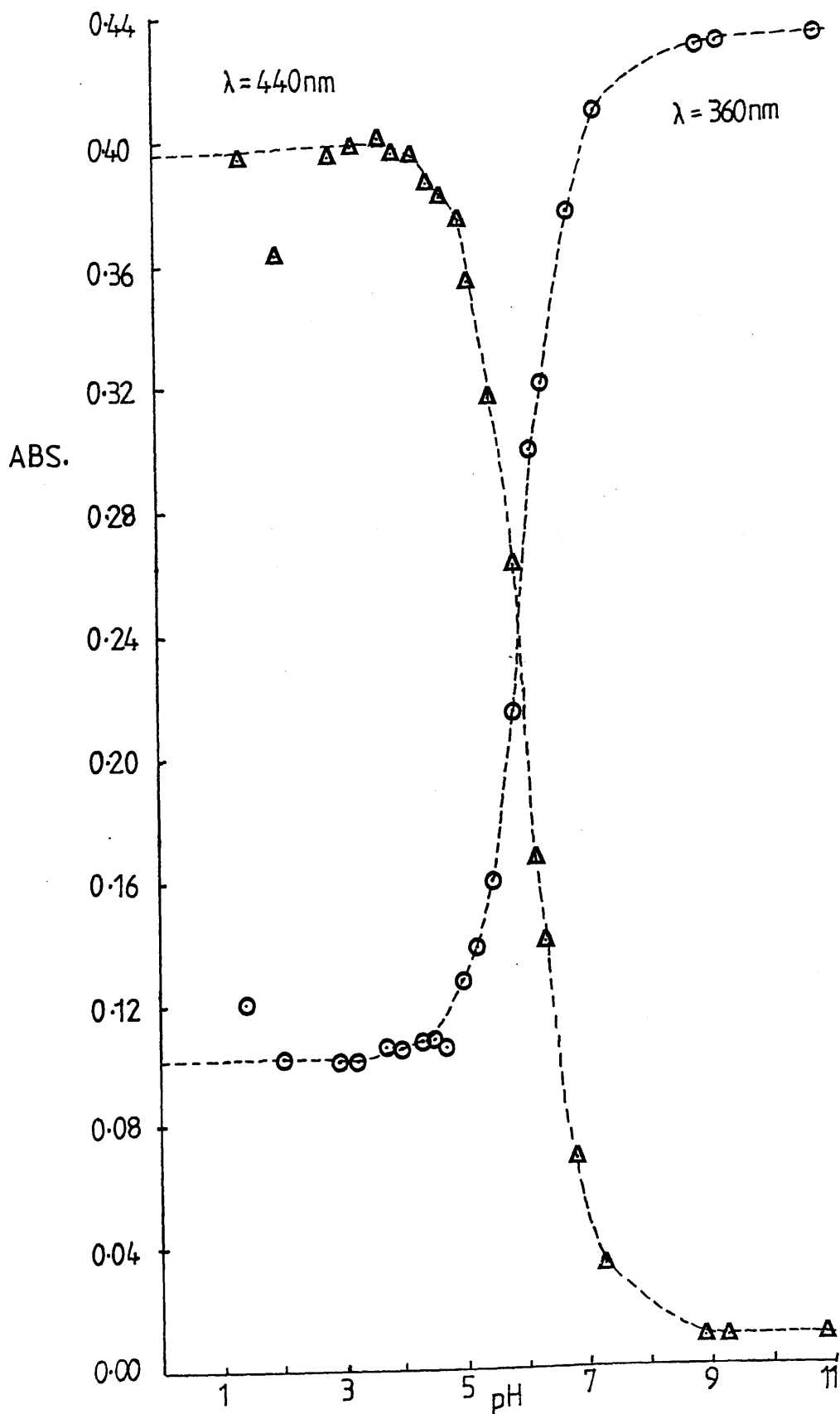
A plot of  $\log [S]/[SH^+]$  versus  $p_{aH}$  should give a straight line with slope equal to unity and intercept

Table 4.14

Table of average values of absorbance (t=0) at 360nm and 440nm and pH values for schiff base hydrolysis reaction in Emulphogene.

Buffer pH	Final pH at end of reaction	Average absorbance at 360nm (t=0secs)	Average absorbance at 440nm (t=0secs)
1.0	1.40	0.1203	0.3941
2.0	1.97	0.1019	0.3630
2.5	2.90	0.1015	0.3965
3.0	3.26	0.1016	0.3990
3.5	3.70	0.1064	0.4025
3.75	3.94	0.1054	0.3985
4.0	4.27	0.1073	0.3957
4.25	4.48	0.1080	0.3875
4.5	4.70	0.1055	0.3832
4.75	4.94	0.1270	0.3762
5.0	5.19	0.1385	0.3536
5.25	5.48	0.1599	0.3168
5.5	5.85	0.2149	0.2629
5.75	6.14	0.2999	0.1674
6.0	6.32	0.3215	0.1399
6.5	6.78	0.3767	0.0693
7.0	7.28	0.4104	0.0340
8.0	8.9	0.4320	0.0093
9.0	9.23	0.4331	0.0095
Butylamine	10.84	0.4347	0.0091

FIGURE 4.30  
pH titration curve for N-retinylidene n-butylamine schiff  
base in Emulphogene detergent.



with the y-axis equal to  $-pK_{sH}$ , where  $pK_{sH}$  is the unperturbed  $pK_s$  of the schiff base.

The micellar hydrogen ion activity ( $a_H$ ) is not directly measurable, but can be related empirically to the measured pH value by using equation 4.4:

$$pa_H = -p\phi + n.pH \quad (4.4)$$

where  $p\phi$  and  $n$  are factors representing any pH shift or non-ideal behaviour due to the reaction taking place in a micellar detergent solution.  $n$  might be naively interpreted as the number of protons involved in the protonation of the schiff base (equation 4.1) and has a value of unity for ideal titration behaviour. The value of  $p\phi$  has arbitrarily been taken as equal to zero for the neutral detergent Emulphogene, so that  $pK_{sH} = 6.1$  on average (from table 4.20).

Taking into account this non-ideal titration behaviour which occurs in the detergent micelles, equation 4.3 becomes:

$$\log [SH^+]/[S] = pK_{sH} + p\phi - n.pH \quad (4.5)$$

so that a plot of  $\log [SH^+]/[S]$  versus pH would give a line with slope =  $-n$  and intercept on the pH axis showing the mid-point ( $pH_{m.i.d.}$ ) of the schiff base titration in the micellar environment. The mid-point pH of the titration is given by equation 4.6:

$$pH_{m.i.d.} = (pK_{sH} + p\phi)/n \quad (4.6)$$

from which  $p\phi$  may be obtained.

Using the results in table 4.14 and figure 4.30, a plot can be drawn for Emulphogene detergent if the ratio  $[SH^+]/[S]$  is available at each wavelength. The ratio can be obtained using equation 4.7;

$$[SH^+]/[S] = (A_H - A)/(A - A_L) \quad (4.7)$$

where  $A_H$  and  $A_L$  are the absorbance readings at high and

low pH respectively, where the pH titration curve has flattened out, and A is the absorbance reading at the pH value of reaction. A plot of  $\log_{10} (A_H - A)/(A - A_L)$  versus pH should therefore give a straight line. Table 4.15 shows the results of  $\log_{10} (A_H - A)/(A - A_L)$  at 360nm and 440nm for Emulphogene and similar results for Ammonyx are shown in tables 4.16, 4.17, figure 4.31 and for DTAB in tables 4.18, 4.19 and figure 4.32.

These results were combined with similar titration experiments carried out on an ultra-violet/visible spectrometer<sup>49</sup> and analysis of the results produced the values of  $pH_{1/2}$ , n and  $pK_a$  in table 4.20 and the plots in figure 4.33.

It is obvious from these results that the different environments created by using different aqueous detergent micelle systems has affected the protonation behaviour of the retinal schiff base. The  $pK_a$  value of the schiff base varies depending on detergent, and the value of n (the number of protons involved in the protonation of the schiff base) also varies depending on detergent. It is interesting to note that in Ammonyx and DTAB the value of n is fractional, equal to 0.77, and in Emulphogene the value of n is equal to unity. This will be considered in more detail later.

#### 4.7 Low Temperature Ultra-Violet Spectroscopy

The schiff base hydrolysis reaction was studied in Ammonyx at pH 4,5 and 6 at a temperature of approximately 3°C (instead of 20°C) in order to examine the effect of decreasing the temperature on the rate of hydrolysis. If both the rates of intermediate formation and decay (rate constants  $\lambda_1$  and  $\lambda_2$ ) are affected by the decrease in temperature then it may be possible to detect the intermediate species using ultra-violet/visible spectroscopy. The problem at 20°C in using UV/visible spectroscopy was that in the time taken to mix solutions manually, any very fast reactions were missed. If the rate of the fast reaction can be decreased by lowering the temperature then the intermediate species may be

Table 4.15

Table listing values of  $\log_{10} (A_H - A) / (A - A_L)$  and pH for 360nm and 440nm in Emulphogene.

pH	$\log_{10} \frac{(A_H - A)}{(A - A_L)}$	$\log_{10} \frac{(A_H - A)}{(A - A_L)}$
	at 360nm	at 440nm
1.40	1.224	1.815
1.97	2.921	0.981
2.90	-	2.044
3.26	3.523	2.591
3.70	1.826	2.197
3.94	1.927	2.414
4.27	1.752	1.954
4.48	1.702	1.481
4.70	1.916	1.348
4.94	1.082	1.188
5.19	0.904	0.871
5.48	0.673	0.568
5.85	0.288	0.268
6.14	-0.167	-0.167
6.32	-0.287	-0.298
6.78	-0.674	-0.739
7.28	-1.099	-1.116
8.9	-2.042	-3.115
9.23	-2.242	-2.893
10.84	-3.046	-3.592

Table 4.16

Table of average values of absorbance (t=0) at 360nm and 440nm and pH values for schiff base hydrolysis reaction in Ammonyx.

Buffer pH	Final pH at end of reaction	Average absorbance at 360nm (t=0secs)	Average absorbance at 440nm (t=0secs)
1.0	1.20	0.0796	0.4148
2.5	3.13	0.0931	0.3997
3.0	3.36	0.1041	0.4073
3.5	3.80	0.1142	0.3801
3.75	4.11	0.1298	0.3486
4.0	4.34	0.2041	0.2540
4.25	4.54	0.2103	0.2498
4.5	4.75	0.2314	0.2252
4.75	4.97	0.2584	0.1870
5.0	5.31	0.2933	0.1437
5.25	5.65	0.3284	0.0941
5.5	6.07	0.3645	0.0549
5.75	6.16	0.3786	0.0431
6.0	6.30	0.3706	0.0339
6.5	6.70	0.3910	0.0216
7.0	7.21	0.3952	-
8.0	8.86	0.4045	-
9.0	8.74	0.4088	-
Butylamine	10.62	0.3922	-

Table 4.17

Table listing values of  $\log_{10} (A_H - A) / (A - A_L)$  and pH for 360nm and 440nm in Ammonyx.

pH	$\log_{10} \frac{(A_H - A)}{(A - A_L)}$	$\log_{10} \frac{(A_H - A)}{(A - A_L)}$
	at 360nm	at 440nm
1.20	2.212	-
3.13	1.319	1.413
3.36	1.065	1.694
3.80	0.909	1.022
4.11	0.725	0.708
4.34	0.205	0.177
4.54	0.172	0.159
4.75	0.058	0.050
4.97	-0.085	-0.115
5.31	-0.279	-0.312
5.65	-0.506	-0.593
6.07	-0.833	-0.923
6.16	-1.047	-1.079
6.30	-0.923	-1.238
6.70	-1.319	-1.594
7.21	-1.460	-
8.86	-2.212	-
10.62	-1.351	-

FIGURE 4.31  
pH titration curve for N-retinylidene n-butylamine schiff  
base in Ammonyx detergent.

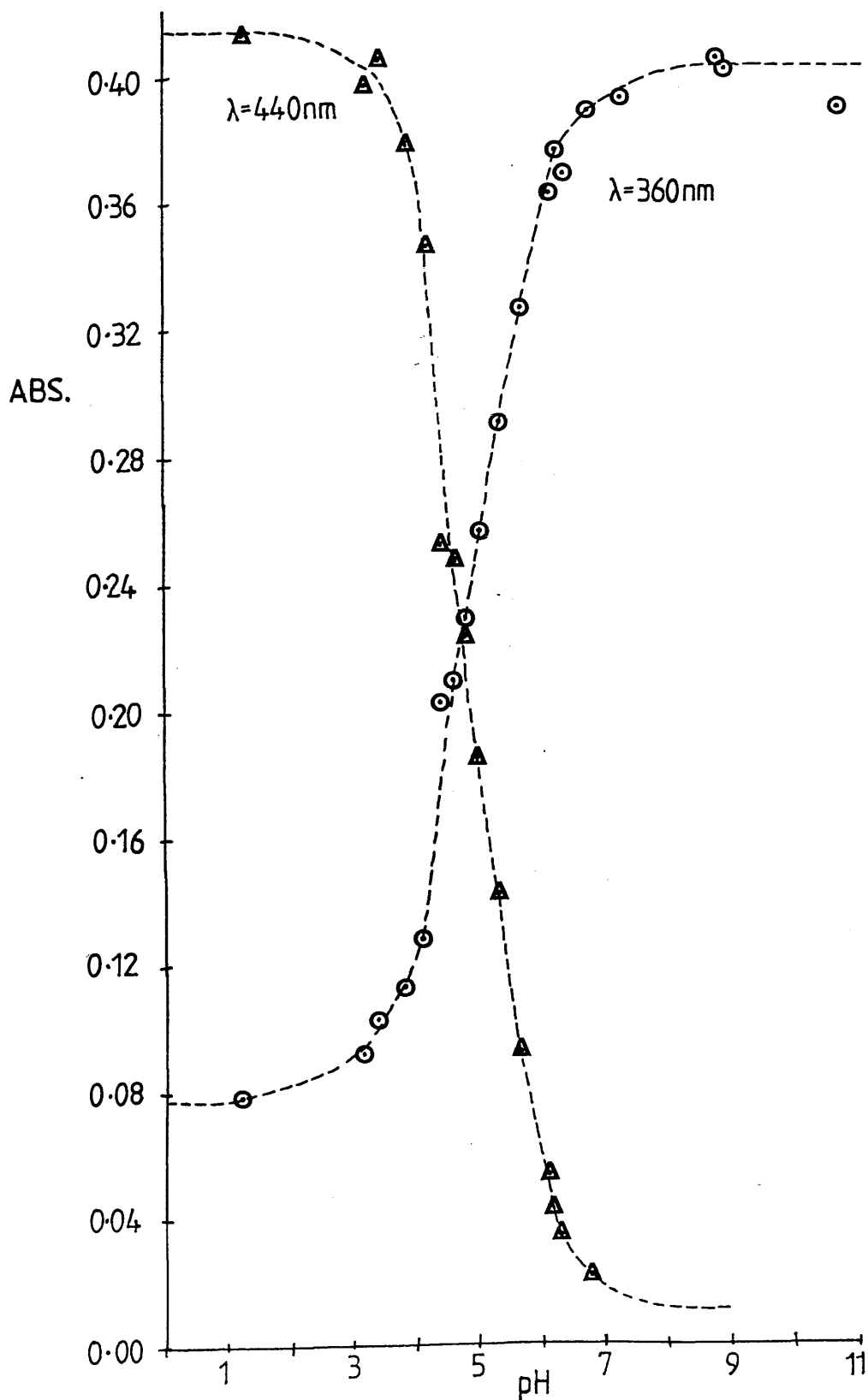


Table 4.18

Table of average values of absorbance (t=0) at 360nm and 440nm and pH values for schiff base hydrolysis reaction in DTAB.

Buffer pH	Final pH at end of reaction	Average absorbance at 360nm (t=0secs)	Average absorbance at 440nm (t=0secs)
1.0	1.37	0.0807	0.4271
2.0	1.95	0.0742	0.4170
2.5	2.87	0.0788	0.4066
3.0	3.21	0.0812	0.4149
3.5	3.65	0.0814	0.3984
3.75	3.90	0.0855	0.4017
4.0	4.20	0.1008	0.3909
4.25	4.44	0.1072	0.3795
4.5	4.68	0.1151	0.3644
4.75	4.91	0.1318	0.3439
5.0	5.20	0.1541	0.3297
5.25	5.50	0.1838	0.2898
5.5	5.88	0.2373	0.2273
5.75	6.11	0.3169	0.1440
6.0	6.32	0.3374	0.1267
6.5	6.76	0.3760	0.0689
7.0	7.28	0.4051	0.0359
8.0	9.67	0.4231	0.0086
9.0	9.12	0.4342	0.0076
Butylamine	10.98	0.4347	0.0087

Table 4.19

Table listing values of  $\log_{10} (A_H - A) / (A - A_L)$  and pH for 360nm and 440nm in DTAB.

pH	$\log_{10} \frac{(A_H - A)}{(A - A_L)}$	$\log_{10} \frac{(A_H - A)}{(A - A_L)}$
	at 360nm	at 440nm
1.37	1.723	-
1.95	3.256	1.834
2.87	1.870	1.386
3.21	1.691	1.701
3.65	1.679	1.201
3.90	1.483	1.267
4.20	1.096	1.077
4.44	0.994	0.931
4.68	0.891	0.784
4.91	0.720	0.628
5.20	0.545	0.538
5.50	0.359	0.325
5.88	0.083	0.049
6.11	-0.313	-0.312
6.32	-0.431	-0.397
6.76	-0.709	-0.764
7.28	-1.044	-1.142
9.67	-1.467	-2.839
9.12	-2.653	-3.016
10.98	-3.080	-2.772

FIGURE 4.32  
pH titration curve for N-retinylidene n-butylamine schiff  
base in DTAB detergent.

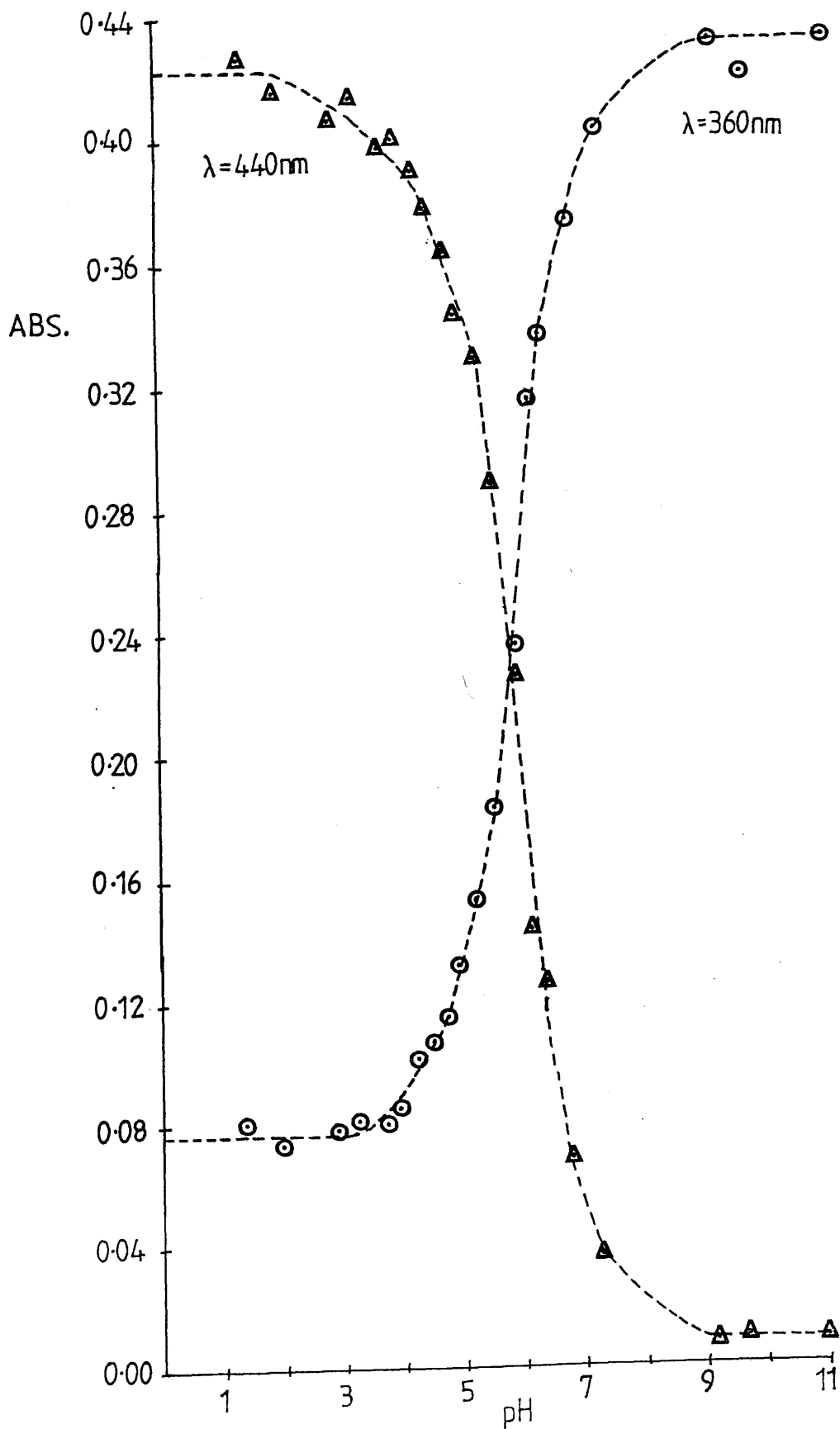


Table 4.20

Results obtained from pH-titrations of N-retinylidene n-butylamine in Ammonyx, Emulphogene, DTAB and SDS.

	Ammonyx	Emulphogene	DTAB	SDS
pH <sub>ind</sub>	4.85	6.1	5.84	9.54
n	0.77	1.0	0.77	1.1
p <sub>s</sub>	-2.37	0	-1.6	4.4

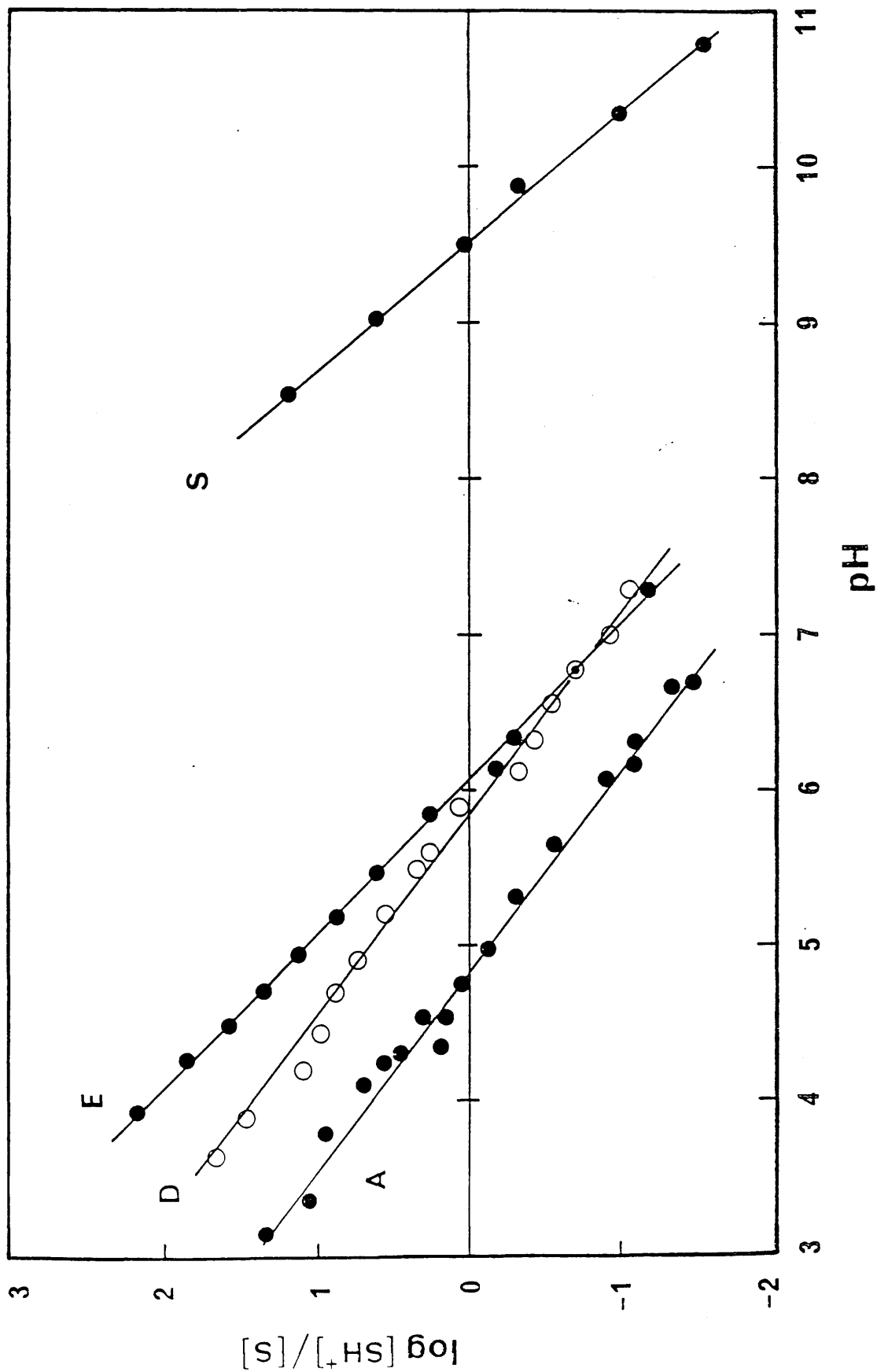
Table 4.21

Table showing values of absorbance at 392nm and 460nm, and time for the schiff base hydrolysis reaction in Ammonyx, pH 4 at 3°C.

Time(mins)	Absorbance (392nm)	Absorbance (460nm)
0	0.251	0.240
3	0.279	0.183
6	0.299	0.144
9	0.315	0.114
12	0.324	0.092
16	0.333	0.072
20	0.341	0.058
26	0.347	0.046
34	0.351	0.038
44	0.353	0.032
75	0.355	0.030

FIGURE 4.33

pH titrations of N-retinylidene n-butylamine in Ammonyx(A), Emulphogene(E), DTAB(D) and SDS(S).



detected.

Two methods of sample preparation were used to study the hydrolysis at low temperature (section 4.1). For the 1:1 mixing method (a), equal volumes (1.8 ml) of schiff base / detergent and buffer/detergent solutions were pipetted into two test tubes and cooled to 3°C in the thermostatted cell holders attached to the UV spectrometer. These solutions were mixed into a cuvette to start the hydrolysis reaction, and on mixing there was a slight increase in temperature of approximately 0.5°C.

In method (b) to try to avoid this increase in temperature a larger volume (3.5ml) of buffer/detergent solution was cooled in the spectrometer and 0.1ml of a concentrated schiff base solution in ethanol, equilibrated to 3°C, was added to the buffer. Unfortunately once again there was a slight increase in temperature and as there was no way to avoid this, methods (a) and (b) were used to mix the reactants. In each case the water bath for the UV/visible spectrometer was continually replenished with ice and the temperature in the cuvette was checked regularly before every spectrum was recorded (approximately every 3 minutes) so that the temperature remained near to 3°C throughout the reactions. The cell compartment in the spectrometer was flushed with argon throughout the experiments to stop the formation of condensation on the cuvette. The pH of the hydrolysis products was recorded at the end of each experiment and this was taken as the pH of reaction.

The UV/visible spectra of the reactions were recorded the same way as previously, with consecutive spectra superimposed on each other, and spectra at pH 4.25, 5.18 and 6.33 are shown in figures 4.34-4.36 respectively. These spectra were recorded after 1:1 mixing of the schiff base and buffer solutions (method a) and very similar spectra were obtained for method (b) (spectra not shown). Comparison of figures 4.34-4.36 with figures 4.5-4.7 shows that the hydrolysis reaction takes place much more slowly at 3°C than at 20°C.

Analysis of the spectra recorded at 3°C involved reading off the absorbance values for different times at

FIGURE 4.34

UV/visible spectrum of schiff base hydrolysis reaction in Ammonyx, pH 4.25 at 3°C.

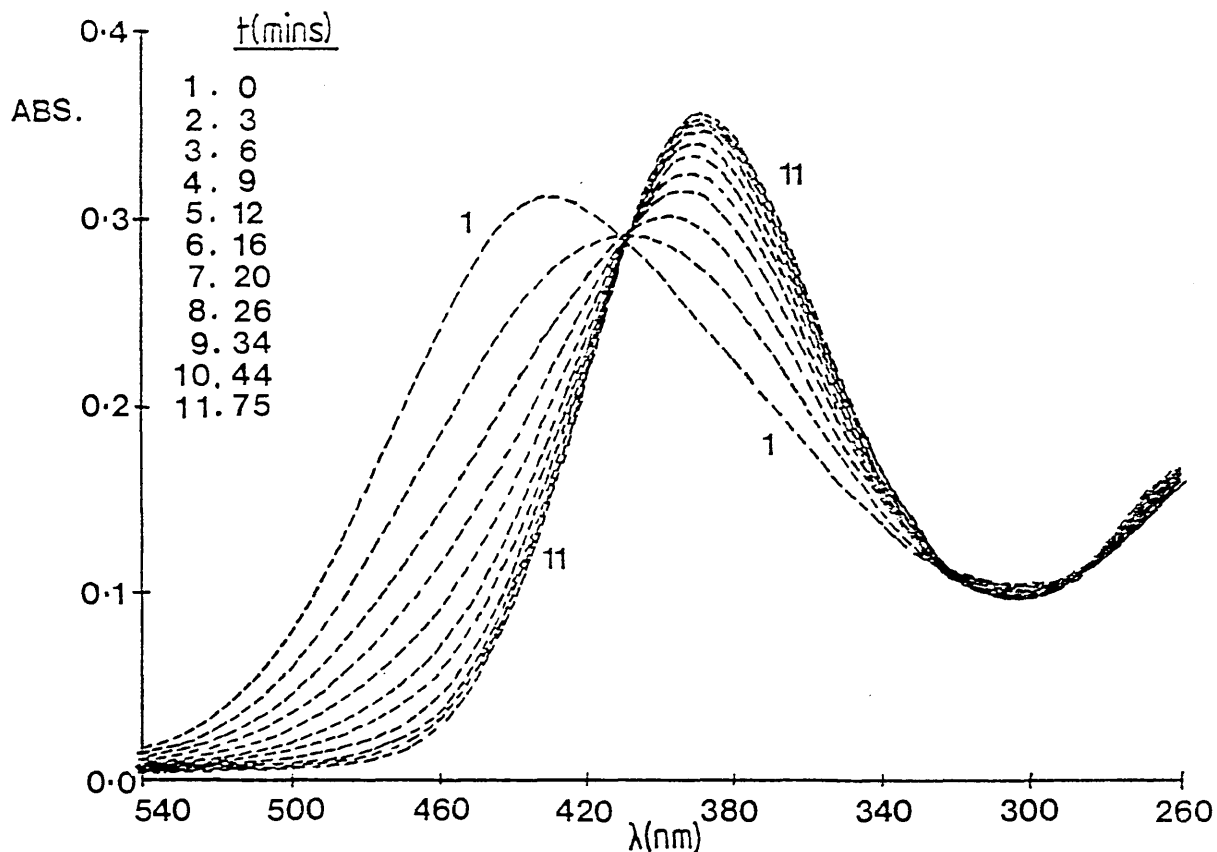


FIGURE 4.35

UV/visible spectrum of schiff base hydrolysis reaction in Ammonyx, pH 5.18 at 3°C.

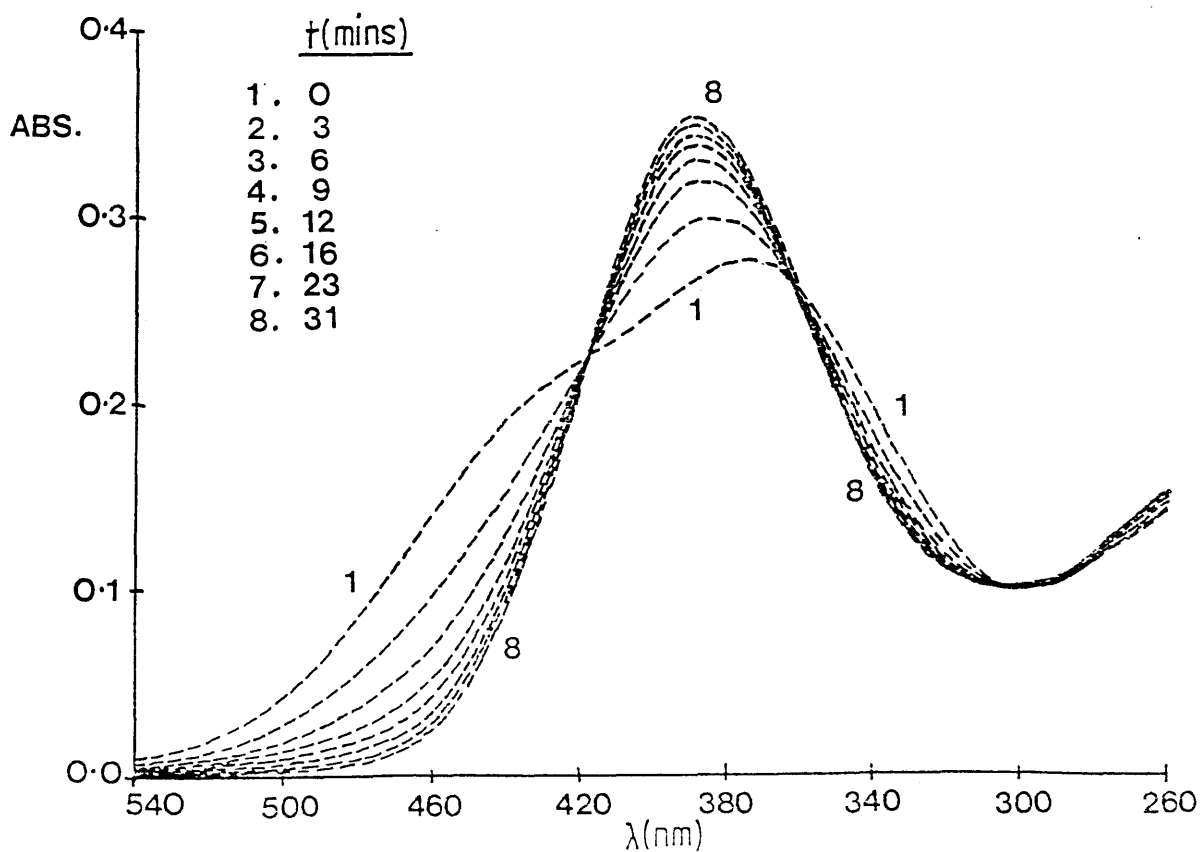
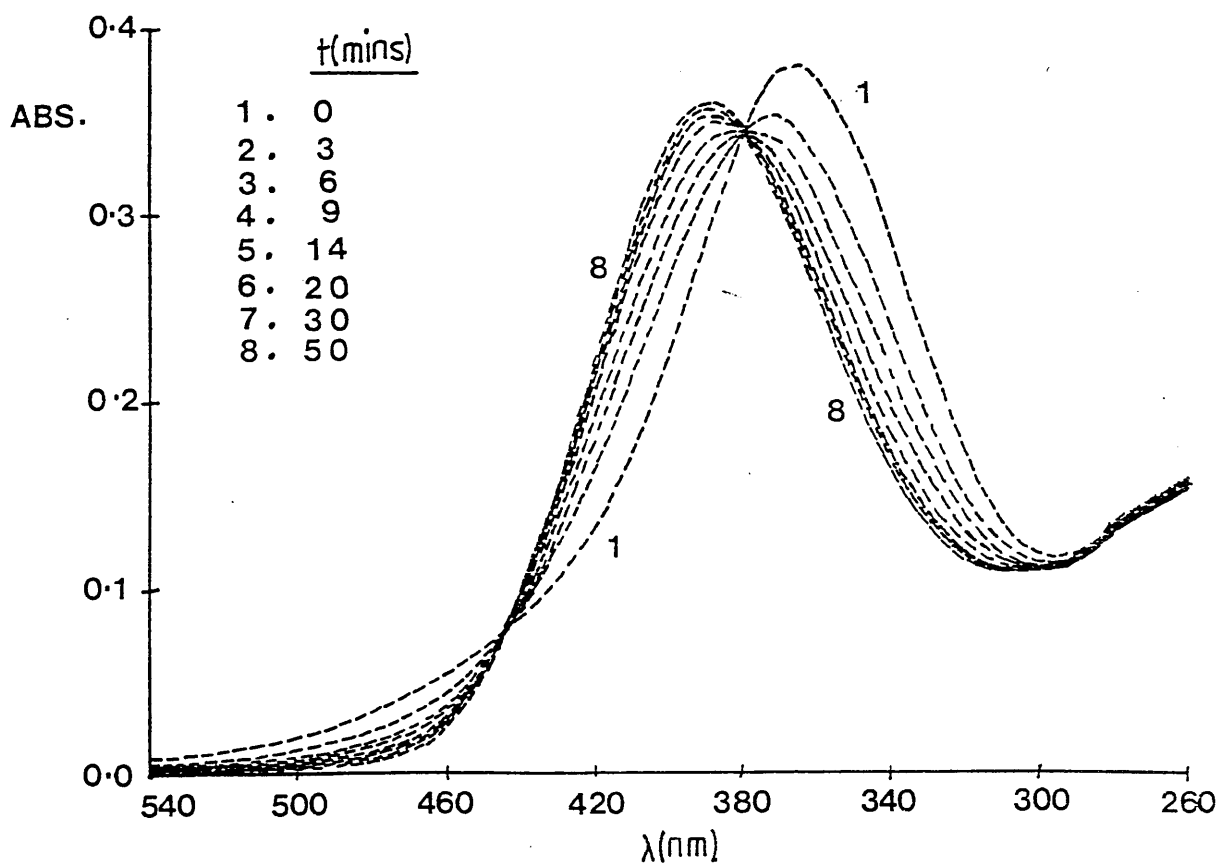


FIGURE 4.36

UV/visible spectrum of schiff base hydrolysis reaction in Ammonyx, pH 6.33 at 3°C.



a fixed wavelength from the ultra-violet/visible spectra and using these absorbance and time values in the Apple and mainframe computer programs. The Discrete program was adapted so that it would accept a small number of absorbance and time readings instead of the 256 readings normally used from the stopped-flow experiments. At pH 4 and 5 absorbance readings were taken at 392nm and 460nm and at pH 6 readings were taken at 360nm and 400nm. These values were chosen because there is a large change in absorbance with time at these wavelengths. The values of absorbance and time for the hydrolysis reactions at pH 4,5 and 6 are given in tables 4.21-4.23 and the final pH readings after 1:1 mixing were 4.25, 5.18 and 6.33. These results are from the 1:1 mixing method, but values from the dilution method (method b) were also analysed in a similar way.

The results from method (a) gave a 2 component fit as the best fit for data at pH 4 (392nm) and at pH 6 (360nm and 400nm) and a 1 component fit as best fit at pH 4 (460nm) and pH 5 (392nm and 460nm). The results from method (b) gave a 1 component fit as the best fit at pH 4 (392nm, 460nm), pH 5 (392nm, 460nm) and pH 6 (360nm) and a 2 component fit at pH 6 (400nm). Overall the reproducibility of the results from the analysis is not very good and this is very probably due to the small number of data points available for analysis.

In the analyses where the 1 component was given as the best fit, the 2 component fit was given as the second best fit and these results are included in table 4.24 which shows values of  $\lambda_1$  and  $\lambda_2$  at pH 4, 5 and 6 obtained from analysis of results of method (a) and method (b).

It is obvious that lowering the temperature has had a marked effect on the overall reaction rate just by examination of the total reaction times at 3°C compared to 20°C. It is also interesting to note that the first spectrum recorded in fig.4.34 does not appear to pass through the isosbestic point which suggests there could be intermediate formation at this stage, however in figs.4.35,4.36 this effect is not seen.

Table 4.22

Table showing values of absorbance at 392nm and 460nm, and time for the schiff base hydrolysis reaction in Ammonyx, pH 5 at 3°C.

Time(mins)	Absorbance (392nm)	Absorbance (460nm)
0	0.262	0.140
3	0.297	0.097
6	0.319	0.068
9	0.329	0.052
12	0.338	0.042
16	0.344	0.033
23	0.349	0.028
31	0.350	0.025

Table 4.23

Table showing values of absorbance at 360nm and 400nm, and time for the schiff base hydrolysis reaction in Ammonyx, pH 6 at 3°C.

Time(mins)	Absorbance (360nm)	Absorbance (400nm)
0	0.373	0.227
3	0.331	0.267
6	0.309	0.289
9	0.292	0.305
14	0.279	0.320
20	0.269	0.329
30	0.265	0.334
50	0.260	0.338

Table 4.24

Table showing rate constants ( $\lambda_1$  and  $\lambda_2$ ) for the schiff base hydrolysis reaction in Ammonyx at pH 4, 5 and 6 at 3°C.

	pH	$\lambda_1$ ( $\text{min}^{-1}$ )	$\lambda_2$ ( $\text{min}^{-1}$ )
Method (a)	4.25	0.155	0.085
	5.18	0.227	0.096
	6.33	0.231	0.105
Method (b)	3.99	0.109	0.061
	4.98	0.224	0.117
	6.07	0.215	0.076
Combined results of Methods (a) and (b)	4	0.132 (0.033)	0.073 (0.017)
	5	0.226 (0.069)	0.103 (0.045)
	6	0.223 (0.011)	0.095 (0.022)

(Figures in brackets are standard deviations.)

The combined results for methods (a) and (b) are included in table 4.24 and comparison of these with results at 20°C in table 4.5 shows that the values of  $\lambda_1$  and  $\lambda_2$  are much smaller at 3°C, as would be expected.

#### 4.8 The Effect of Deuterium Oxide on Schiff Base Hydrolysis Rate

Ultra-violet/visible spectroscopy and stopped-flow spectroscopy were used to study the effect of deuterium oxide on the schiff base hydrolysis rate. The schiff base was made up in Ammonyx/D<sub>2</sub>O solution and was mixed 1:1 with 0.2M acetate buffer pD 4/Ammonyx, D<sub>2</sub>O solution. (The measurement of pD was made following the procedure described in chapter 2.) The pD was measured at the end of the hydrolysis reaction and this was taken as the pD of reaction (pD = 4.01).

The UV/visible spectrum of the hydrolysis reaction in deuterium oxide is shown in figure 4.37. Comparison of this spectrum with that in figure 4.5 shows that the hydrolysis reaction with D<sub>2</sub>O as solvent is significantly slower than the hydrolysis reaction under identical conditions with water as solvent.

The stopped-flow traces were recorded at 20°C using an arithmetic time scale with DT = 12.5msec and total time of 411 seconds. The traces were recorded in duplicate at 340nm, 370nm, 400nm, 460nm and 490nm.

In addition to this, traces were recorded at 340nm and 460nm using a geometric timescale with DT = 75msec, N=32 and total time = 612sec to check the values of rate constants obtained from a longer run as the reaction is quite slow. Figures 4.38 (a-f) show the traces recorded for the arithmetic timescale and there is obviously still some intermediate formation during the first ten to twenty seconds approximately. Comparison of these traces with figures 4.16 (a-d) however shows that the effect in deuterium oxide is much less marked than the effect in water under identical conditions and with the same timing sequence.

FIGURE 4.37

UV/visible spectrum of schiff base hydrolysis reaction in Ammonyx at pD 4.01.

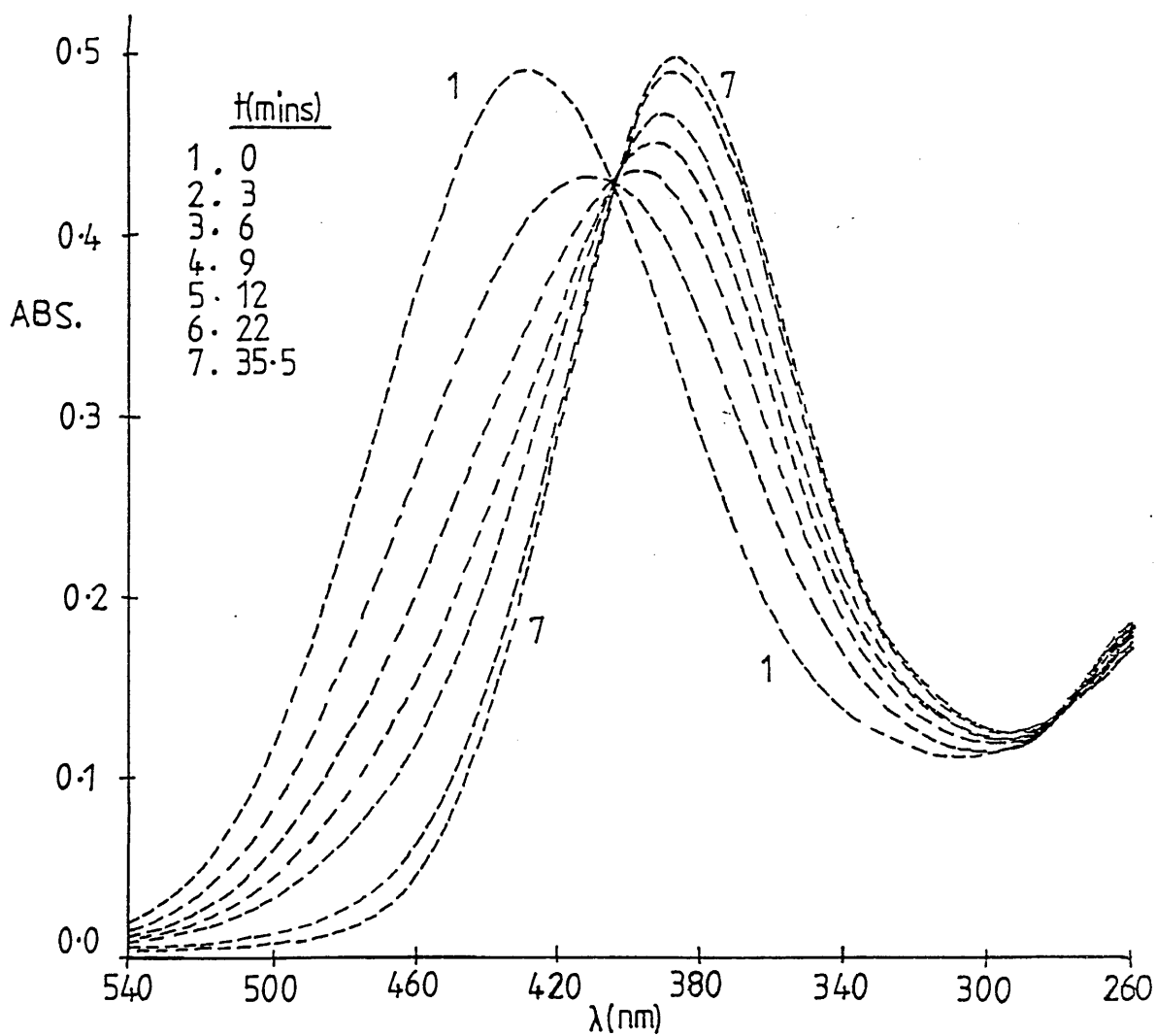
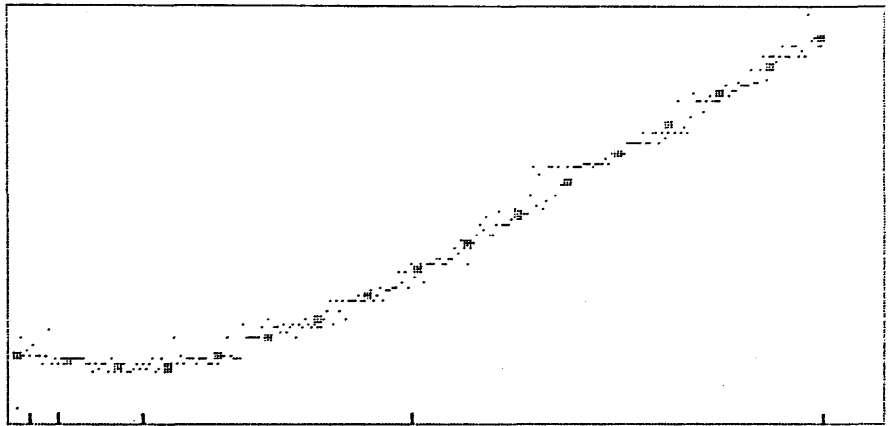


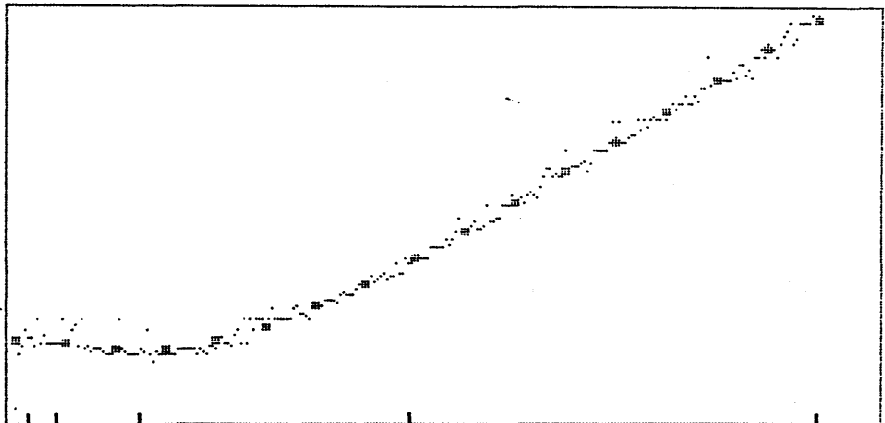
FIGURE 4.38

Stopped-flow traces of schiff base hydrolysis reaction in Ammonyx at pD 4. Timing sequence is arithmetic with DT=12.5msec and total time=411secs.

a.  $\lambda=340\text{nm}$



b.  $\lambda=370\text{nm}$



c.  $\lambda=400\text{nm}$

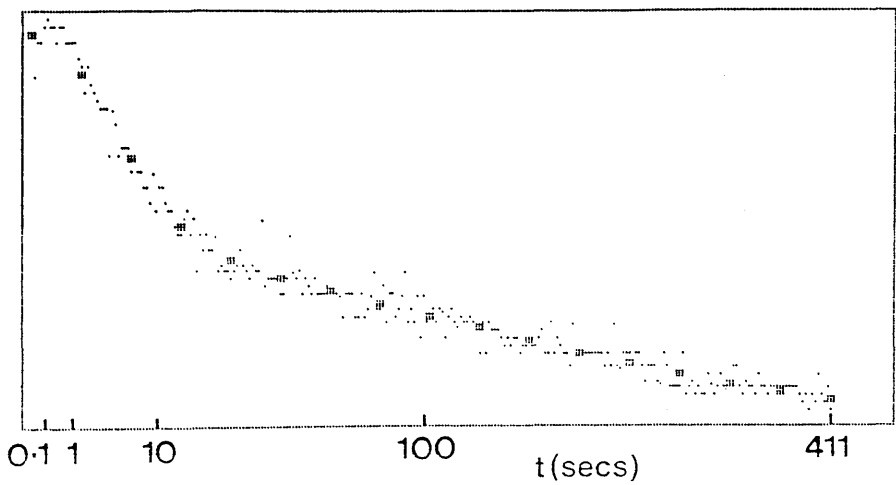
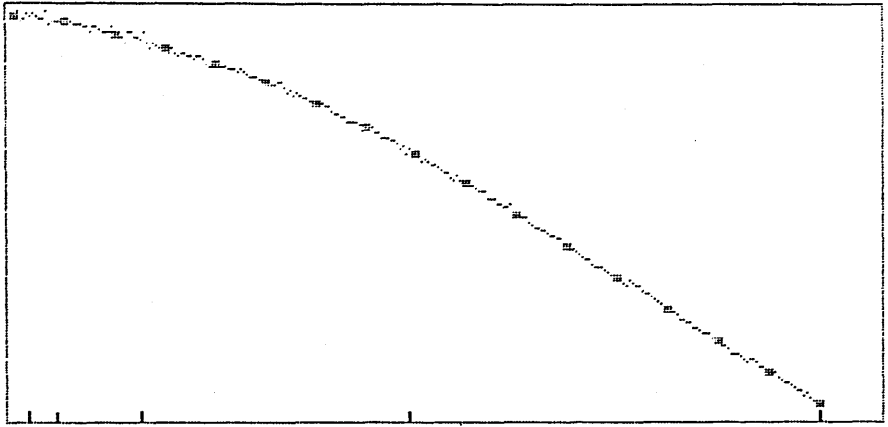
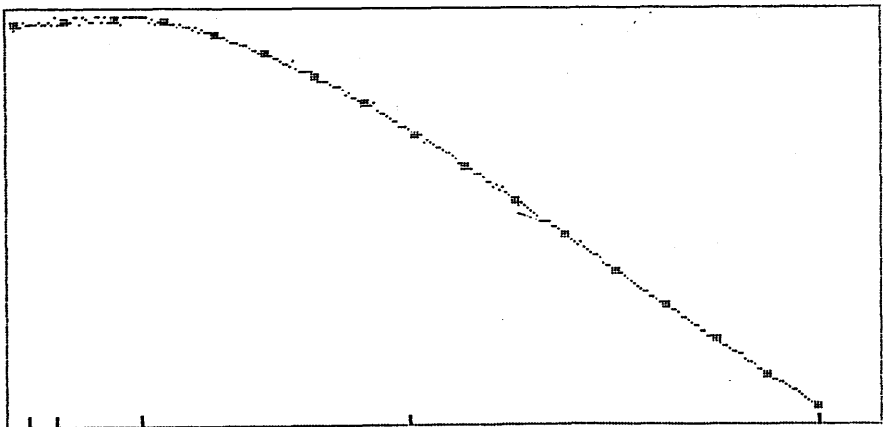


FIGURE 4.38 (cont.)

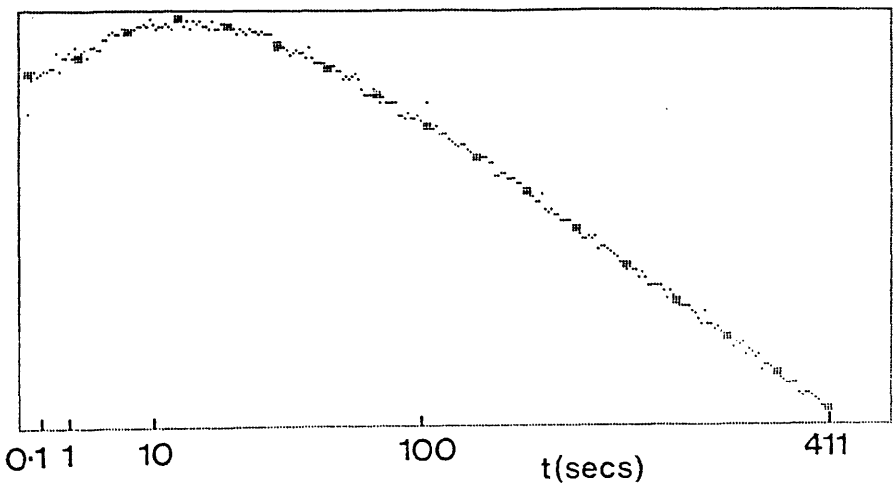
d.  $\lambda=430\text{nm}$



e.  $\lambda=460\text{nm}$



f.  $\lambda=490\text{nm}$



Analysis of the results of absorbance and time using the Discrete program gave 2 components as the best fit in nearly all cases and this best fit is shown on the traces at each wavelength. The values of  $\lambda_1$  and  $\lambda_2$  obtained from the analysis of the arithmetic runs were averaged at each wavelength and the results are given in table 4.25 along with the results for the geometric runs at 340nm and 460nm. The average of these results give values of  $\lambda_1 = 6.821 \text{ min}^{-1}$  and  $\lambda_2 = 0.121 \text{ min}^{-1}$ . Comparison of the results at pD 4 with results at pH 4 (table 4.5) which are  $\lambda_1 = 14.598 \text{ min}^{-1}$  and  $\lambda_2 = 0.651 \text{ min}^{-1}$  shows that there is a solvent isotope effect when deuterium oxide is used in place of water. The isotope effect  $k^H/k^D$  is equal to 2.140 for  $\lambda_1$  and 5.380 for  $\lambda_2$  values obtained from the stopped-flow experiments.

As was mentioned previously, steady-state kinetics provide more accurate hydrolysis rates than non-steady state, and a solvent isotope effect of about 2.3 is obtained if steady-state hydrolysis rates are considered<sup>49</sup>.

This isotope effect is important when considering the resonance Raman spectra of the intermediate species and will be discussed in Chapter 5.

Table 4.25

Table listing values of  $\lambda_1$  and  $\lambda_2$  at different wavelengths for hydrolysis reaction in Ammonyx at pD 4.

Wavelength (nm)	$\lambda_1$ (min <sup>-1</sup> )	$\lambda_2$ (min <sup>-1</sup> )
(Arith) 340	7.140	0.127
370	6.491	0.110
400	7.521	0.114
430	7.061	0.119
460	7.458	0.124
490	7.686	0.111
(Geom) 340	5.618	0.120
460	5.591	0.140
	MEAN = 6.821	0.121
	S.D. = 0.834	0.010

## CHAPTER 5

CHARACTERISATION OF  
INTERMEDIATE FORMED  
DURING SCHIFF BASE  
HYDROLYSIS.

## 5.1 Introduction

The results of the experiments on schiff base formation and hydrolysis (Chapters 3 and 4) provided enough details to enable prediction of conditions where the concentration of the intermediate species is at a maximum. Results from the formation reactions showed that no intermediate species was observable under the reaction conditions which were studied during this work. For the hydrolysis reaction on the other hand, an appreciable amount of intermediate accumulated during schiff base hydrolysis in Ammonyx at pH 4 and 5. This accumulation occurs within the first ten seconds of reaction approximately, according to the stopped-flow traces which were recorded, and this information was used to devise experiments to enable characterisation of the intermediate species.

Intermediate formation during schiff base hydrolysis is also apparent when Emulphogene, DTAB or SDS is the detergent, but in these cases the accumulation occurs at a slightly later stage - approximately 50 - 100 seconds after mixing of reactants. With these detergents a much smaller build up of intermediate occurs than in Ammonyx, and this is due to the fact that the value of  $\lambda_1$  is so much greater when Ammonyx is detergent.

## 5.2 Methods of Characterisation

Two techniques were selected as being particularly useful for the characterisation of the intermediate species and these were:

- (a) freeze-drying of sample followed by infra-red spectroscopy
- (b) resonance Raman spectroscopy using a continuous flow system.

In method (a) the idea was to start the schiff base hydrolysis by 1:1 mixing of schiff base in Ammonyx solution and buffer/Ammonyx solution at pH 4 or 5, allow ten seconds for reaction to occur and then quickly freeze the mixture in liquid nitrogen and dry on a vacuum line.

It would then be possible to record the IR spectrum of the sample present ten seconds after mixing. For this experiment a more concentrated schiff base solution was made up than usual and a less concentrated (0.05 M final concentration) buffer solution was used to try to increase the ratio of schiff base (or intermediate) to salts left after freeze-drying. In addition to this, instead of the acetate buffer normally used, an ammonium acetate buffer at pH 4 was used, as this should be more volatile and evaporate more quickly during freeze-drying.

A trial experiment involved mixing 1ml of the schiff base solution with 1ml of buffer solution, freezing after ten seconds and leaving on a vacuum line for several hours to dry. Unfortunately an oil was formed during the freeze-drying and a second attempt where the concentration of schiff base was reduced gave similar results. Solutions of 2% Ammonyx and 0.1M ammonium acetate were freeze-dried on their own, and with the Ammonyx a white powder was formed whereas the ammonium acetate completely evaporated. It was obvious that it was the retinal which was causing problems, and even at lower concentrations an oil was formed on freeze-drying. As a result of these experimental problems, trial runs using method (b) were carried out to see if this method was more useful.

Method (b) involved the use of a flow system where the schiff base and buffer solutions were pumped separately, using two peristaltic pumps, to a T-piece mixer where the solutions were mixed together and the reaction commenced. The mixture was pumped along a short length of tubing into a 1cm pathlength quartz cell so that the time between mixing and reaching the cell was approximately ten seconds. This flow cell was placed in the Raman spectrometer and a spectrum recorded of the solution ten seconds after mixing which is the optimum time for intermediate accumulation. The fact that the solution is flowing means that it is resident in the laser beam for only a short length of time, less than about 0.15 seconds, reducing the chance of photoisomerisation of retinal occurring. A description of

the set up of the flow cell and pumps is given in Chapter 2. Results from trial experiments using the continuous flow cell and recording the resonance Raman spectra were very encouraging, and it was decided that this technique would be useful in the characterisation of the intermediate species.

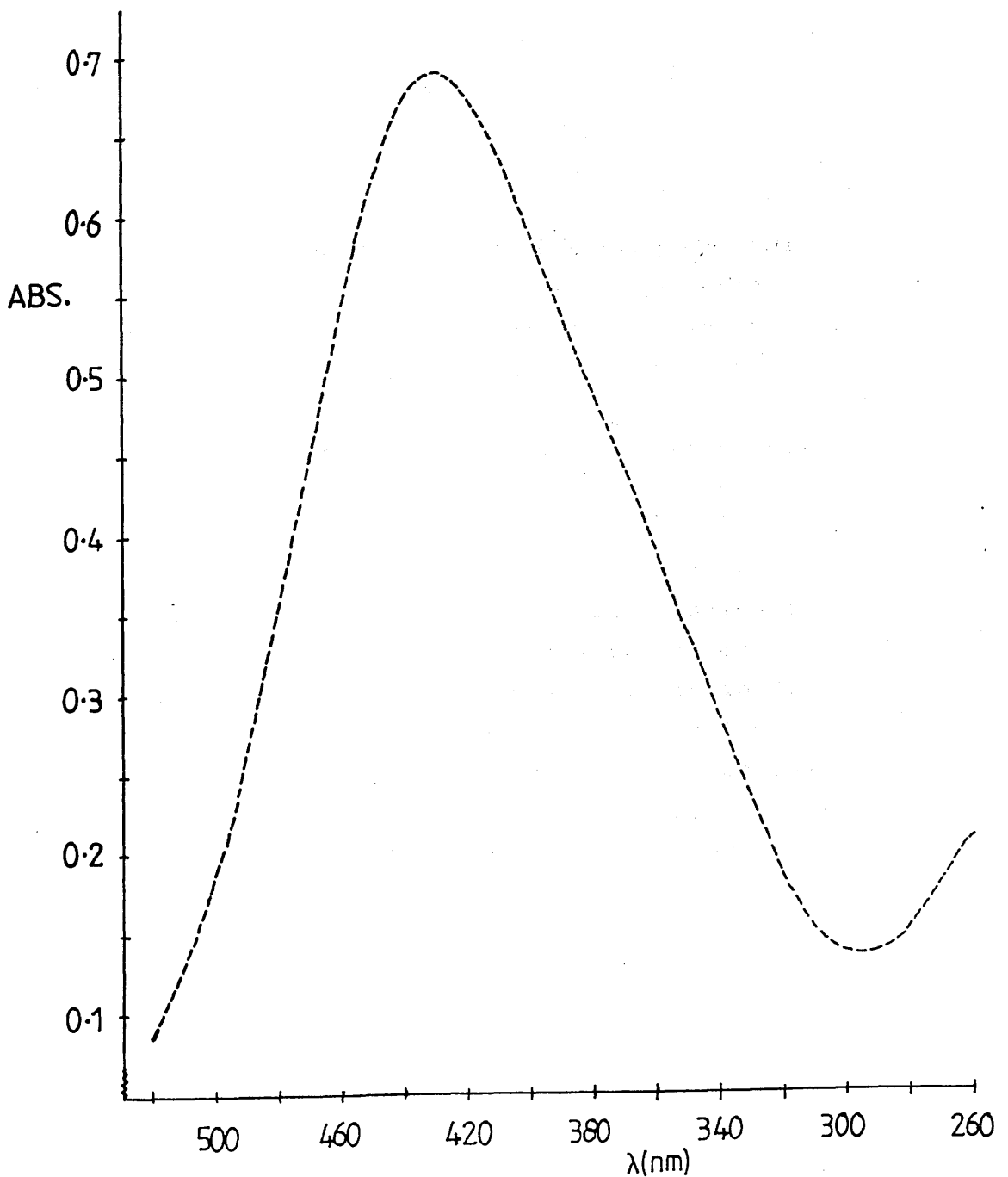
### 5.3 Experimental

The N-retinylidene n-butylamine schiff base was made in the usual way by addition of all-trans retinal dissolved in a small volume of ethanol to 10mM butylamine in aqueous detergent solution. For the resonance enhanced Raman spectroscopy a more concentrated solution of schiff base was used than that for UV/visible and stopped-flow spectroscopy. Trial runs using different concentrations of retinal and observing the spectrum of the unprotonated schiff base suggested an optimum concentration of approximately 0.3mM for the schiff base sample.

Before any resonance Raman experiments were performed, trial experiments on the UV/visible spectrometer using the pump system and flow cell were done. These trials involved mixing the schiff base in 2% (by volume) Ammonyx solution with a 0.2M acetate buffer at pH 4 in 2% Ammonyx solution. The two solutions were pumped separately using the peristaltic pumps to the T-piece mixer, and then the mixture flowed into the cell which was placed in the UV/visible spectrometer and a spectrum was recorded. The diameter of the tubing in the peristaltic pumps was varied, as was the speed of the pumps, until the time between mixing and reaching the cell was near to 10 seconds.

The spectrum in fig.5.1 was recorded using an identical set up to the one used during the Raman runs. The peak maximum in the spectrum is positioned at a wavelength of approximately 430nm and lies between the maxima for the unprotonated and protonated schiff bases which are 360nm and 440nm respectively, but nearer to the protonated schiff base peak. The position of this peak is obviously influenced by the large amount of protonated

FIGURE 5.1  
Continuous flow UV/visible spectrum of N-retinylidene  
n-butylamine schiff base approximately 10 seconds after  
pH-jump to pH 4.13 in 2% Ammonyx solution.



schiff base present at this pH, 10 seconds after mixing, and as a result it is not possible to predict the UV/visible spectrum of the intermediate, except to say that it is probably very similar to the parent schiff base. This trial run on the UV/visible spectrometer confirmed that adequate mixing was achieved by using the flow cell with the peristaltic pumps.

Resonance Raman spectroscopy was used to study the hydrolysis reaction in Ammonyx and Emulphogene at pH 4 and 5 and in SDS at pH 10.5. In each case spectra were recorded of the following species:

- (a) unprotonated schiff base
- (b) protonated schiff base
- (c) intermediate species
- (d) hydrolysis products
- (e) retinal.

For experiments in Ammonyx and Emulphogene, the unprotonated schiff base (a) was made as described previously in 2% detergent solution and the spectrum was recorded by pumping this through a single channel. The protonated schiff base (b) was formed by mixing (a) with 0.2M hydrochloric acid in 2% detergent solution, pumping the solutions separately through 2 channels. The intermediate species (c) was formed by mixing (a) with 0.2M acetate buffer at pH 4 or 5 in 2% detergent solution. The hydrolysis products (d) were formed by leaving (c) to react for 10-20 minutes (recorded stationary), and the retinal (e) was prepared in 0.2M acetate buffer pH 4 or 5 in 2% detergent solution (flowing through 1 channel). (It should be noted that for species (b) - the protonated schiff base - hydrolysis will not occur as the pH is very low due to the hydrochloric acid. Also, for the stationary spectrum of (d), the laser shutter was closed during the 10-20 minutes and re-opened after this time to record the spectrum.)

Controls were prepared for each of the species and these consisted of a solution of 10mM butylamine in 2% detergent solution for (a) - flowing single channel; a mixture of 10mM butylamine / 2% detergent solution and

0.2M hydrochloric acid / 2% detergent solution for (b) - flowing through 2 channels; a mixture of 10mM butylamine / 2% detergent and 0.2M acetate buffer pH 4 or 5 / 2% detergent for (c) - flowing through 2 channels; the same reactants as (c) but stationary instead of flowing for (d) and finally 0.2M acetate pH 4 or 5 / 2% detergent flowing through 1 channel for (e).

For the SDS experiments at pH 10.5 a slightly different procedure was used because of the high pH value required for hydrolysis. A very concentrated schiff base in ethanol was prepared and a small volume added to 10mM butylamine / 12.5mM SDS for (a) - flowing through 1 channel; a small volume of schiff base in ethanol added to 10mM hydrochloric acid / 12.5mM SDS for (b) - flowing through 1 channel; a mixture of (b) with 0.04M borate buffer pH 10.5 / 12.5mM SDS for (c) - flowing through 2 channels; the same reactants as (c) but left for approximately twenty minutes and a stationary spectrum recorded for (d) and retinal dissolved in 0.04M borate pH 10.5 / 12.5mM SDS for (e). Similar control reactions were performed as before with either the schiff base or retinal being omitted in each case. All the experiments were run at a temperature of 20°C. In the case of the intermediate spectrum the pH of a 1:1 mix of reactants was recorded to check that the pH of reaction was what it should be.

#### 5.4 Resonance Raman Spectroscopy

Polarised Raman spectra were obtained using an Applied Photophysics Model 36 multichannel spectrometer (see Chapter 2). Experiments were performed using the 488nm, 514nm and 457.9nm laser lines and similar results were obtained in each case except that background fluorescence was lowest with the 457.9nm line. The spectra recorded consisted of 400 accumulations with a 0.2 second acquisition time, and the spectrum of the relevant solvent control mixture was subtracted from the sample spectrum in each case. The y-axis in the Raman spectra corresponds to the number of photon counts during

the collection period and has arbitrary units.

The first Raman spectra to be recorded were those in Ammonyx at pH 4 and 5 where the concentration of intermediate should be at a maximum. Figures 5.2-5.6 show spectra of the protonated schiff base, intermediate species, unprotonated schiff base, hydrolysis products approximately 20 minutes after the pH-jump and retinal for experiments in Ammonyx, final pH value of 4.13. Table 5.1 lists the frequencies ( $\text{cm}^{-1}$ ) of the main peaks in the unprotonated and protonated schiff base, intermediate species and all-trans retinal obtained from these continuous flow resonance Raman spectra. The values obtained for the schiff base species (protonated and unprotonated) and the all-trans retinal are consistent with published results from Mathies et al<sup>24,25</sup>, taking into account the fact that the published figures are for crystalline species, compared to values in solution in table 5.1. The protonated schiff base spectrum shows a strong retinal C=C stretch band at  $1565\text{cm}^{-1}$ , a protonated imine C=N stretch at  $1656\text{cm}^{-1}$  and major fingerprint vibrations in the  $1100\text{-}1400\text{cm}^{-1}$  region which have been assigned for the all-trans retinal protonated schiff base. Comparison of this protonated schiff base spectrum with the spectrum recorded 10 seconds after pH-jump shows that changes have occurred.

Fig.5.7 shows these two spectra superimposed where SB is the protonated schiff base and X the species present after 10 seconds. The most prominent feature is the appearance of a band at  $1345\text{cm}^{-1}$  in the spectrum of X which is not present in the SB spectrum. In addition to this, there is a decrease in the intensity of bands at  $1240\text{cm}^{-1}$  and  $1656\text{cm}^{-1}$  in the spectrum of X compared to the spectrum of SB. Taking into account the fact that stopped-flow spectroscopy showed that under these same reaction conditions an accumulation of an intermediate occurred in the first 10 seconds, then the difference in spectra of X and SB can be explained by the fact that X contains an appreciable amount of carbinolamine intermediate, formed during the hydrolysis of the schiff base, and it is the presence of this intermediate that is

FIGURE 5.2  
Continuous flow resonance Raman spectrum of protonated  
N-retinylidene n-butylamine schiff base in Ammonyx.

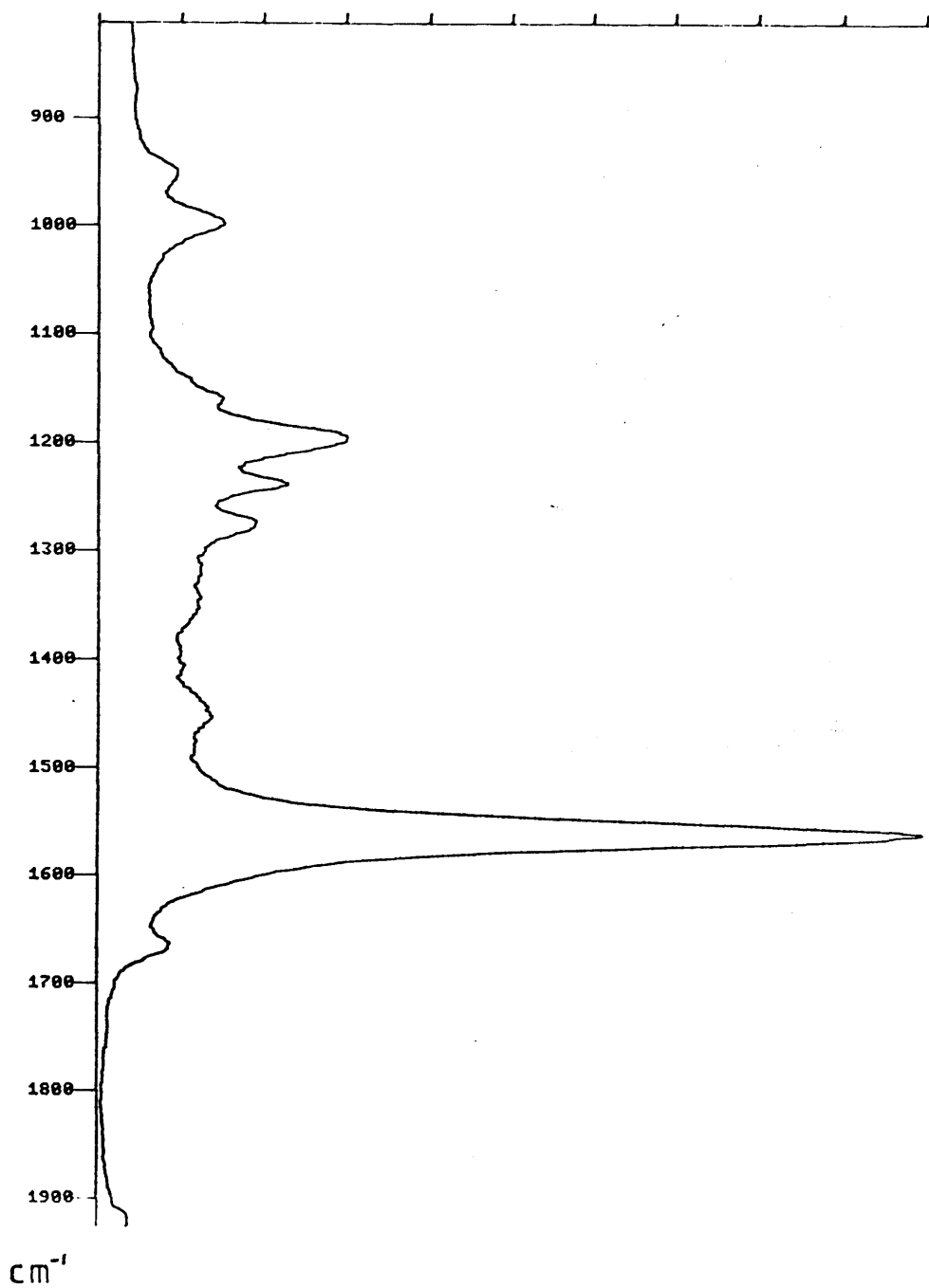


FIGURE 5.3  
Continuous flow resonance Raman spectrum of N-retinylidene  
n-butylamine schiff base in Ammonyx approximately 10 secs  
after pH-jump to pH 4.13.

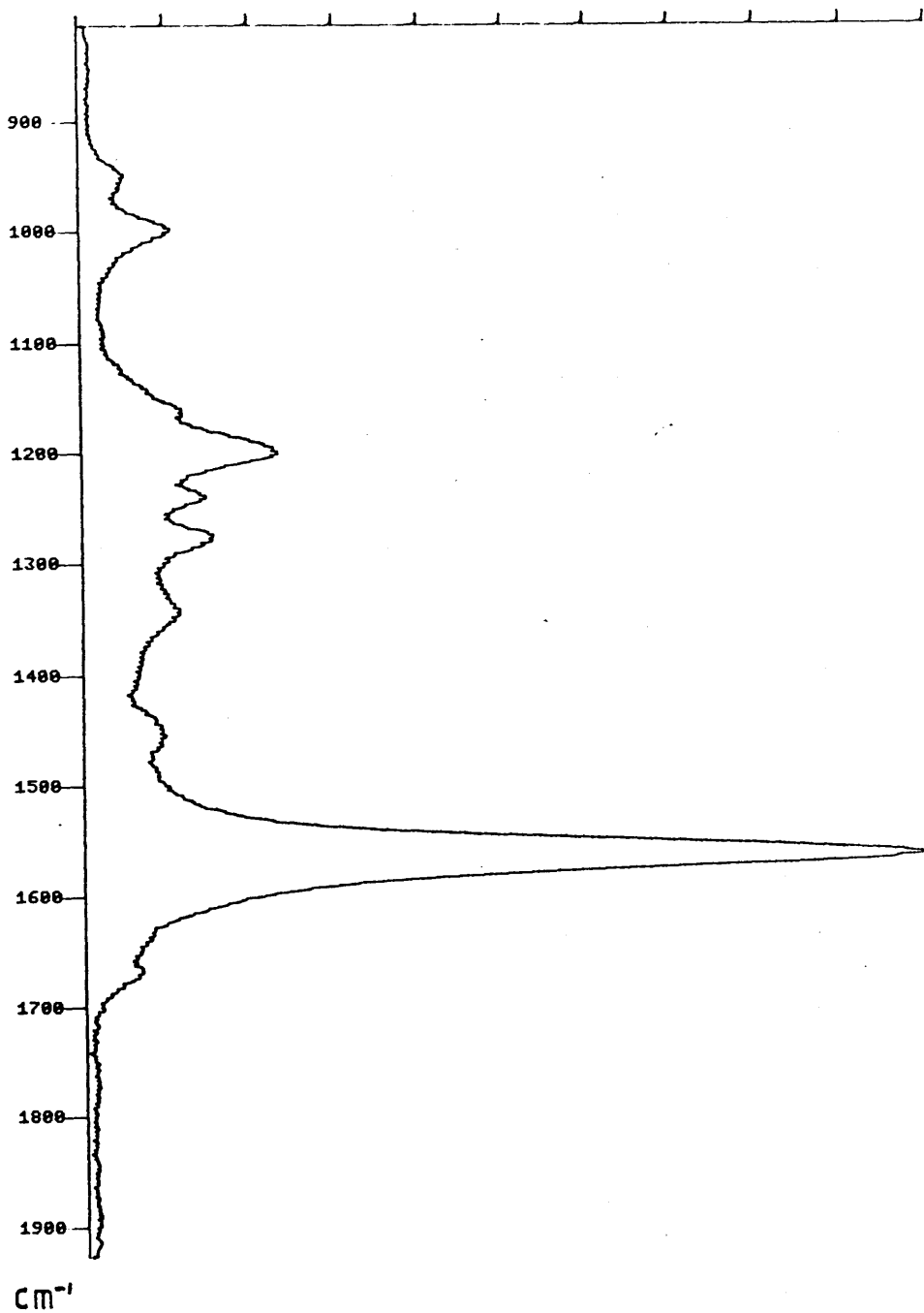


FIGURE 5.4  
Continuous flow resonance Raman spectrum of unprotonated  
N-retinylidene n-butylamine schiff base in Ammonyx.

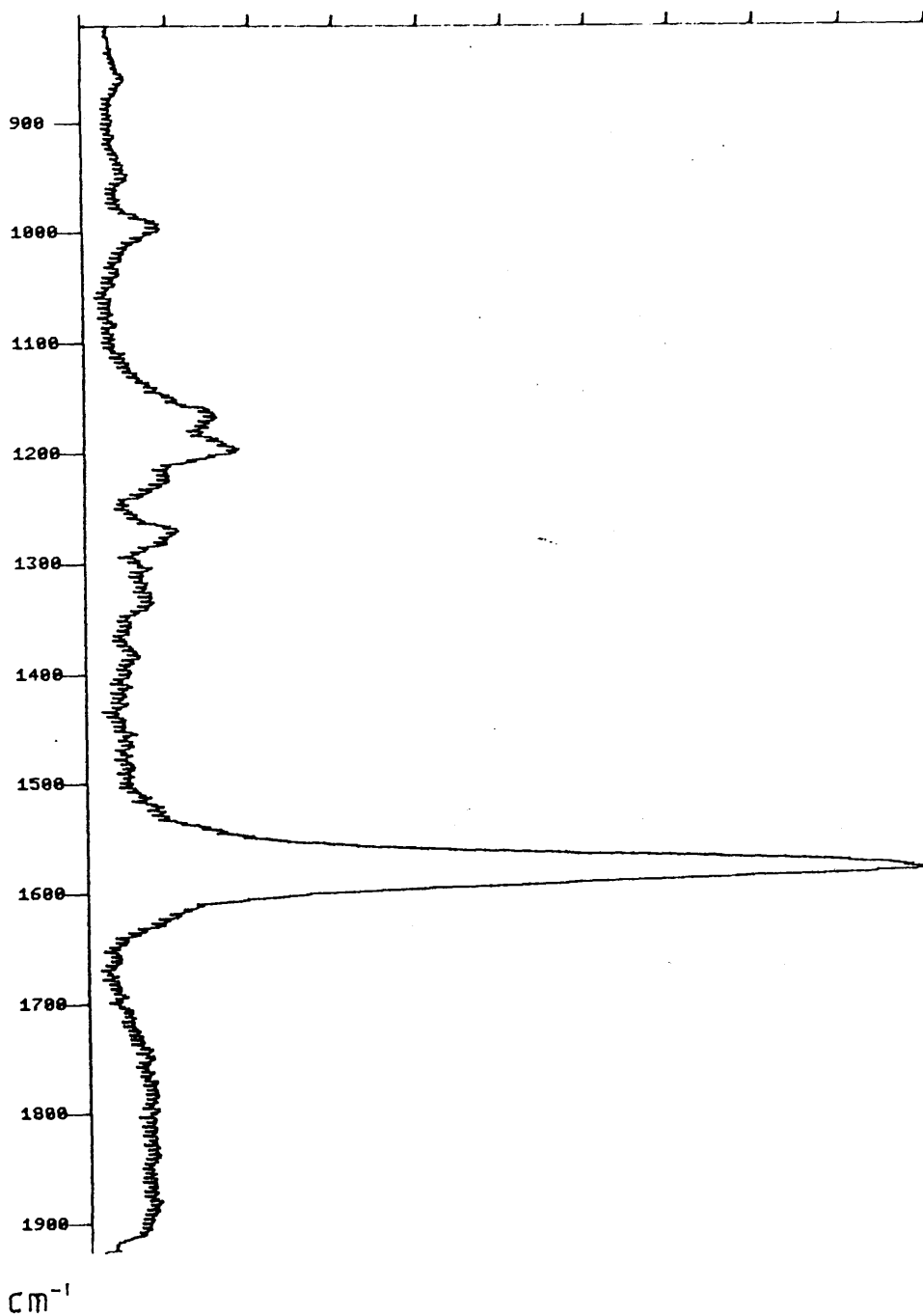


FIGURE 5.5  
Stationary resonance Raman spectrum of hydrolysis products  
of N-retinylidene n-butylamine in Ammonyx approximately  
20 minutes after pH-jump to pH 4.13.

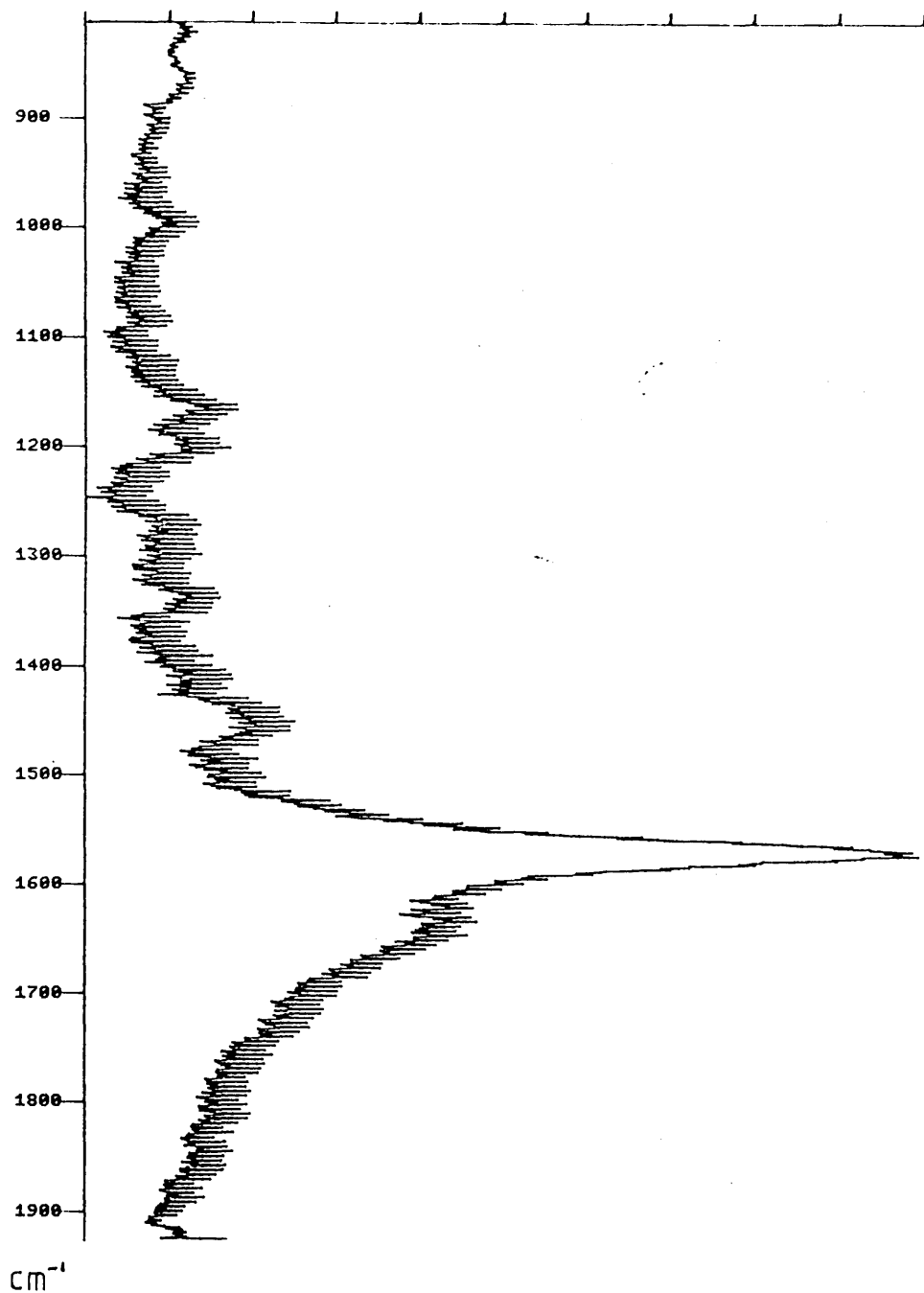


FIGURE 5.6  
Continuous flow resonance Raman spectrum of all-trans  
retinal in pH 4 buffer/Ammonyx.

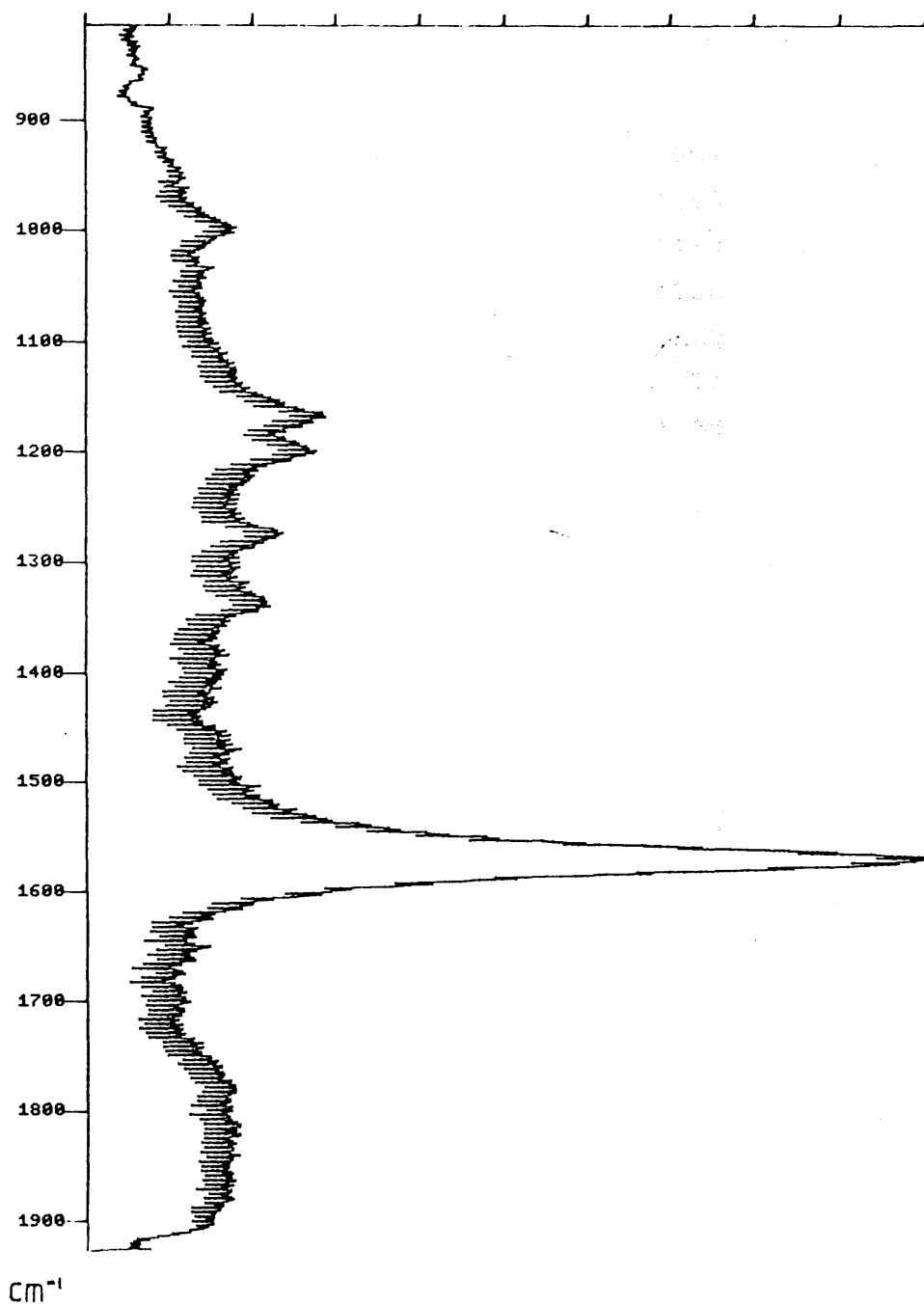


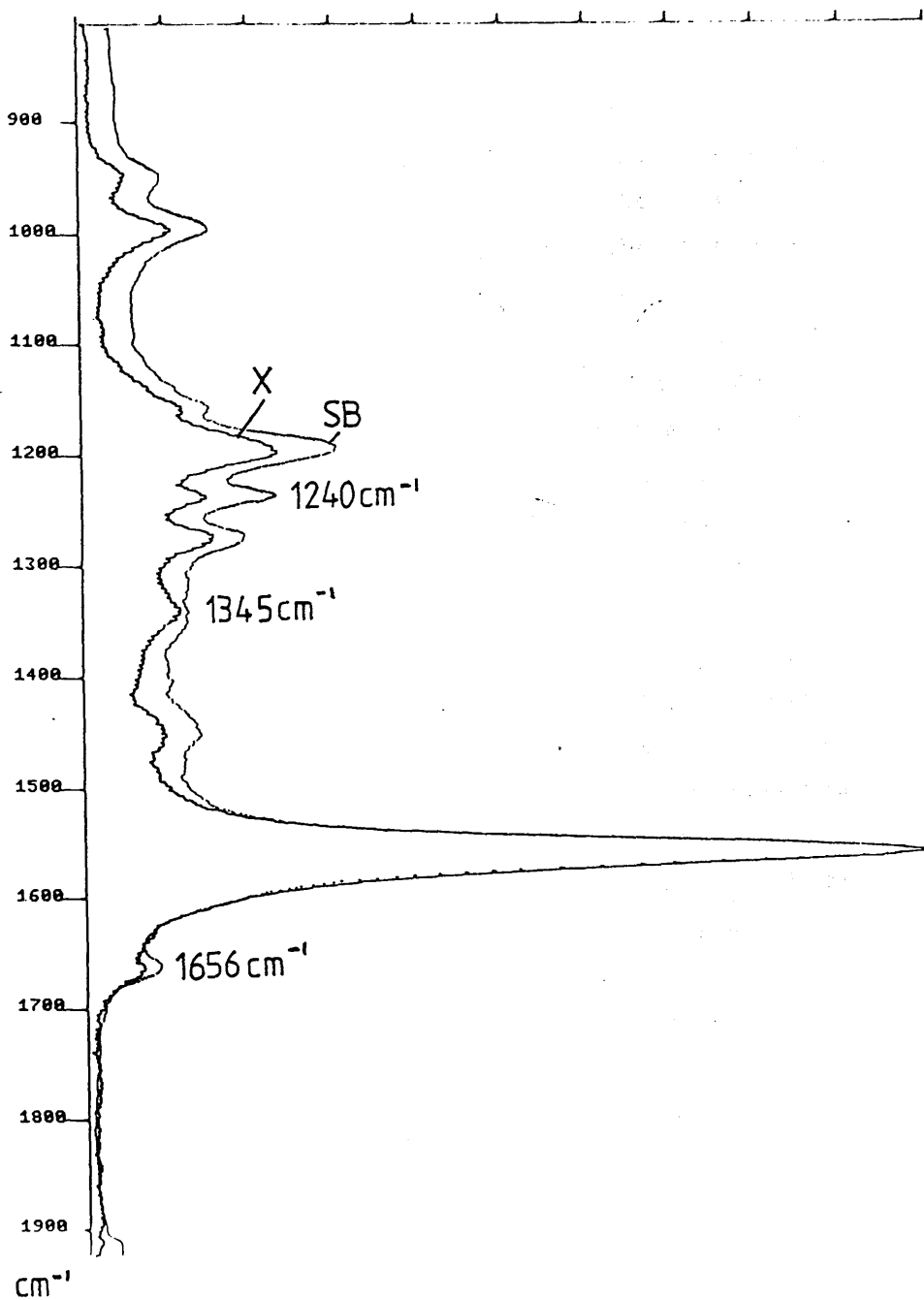
Table 5.1

Table of frequencies ( $\text{cm}^{-1}$ ) of main peaks in the resonance Raman spectra of N-retinylidene n-butylamine and its hydrolysis products in Ammonyx, pH 4.13.

Unprotonated schiff base	Protonated schiff base	Intermediate species	All-trans retinal
965	967	967	969
1010	1012	1012	1009
1164	1160	1160	1164
1195	1200	1200	1200
1223	1239	1240	1222
1270	1275	1276	1274
-	-	1345	1336
-	1453	1453	-
1582	1565	1565	1574
1625	1656	1656	-

FIGURE 5.7

Superimposed Raman spectra of N-retinylidene n-butylamine protonated schiff base (SB) and species present approx. 10secs after pH-jump to pH 4.13 in 2% Ammonyx solution (X).



responsible for the differences in the spectra. (The mixture X will still contain a large amount of protonated schiff base as the maximum amount of intermediate is estimated to be 50% of the schiff base concentration.)

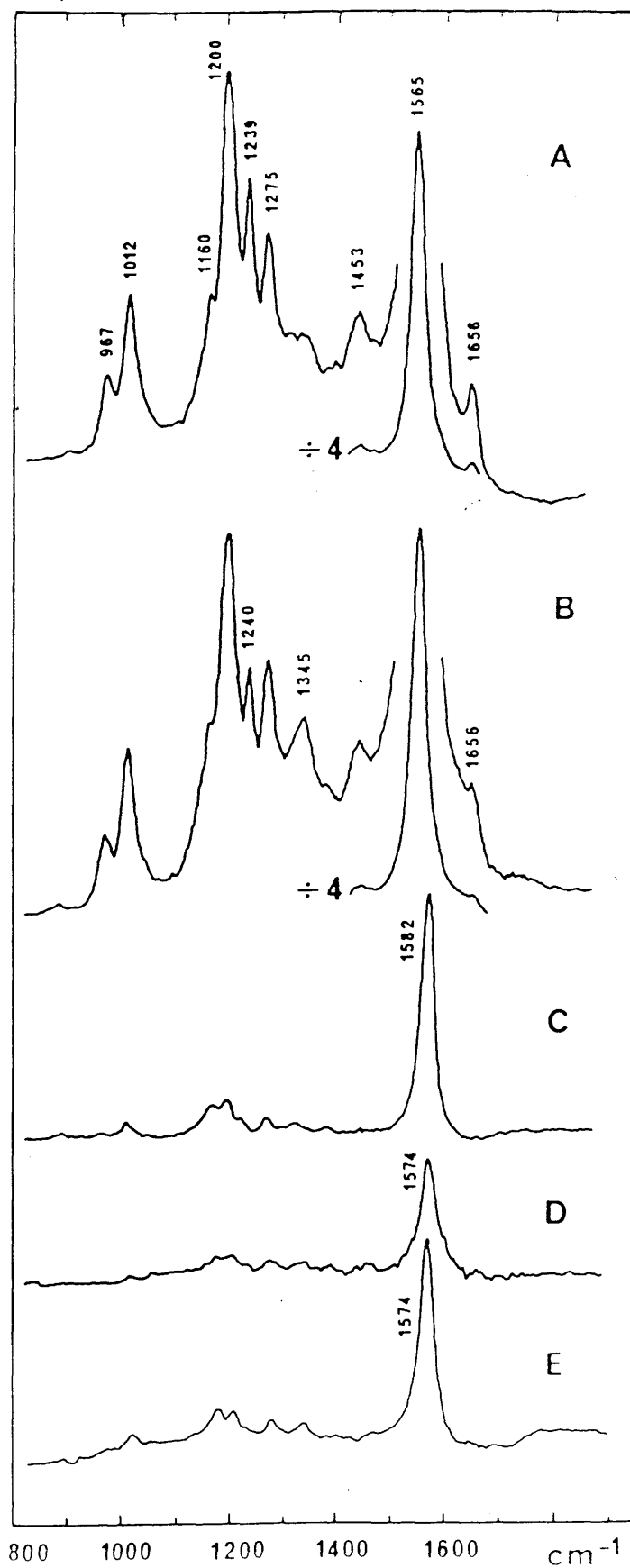
Examination of spectra of the unprotonated schiff base (fig.5.4) and all-trans retinal (fig.5.6) and values in table 5.1 show characteristic bands at  $1582\text{cm}^{-1}$  for the retinal C=C stretch in the unprotonated schiff base and at  $1574\text{cm}^{-1}$  in the all-trans retinal. These spectra, and indeed the spectrum of the hydrolysis products (fig.5.5), are very noisy compared to those of the unprotonated schiff base and the protonated schiff base 10 seconds after pH-jump because there is less resonance enhancement of these species. Figure 5.8 shows all the spectra together on the same diagram, drawn to scale (except where indicated), in order to show the different extents of resonance enhancement that occur on illumination with the 457.9nm laser line. Spectra A and B in fig.5.8 are of the protonated schiff base and the intermediate species approximately 10 seconds after pH jump, respectively. Both these spectra show intense resonance enhancement compared to spectra C,D and E (unprotonated schiff base, hydrolysis products after approximately 20 minutes and all-trans retinal respectively) which were run under the same conditions.

The reason for this enhancement is that Raman bands increase in intensity as the exciting frequency approaches the electronic absorption maximum. In spectra of A and B the maxima for the protonated schiff base (440nm) and the intermediate species (around 430nm ?) are close to the wavelength of the exciting laser line (457.9nm) when compared to the absorbance maxima of the unprotonated schiff base (360nm), retinal (380nm) and hydrolysis products which will contain mostly retinal as the absorbing species.

From figure 5.8 it is obvious that the features present in B which are different from A cannot be explained by suggesting they are due to the presence of unprotonated schiff base or all-trans retinal. Firstly the peak at  $1345\text{cm}^{-1}$  present in spectrum B is not present

FIGURE 5.8

Raman spectra of; A- N-retinylidene n-butylamine protonated schiff base, B- schiff base approximately 10 secs after pH-jump to pH 4.13, C- unprotonated schiff base, D- hydrolysis products approximately 20 minutes after pH-jump to pH 4.13 and E- all-trans retinal in pH 4 buffer.  
Drawn to scale except where shown.  
(Taken from ref.69)



in spectra of unprotonated schiff base or retinal and, more importantly, because of the resonance enhancement in spectra A and B, any contamination from unprotonated schiff base or retinal would not produce a peak as intense as the  $1345\text{cm}^{-1}$  peak in spectrum B anyway. It should also be noted that the presence of these contaminating species would produce a shift in the  $1565\text{cm}^{-1}$  C=C band which does not occur, and that at pH 4 the schiff base is predominantly in the protonated form.

Similar results to these were obtained when examining the schiff base hydrolysis at pH 5 in Ammonyx. The reaction conditions were the same as those in the pH 4 experiments except that the intermediate spectrum was obtained by mixing unprotonated schiff base in 2% Ammonyx solution with 0.2M acetate buffer pH 5 / 2% Ammonyx detergent.

Spectra were recorded and fig.5.9 shows superimposed continuous flow Raman spectra of the protonated schiff base and the intermediate species approximately 10 seconds after pH jump to pH 5.12. Exactly the same features can be identified as those in spectra at pH 4, with a peak appearing at  $1345\text{cm}^{-1}$  in the spectrum of X which is not present in the spectrum of SB, and peaks at  $1240\text{cm}^{-1}$  and  $1656\text{cm}^{-1}$  having lower intensity in the spectrum of X compared to that of SB. Table 5.2 lists the frequencies of the main peaks in the spectra.

Again at this pH value in Ammonyx, stopped-flow traces have shown that 10 seconds after pH jump to 5.12 is the time when the optimum concentration of intermediate is present, and so these features must be due to the presence of this intermediate species. Repetition of spectra of unprotonated schiff base, hydrolysis products after 20 minutes and all-trans retinal confirms the previous results that resonance enhancement of these species is much lower than the protonated schiff base / intermediate species.

The experiments in Ammonyx detergent were repeated in Emulphogene detergent, and reaction conditions and solutions were identical except that solutions were made in 2% Emulphogene detergent instead of 2% Ammonyx

FIGURE 5.9

Superimposed Raman spectra of N-retinylidene n-butylamine protonated schiff base (SB) and species present approx.10 secs after pH-jump to pH 5.12 (X), in 2% Ammonyx solution.

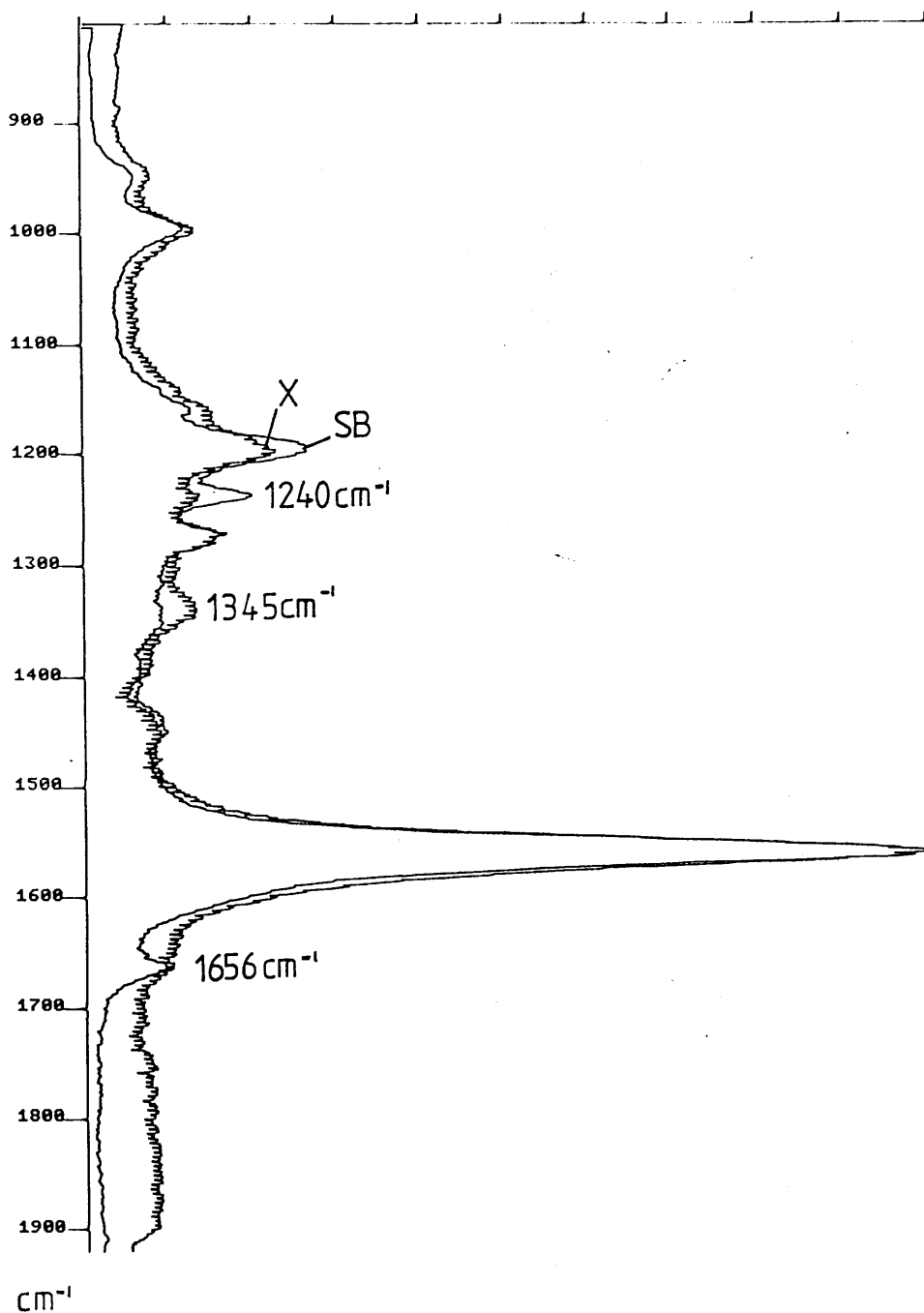


Table 5.2

Table of frequencies ( $\text{cm}^{-1}$ ) of main peaks in the resonance Raman spectra of N-retinylidene n-butylamine protonated schiff base and its hydrolysis product 10 seconds after pH jump to pH 5.12, in Ammonyx.

Protonated schiff base	Intermediate species
968	968
1012	1012
1160	1160
1200	1200
1239	1241
1275	1275
-	1345
1452	1453
1565	1565
1656	1656

detergent. Results from stopped-flow traces showed that the maximum accumulation of intermediate occurred approximately 100 seconds after pH jump to pH 4 or 5. The accumulation is also much lower than in Ammonyx, so that for the spectra in Emulphogene there should be hardly any evidence of intermediate 10 seconds after pH jump.

The continuous flow resonance Raman spectrum of the protonated schiff base in Emulphogene is shown in figure 5.10, and the frequencies ( $\text{cm}^{-1}$ ) are shown in table 5.3. Once again the major features of the crystalline protonated schiff base, assigned by Mathies et al, can be identified. The change of detergent from Ammonyx to Emulphogene has caused a small shift in some of the frequencies (comparison of values in table 5.3 with those in table 5.1), but overall the protonated schiff base peaks in solutions are similar.

Figures 5.11 and 5.12 show the continuous flow resonance Raman spectra of the N-retinylidene n-butylamine schiff base approximately 10 seconds after pH jump to pH 4.11 and pH 5.11 respectively, and table 5.3 lists the frequencies of the major peaks in these spectra. It is obvious from examination of the spectra that the difference between protonated schiff base (fig.5.10) and species present 10 seconds after pH jump (figures 5.11, 5.12) is much less marked in Emulphogene than in Ammonyx.

It is possible that in figures 5.11 and 5.12 there is a peak appearing at around  $1350\text{cm}^{-1}$  which is not so obvious in the protonated schiff base spectrum in figure 5.10. In the spectrum of pH jump to pH 5.11, the peaks at  $1242\text{cm}^{-1}$  and  $1660\text{cm}^{-1}$  are less intense than in the protonated schiff base spectrum, and for pH jump to 4.11 these peaks are approximately the same as the protonated schiff base spectrum. This seems reasonable as the reaction in Emulphogene is slightly faster at pH 5 than at pH 4 and it is more likely that intermediate will have formed.

FIGURE 5.10  
Continuous flow resonance Raman spectrum of protonated  
N-retinylidene n-butylamine schiff base in Emulphogene.

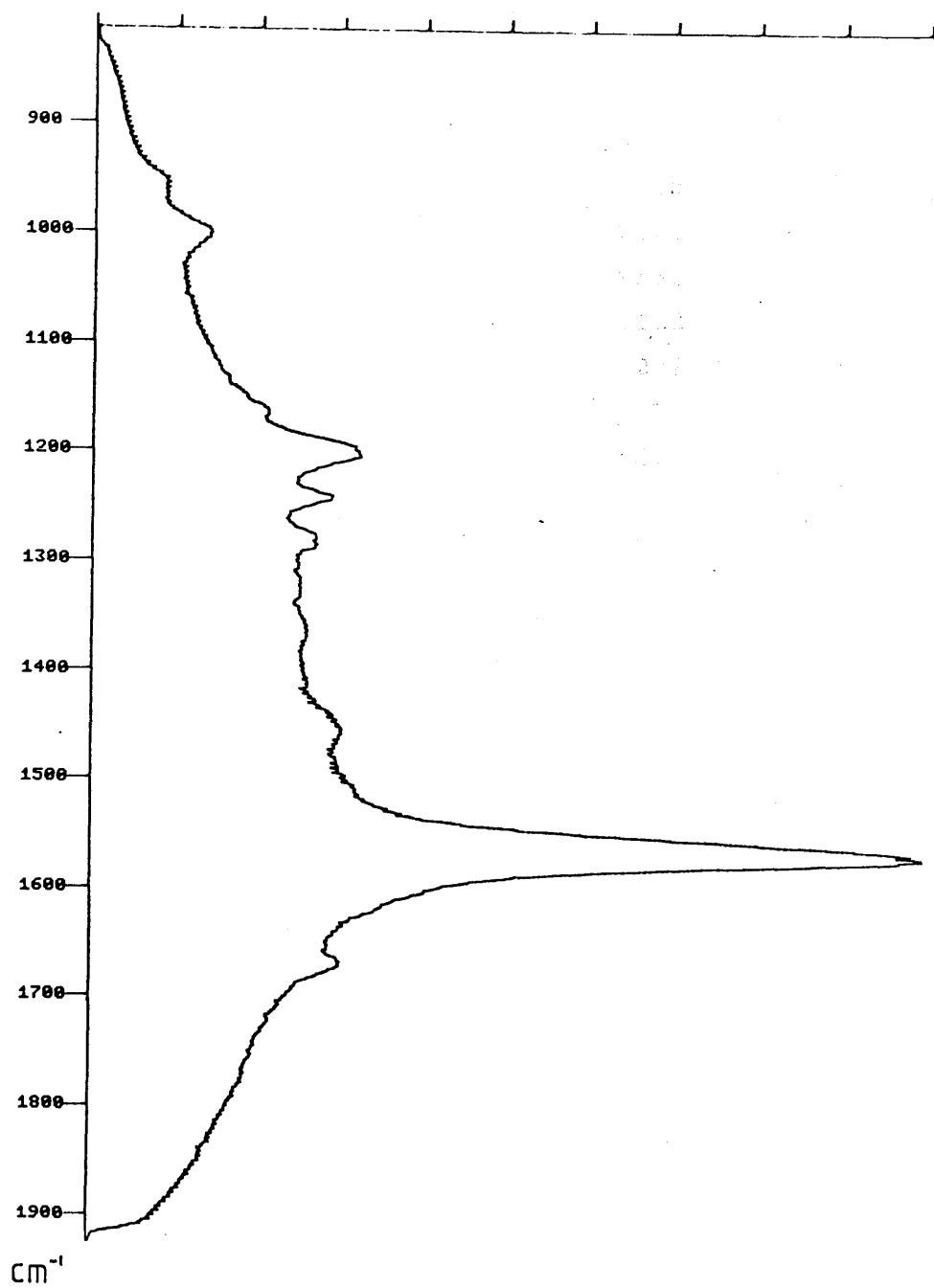


Table 5.3

Table of frequencies ( $\text{cm}^{-1}$ ) of main peaks in the resonance Raman spectra of N-retinylidene n-butylamine protonated schiff base and its hydrolysis product 10 seconds after pH jump to pH 4.11 and pH 5.11, in Emulphogene.

Protonated schiff base	Hydrolysis product after pH jump to pH 4.11	Hydrolysis product after pH jump to pH 5.11
968	968	968
1012	1012	1013
1162	1162	1162
1203	1202	1202
1242	1242	1242
1277	1277	1277
-	1353	1351
1455	1456	1455
1570	1570	1566
1660	1660	1660

FIGURE 5.11  
Continuous flow resonance Raman spectrum of N-retinylidene  
n-butylamine schiff base in Emulphogene approximately 10secs  
after pH-jump to pH 4.11.

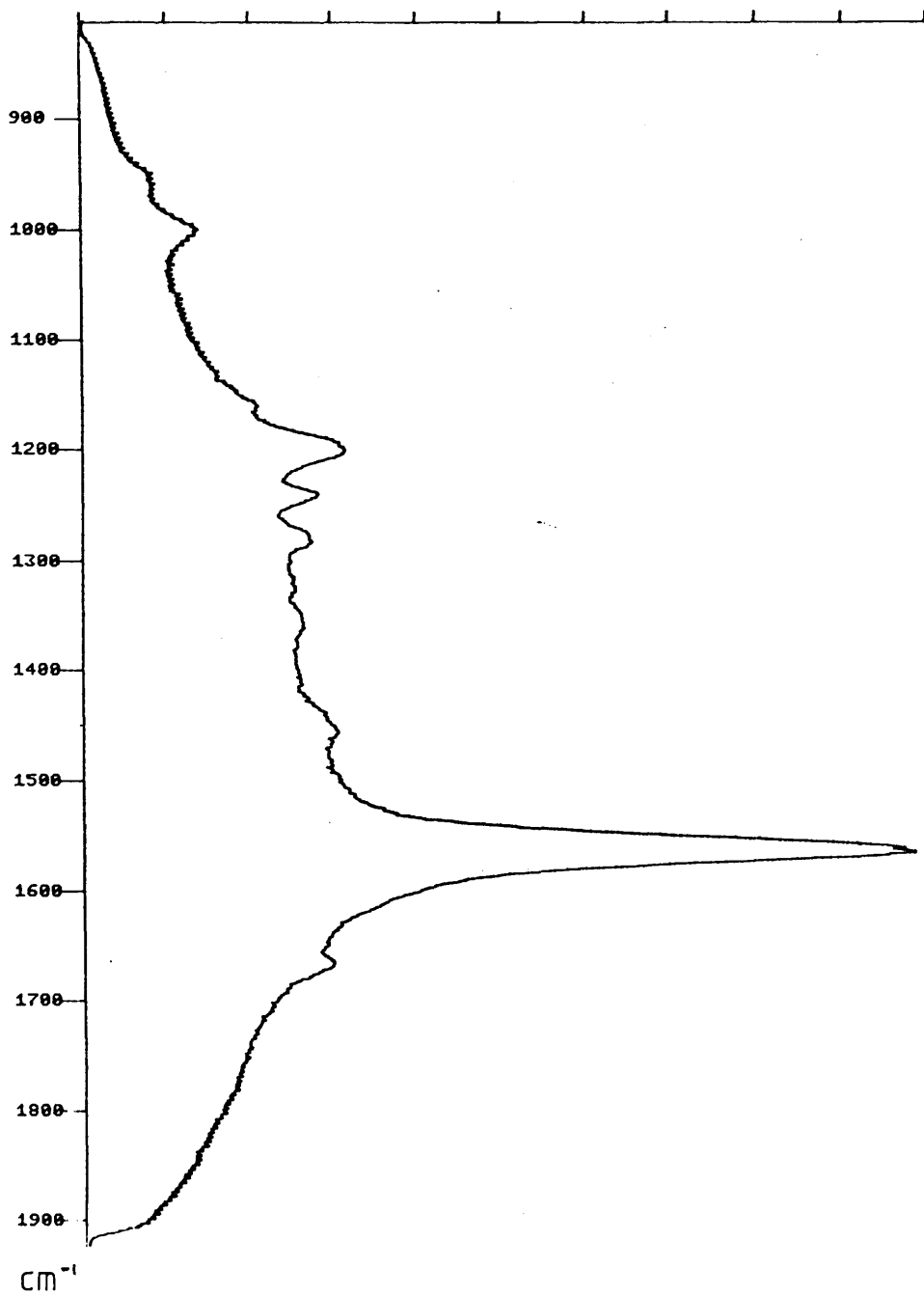
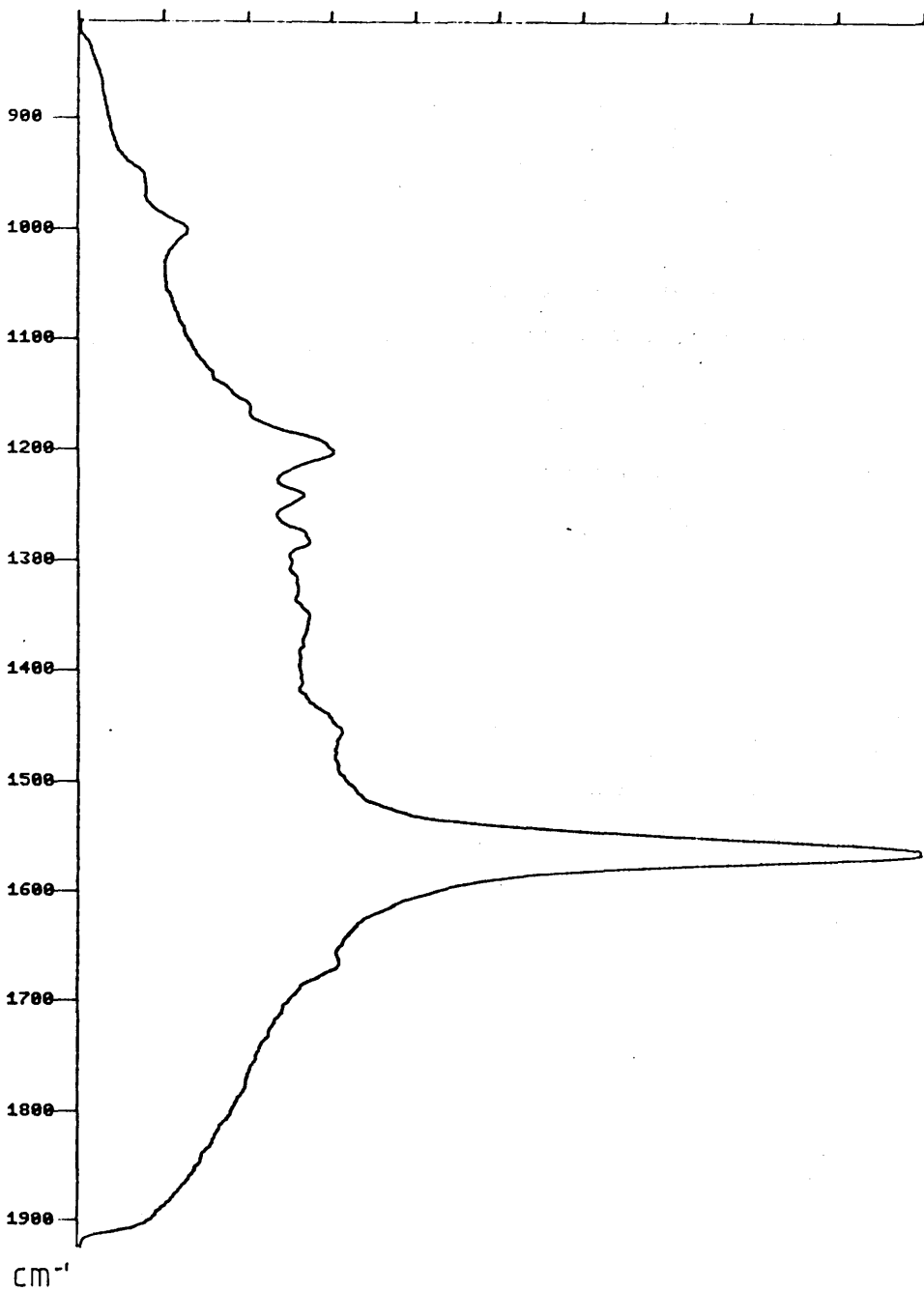


FIGURE 5.12

Continuous flow resonance Raman spectrum of N-retinylidene n-butylamine schiff base in Emulphogene approximately 10secs after pH-jump to pH 5.11.



Overall, the similarity in these figures shows that very little intermediate formation has occurred during the 10 seconds after pH jump, and the species present at this time in Emulphogene is very predominantly protonated schiff base.

These experiments with Emulphogene can act as a control reaction for the set up with the pump system where the solutions are reaching the flow cell 10 seconds after mixing. The fact that the features present in the intermediate spectrum in Ammonyx are not seen in Emulphogene shows that these features are not simply due to mixing the schiff base solution with any buffer/detergent mixture, nor due to photoisomerisation, but are specific features seen when an appreciable amount of intermediate species is present.

Experiments in SDS detergent were done and the solutions were prepared as described previously (section 5.3). Continuous flow resonance Raman spectra of the protonated schiff base and species present 10 seconds after pH jump to 10.34 are shown in figures 5.13 and 5.14 respectively, and the frequencies ( $\text{cm}^{-1}$ ) of the main peaks are shown in table 5.4.

It is very difficult to establish any differences in these spectra because the spectrum in figure 5.14 is so noisy, and the intensity of some peaks in figure 5.13 is very low. The intensity of peaks at  $1232\text{cm}^{-1}$ ,  $1450\text{cm}^{-1}$  and  $1656\text{cm}^{-1}$  in figure 5.13 is greater than in figure 5.14, and it would appear that peaks at  $1324\text{cm}^{-1}$  and  $1336\text{cm}^{-1}$  in the protonated schiff base spectrum have converged in the pH jump spectrum, but this region is so noisy it is impossible to even assign accurate frequencies to these peaks.

The results of stopped-flow traces would suggest that accumulation of intermediate for the hydrolysis reaction in SDS at pH 10.5 occurs in approximately 30-40 seconds, but again the concentration of the intermediate is much smaller than that in Ammonyx. It is not possible to decide from the spectra recorded whether the species present in figure 5.14 is the intermediate, but there are differences between this spectrum and the protonated

FIGURE 5.13  
Continuous flow resonance Raman spectrum of protonated  
N-retinylidene n-butylamine schiff base in SDS.

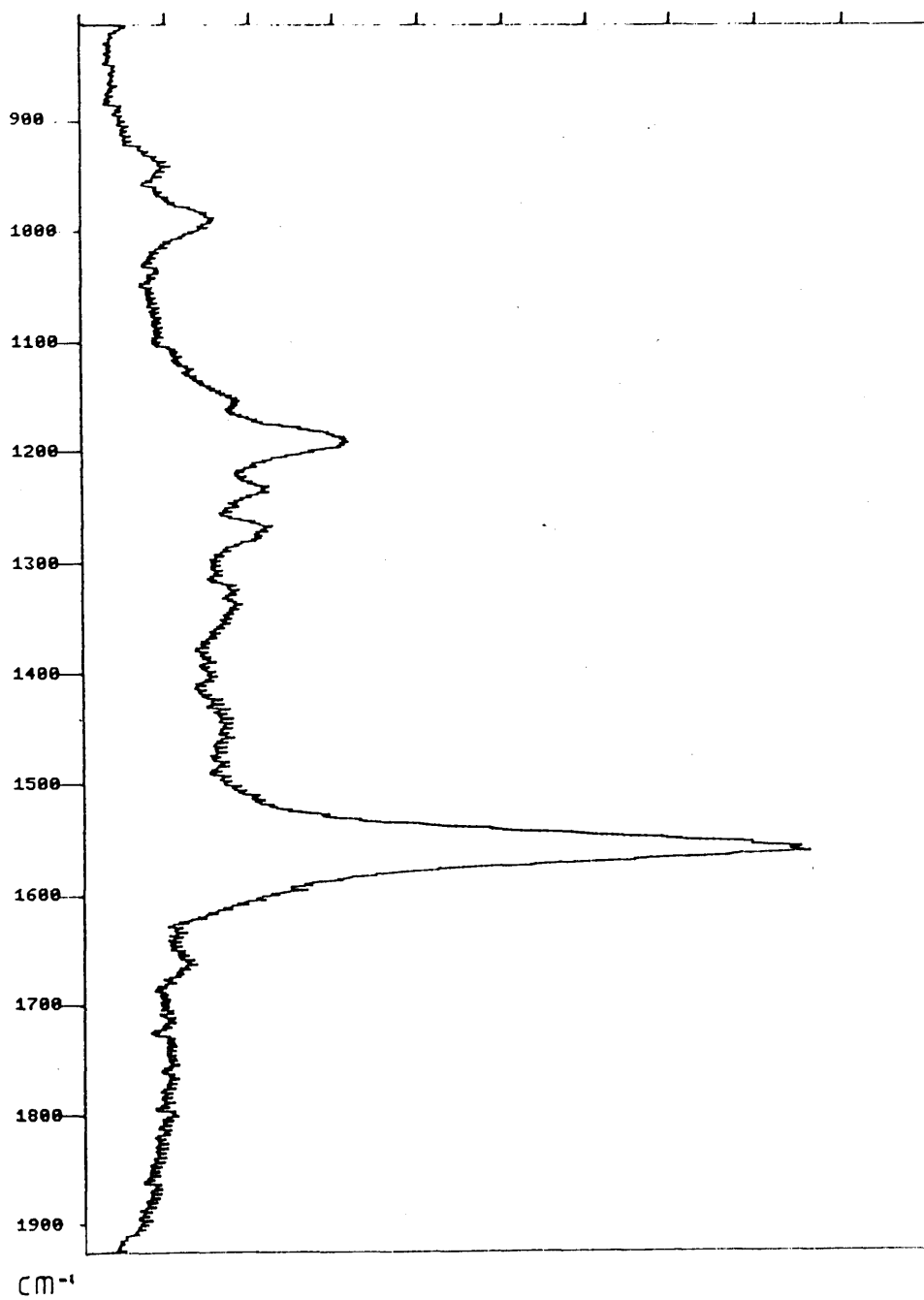


FIGURE 5.14  
Continuous flow resonance Raman spectrum of N-retinylidene  
n-butylamine schiff base in SDS approximately 10secs after  
pH-jump to pH 10.34.

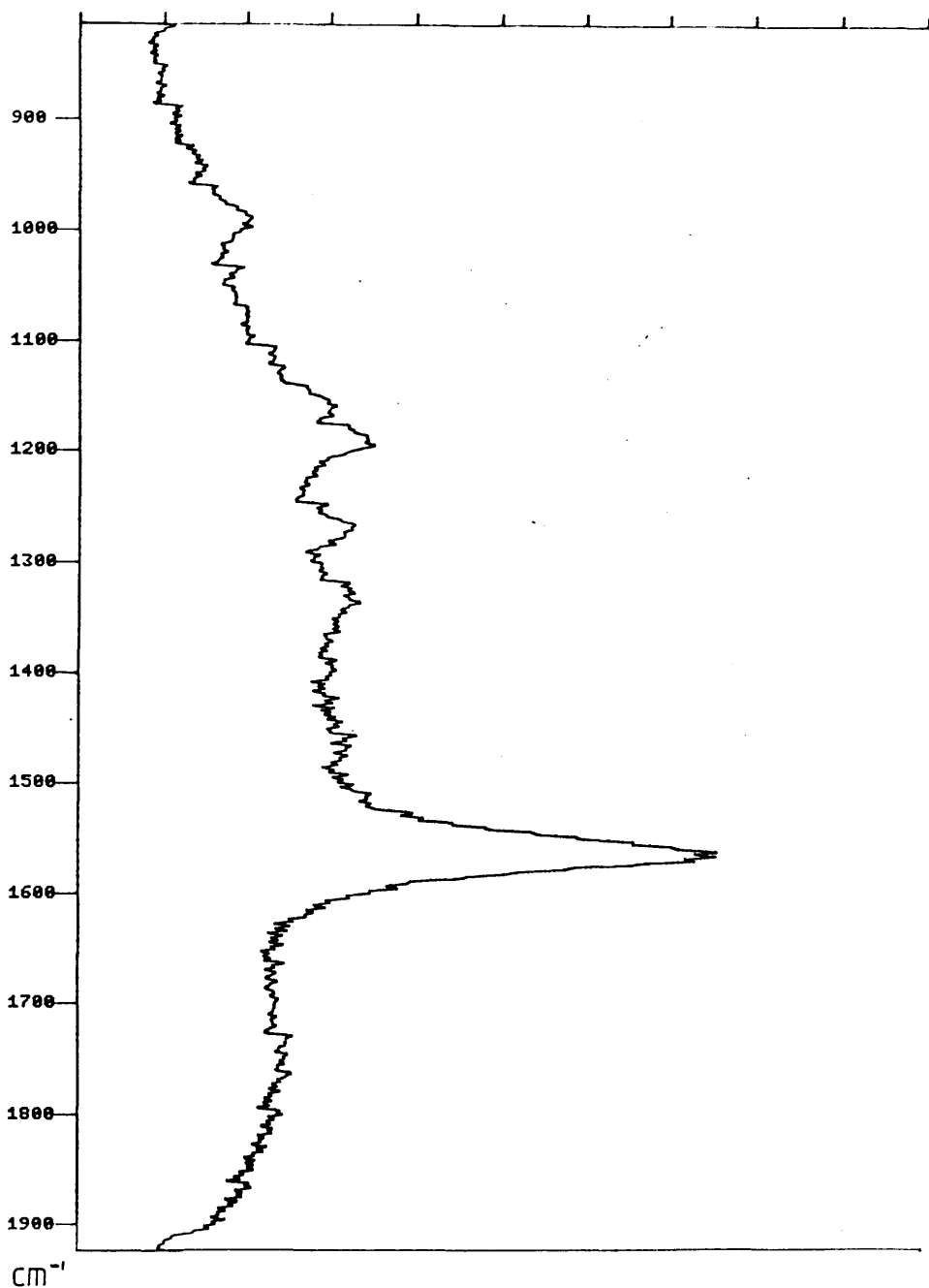


Table 5.4

Table of frequencies ( $\text{cm}^{-1}$ ) of main peaks in the resonance Raman spectra of N-retinylidene n-butylamine protonated schiff base and its hydrolysis product 10 seconds after pH jump to pH 10.34 in SDS.

Protonated schiff base	Hydrolysis product after pH jump to pH 10.34
958	958
1002	1002
1153	1160
1190	1190
1232	-
1273	1270
1324	
1336	1330
1450	-
1558	1563
1656	-

schiff base spectrum in SDS.

Overall, the best evidence for the presence of the intermediate is obtained in the Ammonyx experiments at pH 4 and 5, as would be expected from previous results. The main differences in the spectra of the protonated schiff base and intermediate species in Ammonyx at pH 4 and 5, as previously stated, are the loss of intensity of the  $1240\text{cm}^{-1}$  and  $1656\text{cm}^{-1}$  bands in the intermediate spectrum compared to the protonated schiff base spectrum, and the presence of the new band at  $1345\text{cm}^{-1}$  in the intermediate spectrum.

The band at  $1656\text{cm}^{-1}$  has previously been assigned<sup>8,5</sup> and is predominantly due to the C=N stretch of the protonated schiff base. It is therefore not surprising that the intensity of this band should decrease after the pH jump when the intermediate species accumulates, because the C=N group is not present in the carbinolamine intermediate. The band at  $1240\text{cm}^{-1}$  in the protonated schiff base is thought to be a highly mixed combination of C-C, C=C, C-CH<sub>3</sub> stretches and CCH in-plane hydrogen rocks involving carbon atoms 11-15<sup>8,5</sup>. The changes occurring at C-15 during the formation of the carbinolamine (formation of C<sub>15</sub>-OH bond and conversion of C=N to C-N) could therefore cause a change of intensity in the  $1240\text{cm}^{-1}$  band. It should however be noted that this peak is more intense in the detergent solution spectra than in the crystalline spectra, and this could be due to the fact that the conformation of the schiff base is slightly different in the micelle and the crystal, which may affect mode assignment.

The assignment of the band at  $1345\text{cm}^{-1}$  in the intermediate spectrum is more difficult as there are no carbinolamine spectra in the literature with which to compare the spectrum recorded here. The frequency of this vibration is possibly due to an alcoholic O-H in-plane deformation of the carbinolamine intermediate, and deuterium labelling experiments were done in order to test this possibility.

If the band at  $1345\text{cm}^{-1}$  is due to the presence of the -OH group in the carbinolamine, then replacement of water

by deuterium oxide will result in a shift of frequency to a lower value. This is because the -OH group on the carbinolamine is replaced by an -OD group in deuterium oxide, and the increase in mass due to the presence of deuterium instead of hydrogen will cause a decrease in frequency.

### 5.5 Use of Deuterium Oxide in Schiff Base Hydrolysis

The hydrolysis experiment in Ammonyx at pH 4 was repeated in Ammonyx at pD 4, replacing all water by deuterium oxide. The experimental set up was exactly the same as before, and spectra of the protonated schiff base and hydrolysis products 10 seconds after pD jump to pD 4.01 are shown in figures 5.15 and 5.16 with values of frequencies ( $\text{cm}^{-1}$ ) listed in table 5.5.

The spectra recorded seemed disappointing at first because there was very little difference in spectra of the protonated schiff base and hydrolysis products - there was possibly a peak at around  $1349\text{cm}^{-1}$  in the "intermediate" spectrum, but the intensity is very low and the spectrum is noisy in this region anyway. However the ultra-violet and stopped-flow spectroscopy experiments using deuterium oxide (Chapter 4) confirmed that the reaction occurred much more slowly when deuterium oxide was used as solvent, and this has obviously resulted in the formation of much smaller concentrations of carbinolamine intermediate. Because of these kinetic isotope effects, the deuterium labelling experiment was unable to assist in the assigning of the  $1345\text{cm}^{-1}$  band in the carbinolamine intermediate spectrum.

It is interesting to note that most of the bands listed in table 5.5 for the deuterium oxide experiment are essentially identical to those listed in table 5.1 for the water experiment, with the exception that the  $1656\text{cm}^{-1}$  band has moved to  $1638\text{cm}^{-1}$  in  $\text{D}_2\text{O}$ . This is not surprising as the hydrogen atom on the protonated nitrogen in the schiff base will exchange with deuterium from the  $\text{D}_2\text{O}$ , thus affecting the frequency of the  $1656\text{cm}^{-1}$  C=N protonated schiff base band, causing a

FIGURE 5.15  
Continuous flow resonance Raman spectrum of protonated  
N-retinylidene n-butylamine schiff base in Ammonyx, D<sub>2</sub>O.

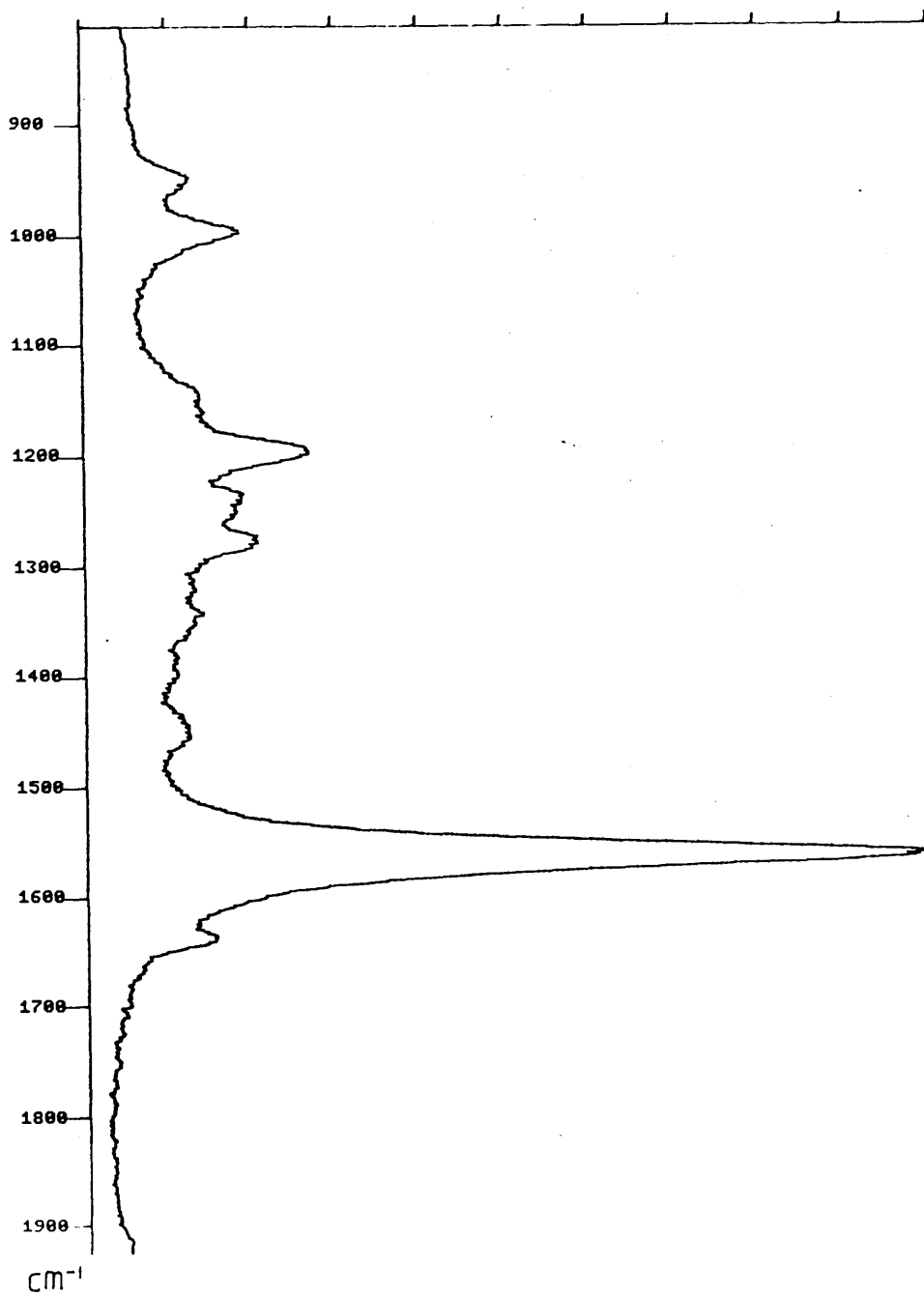


FIGURE 5.16  
Continuous flow resonance Raman spectrum of N-retinylidene  
n-butylamine schiff base in Ammonyx, D<sub>2</sub>O approximately 10  
secs after pD-jump to pD 4.01.

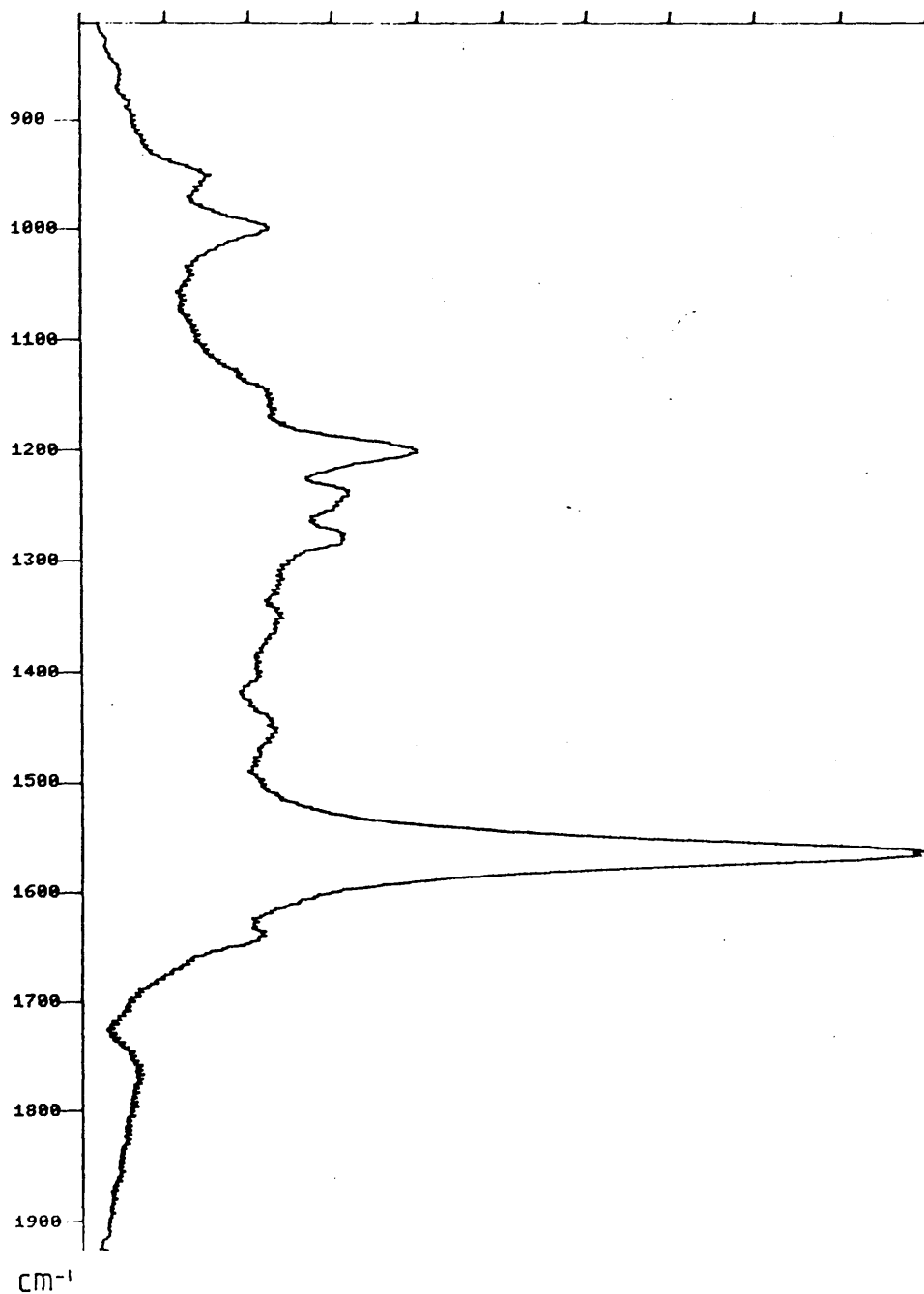


Table 5.5

Table of frequencies ( $\text{cm}^{-1}$ ) of main peaks in the resonance Raman spectra of N-retinylidene n-butylamine protonated schiff base and its hydrolysis product 10 seconds after pH jump to pD 4, in Ammonyx/D<sub>2</sub>O.

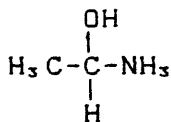
Protonated schiff base	Hydrolysis product after pH jump to pD 4.01
967	967
1012	1012
1158	1158
1200	1200
1239	1239
1276	1276
-	? 1349
1453	1453
1567	1567
1638	1638

decrease in frequency to  $1638\text{cm}^{-1}$ .

In the absence of any further information it is not possible to make a definite assignment for the  $1345\text{cm}^{-1}$  band in the carbinolamine intermediate spectrum.

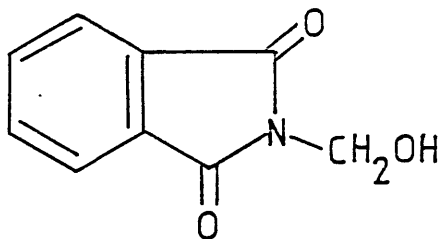
Infra-red spectra of some carbinolamine species have been recorded, for example 1-aminoethanol (a) and N-(hydroxymethyl) phthalimide (b) shown below, and both of these have bands at around  $1350\text{cm}^{-1}$  in their spectra. In general, primary and secondary alcohols would be expected to have bands in the infra-red spectrum in the region  $1250\text{-}1350\text{cm}^{-1}$  due to an -OH bending mode. In the absence of any Raman spectra of carbinolamine species, comparison with infra-red spectra would suggest that the  $1345\text{cm}^{-1}$  could be explained by the -OH bend.

(a)



secondary alcohol

(b)



primary alcohol

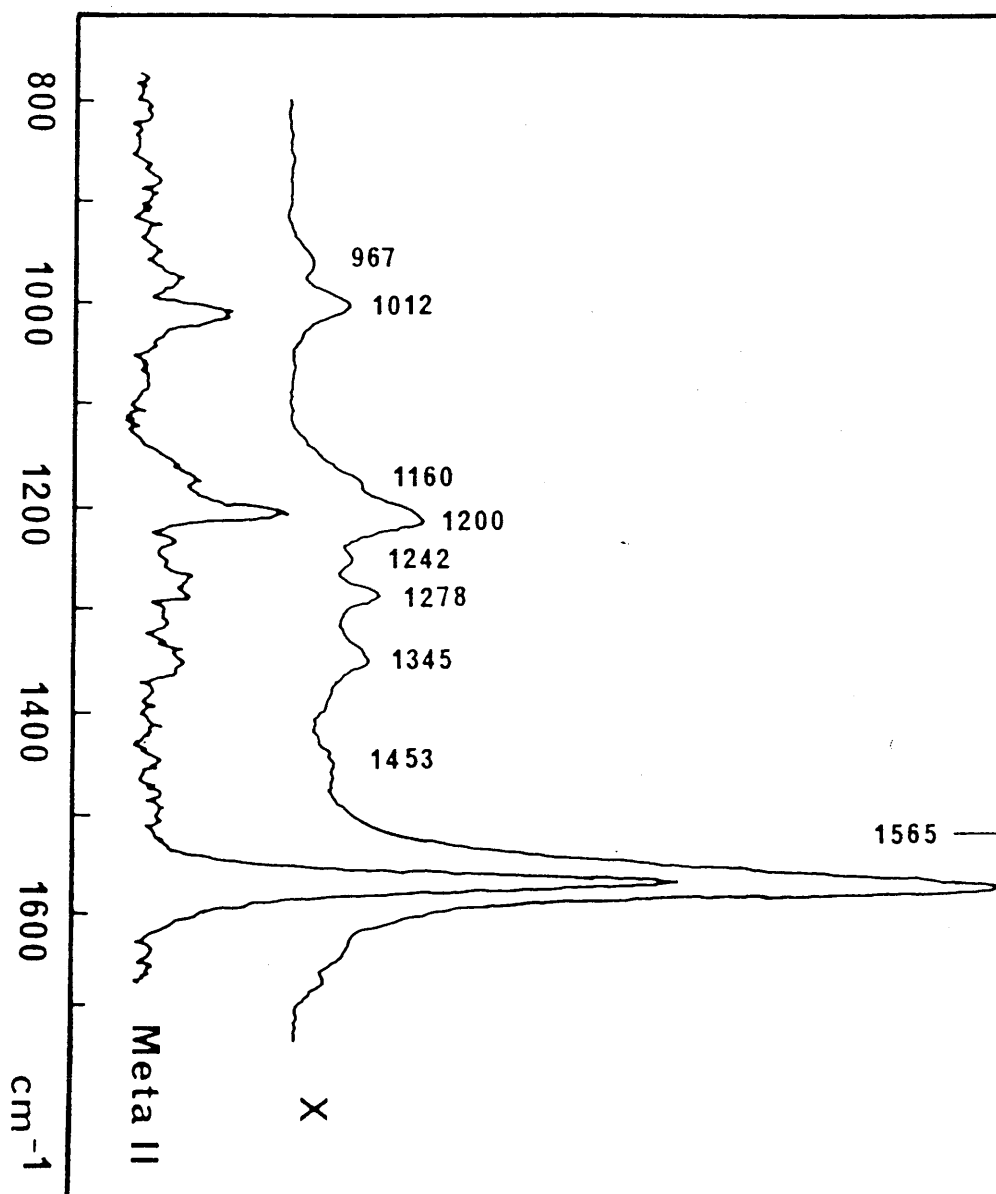
## 5.6 The Resonance Raman Spectrum of the Carbinolamine Intermediate

As was previously mentioned, the spectrum in figure 5.3, of the N-retinylidene n-butylamine schiff base 10 seconds after pH jump to pH 4 in Ammonyx, actually consists of a mixture of the carbinolamine intermediate formed during the hydrolysis reaction, and the protonated schiff base itself, in roughly equal proportions. It is therefore possible to subtract 50% of the protonated schiff base spectrum in figure 5.2 from figure 5.3 and obtain the resonance Raman spectrum of the pure carbinolamine intermediate. This spectrum is shown in figure 5.17 and clearly demonstrates the decrease in intensity of the  $1240\text{cm}^{-1}$  and  $1656\text{cm}^{-1}$  bands, along with the appearance of the  $1345\text{cm}^{-1}$  band in the carbinolamine intermediate (X).

What is even more interesting is the similarity of this spectrum to the published spectrum of the metarhodopsin II intermediate which is one of the intermediate species formed during the hydrolysis of bovine rhodopsin<sup>28, 29</sup>. This spectrum of the metarhodopsin II intermediate led to controversy as to whether the species is an unprotonated retinal-opsin schiff base<sup>28</sup>, so that the meta I to meta II stage in the bleaching sequence is a deprotonation step (meta I being a protonated schiff base), or whether the species is retinal formed from the hydrolysis of meta I, the protonated schiff base<sup>29</sup>. The spectrum clearly does not have a band at  $1630\text{cm}^{-1}$  which is the C=N stretch characteristic of unprotonated schiff bases, and it does have a peak at  $1350\text{cm}^{-1}$  which corresponds to the peak in the carbinolamine intermediate spectrum at  $1345\text{cm}^{-1}$ .

The metarhodopsin II intermediate spectrum was obtained by computer subtraction of a percentage (approximately 40%) of a meta I spectrum from the spectrum of a solution containing a mixture of meta I and meta II (predominantly meta II as mixture was at pH 5.3). The meta I spectrum had also been corrected by subtraction of 7% of an isorhodopsin spectrum and it was

FIGURE 5.17  
Continuous flow resonance Raman spectra of carbinolamine intermediate (X) formed during hydrolysis of N-retinylidene n-butylamine in Ammonyx pH4 and of the metarhodopsin II intermediate (Meta II). (Taken from ref.69)



still estimated that the meta I spectrum could contain up to 5% of isorhodopsin or rhodopsin. It is obvious therefore that the meta II spectrum may not be entirely accurate, but the carbinolamine spectrum is very similar to it, more so than the model unprotonated schiff base spectrum.

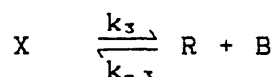
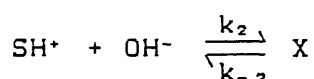
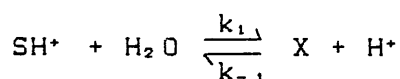
It would seem very likely from these results that the metarhodopsin II intermediate of the rhodopsin bleaching sequence is a stabilised form of a carbinolamine intermediate, formed during the hydrolysis of the retinal schiff base linkage of rhodopsin.

## CHAPTER 6

EQUILIBRIUM AND RATE  
EXPRESSIONS FOR THE  
REACTION MECHANISM.

## 6.1 Equilibrium and Rate Expressions

The mechanism of the hydrolysis and formation reactions of a schiff base is represented in the scheme below, where  $\text{SH}^+$  is the protonated schiff base, X is the neutral or zwitterionic form of the tetrahedral carbinolamine intermediate, R is the aldehyde (retinal) and B is the amine (butylamine)<sup>64, 67</sup>.



(scheme 1)

The hydrolysis and formation reactions have the same mechanism and the carbinolamine X is formed by attack of water or hydroxide ion on the protonated schiff base during hydrolysis, or by attack of amine on the retinal during formation.

For the hydrolysis and formation reactions studied during this work, all the solutions were prepared in detergent micelles and so we assume any species containing retinal are in the micellar phase whereas the free butylamine is in the aqueous phase.

The acid dissociation constants for the schiff base and the butylamine respectively can be defined as:

$$K_{sH} = [\text{S}]a_H / [\text{SH}^+]$$

$$K_{bH} = [\text{B}][\text{H}^+] / [\text{BH}^+]$$

where  $a_H$  is the hydrogen ion activity in the micellar phase, estimated from the schiff base titrations as described in Chapter 4, and  $[\text{H}^+]$  is the concentration of the hydrogen ions (or activity) in the bulk aqueous phase, measured using the pH electrode.

The overall observed equilibrium constant for the reaction ( $K_{obs}$ ) can be written as follows:

$$\begin{aligned}
 K_{obs} &= [B]_{tot}[R]/[S]_{tot} \\
 &= [R]([B] + [BH^+])/([S] + [SH^+]) \\
 &= [R] \left( [B] + \frac{[B][H^+]}{K_{BH}} \right) / \left( [S] + \frac{[S]a_H}{K_{SH}} \right) \\
 K_{obs} &= K_0 (1 + [H^+]/K_{BH}) / (1 + a_H/K_{SH})
 \end{aligned} \tag{6.1}$$

where  $K_0 = [R][B]/[S]$  is the dissociation constant at the high pH limit.

The principle of microscopic reversibility produces some useful relationships between the equilibrium and rate constants, as shown below.

$$\text{At equilibrium, } k_3[X] = k_{-3}[R][B]$$

$$k_2[SH^+]a_{OH} = k_{-2}[X]$$

$$k_1[SH^+] = k_{-1}[X]a_H$$

therefore,

$$\frac{k_1 k_{-2}}{k_{-1} k_2} = a_H a_{OH} = K_w$$

(6.2)

$$K_0 = [R][B]/[S] = [X]k_3/[S]k_{-3}$$

$$= [X]k_3 a_H / k_{-3} K_{SH} [SH^+]$$

$$= k_2 k_3 a_H [SH^+] a_{OH} / k_{-2} k_{-3} K_{SH} [SH^+]$$

$$= k_2 k_3 K_w / k_{-2} k_{-3} K_{SH} \tag{6.3}$$

$$= k_1 k_3 / k_{-1} k_{-3} K_{SH} \tag{6.4}$$

In the reaction sequence for the formation / hydrolysis of the schiff base, the steady-state approximation can be used and after a short time it will be a good approximation to assume that the rate of formation of X is equal to the rate of breakdown, i.e. the first derivative of the concentration of X is equal to zero.

$$\frac{d[X]}{dt} = 0$$

If the steady-state approximation is applied to reaction scheme 1 then, following established procedures<sup>22</sup>, steady-state observed rate constants for formation and hydrolysis can be obtained.

For hydrolysis the pseudo-first order observed rate constant can be written as:

$$k_{hydroly} [S]_{tot} = k_3 [X] \quad (6.5)$$

From the steady-state approximation the concentration of X, the reactive intermediate, can be written as:

$$[X] = \frac{k_1 [SH^+] + k_2 [SH^+] a_{OH}}{k_3 + k_{-2} + k_{-1} a_H} \quad (6.6)$$

It is known that,

$$[S]_{tot} = [S] + [SH^+]$$

$$= \frac{K_{SH} [SH^+]}{a_H} + [SH^+]$$

$$= [SH^+] (1 + K_{SH}/a_H)$$

therefore,  $[SH^+] = [S]_{tot} / (1 + K_{SH}/a_H)$

and substitution into equation 6.6 gives:

$$[X] = \frac{[S]_{tot} (k_1 + k_2 a_{OH})}{(1 + K_{SH}/a_H) (k_3 + k_{-2} + k_{-1} a_H)}$$

Substitution of [X] into equation 6.5 gives:

$$\begin{aligned}
 k_{\text{hydrolysis}} &= \frac{k_3 (k_1 + k_2 a_{\text{OH}})}{(1 + K_{\text{BH}}/a_{\text{H}})(k_3 + k_{-2} + k_{-1} a_{\text{H}})} \\
 &= \frac{k_3 (k_1 a_{\text{H}} + k_2 K_{\text{H}})}{(a_{\text{H}} + K_{\text{BH}})(k_3 + k_{-2} + k_{-1} a_{\text{H}})} \quad (6.7)
 \end{aligned}$$

For the formation reaction the second order observed rate constant can be written as:

$$k_{\text{formation}} [\text{B}]_{\text{total}} [\text{R}] = [\text{X}](k_{-1} a_{\text{H}} + k_{-2}) \quad (6.8)$$

From the steady-state approximation,

$$[\text{X}] = \frac{k_{-3} [\text{R}][\text{B}]}{k_3 + k_{-2} + k_{-1} a_{\text{H}}} \quad (6.9)$$

It is known that:

$$\begin{aligned}
 [\text{B}]_{\text{total}} &= [\text{B}] + [\text{BH}^+] \\
 &= [\text{B}] + ([\text{B}][\text{H}^+]/K_{\text{BH}}) \\
 &= [\text{B}](1 + [\text{H}^+]/K_{\text{BH}})
 \end{aligned}$$

therefore,  $[\text{B}] = [\text{B}]_{\text{total}} / (1 + [\text{H}^+]/K_{\text{BH}})$

Substitution into equation 6.9 gives:

$$[\text{X}] = \frac{[\text{B}]_{\text{total}} k_{-3} [\text{R}]}{(1 + [\text{H}^+]/K_{\text{BH}}) (k_3 + k_{-2} + k_{-1} a_{\text{H}})}$$

and substitution of [X] into equation 6.8 gives:

$$\begin{aligned}
 k_{\text{formation}} &= \frac{k_{-3} (k_{-1} a_{\text{H}} + k_{-2})}{(1 + [\text{H}^+]/K_{\text{BH}}) (k_3 + k_{-2} + k_{-1} a_{\text{H}})} \\
 &= \frac{k_{-3} K_{\text{BH}} (k_{-1} a_{\text{H}} + k_{-2})}{(K_{\text{BH}} + [\text{H}^+]) (k_3 + k_{-2} + k_{-1} a_{\text{H}})} \quad (6.10)
 \end{aligned}$$

Equations 6.7 and 6.10 are expressions for the steady-state rates of hydrolysis and formation respectively. These expressions are related by the equilibrium constant  $K_{obs} = k_{hydrolysis}/k_{formation}$ , and so either hydrolysis or formation data can be used to give the same information. As a check it is therefore possible to use equations 6.7 and 6.10 to compare with equation 6.1.

$$\begin{aligned}
 K_{obs} &= \frac{k_{hydrolysis}}{k_{formation}} \\
 &= \frac{k_3 (k_1 a_H + k_2 K_W) ([H^+] + K_{BH}) (k_3 + k_{-2} + k_{-1} a_H)}{k_{-3} K_{BH} (a_H + K_{BH}) (k_3 + k_{-2} + k_{-1} a_H) (k_{-1} a_H + k_{-2})} \\
 &= \frac{(k_1 k_3 a_H + k_2 k_3 K_W) ([H^+] + K_{BH})}{(k_{-1} k_{-3} a_H K_{BH} + k_{-2} k_{-3} K_{BH}) (a_H + K_{BH})} \\
 &= \frac{k_1 k_3 K_{BH} (a_H + k_2 K_W/k_1) (1 + [H^+]/K_{BH})}{k_{-1} k_{-3} K_{BH} K_{BH} (a_H + k_{-2}/k_{-1}) (1 + a_H/K_{BH})} \\
 &= \frac{k_1 k_3 (1 + [H^+]/K_{BH})}{k_{-1} k_{-3} K_{BH} (1 + a_H/K_{BH})} \\
 &= K_o \frac{(1 + [H^+]/K_{BH})}{(1 + a_H/K_{BH})}
 \end{aligned} \tag{6.11}$$

Equation 6.11 is consistent with equation 6.1 and gives an expression for the observed dissociation constant.

In the equilibrium study of the schiff base N-retinylidene n-butylamine<sup>6,9</sup>, data was obtained by studying the hydrolysis reaction at low to neutral pH and the formation reaction at high pH. It is not possible however to obtain all of the rate constants in scheme 1 from the steady-rate pH-rate profiles on their own. Three parameters can be determined independently, as shown below.

If equation 6.7 is divided by  $k_3$  then the following equation is obtained:

$$k_{hydrolysis} = \frac{(k_1 a_H + k_2 K_W)}{(a_H + K_{BH}) (1 + k_{-2}/k_3 + k_{-1} a_H/k_3)}$$

and in this equation there are four parameters namely  $k_1$ ,  $k_2$ ,  $k_{-2}/k_3$  and  $k_{-1}/k_3$ . However only three of these are independent because they are related by microscopic reversibility. Equations 6.3 and 6.4 gave:

$$K_o = \frac{k_2 k_3 K_w}{k_{-2} k_{-3} K_{BH}} = \frac{k_1 k_3}{k_{-1} k_{-3} K_{BH}}$$

therefore,

$$\frac{k_{-2}}{k_3} = \frac{k_2 K_w k_{-1}}{k_1 k_3}$$

for example, and so only three of the four parameters are independent. Similarly for formation, equation 6.10 can be written:

$$k_{f o r m} = \frac{k_{-3} K_{BH} (k_{-1} a_H / k_3 + k_{-2} / k_3)}{(K_{BH} + [H^+]) (1 + k_{-2} / k_3 + k_{-1} a_H / k_3)}$$

and so in this case three parameters, namely  $k_{-3}$ ,  $k_{-1}/k_3$  and  $k_{-2}/k_3$  can be obtained.

It is therefore necessary to obtain additional information and this is possible by analysis of the complete, non-steady-state rate equations used during this work. The value of the rate constant  $k_3$  can be obtained in this way, giving a complete set of rate constants for scheme 1.

For consecutive two-step reactions of the type in scheme 1 with a reversible first step, the absorbance versus time curves are biphasic and can be represented by equation 2.14,

$$A(t) = \alpha_0 + \alpha_1 (\exp -\lambda_1 t) + \alpha_2 (\exp -\lambda_2 t) \quad (2.14)$$

In this expression  $\lambda_1$  and  $\lambda_2$  are actually functions of the individual rate constants, and it is necessary to derive expressions to relate them to the actual rate constants of the reaction.

A general reaction scheme which involves the reversible formation of an intermediate B during the transformation of A to C is shown below.



(Scheme 2)

The differential rate equations for this scheme are:

$$\frac{-d[A]}{dt} = k_1[A] - k_{-1}[B]$$

$$\frac{d[B]}{dt} = k_1[A] - k_{-1}[B] - k_2[B]$$

$$\frac{d[C]}{dt} = k_2[B]$$

The solutions (taking  $[B]_0 = [C]_0 = 0$ ) are:

$$[A] = \frac{k_1[A]_0}{\lambda_1 - \lambda_2} \left[ \frac{\lambda_1 - k_2}{\lambda_1} \exp(-\lambda_1 t) - \frac{\lambda_2 - k_2}{\lambda_2} \exp(-\lambda_2 t) \right] \quad (6.12)$$

$$[B] = \frac{k_1[A]_0}{\lambda_1 - \lambda_2} [\exp(-\lambda_2 t) - \exp(-\lambda_1 t)] \quad (6.13)$$

where  $\lambda_1 = 1/2(p+q)$

$$\lambda_2 = 1/2(p-q)$$

$$p = k_1 + k_{-1} + k_2$$

$$q = (p^2 - 4k_1k_2)^{1/2}$$

It can be seen that:

$$\begin{aligned} \lambda_1 \lambda_2 &= 1/4(p^2 - q^2) \\ &= 1/4(p^2 - p^2 + 4k_1k_2) \\ &= k_1k_2 \end{aligned}$$

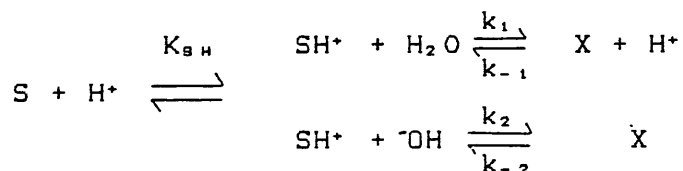
Comparison of scheme 2 with scheme 1 shows that:

$$\begin{aligned}
 "k_1" &= k_1 + k_2 a_{OH} \\
 &= k_1 + k_2 K_W / a_H \\
 "k_{-1}" &= k_{-1} a_H + k_{-2} \\
 "k_2" &= k_3
 \end{aligned}$$

so that:

$$\lambda_1 \lambda_2 = k_3 (k_1 + k_2 K_W / a_H)$$

However it must be remembered that the very first step in scheme 1 is actually the protonation of the schiff base and this must be included in the scheme.



The fraction of the total schiff base which is in the protonated form and can be hydrolysed by H<sub>2</sub>O or OH can be calculated as follows:

$$K_{SH} = [S]a_H / [SH^+]$$

$$[S]_{tot} = [S] + [SH^+] = [SH^+] (1 + K_{SH} / a_H)$$

therefore,

$$[SH^+] / [S]_{tot} = 1 / (1 + K_{SH} / a_H)$$

This then gives a value of "k<sub>1</sub>" as:

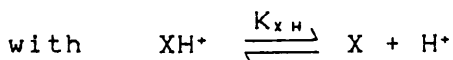
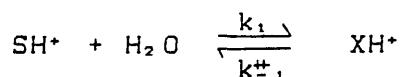
$$"k_1" = \frac{(k_1 + k_2 K_w / a_H)}{(1 + K_{SH} / a_H)} \quad (6.14)$$

so that,

$$\lambda_1 \lambda_2 = k_3 (k_1 a_H + k_2 K_w) / (a_H + K_{SH}) \quad (6.15)$$

$\lambda_1$  and  $\lambda_2$  are obtained directly from the mainframe analysis of the non-steady-state kinetics and are the values quoted in Chapters 3 and 4,  $k_1$  and  $k_2$  can be obtained from the steady-state kinetics and so  $k_3$  can be obtained from equation 6.15 giving a full set of rate constants for scheme 1.

The reaction mechanism in scheme 1 can be written in different kinetically equivalent forms. For example, the carbinolamine intermediate, like the parent schiff base species, can exist in a protonated and an unprotonated form, and this protonation step could be included in the scheme so that the first line of scheme 1 would be:



where  $K_{XH}$  is the acid dissociation constant of the carbinolamine. In this case rate constant  $k_{-1}$  in scheme 1 would be replaced by  $k_{-1}^{\ddagger} / K_{XH}$  and the rate expressions in equations 6.7 and 6.10 would still be obtained. There is no real advantage in including this protonation step as the  $pK_a$  of the carbinolamine cannot be determined independently.

In scheme 2 the absorbance at any time ( $Abs_t$ ) is given by:

$$Abs_t = \epsilon_A [A] + \epsilon_B [B] + \epsilon_C [C]$$

and  $[C] = [A]_0 - [A] - [B]$  (where  $[A]_0$  is the concentration of A at time = 0secs, assuming  $[B]_0 = [C]_0 = 0$ , and where  $\epsilon_A$  is the molar extinction coefficient of A in  $lcm^{-1}mole^{-1}$ ).

Therefore,

$$Abs_t = (\epsilon_A - \epsilon_C) [A] + (\epsilon_B - \epsilon_C) [B] + \epsilon_C [A]_0.$$

Using the solutions of the differential rate equations 6.12.6.13 then:

$$\begin{aligned} Abs_t &= (\epsilon_A - \epsilon_C) \frac{k_1 [A]_0}{\lambda_1 - \lambda_2} \left[ \frac{\lambda_1 - k_2}{\lambda_1} e^{-\lambda_1 t} - \frac{\lambda_2 - k_2}{\lambda_2} e^{-\lambda_2 t} \right] \\ &+ (\epsilon_B - \epsilon_C) \frac{k_1 [A]_0}{\lambda_1 - \lambda_2} \left[ e^{-\lambda_2 t} - e^{-\lambda_1 t} \right] + \epsilon_C [A]_0 \\ &= \frac{k_1 [A]_0}{\lambda_1 - \lambda_2} \left[ (\epsilon_A - \epsilon_C) \frac{\lambda_1 - k_2}{\lambda_1} - (\epsilon_B - \epsilon_C) \right] e^{-\lambda_1 t} \\ &+ \frac{k_1 [A]_0}{\lambda_1 - \lambda_2} \left[ (\epsilon_B - \epsilon_C) - (\epsilon_A - \epsilon_C) \frac{\lambda_2 - k_2}{\lambda_2} \right] e^{-\lambda_2 t} \\ &+ \epsilon_C [A]_0 \end{aligned}$$

therefore,

$$Abs_t = \alpha_0 + \alpha_1 e^{-\lambda_1 t} + \alpha_2 e^{-\lambda_2 t}$$

where  $\alpha_0 = \epsilon_C [A]_0$ ,

$$\alpha_1 = \frac{k_1 [A]_0}{\lambda_1 - \lambda_2} \left[ (\epsilon_A - \epsilon_C) \frac{\lambda_1 - k_2}{\lambda_1} - (\epsilon_B - \epsilon_C) \right]$$

$$\text{and } \alpha_2 = \frac{k_1 [A]_0}{\lambda_1 - \lambda_2} \left[ (\epsilon_B - \epsilon_C) - (\epsilon_A - \epsilon_C) \frac{\lambda_2 - k_2}{\lambda_2} \right]$$

This is the derivation of equation 2.13.

## 6.2 Calculated Spectrum of the Intermediate Species

In Chapters 3 and 4 it was shown that spectra of retinal and schiff base could be constructed by use of equation 2.13.

At time = 0,  $A = \alpha_0 + \alpha_1 + \alpha_2$  for biphasic reactions, and at time = infinity (at the end of the reaction),  $A = \alpha_0$ . Values of  $\alpha_0$ ,  $\alpha_1$  and  $\alpha_2$  were obtained from mainframe analysis, and so in the hydrolysis reaction the spectra of the absorbing species present at the start of reaction (schiff base) and at the end of reaction (retinal) could be constructed, and similarly for formation, the species at the start of reaction (retinal) and at the end of reaction (schiff base), by using the above equations.

It is also possible to construct the spectrum of the intermediate species if an appropriate expression can be derived, and by trial and error the following expression was found to be suitable:

$$\begin{aligned}
 \alpha_1 \lambda_1 + \alpha_2 \lambda_2 &= \frac{k_1 [A]_0}{\lambda_1 - \lambda_2} [(\epsilon_A - \epsilon_C)(\lambda_1 - k_2) - \lambda_1(\epsilon_B - \epsilon_C) + \\
 &\quad \lambda_2(\epsilon_B - \epsilon_C) - (\epsilon_A - \epsilon_C)(\lambda_2 - k_2)] \\
 &= \frac{k_1 [A]_0}{\lambda_1 - \lambda_2} (\epsilon_A \lambda_1 - \epsilon_B \lambda_1 + \epsilon_B \lambda_2 - \epsilon_A \lambda_2) \\
 &= \frac{k_1 [A]_0}{\lambda_1 - \lambda_2} [(\epsilon_A - \epsilon_B)(\lambda_1 - \lambda_2)] \\
 &= k_1 [A]_0 (\epsilon_A - \epsilon_B) \qquad (6.16)
 \end{aligned}$$

Rearrangement of equation 6.16 gives:

$$[A]_0 \epsilon_B = [A]_0 \epsilon_A - (\alpha_1 \lambda_1 + \alpha_2 \lambda_2) / k_1 \qquad (6.17)$$

If  $[A]_0 \epsilon_B$  values can be calculated over a wavelength range using equation 6.17 then the spectrum of the intermediate can be constructed.

$[A]_0$ ,  $\epsilon_A$  is the absorbance of A, the species present at the start of reaction, and this absorbance is given by  $A = \alpha_0 + \alpha_1 + \alpha_2$ , which can be easily calculated. The term  $\alpha_1 \lambda_1 + \alpha_2 \lambda_2$  can be calculated using mainframe values of  $\alpha$  and  $\lambda$ , and the value of " $k_1$ " can be estimated as being either very similar to  $\lambda_1$  or  $\lambda_2$  values obtained from analysis. This ambiguity arises because it is not possible to say for definite which one of  $\lambda_1$  or  $\lambda_2$  corresponds to " $k_1$ " and " $k_2$ ".

Results of schiff base hydrolysis in Ammonyx at pH 4 are shown in table 6.1. The average values of  $\lambda_1$  and  $\lambda_2$  obtained from mainframe hydrolysis were  $0.254\text{sec}^{-1}$  and  $0.010\text{sec}^{-1}$  respectively and table 6.1 shows values obtained assuming that " $k_1$ " =  $\lambda_1$  and table 6.2 assuming that " $k_1$ " =  $\lambda_2$ .

Examination of the values of  $\epsilon_b [A]_0$  in tables 6.1 and 6.2 shows that those in table 6.1 are reasonable absorbance values whereas those in table 6.2 are not, as there are negative values. It would therefore seem reasonable to say that " $k_1$ " is approximately equal to  $\lambda_1$  and a plot of  $\epsilon_b [A]_0$  values in table 6.1 versus wavelength (nm) is shown in figure 6.1.

Similar calculations can be done for results of schiff base hydrolysis in Ammonyx at pH 5. Values of  $\epsilon_b [A]_0$  are shown in table 6.3 and a plot of these values versus wavelength is shown in figure 6.2. Once again the use of " $k_1$ " =  $\lambda_2$  gave negative absorbance values and so it was assumed that " $k_1$ " =  $\lambda_1$  (the average value of  $\lambda_1$  being  $0.329 \text{ sec}^{-1}$  in this case).

It is possible to construct a spectrum of species present 10 seconds after pH jump by reading the value of absorbance at  $t = 10$  secs from the mainframe printout at each wavelength. Table 6.4 lists the values of wavelength and absorbance at  $t = 10$  secs for the hydrolysis reaction in Ammonyx at pH 4 and 5, and figure 6.3 shows the spectra constructed using these values. Comparison of these spectra with those in figures 6.1, 6.2 shows that these two methods give very similar results. It is also possible to obtain spectra of retinal and protonated schiff base by reading off absorbance values at  $t = 420$

Table 6.1

Table listing calculated values of carbinolamine intermediate absorbance during schiff base hydrolysis in Ammonyx at pH 4, assuming " $k_1$ " =  $\lambda_1$ .

Wavelength (nm)	$\epsilon_a$ [A] <sub>0</sub>	$\frac{\alpha_1 \lambda_1 + \alpha_2 \lambda_2}{\text{"}k_1\text{"}}$	$\epsilon_b$ [A] <sub>0</sub>
330	0.1941	0.0165	0.1776
340	0.2077	0.0224	0.1853
350	0.2479	0.0248	0.2231
360	0.2754	0.0276	0.2478
370	0.2904	0.0240	0.2664
380	0.2966	0.0209	0.2757
390	0.3014	0.0087	0.2927
410	0.3451	-0.0087	0.3538
420	0.3654	-0.0039	0.3693
430	0.3668	-0.0079	0.3747
440	0.3603	-0.0142	0.3745
450	0.3295	-0.0221	0.3516
460	0.2901	-0.0221	0.3122
470	0.2436	-0.0236	0.2672
480	0.1878	-0.0252	0.2130
490	0.1431	-0.0055	0.1486
500	0.0990	-0.0181	0.1171
510	0.0715	-0.0158	0.0873
520	0.0494	-0.0130	0.0624
530	0.0375	-0.0079	0.0454

Table 6.2

Table listing calculated values of carbinolamine intermediate absorbance during schiff base hydrolysis in Ammonyx at pH 4, assuming " $k_1$ " =  $\lambda_2$ .

Wavelength (nm)	[A] <sub>0</sub> ε <sub>A</sub>	$\frac{\alpha_1 \lambda_1 + \alpha_2 \lambda_2}{\text{"}k_1\text{"}}$	ε <sub>B</sub> [A] <sub>0</sub>
330	0.1941	0.4106	-0.2165
340	0.2077	0.5572	-0.3495
350	0.2479	0.6158	-0.3679
360	0.2754	0.6843	-0.4089
370	0.2904	0.5963	-0.3059
380	0.2966	0.5181	-0.2215
390	0.3014	0.2151	0.0863
410	0.3451	-0.2151	0.5602
420	0.3654	-0.0978	0.4632
430	0.3668	-0.1955	0.5623
440	0.3603	-0.3519	0.7122
450	0.3295	-0.5474	0.8769
460	0.2901	-0.5474	0.8375
470	0.2436	-0.5865	0.8301
480	0.1878	-0.6256	0.8134
490	0.1431	-0.1368	0.2799
500	0.0990	-0.4497	0.5487
510	0.0715	-0.3910	0.4625
520	0.0494	-0.3226	0.3720
530	0.0375	-0.1955	0.2330

FIGURE 6.1  
Reconstructed spectrum of carbinolamine intermediate formed during schiff base hydrolysis in Ammonyx at pH 4, obtained by plotting  $\epsilon_B(A)_O$  values in Table (6.1) versus wavelength (nm).

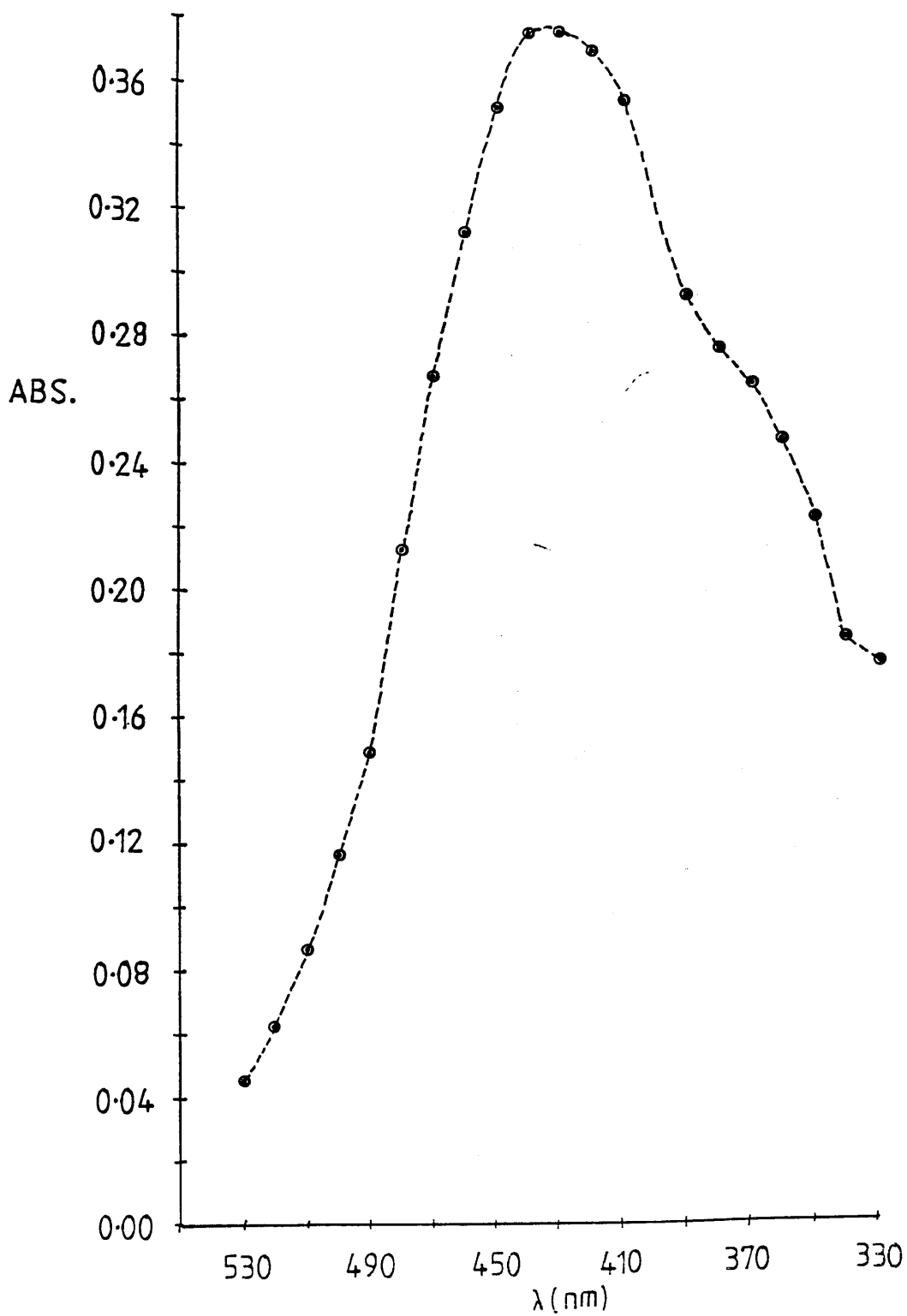


Table 6.3

Table listing calculated values of carbinolamine intermediate absorbance during schiff base hydrolysis in Ammonyx at pH 5, assuming " $k_1$ " =  $\lambda_1$ .

Wavelength (nm)	$\epsilon_A [A]_0$	$\frac{\alpha_1 \lambda_1 + \alpha_2 \lambda_2}{k_1}$	$\epsilon_B [A]_0$
330	0.2517	0.0088	0.2429
340	0.3016	0.0158	0.2858
350	0.3524	0.0182	0.3342
360	0.3727	0.0155	0.3572
380	0.3251	0.0082	0.3169
390	0.2705	-0.0128	0.2833
400	0.2275	-0.0097	0.2372
410	0.1944	-0.0103	0.2047
420	0.1788	-0.0094	0.1882
430	0.1817	-0.0112	0.1929
440	0.1718	-0.0137	0.1855
450	0.1498	-0.0128	0.1626
460	0.1319	-0.0131	0.1450
470	0.1175	-0.0118	0.1293
480	0.0904	-0.0131	0.1035
490	0.0664	-0.0094	0.0758
500	0.0525	-0.0097	0.0622
510	0.0411	-0.0058	0.0469
520	0.0235	-0.0070	0.0305
530	0.0212	-0.0058	0.0270

FIGURE 6.2

Reconstructed spectrum of carbinolamine intermediate formed during schiff base hydrolysis in Ammonyx at pH 5, obtained by plotting  $\epsilon_B(\lambda)_0$  values in Table (6.3) versus wavelength (nm).

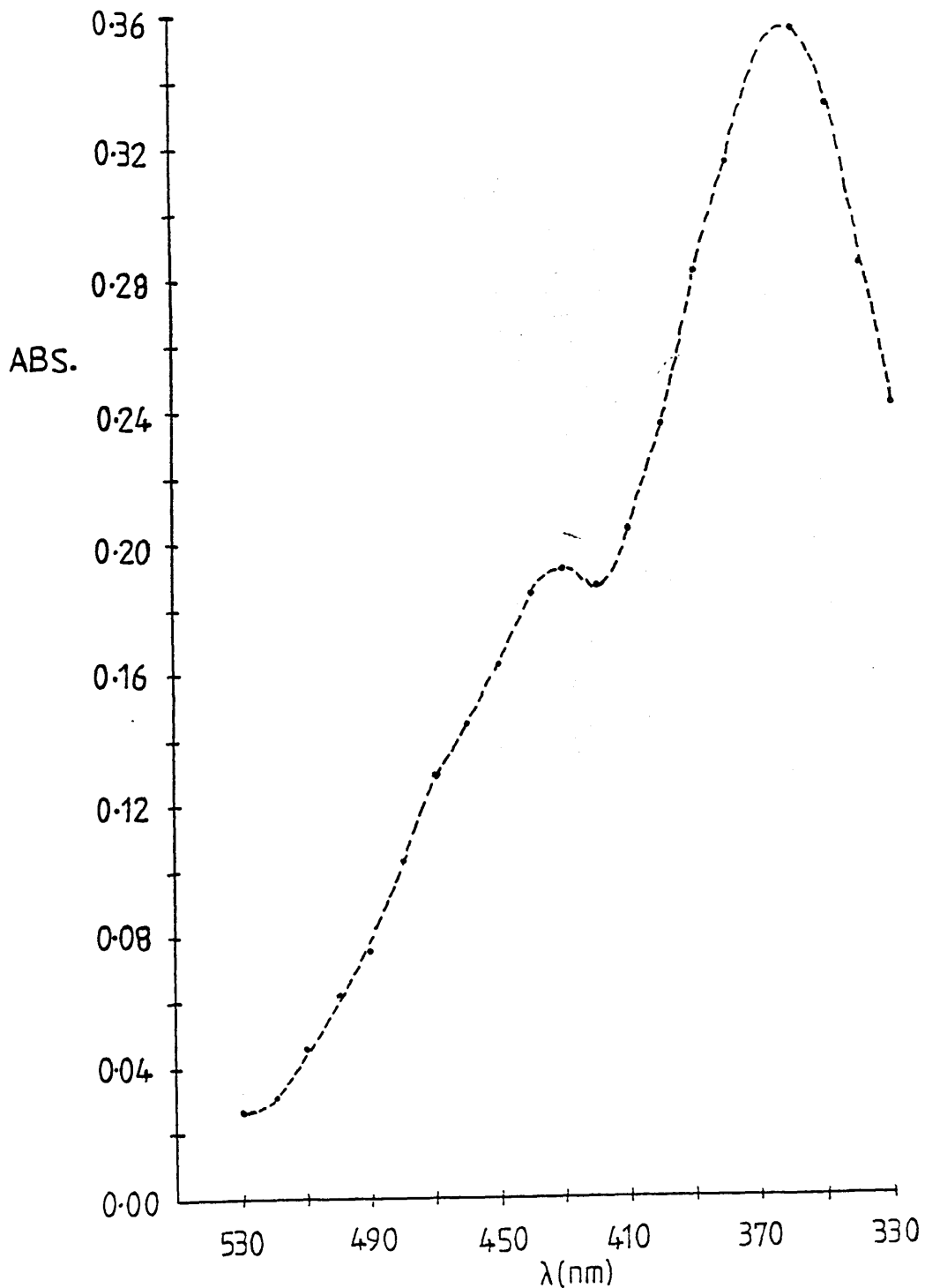


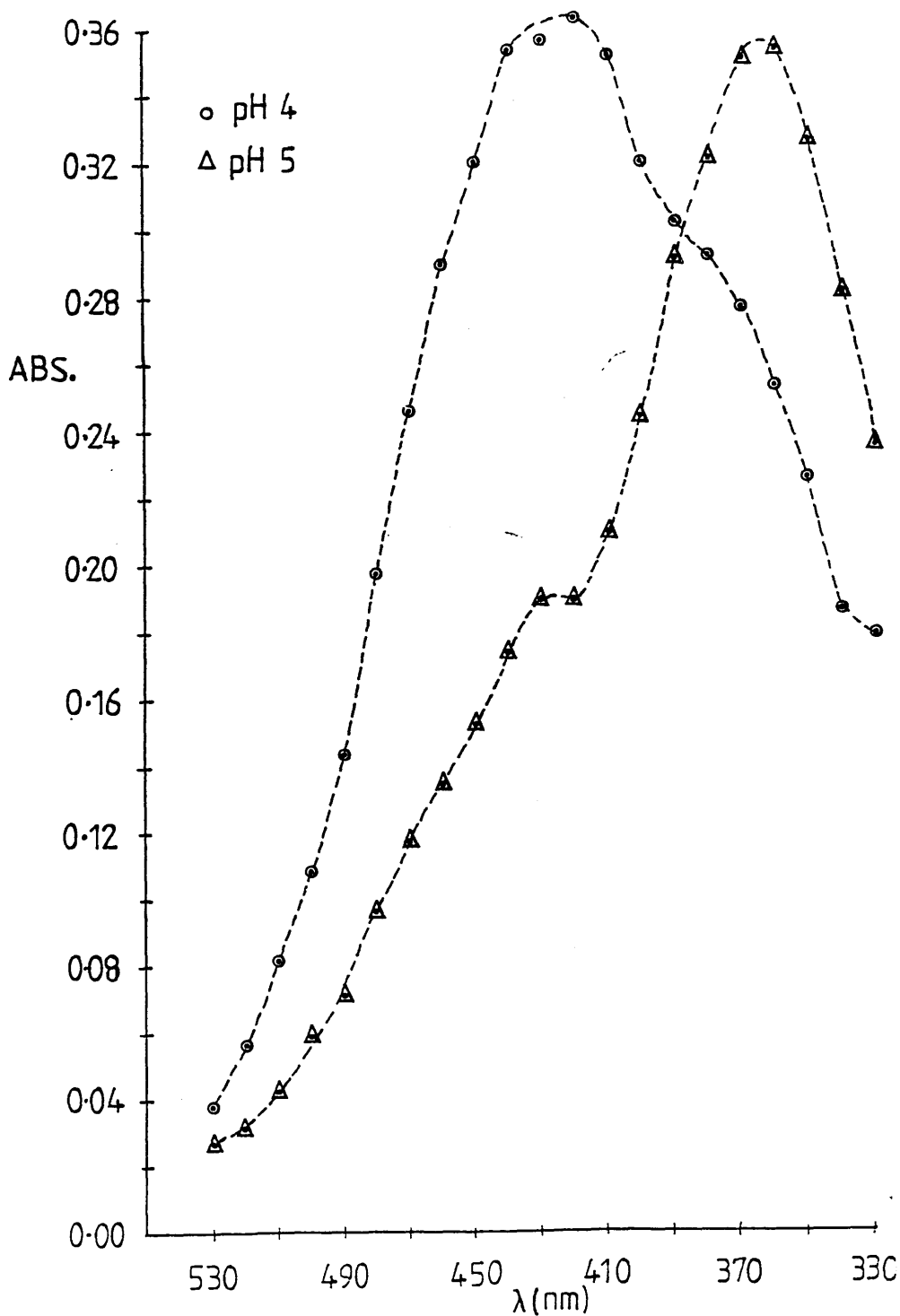
Table 6.4

Table showing values of wavelength (nm) and absorbance (t=10secs) at pH 4 and pH 5 obtained from mainframe analysis of hydrolysis reaction in Ammonyx.

Wavelength (nm)	Absorbance (t=10secs) pH 4	Absorbance (t=10secs) pH 5
330	0.1801	0.2375
340	0.1883	0.2827
350	0.2284	0.3291
360	0.2549	0.3558
370	0.2787	0.3542
380	0.2941	0.3226
390	0.3040	0.2929
400	0.3223	0.2460
410	0.3542	0.2114
420	0.3647	0.1905
430	0.3580	0.1905
440	0.3547	0.1749
450	0.3214	0.1533
460	0.2902	0.1349
470	0.2465	0.1181
480	0.1982	0.0970
490	0.1439	0.0715
500	0.1090	0.0593
510	0.0815	0.0433
520	0.0569	0.0319
530	0.0388	0.0275

FIGURE 6.3

Reconstructed spectra of species present 10 secs after pH-jump of N-retinylidene n-butylamine in Ammonyx to pH 4 and 5, obtained by plotting values of Abs.(t=10secs) in Table (6.4) from mainframe analysis versus wavelength (nm).



secs and  $t = 0$  secs respectively (spectra not shown).

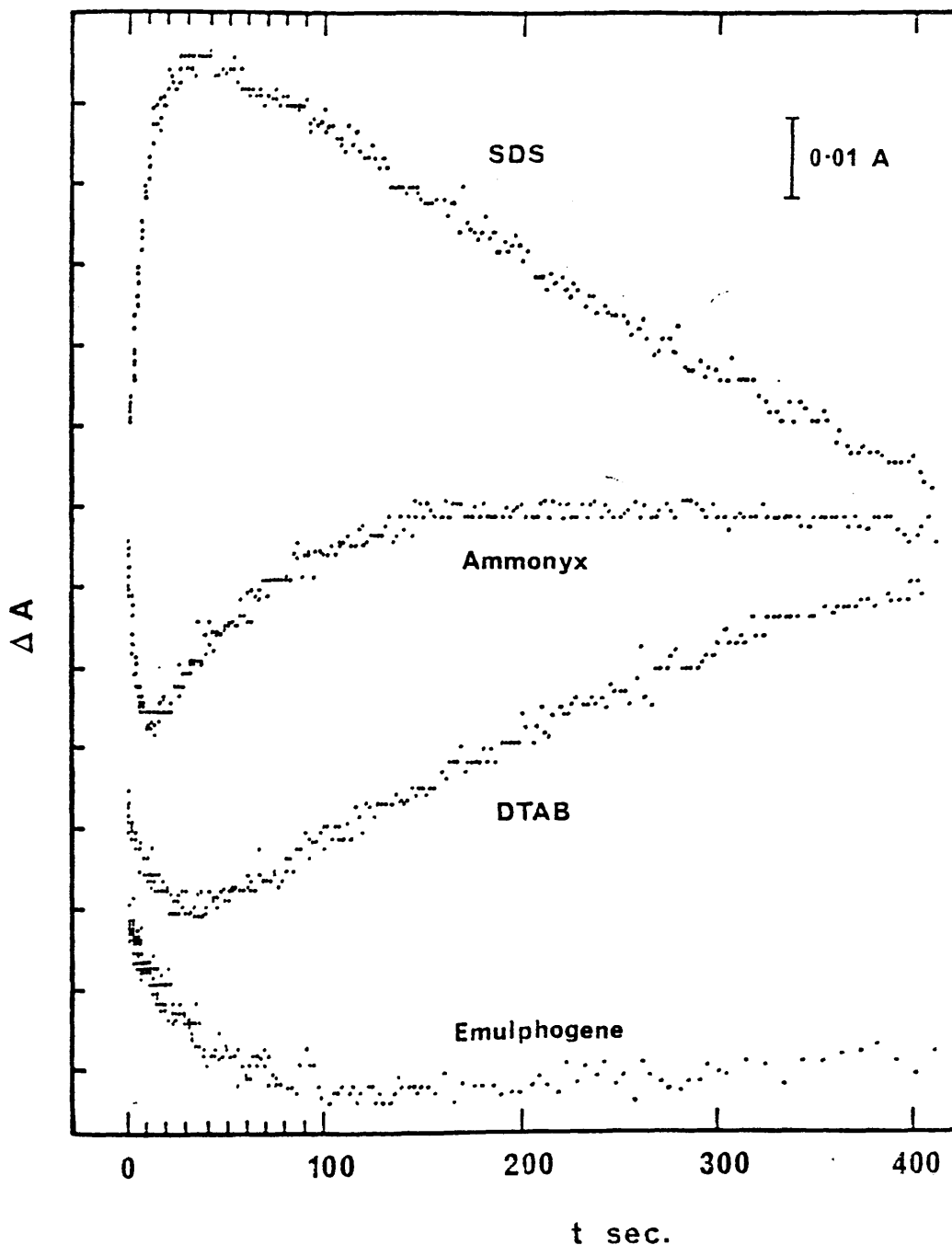
The constructed spectra at pH 4 (figs. 6.1, 6.3) can in turn be compared with the actual continuous flow UV/vis. spectrum recorded 10 seconds after mixing the N-retinylidene n-butylamine schiff base with 0.2M acetate buffer pH 4 (fig. 5.1) and again there is a good similarity. The spectrum in fig. 5.1 does not have such a pronounced shoulder at around 370nm as the constructed spectra, but the peak is obviously not symmetric. It must be remembered that these spectra contain contributions due to unprotonated/protonated schiff base and unprotonated/protonated intermediate. At pH 4 the majority of the schiff base is protonated with absorbance maximum at around 440nm, whereas at pH 5 the majority of the schiff base is in the unprotonated form with absorbance maximum at around 360nm. The proportion of the carbinolamine intermediate in the protonated/unprotonated form is dependent on the  $pK_a$  value of this species.

### 6.3 Prediction of the $pK_a$ Value of the Intermediate Species

Examination of the stopped-flow traces recorded during the hydrolysis reaction in the various detergents enables a prediction of the  $pK_a$  value for the carbinolamine intermediate. Figure 6.4 shows traces in SDS (360nm, pH 11), Ammonyx (370nm, pH 5), DTAB (370nm, pH 5.5) and Emulphogene (370nm, pH 6). It can be seen that in the traces recorded at pH 5-6 in Ammonyx, DTAB and Emulphogene, the initial absorbance at 370nm decreases during the first stage of reaction, whereas at pH 11 in SDS the initial absorbance increases at 360nm.

In the case of the schiff base a red-shift is indicative of protonation, with the protonated form having an absorbance maximum at 440nm compared to 360nm for the unprotonated form. If this is also true for the carbinolamine species then at low pH (pH 5-6, Ammonyx, DTAB and Emulphogene) the red-shift observed in the stopped-flow traces would suggest an increase in protonation, and at high pH (pH 11, SDS) the blue-shift

FIGURE 6.4  
Stopped-flow traces showing transient absorbance changes during the initial stages of hydrolysis of N-retinylidene n-butylamine in SDS (360nm, pH11), Ammonyx (370nm, pH5), DTAB (370nm, pH5.5) and Emulphogene (370nm, pH6).  
(Taken from ref.69)



observed would suggest a decrease in protonation of the carbinolamine. This means that the  $pK_a$  value of the carbinolamine is possibly around 7 - 9.

The  $pK_a$  value of organic molecules may be predicted by use of the Taft equation<sup>99</sup>. The retinal carbinolamine can be considered as a secondary amine ( $R_1R_2NH_2^+$ ) so that the form of the Taft equation which is applicable in this case is:

$$pK = 10.59 - 3.23 \sum \sigma^*$$

where  $\sigma^*$  is an increment for substituents.

For the retinal carbinolamine,  $R_1 = C_6H_5$ , which gives a value of -0.25 for  $\sigma^*$ .

$R_2$  is of general form  $\begin{array}{c} H \\ | \\ -C-Y \\ | \\ Z \end{array}$  where  $Y = -OH$  and

$Z = -CH=C(CH_3)_2$  (as a model for the retinyl group).

For  $R_2$ ,  $\sigma^* = \sigma^*$  for  $-CH_2OH$  (0.62) +  $\sigma^*$  for  $-CH_2-CH=C(CH_3)_2$  (0), therefore  $\sigma^* = 0.62$ .

$$\sum \sigma^* = 0.62 - 0.25 = 0.37$$

and so the predicted  $pK_a$  value is around 9.4. This seems to be a reasonable value for the  $pK_a$  of the carbinolamine intermediate, but is obviously only an estimate.

CHAPTER 7

DISCUSSION AND CONCLUSIONS.

## Discussion and Conclusions

A study of the formation and hydrolysis reactions of N-retinylidene n-butylamine schiff base in various aqueous detergent micelle systems has shown that these reactions have many features similar to classical imine reactions. The N-retinylidene n-butylamine schiff base was chosen as a model for the visual pigment rhodopsin and the n-butylamine moiety represents the lysine group in opsin to which the retinal is attached. The detergent micelle systems allow some control over the environment of the model compound.

In a classical schiff base system the steady-state rate of formation increases as the pH is raised<sup>7</sup>. This is because the formation reaction occurs by attack of unprotonated amine on the carbonyl group of the aldehyde, and as this is usually the rate limiting step, the reaction rate increases with pH because more of the amine is in the unprotonated form at high pH.

The steady-state rate of hydrolysis for a classical schiff base system gives a bell-shaped rate profile when plotted versus pH<sup>7</sup>. This is because hydrolysis involves the nucleophilic attack of water or hydroxide ion on the protonated schiff base species to form a carbinolamine intermediate. At high pH this step is rate-determining and so as the pH is lowered the rate increases. There is however a transition in rate determining step from the attack of water under neutral conditions, to decomposition of the carbinolamine intermediate under acidic conditions. This is because the breakdown of the intermediate requires de-protonation of the carbinolamine species to form the zwitterionic form, and this is rate limiting at low pH.

Examination of the pH dependence of the steady-state rates of formation and hydrolysis of N-retinylidene n-butylamine shows that the results are consistent with the classical schiff base system<sup>9</sup>. The steady-state rate of formation of N-retinylidene n-butylamine in Ammonyx, Emulphogene, DTAB and SDS detergents increases as the pH

is raised from 2-13, (fig.3.17) and the steady-state rate of hydrolysis of N-retinylidene n-butylamine, in the same detergents, exhibits a bell-shaped pH-rate profile (fig.1.17), as would be expected from the classical reactions. This means that the formation and hydrolysis reactions of N-retinylidene n-butylamine schiff base, like other schiff bases, should involve the formation of a tetrahedral carbinolamine intermediate.

Kinetic transients consistent with this intermediate have been observed during the hydrolysis reaction using stopped-flow spectroscopy. These transients can only be seen during hydrolysis at a pH near to the maxima on the pH-rate profiles and cannot be seen at all during the formation reactions. The reason for this is that the rate limiting step during formation in the pH range 8-12 (the range observable using stopped-flow spectroscopy) is the nucleophilic attack of the amine on the aldehyde, which is the step where formation of carbinolamine occurs.

It is interesting to note that in figure 3.17 the pH dependence of the rate of formation is very similar in the different detergent micelles, with the rate falling as the amine becomes protonated. In the case of hydrolysis (figure 1.17) the position and magnitude of the bell-shaped pH-rate profiles are, however, influenced by the different micellar environments. This is most marked with SDS where the entire pH-rate curve is shifted to high pH, but even in this case the shape of the curve is still the same.

The differences in the pH-rate curves of hydrolysis can be explained by examination of the acid-base dissociation of the schiff base in the different detergents. As was previously mentioned in Chapter 4, the apparent  $pK_a$  ( $pH_{1/2}$ ) of the retinyl schiff base changes depending on detergent (table 7.1) and this affects the position and magnitude of the rate curves. These variations in apparent  $pK_a$  can be correlated to the anionic or cationic nature of the detergent which suggests that there is an electrostatic effect on the protonation equilibria.

The apparent  $pK_a$  in the non-ionic detergent

TABLE 7.1 Kinetic and Equilibrium Parameters for the Retinal/  
n-Butylamine Reaction in Detergent Micelles\*.

	Ammonyx	Emulphogene	DTAB	SDS
$pK_{BH}$	10.75	10.75	10.75	~ 11
$pH_{mid}$	4.85	6.1	5.84	9.54
$n$	0.77	1	0.77	1.1
$p\theta$	-2.37	0	-1.6	4.4
$K_0$ (mM)	0.22	0.13	0.25	~0.25
$k_1$ ( $s^{-1}$ )	0.31	$6.1 \times 10^{-4}$	$7.9 \times 10^{-3}$	~0.01
$k_2$ ( $M^{-1}s^{-1}$ )	$1.2 \times 10^4$	$2.0 \times 10^4$	$2.6 \times 10^4$	~ $3 \times 10^5$
$k_3$ ( $s^{-1}$ )	.028	.026	.025	~.05
$k_{-1}$ ( $M^{-1}s^{-1}$ )	$4.0 \times 10^5$	420	6500	~ $2 \times 10^5$
$k_{-2}$ ( $s^{-1}$ )	$1.1 \times 10^{-4}$	$9.4 \times 10^{-5}$	$1.5 \times 10^{-4}$	~0.05
$k_{-3}$ ( $M^{-1}s^{-1}$ )	124	371	153	~10
$k_1/k_{-1}$	$7.8 \times 10^{-7}$	$1.5 \times 10^{-6}$	$1.2 \times 10^{-6}$	~ $5 \times 10^{-8}$
$k_2/k_{-2}$	$1.1 \times 10^9$	$2.2 \times 10^9$	$1.7 \times 10^9$	~ $6 \times 10^9$
$k_3/k_{-3}$	$2.3 \times 10^{-4}$	$7.0 \times 10^{-5}$	$1.6 \times 10^{-4}$	~ $5 \times 10^{-3}$

\* Except as indicated for SDS, where only order-of-magnitude estimates are available, typical maximum estimated error limits are as follows:  $pK_{BH}$ ,  $pH_{mid}$ ,  $n$ ,  $p\theta$  (+/- 0.05);  $K_0$  (+/- 10%); rate constants (+/- 20%).

(Taken from ref.69)

Emulphogene is equal to 6.1 which is in agreement with values obtained in other neutral detergents<sup>90,91</sup>. In the case of Ammonyx, which is neutral at high pH and cationic below neutral pH,  $pK_a = 4.85$ . for DTAB which is a cationic detergent,  $pK_a = 5.84$  and finally for SDS which is anionic,  $pK_a = 9.54$ . It can be seen therefore that a cationic detergent has the effect of lowering the  $pK_a$  value of the schiff base because the presence of positive charge on the detergent micelle surface makes protonation of the schiff base more difficult. An anionic detergent has the opposite effect and raises the  $pK_a$  value of the schiff base as the negative charges on the detergent micelle allow protonation to occur more easily. Similar effects in the presence of charged micelles have been reported elsewhere<sup>91,92</sup>.

In the case of SDS, the rate curve is shifted to such an extent that it seems likely that there are specific interactions between the cationic sulphonic acid head group of the SDS and the nitrogen in the schiff base, rather than the non-specific delocalised effect of micellar surface potential in the case of Ammonyx and DTAB.

For the formation reactions, any effects of the different detergents on the protonation behaviour of the butylamine would be important, but the  $pK_a$  value of the butylamine was found to be equal to 10.75 in Ammonyx, Emulphogene and DTAB (table 7.1). This value is consistent with the  $pK_a$  value of butylamine in aqueous solution and suggests that these three detergents have a negligible effect on the protonation behaviour of the n-butylamine. However pH titration of butylamine in the presence of SDS detergent gave  $pK_a$  values greater than 11 which again suggests a specific interaction between SDS and, in this case, the butylamine.

Another feature which evolved from the spectral acid-base titrations in the detergent micelle systems was that in the plots of  $\log [SH^+]/[S]$  versus pH (fig.4.33), the slope of the line is equal to unity only in the case of Emulphogene. The slopes with Ammonyx and DTAB are equal to 0.77 and with SDS equal to 1.1 which means that

there is a deviation from ideal titration behaviour with these three detergents. This behaviour is observed even when different buffers are used and with different absorbance wavelengths.

In the case of Ammonyx it may be explained perhaps by the fact that this amine oxide protonates in a similar pH range to the schiff base. This means that the positive charges in the detergent micelle could affect the protonation of the schiff base in such a way that  $n \neq 1$ . Unfortunately there is not such an obvious explanation for titration behaviour in DTAB or SDS. It is possible that the non-ideal behaviour in these detergents is due to changes in micelle surface potential as a result of ionic strength changes in the buffer counter-ions during the titration of the schiff base.

In Chapter 4 an empirical relationship between the micellar hydrogen ion activity ( $a_w$ ) and the measured pH was given where:

$$p a_w = -p_{\#} + n.pH \quad (4.4)$$

In this expression  $p_{\#}$  and  $n$  were used to represent the apparent pH shift and non-ideality respectively in the micellar detergent solutions. In the case of ideal titration behaviour  $n = 1$  and  $p_{\#}$  is arbitrarily taken as equal to 0 for the neutral detergent Emulphogene. This type of non-ideal titration behaviour can also be represented by a fractional protonation scheme where an unprotonated schiff base (S) picks up  $n$  protons to form the species  $SH_n^+$ .



The dissociation constant of this protonation reaction is given by:

$$K = [S] [H^+]^n / [SH_n^+]$$

It is interesting to note that a very similar situation is encountered with the visual pigment

rhodopsin itself. The deviation of rhodopsin from ideal titration behaviour was first noted by Matthews et al<sup>27</sup> who were studying the effect of pH on the metarhodopsin equilibrium and found that the titration curve for meta I - meta II equilibrium was not convergent with that of a monoprotic indicator base. They thought that the differences may be due to the ionic strength of their solvent as the departure from ideal behaviour was even greater at higher ionic strengths.

Later Parkes and Liebman<sup>34</sup> obtained the fractional value of  $n = 0.7$  for the meta I - meta II equilibrium and stated that as other investigators had also obtained fractional values it could not be due to systematic experimental error. In the case of rhodopsin this "fractional protonation" is possibly due to non-ideal titration behaviour of some groups present in the protein environment.

If these abnormalities in the schiff base protonation behaviour of N-retinylidene n-butylamine are taken into account, then the experimental data obtained from steady-state and non-steady-state kinetics (table 7.1) are consistent with the mechanism proposed in Scheme 1 (Chapter 4), and the pH-rate curves of N-retinylidene n-butylamine are consistent with those for classical schiff base formation and hydrolysis.

Another feature of classical schiff base reactions is that attack of water on the protonated schiff base can be catalysed, and when conditions are such that this step is rate limiting, then the entire hydrolysis reaction may be subject to general base catalysis.

The effect of increasing the buffer concentration on the hydrolysis rate of N-retinylidene n-butylamine has been studied in Emulphogene<sup>49</sup> and Ammonyx (Chapter 4). The results obtained for Emulphogene showed that steady-state rates of hydrolysis in the pH range 4-6 (where attack of water on protonated schiff base is rate limiting) are dependent on buffer type and concentration, and are subject to general base catalysis. In the case of Ammonyx this effect was not seen as the values of  $\lambda_1$  and  $\lambda_2$  changed very little when the final concentration of

buffer was increased from 0.01 - 0.20 molar.

However, it is interesting to note that the value of  $k_1$  obtained in Ammonyx experiments is much higher than the value of  $k_1$  obtained in other detergents (table 7.1). As  $k_1$  is the rate constant for the base catalysed attack of water on protonated schiff base, this observation would suggest that the hydrolysis reaction is already subject to base catalysis from the amine oxide groups in the Ammonyx detergent, and this will therefore mask the catalytic effect of other bases in solution.

Examination of the other rate constants in table 7.1 shows that there is little variation in the values of  $k_2, k_3, k_{-2}$  and  $k_{-3}$  obtained in the different detergents (with the exception of SDS once again) and little variation in the ratios  $k_1/k_{-1}, k_2/k_{-2}$  and  $k_3/k_{-3}$ . The fact that the value of the ratio  $k_1/k_{-1}$  hardly changes, despite  $k_1$  being much greater in Ammonyx than in other detergents, would suggest that the Ammonyx micelles do have a catalytic effect on the hydrolysis as the rate of forward and reverse reaction ( $k_1$  and  $k_{-1}$  respectively) are both affected.

As was previously mentioned, the formation and decay of an intermediate species was directly observed during hydrolysis reactions using stopped-flow spectroscopy and the kinetic data from these runs can be described by equation 2.14 which represents the rate expression for a biphasic reaction. The stopped-flow spectroscopy showed that the formation and decay of intermediate could be observed most easily during hydrolysis reactions at a pH near to the peak in the pH-rate curve.

It is possible to estimate the steady-state accumulation of intermediate from equation 6.5;

$$\frac{[X]}{[S]_{tot}} = \frac{k_{hydro1}}{k_3} \quad (6.5)$$

and this shows that in most cases the build up is less than around 5% of the total schiff base concentration. However, in the case of Ammonyx, the high value of  $k_1$  under certain conditions (which will affect the value of

$k_{hydrolysis}$ ) causes an increase in intermediate concentration to around 50% of the total schiff base concentration, making determination of the intermediate an easier process.

The absorbance spectrum of the intermediate has been estimated (Chapter 6) and is very similar to that of the schiff base itself. The spectrum is dependent on pH, and the  $pK_a$  value of the carbinolamine is estimated to be in the region 7-9.

The continuous-flow resonance Raman spectrum of the intermediate has been recorded in aqueous Ammonyx micelles during experiments involving a pH-jump to pH 4 or 5 (Chapter 5). Definite changes have been observed between the carbinolamine intermediate spectrum and the parent schiff base spectrum. These differences are much less marked when Emulphogene or SDS are used as detergent, presumably because the concentration of intermediate present is so much lower.

Hydrolysis reactions in Ammonyx detergent/ $D_2O$  at pD 4 occurred much more slowly than reactions in water at pH 4, giving a solvent isotope effect,  $k(H_2O)/k(D_2O)$ , of around 2.3 (Chapter 4). This value is similar to the observed solvent isotope effects of other schiff bases<sup>93</sup> and led to the conclusion that the transition states for these hydrolysis reactions resemble the protonated carbinolamine more closely than the reactants<sup>93,94</sup>.

The continuous-flow resonance enhanced Raman spectrum of the carbinolamine intermediate is very similar to the published spectrum of the metarhodopsin II intermediate formed during the bleaching sequence of the visual pigment rhodopsin (figure 5.17). This would suggest that the metarhodopsin II intermediate is a stabilised form of a carbinolamine intermediate which has been formed during the hydrolysis of the schiff base linkage present in the visual pigment rhodopsin. This means that the hydrolysis of the schiff base must have started at the metarhodopsin stage of the bleaching sequence, as previously suggested by Cooper and Converse<sup>20</sup>.

Support for this theory was obtained from isotopic labelling experiments involving photoreceptor

membranes<sup>6,7</sup>. Bovine rod outer segment membranes were exposed to oxygen - 18 enriched water during the metarhodopsin I - metarhodopsin II transition of the rhodopsin bleaching sequence. Retinal was extracted and low-resolution mass spectrometry showed that <sup>18</sup>O had been incorporated into the retinal. Infra-red spectra of the retinal showed that there was an isotopic shift in the carbonyl stretch mode of this extracted retinal, compared to commercial all-trans retinal or retinal extracted from bleached rod outer segment membranes. These results show that hydrolysis of the schiff base linkage occurs during the meta I - meta II transition. No isotopic labelling by <sup>18</sup>O enriched water was observed prior to the meta I intermediate nor when meta I - containing membranes were incubated in labelled water.

G. Wald et al in 1950<sup>30</sup> had observed that the bleaching sequence of rhodopsin stops at the meta I stage in the absence of water, and that meta II and subsequent intermediates were formed when water was added which would suggest that hydrolysis was occurring at this stage. In addition to this it is known that small, water-soluble molecules like sodium borohydride and hydroxylamine do not attack the chromophore of rhodopsin before the metarhodopsin stage in the bleaching cycle, presumably because at this stage the schiff base linkage is exposed through unfolding of the protein, whereas beforehand it was buried<sup>14,95</sup>. It would therefore seem likely that a similar situation would occur with water itself.

Cooper and Converse<sup>20</sup> studied the energetics of the meta I - meta II transition and found that this stage involved the uptake of 10kcal/mole which is similar to enthalpies of hydrolysis of model schiff base compounds (8-12 kcal/mole). Furthermore this transition was found to be the only spontaneous endothermic step to occur during the bleaching sequence<sup>74</sup>.

Features which have been observed during the hydrolysis reactions of model retinal schiff bases<sup>6,7</sup> have also been observed during kinetic studies of the meta I - meta II transition<sup>24,33,34</sup>. These similarities include

complex reaction kinetics, protonation changes and possible base catalysis.

When all this information is considered along with results of the experiments with  $^{18}\text{O}$  enriched water<sup>49</sup> and the resonance Raman spectra (this work) then there certainly would appear to be evidence that hydrolysis has started at the metarhodopsin stage of the bleaching sequence. It is not possible to establish from the labelling experiments if the formation of the aldehyde is complete by the meta II stage and the resonance Raman spectra would certainly suggest that meta II is more likely to be a stabilised carbinolamine intermediate. Extraction of the retinal from meta II after the labelling experiments would cause the formation of labelled retinal as the carbinolamine intermediate would collapse.

It is interesting to note that when Matthews et al<sup>27</sup> were studying the tautomeric forms of metarhodopsin they noted that meta II "has an absorption spectrum close to that of free retinal, but contains all-trans retinal still attached to opsin at the chromophoric site". They did not think that hydrolysis had started at the metarhodopsin stage because of the fact that irradiation of meta II with UV light produced the parent rhodopsin, and because of the rapid interconversion of meta I and meta II. However, if meta II is a stabilised tetrahedral carbinolamine intermediate, held in the specific retinal binding site of opsin by non-covalent interactions or by the carbinolamine linkage, then the above observations would hold true, even though hydrolysis had started.

In order to allow a mechanism for schiff base hydrolysis to be postulated it is necessary to consider the types of molecular interactions which could occur in the rhodopsin chromophore binding site and which would stabilise the carbinolamine linkage. Before this is possible there are certain differences between the model schiff base compounds and rhodopsin which must be considered.

One major difference is the fact that in the formation reactions of the model schiff base compounds it

is known that the attacking amine must be in the unprotonated form and, as the attack of amine on the aldehyde is usually rate-limiting, reaction rates fall rapidly with pH below the  $pK_a$  of the base. This schiff base formation reaction is analogous to the regeneration of pigment by recombination of the appropriate retinal chromophore with either bleached rhodopsin or bacteriorhodopsin, both of which are rapid and spontaneous at physiological pH<sup>7,9</sup>.

If the formation mechanism is the same for the model schiff bases and the retinal pigments then it means that the active lysine group in opsin must be unprotonated, or only partially protonated, at physiological pH. This lysine group must therefore have a  $pK_a$  value of around 7, rather than the more typical value of around 10 for a primary amine, and it must be subject to environmental effects which have caused this decrease in  $pK_a$  value.

Previous studies on the energetics and protonation of bovine rhodopsin showed that an additional titrating group on opsin with a  $pK_a$  value of around 7 is exposed during photolysis, and it was suggested that this group is the schiff base lysine and that the low  $pK_a$  value may be induced by a nearby positively charged group on the protein (possibly another lysine group or an arginine group)<sup>20</sup>.

It has been shown that the schiff base enzyme acetoacetate decarboxylase contains an active lysine group with a  $pK_a$  value of around 6, and this low  $pK_a$  value was ascribed to the electrostatic effect of nearby positive charges<sup>9</sup>. In addition to this, work on diamines has suggested that the  $pK_a$  value can be reduced by 3-4 units in the presence of a single positive charge positioned within a few Angstroms of an amino group<sup>10</sup>.

It would seem likely therefore that the active lysine in the retinal binding site has an anomalously low  $pK_a$  value, possibly due to electrostatic interactions of an adjacent positively charged group.

This theory leads to problems when considering the unbleached visual pigment, because the interactions which caused the lowering of the lysine  $pK_a$  value in the

apo-protein would also be expected to lower the  $pK_a$  of the retinal schiff base linkage in rhodopsin. It is known however that the schiff base linkage in unbleached rhodopsin is protonated and remains protonated over a wide pH range which would suggest a high  $pK_a$  value.

The actual value of the schiff base  $pK_a$  has not been determined for rhodopsin but a value of 13.3 has been measured in the case of bacteriorhodopsin<sup>101</sup>. This anomalously high  $pK_a$  value could be explained by suggesting that there are major protein conformational differences between opsin and rhodopsin which would cause changes in the electrostatic environment of the binding site. Model schiff base hydrolysis experiments in aqueous detergent micelles have shown that the micellar environment can have a marked effect on the  $pK_a$  value of the schiff base - especially in the case of the anionic detergent SDS, where a value of 9.5 was obtained for the  $pK_a$ . It is possible therefore that major conformational changes could introduce a negatively charged group into the vicinity of the schiff base in rhodopsin and cause a high  $pK_a$  value.

Alternatively it can be assumed that the retinal binding site does not change markedly during recombination, and if this is the case, it is possible to devise a scheme which can account for many basic observations in rhodopsin chemistry. If the chromophore binding site is the same in opsin and rhodopsin, then the adjacent positively charged group responsible for the low  $pK_a$  value of the active lysine in the retinal binding site could form an  $(-NH\dots\dots N-)^+$  hydrogen bond with the nitrogen atom in the retinyl schiff base, thus causing the schiff base to have an anomalously high  $pK_a$  value. This explanation is consistent with the fact that there is no overall change in protonation during bleaching and regeneration of rhodopsin or bacteriorhodopsin at neutral  $pH^{20, 102}$  and has been suggested previously by Cooper and Converse<sup>20</sup>.

One problem with this explanation is the fact that the nitrogen atom on the adjacent lysine group is more basic than that in the schiff base linkage, which means

that in the hydrogen bond the proton is likely to be nearer to the more basic donor group. It has, however, been shown that the position of the H-bond proton in protonated amine-imine hydrogen bonds is dependent on the relative orientations of the donor and acceptor groups, and that slight changes in orientation can cause reversal of the relative  $pK_a$  values of these groups, along with proton transfer from one nitrogen to another<sup>103</sup>. It has been suggested that a process of this type may be involved in the mechanism of the proton translocation in bacteriorhodopsin<sup>103</sup>.

Picosecond spectroscopy has been used to study the kinetics of the primary intermediate bathorhodopsin formed during the visual process, and deuterium labelling experiments led to the theory that this step involves a proton translocation<sup>104</sup>. It would seem likely that the cis-trans photoisomerisation of the rhodopsin chromophore would cause slight changes in orientation of groups in the region of the binding site, and this could result in a proton translocation within the -NH.....N- hydrogen bond.

The fact that the bathorhodopsin intermediate is red-shifted with respect to the parent rhodopsin would suggest that the schiff base in rhodopsin is only partially protonated, and that the proton translocation results in the proton lying nearer to the nitrogen of the schiff base linkage in bathorhodopsin than in rhodopsin. Alternatively it could be that the red shift is due to strain in the molecule as a result of the chromophoric isomerisation, and the proton transfer could be away from the nitrogen of the schiff base.

Recently it has been shown that it is possible to form a permethylated rhodopsin where the ten non-active site lysines are methylated, and this pigment behaves in the same way as rhodopsin as far as bleaching, regeneration and activation of GTPase (G protein) when photolysed, and has an identical UV/visible spectrum to rhodopsin<sup>105</sup>. If the proposed model for the binding site of rhodopsin is correct, where protonation of the schiff base nitrogen is by H-bonding to an adjacent lysine

group, then this H-bonding would still be possible after methylation of the adjacent lysine. It would seem likely however that dimethylation of this lysine would cause slight changes in the chromophoric region which would change the spectrum. As the spectrum is unchanged it may be that the adjacent group involved in H-bonding is in fact an arginine group.

Further work on this permethylated pigment produced a pigment with a methylated active-site lysine and permethylated non-active site lysines<sup>106</sup>. This pigment absorbs at 520nm (i.e. is red-shifted with respect to rhodopsin itself) and, as the methylated schiff base nitrogen must carry the full positive charge due to its inability to H-bond, this red-shift would suggest that rhodopsin itself is only partially protonated.

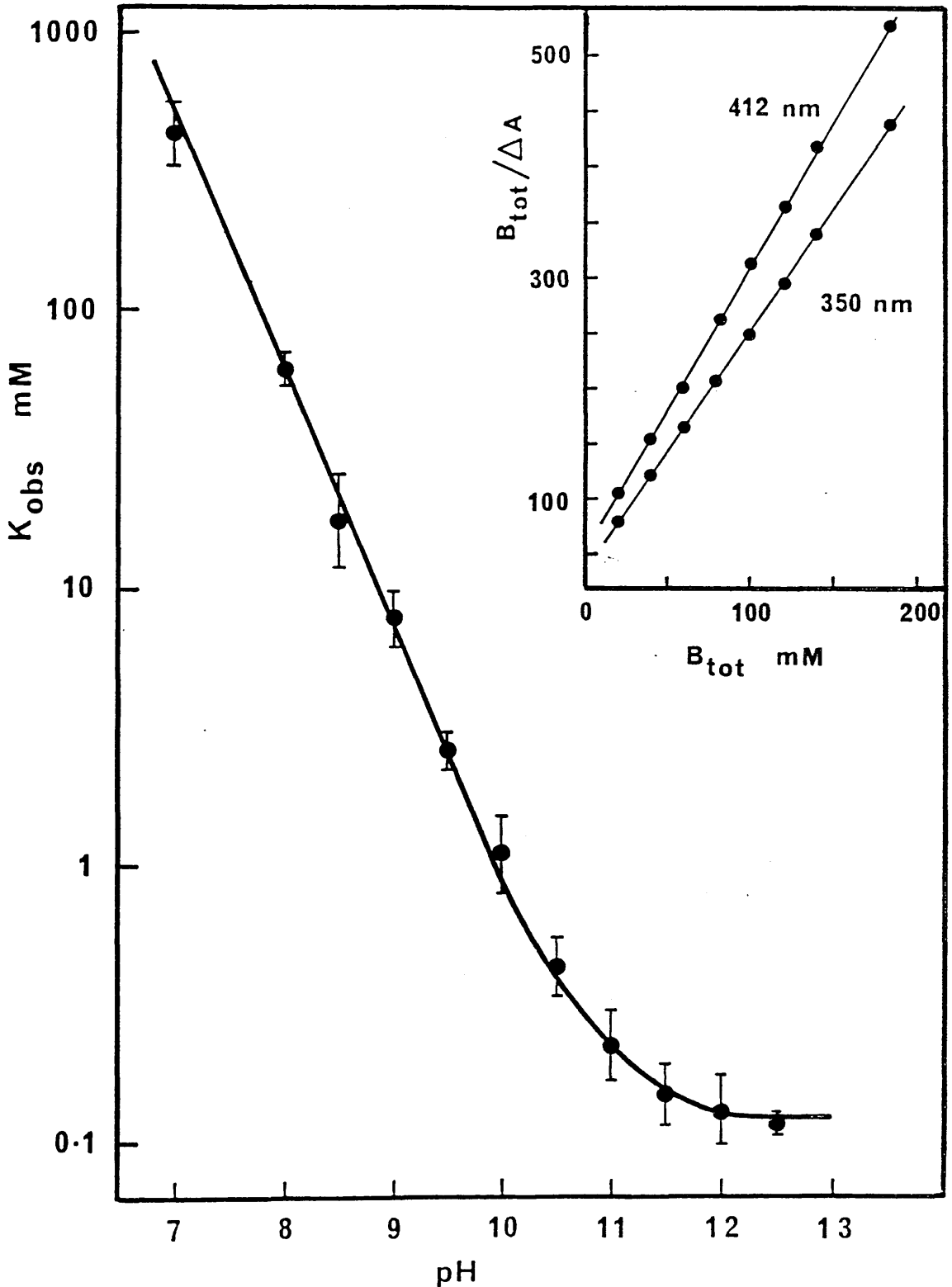
No matter what is causing the perturbations, and the abnormal  $pK_a$  values, the effect on the rhodopsin system is to stabilise the retinyl chromophore under physiological conditions. In the model compounds it can be seen that the amine (butylamine in this case) has a high  $pK_a$  value of around 10.75 and the imine has a low  $pK_a$  value of around 6. In rhodopsin however the values are reversed so that the amine group (lysine) has a low  $pK_a$  value of around 7 and the imine would appear to have a high  $pK_a$  value.

In the model schiff bases the fact that  $pK_{B_H} > pK_{S_H}$  means that  $K_{S_H} > K_{B_H}$  and it can be seen from figure 7.1 and equation 6.1 that the thermodynamic stability of these model compounds decreases rapidly below the  $pK$  of the amine ( $pK_{B_H}$ ).

Rhodopsins on the other hand are stable at neutral pH and their chromophores do not hydrolyse in the way that model schiff bases do under these conditions. This is because reversal of the  $pK_a$  values means that  $K_{S_H} < K_{B_H}$  and so thermodynamic stability of the schiff base linkage in rhodopsin is greatest at low pH. The stability of the schiff base in rhodopsin cannot simply be kinetic, due to protonation or inaccessibility of water molecules, because the regeneration of the schiff base from retinal and opsin is spontaneous under the same physiological

FIGURE 7.1

Observed dissociation constants ( $K_{obs}$ ) as a function of pH for N-retinylidene n-butylamine in 2% aqueous Emulphogene, determined from equilibrium absorbance changes ( $\Delta A$ ) over a range of butylamine concentrations ( $B_{tot}$ ).



(Taken from ref.69)

conditions.

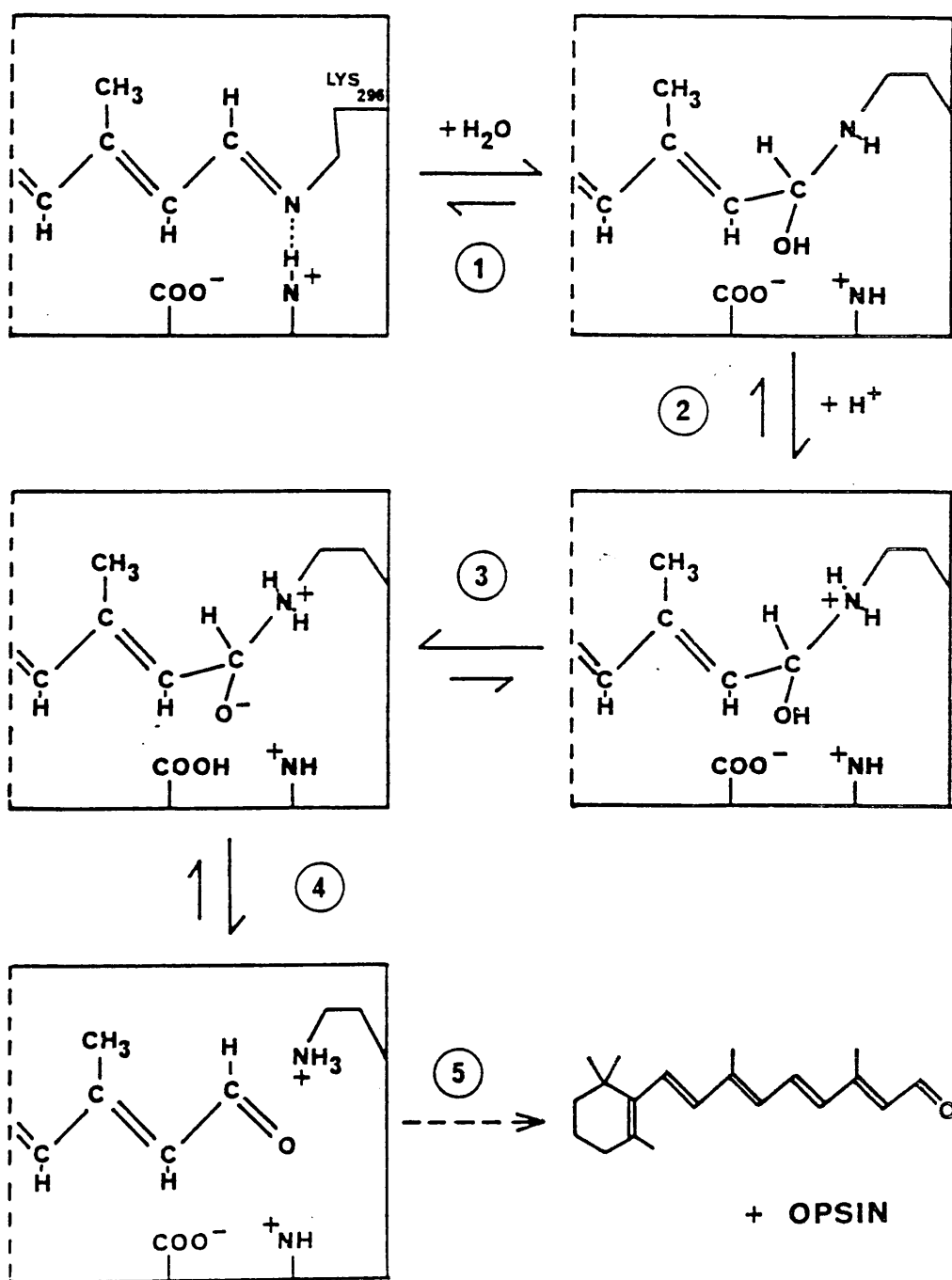
There are therefore many points which must be considered when working out a plausible mechanism for the metarhodopsin transition, and these include: (a) the meta I - II transition is an equilibrium reaction involving the uptake of a proton<sup>20,27</sup> and the bleaching sequence does not proceed past meta I in the absence of water<sup>30</sup> (b) labelling experiments have shown that <sup>18</sup>O is incorporated into retinal from <sup>18</sup>O labelled water at the metarhodopsin stage<sup>9</sup> (c) the kinetics of the meta transition exhibit specific base catalysis<sup>34</sup> (d) the opsin shift can be rationalised by placing a negative point charge near to the schiff base linkage in rhodopsin<sup>44</sup> (e) it would seem likely that there is an additional basic group (arginine or lysine) in the vicinity of the schiff base nitrogen and this basic group is possibly -NH.....N- hydrogen bonded to the schiff base group<sup>20</sup> (f) the retinal binding site is electrically neutral<sup>107</sup> and (g) the continuous flow resonance Raman spectrum of the carbinolamine intermediate formed during schiff base hydrolysis is very similar to the Raman spectrum of the meta II intermediate (this work).

Taking these points into account, a scheme for the reactions occurring at the metarhodopsin transition is shown in figure 7.2, and events leading up to this scheme can be suggested.

The initial photon absorption by rhodopsin causes a rapid isomerisation of the 11-cis retinal chromophore to the all-trans retinal isomer, which leads to slight changes in the relative positions of the schiff base group and the adjacent group which is donating the H-bond. This reorientation causes a reversal of the relative pK<sub>a</sub> values of the two groups and results in proton translocation along the H-bond towards the nitrogen of the schiff base group to form the bathorhodopsin intermediate. The fact that bathorhodopsin is fully protonated explains the red-shift which occurs during this initial stage of the bleaching sequence. It is also possible that the large energy storage observed at this stage<sup>109,51</sup> may be partly attributed to the

FIGURE 7.2

Suggested scheme for the hydrolysis of the retinal schiff base chromophore in the active site of rhodopsin as a possible model for the meta I-II transition.



(Taken from ref.69)

destabilisation of the -NH...N- bond during proton translocation. It is unlikely that any other protein conformational changes occur as this conversion of rhodopsin to bathorhodopsin takes place in less than 6 picoseconds.

It is envisaged that structural relaxation in the active site vicinity occurs at the lumirhodopsin stage, followed by more widespread conformational changes at the meta I stage as the protein relaxes to accommodate the all-trans retinal configuration.

It is now likely that the stabilisation of the schiff base by the groups in the active site has been reduced as a result of the protein conformational changes, and that water may gain access to the active site. This water can attack the schiff base linkage to form the carbinolamine species (step 1, figure 7.2) and the hydrolysis reaction could be base catalysed by the nearby point charge (conjugate base of glutamic or aspartic acid).

The configuration about the carbon atom of the schiff base linkage changes from trigonal to tetrahedral which results in reorientation of groups in the active site, breaking the hydrogen bond between the adjacent group and the schiff base nitrogen. This allows the more basic carbinolamine to become protonated (step 2) and is the step involving proton uptake.

The carbinolamine can exist in various ionisation states and it is the zwitterionic form which decays to form the hydrolysis products. This step involves deprotonation of the carbinol releasing the proton to the solvent, but this is inhibited by the presence of the adjacent carboxylate anion.

It is possible that this released proton could be transferred to the carboxylate group to form a carboxylic acid group and this is consistent with FTIR difference spectra which show that changes occur in carboxylate protonation at the metarhodopsin stage of the bleaching sequence<sup>109, 110</sup>. This carboxylate anion protonation is step 3 in the mechanism and results in zwitterion formation. This zwitterion can then collapse breaking the schiff base linkage and leaving retinal in the active

site, still held in place by non-covalent interactions (step 4). This complex will however be very unstable because of the presence of the all-trans retinal isomer in the 11-cis isomer binding site, and this instability leads to irreversible retinal dissociation (step 5) which could involve the formation of other schiff base linkages with amine groups present in the vicinity.

It is difficult to say which of the species in this scheme can be assigned to the meta I and meta II intermediates of rhodopsin photolysis. The resonance Raman spectra would suggest that the meta II intermediate is similar to the carbinolamine intermediate, but the  $\lambda_{max}$  value of 380nm for meta II would suggest the presence of the retinal aldehyde. It would seem likely that the metarhodopsin II intermediate is a mixture of carbinolamine / retinal and that the individual species cannot be resolved in the UV/visible spectra.

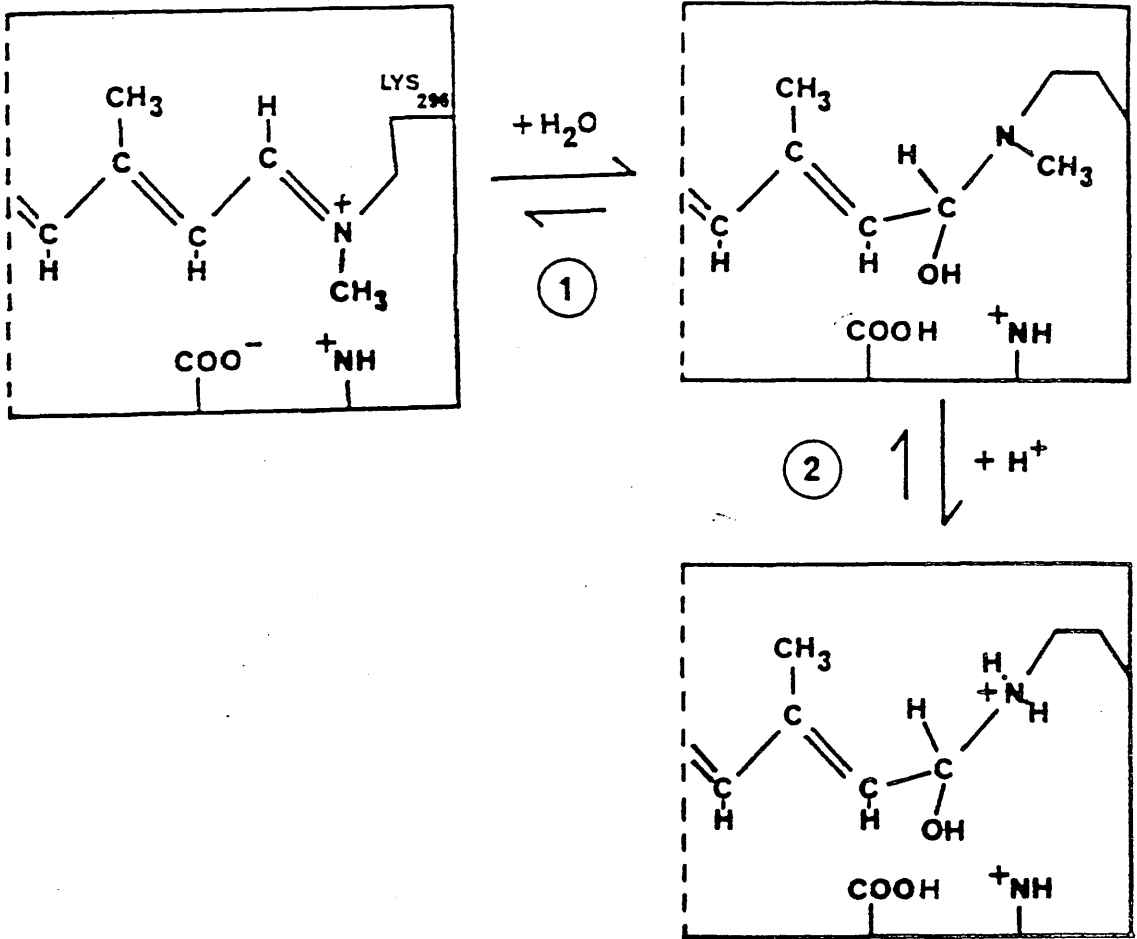
The meta I - meta II transition is a very important stage of the bleaching sequence because it has been shown that chemical inhibition of this transition blocks the activation of the G-protein and subsequent biochemical steps which are thought to be involved in the generation of the nerve impulse<sup>106</sup>. It is possible that the change from trigonal to tetrahedral configuration at the retinal-opsin linkage during carbinolamine formation could therefore be the driving force for activation of the enzyme cascade.

It is also interesting to note that if the mechanism in figure 7.2 is correct, then monomethylation of the active site lysine<sup>106</sup> would affect a hydrolysis reaction as much as a deprotonation.

If the schiff base nitrogen had a methyl substituent in place of hydrogen, then it would seem likely that the electron-donating methyl group would stabilise the positive charge on the nitrogen group, slightly reducing the susceptibility of the schiff base linkage to hydrolysis. The presence of the methyl group may also change the ease of occurrence of some of the steps in the mechanism. Figure 7.3 shows what may happen in the presence of a methyl substituent.

FIGURE 7.3

Scheme for the hydrolysis of the retinal schiff base chromophore in the binding site of rhodopsin when the nitrogen of the active lysine group is methylated.



The first step involving addition of water would result in the formation of the carbinolamine species, but would leave  $H^+$  ions which could protonate the nitrogen of the active lysine, or more likely, the carboxylate anion.

Step 2 would be as before, where a proton is taken up by the nitrogen of the lysine, but it is now very difficult to form a zwitterionic species as the carboxylate group is already protonated, and this would very likely cause a reduction in the rate of hydrolysis, as was observed during these methylation experiments.

The methylation experiments do not therefore prove that the meta I - meta II transition is schiff base deprotonation, but rather that the presence of a methyl substituent on the nitrogen of the active lysine inhibits the formation of meta II, the species responsible for activation of the photoreceptor response.

Overall, the results of experiments in this thesis, along with evidence from other work, would strongly suggest that the hydrolysis of the specific schiff base linkage in the visual pigment rhodopsin starts at the metarhodopsin stage of the bleaching sequence.

It has already been suggested that metarhodopsin II is the trigger which activates the enzyme cascade and further work will need to be done in this area before the complete sequence of events leading to the nerve impulse is discovered.

## APPENDICES

## Appendix 1

### Principles of Raman Spectroscopy

To obtain a Raman spectrum of a molecule the sample is irradiated with monochromatic radiation usually in the visible region. The fixed frequency exciting light is a travelling wave of electric and magnetic fields and it is the electric component which produces Raman scattering. The electric field exerts a force on all the electrons in the molecule causing them to oscillate and displacing them from their average positions around the positively charged nuclei. For the Raman effect these displacements must result in an induced dipole moment  $\mu$  in the molecule, which is proportional to the electric field strength,  $E$  <sup>74</sup>.

$$\mu = \alpha E$$

The proportionality constant  $\alpha$  is called the polarisability tensor. In anisotropic molecules i.e. molecules that are not spherically symmetrical, the vectors  $\mu$  and  $E$  have different directions and the magnitudes of the three components defining  $\mu$ , namely  $\mu_x$ ,  $\mu_y$ ,  $\mu_z$  are related to the magnitude of the electric field  $E$  by the following relationships:

$$\mu_x = \alpha_{xx} E_x + \alpha_{xy} E_y + \alpha_{xz} E_z$$

$$\mu_y = \alpha_{yx} E_x + \alpha_{yy} E_y + \alpha_{yz} E_z$$

$$\mu_z = \alpha_{zx} E_x + \alpha_{zy} E_y + \alpha_{zz} E_z$$

Thus each component ( $\mu_x$ ,  $\mu_y$ ,  $\mu_z$ ) of the induced dipole moment  $\mu$  is dependent on each component ( $E_x$ ,  $E_y$ ,  $E_z$ ) of the electric field  $E$ . The nine components  $\alpha_i$ , are called the components of the polarisability tensor which are constants independent of  $\mu$  and  $E$ .

As the molecule vibrates it undergoes nuclear displacements and the charge distribution, and therefore the polarisability, constantly changes. For small displacements from the equilibrium configuration the polarisability for say the  $\alpha_{xx}$  component can be written as:

$$\alpha_{xx} = \alpha_0 + \left( \frac{d\alpha_{xx}}{dQ_p} \right)_0 Q_p$$

where  $\alpha_0$  is the induced equilibrium polarisability along the x direction by the electric field component  $E_x$  (i.e. the polarisability element of the non-vibrating molecule). For a normal mode p undergoing simple harmonic motion, the normal coordinate  $Q_p$  varies as a function of time:

$$Q_p = Q_p^0 \cos 2\pi\nu_p t$$

where  $Q_p^0$  is the time independent amplitude of the normal coordinate  $Q_p$  and  $\nu_p$  is the frequency of the normal vibration of the molecule.

The electric field of the light wave also varies with time:

$$E_x = E^0 \cos 2\pi\nu t$$

where  $\nu$  is the frequency of monochromatic radiation which is plane polarised in the x direction and  $E^0$  is the amplitude of the electric field.

The induced dipole moment becomes:

$$\begin{aligned} \mu_x &= \alpha_{xx} E_x = \left[ \alpha_0 + \left( \frac{d\alpha_{xx}}{dQ_p} \right)_0 Q_p^0 \cos 2\pi\nu_p t \right] E^0 \cos 2\pi\nu t \\ &= \alpha_0 E^0 \cos 2\pi\nu t + \left( \frac{d\alpha_{xx}}{dQ_p} \right)_0 Q_p^0 E^0 \cos 2\pi\nu_p t \cos 2\pi\nu t \\ &= \alpha_0 E^0 \cos 2\pi\nu t + 1/2 \left( \frac{d\alpha_{xx}}{dQ_p} \right)_0 Q_p^0 E^0 \left[ \cos 2\pi(\nu + \nu_p) t \right. \\ &\quad \left. + \cos 2\pi(\nu - \nu_p) t \right] \end{aligned}$$

(using  $\cos A \cos B = 1/2[\cos(A+B) + \cos(A-B)]$ )

This equation demonstrates that when a light wave interacts with a vibrating molecule, the induced dipole moment ( $\mu_x$  in this case), has three components contributing to its time dependence. The first term on the right hand side of the equation is a component which is vibrating with the frequency of the incident light ( $\nu$ ) with a magnitude determined by  $\alpha_0$  and  $E^0$ . This is the Rayleigh line which is due to light emission of the same frequency as the incident but is observable in directions which differ from the incident.

The second term is due to the anti-Stokes scattering which occurs at the shifted frequency ( $\nu + \nu_p$ ) i.e. the sum of the frequencies of the light and the molecular vibration. Finally the third term is from the Stokes line at a frequency of ( $\nu - \nu_p$ ) which is the light frequency minus the molecular vibration. Both the second and third term have magnitudes which depend on the field strength of the light, the amplitude of vibration and the polarisability derivative,

$$\left( \frac{d\alpha_{xx}}{dQ_p} \right)_0$$

which is proportional to the intensity of a vibrational Raman band.

Although this classical derivation illustrates the Raman shifted frequencies at ( $\nu + \nu_p$ ) and ( $\nu - \nu_p$ ), it also incorrectly implies that the two sets will occur with equal intensity. The actual intensities of the Stokes and anti-Stokes lines are principally determined by the Boltzmann factor characterising the vibrational population:

$$\frac{N}{N_0} = \exp(-\Delta E/kT)$$

where  $N_0$  is the population of the initial state,  $N$  the population of the final state and  $\Delta E$  the energy

difference between the initial and final energy levels. For high frequency vibrations the Stokes lines are relatively intense, whereas the anti-Stokes lines are extremely weak or non-existent as they depend on significant population of the upper vibrational levels.

This derivation has only considered the  $\alpha_{xx}$  component of the polarisability tensor but the other components can be written in a similar way.

## Appendix 2

### Electronic Spectra of Retinal

The primary reaction in vision is the cis-trans isomerisation of retinal which follows the absorption of light by rhodopsin. Retinal is a polyene aldehyde which contains a chain of five carbon-carbon double bonds in conjugation with a carbonyl group. The mobile  $\pi$  electrons of polyenes are responsible for most of the known spectroscopic properties, and these  $\pi$  electrons are delocalised over the molecule leading to a resonance stabilisation of the system. The single bonds obtain some double bond character and the double bonds cease to be pure double bonds, so that all the bonds in the polyene backbone have some double bond character and this tends to result in polyenes having a planar configuration.

In the isomers of retinal there is steric hindrance due to bulky methyl substituents on carbon atoms 1,5,9 and 13 causing strain in the molecules. The relaxation of this strain takes place via torsional motion about rotatable bonds, along with some bond stretching and bond angle bending, preventing the typical planar configuration.

Usually this steric hindrance is greater in the cis configuration so that isomers containing cis bonds are usually less stable than those with trans bonds. This steric hindrance in cis isomers is accompanied by a shift in maximum absorbance to shorter wavelength and this shift is associated with the distortion of the polyene chain from planarity.

The electronic spectrum of a molecule containing just one isolated double bond or a lone pair of electrons would consist of a strong absorption maximum at around 190nm in the ultra-violet region. When the molecular orbitals of two isolated double bonds are brought into conjugation, the energy of the highest occupied bonding orbital is raised and that of the lowest unoccupied anti-bonding orbital is lowered, so that the energy of

the transition from the  $\pi$  bonding orbital to the  $\pi^*$  anti-bonding orbital is lowered resulting in a transition at longer wavelength.

When more than two  $\pi$  bonding orbitals overlap, such as in a longer conjugated system like retinal, the separation of the energy levels is even further reduced and absorption can occur at longer wavelength, in the visible region. This accounts for the fact that retinal absorbs in the visible region.

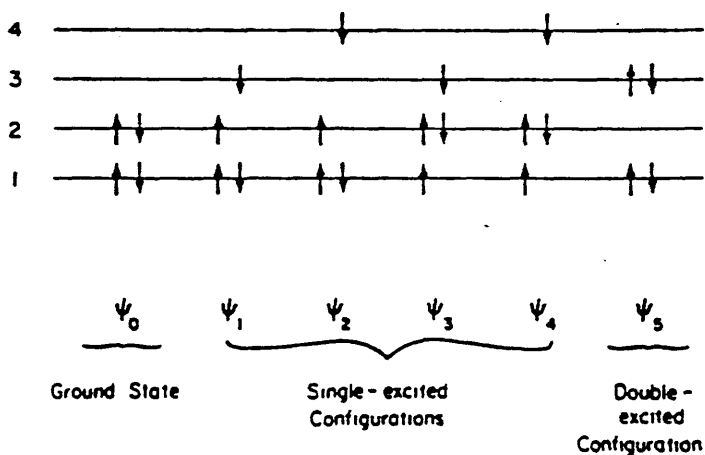
With polyene aldehydes, in addition to the transitions of  $\pi$  electrons from  $\pi \rightarrow \pi^*$  molecular orbitals, there are transitions from the non-bonding orbital (n) on the oxygen atom of the carbonyl group, to the anti-bonding orbital  $\pi^*$ . These  $n \rightarrow \pi^*$  transitions tend to be very weak and could be partially responsible for the observed broadening of the bands in the absorption spectra of polyene aldehydes.

During this work all-trans retinal was the chromophore in the model schiff base compounds, and there are two absorption bands present in the electronic spectra of the retinal, an intense peak at approximately 380nm and a weaker band at around 280nm. Assignments of these transitions are normally made in terms of the transitions to the lowest  $\pi^*$  excited states of linear polyenes<sup>1,2,111</sup>.

As an example butadiene, which is the simplest polyene, has four  $\pi$  electron molecular orbitals which can be labelled 1 to 4 in order of increasing energy (fig. 1). Orbitals 1 and 2 are bonding orbitals and 3 and 4 are anti-bonding orbitals. In the ground state configuration ( $\Psi_0$ ), orbitals 1 and 2 each contain two electrons while orbitals 3 and 4 remain empty. There are four singlet  $\pi$  electron excited state configurations ( $\Psi_1, \Psi_2, \Psi_3, \Psi_4$ ) where a single electron is removed from orbital 1 or 2 and added to orbital 3 or 4. The arrows indicate the spin pairing corresponding to the singlet configurations.

From these four excited configurations it is possible to form four excited singlet states namely,  $^1A_g, ^1B_u, ^1A_g$  and  $^1B_u$ . These excited states are assigned the labels which are determined by their symmetry properties. Linear

FIGURE 1  
 Ground state and excited state electronic configurations  
 of butadiene.



(Taken from ref.111)

polyenes such as *s*-trans butadiene belong to the  $C_{2h}$  point group. The ground state is totally symmetric and is represented by  ${}^1A_g$  where the *g* indicates that the state is symmetric with respect to inversion through the centre of symmetry of the molecule (*u* is anti-symmetric). The excited states have dominant contributions as follows:

${}^1B_u, \Psi_1$ ;  ${}^1A_g, \Psi_2 + \Psi_3$ ;  ${}^1A_g, \Psi_2 - \Psi_3$ ;  ${}^1B_u, \Psi_4$ .

Triplet excited states also exist but as the ground state configuration is singlet, transitions to triplet excited states are spin forbidden. Only *g*→*u* transitions should be allowed for molecules with a centre of symmetry.

The transition from the  ${}^1A_g$  ground state to the  ${}^1B_u$  excited state is strongly allowed and corresponds to the main absorbance band in polyene spectra. The two  ${}^1A_g$  states correspond to forbidden transitions from the ground state and the  ${}^1B_u$  is weakly allowed. If one or more of the double bonds becomes *cis* then the centre of symmetry is destroyed and a transition to the  ${}^1A_g$  state becomes allowed (the subscript *g* is no longer valid as the centre of symmetry has been destroyed). This explains the extra "cis peak" that is seen on the spectra of the *cis* isomers<sup>1,2</sup>. The other  ${}^1A_g$  excited state remains forbidden even in *cis* polyenes.

It is very difficult to assign the level order of the low-lying excited singlet states of polyenes because of the broadening of the peaks in the spectra which has been shown to be mostly due to torsional inhomogeneity around the 6-7 single bond<sup>1,3</sup>. Spectroscopic and theoretical studies have led to controversy over the ordering because there are three low-lying excited states that are very close in energy, namely the  ${}^1B_u$  and  ${}^1A_g$  states giving rise to  $\pi \rightarrow \pi^*$  transitions, and the  ${}^1n\pi^*$  state giving rise to an  $n \rightarrow \pi^*$  transition. There is also evidence to suggest that the relative ordering of these excited levels is dependent on solvent, temperature and conformation<sup>1,4</sup>.

With all-trans retinal, the main absorption band at 380nm has generally been accepted to be due to the allowed transition from the  ${}^1A_g$  ground state to the

low-lying  $^1B_u$  excited state. The assignment of the 280nm band has also been subject to considerable controversy. It was suggested that it may be associated with a transition to the lowest  $^1n\pi^*$  state<sup>114</sup> but later work shows that it is more likely to be due to the transition to the  $^1A_g$  state which was referred to as the "cis peak"<sup>115</sup>. This should be forbidden in the spectra of the all-trans polyenes but is weakly allowed in the polyene aldehydes. This is because, although most of the features that characterise the various states in the polyenes are still present in the polyene aldehydes (even though the symmetry designations are no longer valid), there is a difference in that all the transitions become weakly allowed even in the trans isomer. The "cis peak" has a very weak intensity in the all-trans isomer, gains intensity in the s-cis isomer and becomes even more intense when the cis bond approaches the centre of the polyene chain. Honig and co-workers<sup>115</sup> assign the 280nm band as the "cis peak" by showing that the intensity of the transition is very sensitive to the 6,7 dihedral angle.

During these experiments the absorption peaks of most interest are those due to the main transition to the  $^1B_u$  state i.e. the 380nm band for all-trans retinal, the 360nm band for the unprotonated retinal schiff base and the 440nm band for the protonated schiff base.

### Appendix 3

The Mechanism of Retinal Schiff Base Formation and Hydrolysis in Relation to Visual Pigment Photolysis and Regeneration: Resonance Raman Spectroscopy of a Tetrahedral Carbinolamine Intermediate and Oxygen-18 Labelling of Retinal at the Meta-Rhodopsin Stage in Photoreceptor Membranes.

Alan Cooper\*, Sheila F. Dixon, Margaret A. Nutley  
and Jenifer L. Robb

Contribution from the Department of Chemistry,  
Glasgow University, Glasgow G12 8QQ, Scotland, U.K.

## ABSTRACT

The mechanism of formation and hydrolysis of N-retinylidene-n-butylamine, as a model of the rhodopsin chromophore, has been investigated by a study of the kinetic and equilibrium properties in aqueous anionic, cationic and neutral detergent micelle systems. The pH dependence of steady-state formation and hydrolysis rate constants is consistent with the classical imine reaction mechanism involving tetrahedral carbinolamine intermediates. Kinetic transients consistent with such intermediates can be seen using rapid stopped-flow techniques. Hydrolysis rates in neutral detergent micelles exhibit general base catalysis, and there are pronounced detergent-specific effects which can be qualitatively interpreted in terms of ionic effects on Schiff base  $pK_a$  and micellar hydrogen ion activities. This suggests a rational explanation for the anomalous  $pK_a$  and thermodynamic stability of visual pigment chromophores under physiological conditions. The tetrahedral intermediate has been observed directly at room temperature by continuous-flow, pH-jump resonance Raman spectroscopy, and the spectrum of this transient species shows remarkable similarity with the previously reported Raman spectrum of the metarhodopsin II intermediate of bovine rhodopsin photolysis. Isotope-labelling experiments on bovine photoreceptor membranes exposed to oxygen-18 enriched water during bleaching show incorporation of  $^{18}O$  at the retinal aldehyde site during the metarhodopsin I  $\rightarrow$  II transition. These observations support the hypothesis that the vertebrate Meta I  $\rightarrow$  Meta II transition involves hydrolytic attack by water on the retinyl-lysine Schiff base linkage of the rhodopsin chromophore.

## INTRODUCTION

Visual pigment rhodopsins and related proteins from various organisms are characterized by the presence of the retinal chromophore, attached via a Schiff base (imine) linkage to a specific lysine side chain<sup>1</sup>. In vertebrate rhodopsins, at least, this linkage is hydrolysed at some stage during the visual photochemical cycle (after cis-trans photoisomerization) and must be re-formed (with 11-cis retinal) during regeneration. Neither the precise stage at which this hydrolysis occurs nor, indeed, the mechanism of Schiff base formation and hydrolysis in the protein active site environment are known. We report here on a series of experiments designed to clarify the situation. Firstly, using conventional equilibrium and kinetic techniques, we examine the formation and hydrolysis of a model retinal Schiff base in different detergent micelle environments in relation to the standard tetrahedral carbinolamine intermediate mechanism of imine chemistry<sup>2</sup>. The presence of this intermediate is demonstrated by stopped-flow kinetic measurements and its resonance Raman spectrum obtained under continuous flow conditions. Finally, using isotope labelling techniques, we examine the possible onset of Schiff base hydrolysis during the metarhodopsin stage of photolysis in bovine photoreceptor membranes.

## EXPERIMENTAL SECTION

Model Compound Equilibrium & Kinetics

All-trans retinal (vitamin A aldehyde, retinaldehyde, from Fluka or Sigma) was used without further purification. Mass spectrometry and HPLC analysis showed no detectable impurities other than traces of other geometric isomers. Detergents used include: Emulphogene BC-720 (a commercial poly-oxyethylene-10-tridecyl-ether preparation from GAF), Ammonyx-LO (primarily lauryl dimethylamine oxide, from Onyx Corp.), sodium dodecylsulfate (SDS, from BDH Ltd.) and dodecyl-trimethylammonium bromide (DTAB, from Sigma). n-Butylamine was redistilled before use, and all other reagents were of appropriate analytical grade. Glass-distilled water was used throughout, and all manipulations involving retinal were done under argon in the dark or dim light conditions.

Retinal solutions for kinetic and equilibrium experiments were made up fresh daily by first dissolving the solid in a small quantity of ethanol, followed by rapid dispersal in a large volume of the appropriate detergent buffer (final EtOH concentration less than 1%). Stock solutions of the model Schiff base, N-retinylidene-n-butylamine, were prepared by addition of retinal to a large excess of 10mM n-butylamine in ethanol or unbuffered aqueous detergent. Incubation at room temperature for 30min. was sufficient for complete reaction. All experiments were performed at 20°C. Buffer concentrations were generally 0.1M, except in the case of SDS where poor solubility limited buffer concentrations to 0.02M. Detergent concentrations used were well above critical micelle concentrations: 2% v/v (Ammonyx, Emulphogene), 25mM (DTAB) and 12.5mM (SDS). Spectral changes in the 300-550nm range were observed using Pye-Unicam SP-1800 or SPB-200 spectrophotometers fitted with thermostatted cell holders.

Dissociation constants ( $K_{diss}$ ) for the retinal-butylamine reaction were determined in the pH range 7-13 using phosphate, borate or NaOH/NaCl buffers, as appropriate. Retinal in

detergent buffer was mixed, under argon, in a series of stoppered volumetric flasks with appropriate volumes of n-butylamine in the same buffer mixture, to give a final retinal concentration of about  $10^{-6}$ M and butylamine concentrations in the range 0.02mM to 1M. After incubation for 2-4 hrs. at 20°C spectra were taken to determine the extent of reaction. The pH of each mixture was checked before and after incubation. Longer reaction times gave identical results, as did trial experiments in which equilibrium was approached from the opposite direction by pH and concentration adjustment of solutions of the pre-formed Schiff base. Data were analyzed by a linear least-squares Benesi-Hildebrand method<sup>3</sup> using absorbances at a minimum of two different wavelengths for each sample.

Steady-state rates of Schiff base formation and hydrolysis were obtained from absorbance changes, again at at least two wavelengths, after mixing retinal or the Schiff base with the relevant detergent buffer mixture. Variation of the butylamine content verified that formation rates were first order in amine concentration. Absorbance changes were recorded either at fixed wavelengths or, for slower reactions, by repetitive spectral scans, and the pH of each reaction mixture was determined at the end of each kinetic run using a sodium ion correction at high pH if appropriate. Pseudo-first order rate constants ( $k_{form}$  or  $k_{hydro}$ ) were obtained by least-squares analysis according to the appropriate first order rate expression, and formation rate constants were corrected for hydrolysis in the reverse direction when necessary. This latter correction is only significant at the lower pH limit and never amounted to more than 10% of the whole. A limited examination of possible solvent isotope effects was undertaken for hydrolysis in Ammonyx with  $D_2O$  (99.8%, Fluorochem, pD 4.0).

General base catalysis of the hydrolysis reaction in Emulphogene or Ammonyx micelles was investigated in the pH range 4-7 by use of various different buffers over a concentration range of 0.01 to 0.2M. Higher concentrations could not be used because of problems with solubility of the detergents. Control experiments with added NaCl showed that ionic strength had no

significant effect on hydrolysis rates in this pH range.

Transient kinetics were studied using an Applied Photophysics stopped-flow kinetic spectrophotometer, interfaced to an Apple II microcomputer giving non-linear, programmable time-base data acquisition. The effective dead-time of this apparatus is about 8 msec. and the non-linear time-base allows data in the time range from about 10 msec. to 12 minutes to be sampled in a single run. Rapid formation or hydrolysis reactions were initiated by pH-jump or reagent mixing, as appropriate and the kinetic behaviour was analysed by a multi-exponential fitting procedure (DISCRETE) kindly provided by Dr. Provencher<sup>4</sup>.

The hydrogen ion titration behaviour of the model Schiff base in different detergents was obtained from the absorbance changes associated with the protonation-induced red shift of the retinyl chromophore during pH-jump experiments. Absorbances at 360 and 440nm, extrapolated to zero time, were obtained from the initial phases of stopped-flow measurements ( $< 100$  msec.) and were confirmed, in the slower hydrolysis ranges, by manual mixing techniques. Data were analyzed from the pH-dependence of the quantity:

$$[\text{SH}^+]/[\text{S}] = (\text{A}_H - \text{A})/(\text{A} - \text{A}_L)$$

where  $\text{A}_H$ ,  $\text{A}_L$  are the initial absorbances at high and low pH extremes,  $\text{A}$  is the initial absorbance after pH-jump, and  $\text{SH}^+$ ,  $\text{S}$  are the protonated and unprotonated Schiff base, respectively.

Defining the acid dissociation constant of the Schiff base:

$$K_{aH} = [\text{S}] a_H / [\text{SH}^+]$$

where  $a_H$  is the hydrogen ion activity in the micelle shows that, for simple titration behaviour, a plot of  $\log[\text{S}]/[\text{SH}^+]$  versus  $\text{p}a_H$  should be linear, with slope unity and an intercept of  $\text{p}K_{aH}$  on the  $\text{p}a_H$  axis. To relate the micellar hydrogen ion activity to the measured bulk pH we use the empirical relation:

$$\text{p}a_H = -\text{p}\phi + n.\text{pH} \quad \dots\dots\dots\text{Equ. (1)}$$

where  $\text{p}\phi$  and  $n$  represent any apparent pH shift and non-ideality at the micelle, respectively. ( $n=1$  for ideal titration

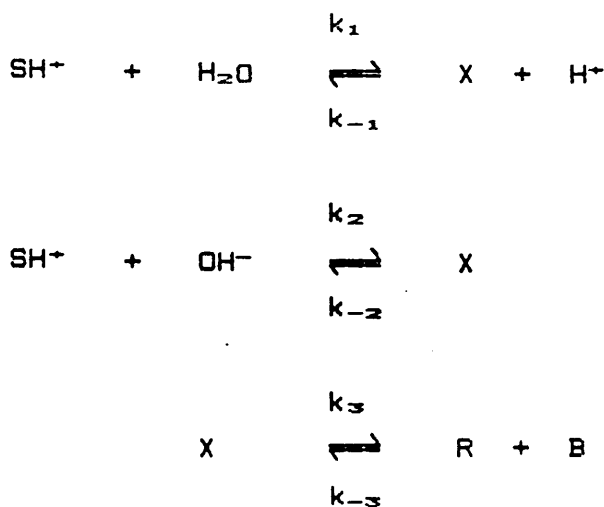
behaviour.) We arbitrarily take  $p\emptyset = 0$  for the neutral detergent, Emulphogene. The mid-point pH of the titration is given, in these terms, by:

$$pH_{mid} = (pK_{SH} + p\emptyset)/n$$

### Reaction Mechanism: Equilibrium and Rate Expressions

We assume the standard<sup>2</sup> imine mechanism (Scheme I) in which retinal Schiff base hydrolysis and formation share a common tetrahedral carbinolamine intermediate (X).

Scheme 1



X is formed solely by attack of water or hydroxide on the protonated imine ( $SH^+$ ), or by reaction of unprotonated amine (B) on the aldehydic retinal (R). Assuming that all retinyl species are confined to the micellar phase, whereas the much more soluble free butylamine resides in the aqueous phase, we can define the following acid dissociation constants for the amine and imine, respectively:

$$K_{BH} = [B][H^+]/[BH^+] \quad ; \quad K_{SH} = [S]a_H/[SH^+]$$

where  $[H^+]$  is the hydrogen ion concentration (strictly activity) in the bulk aqueous phase (as measured by the pH electrode) and  $a_H$  is the hydrogen ion activity in the micellar phase estimated from the Schiff base titrations in the appropriate detergents as described above.

The overall observed equilibrium constant for the reaction ( $K_{obs}$ ) may be written:

$$\begin{aligned} K_{obs} &= [B]_{Tot}[R]/[S]_{Tot} \\ &= K_0(1 + [H^+]/K_{BH})/(1 + a_H/K_{SH}) \end{aligned} \quad \dots\dots\text{Equ. (2)}$$

where  $K_0 = [R][B]/[S]$  is the dissociation constant at the high pH limit. Application of detailed balance gives several useful relations between the equilibrium and rate constants:

$$k_1k_{-2}/k_{-1}k_2 = a_H a_{OH} = K_w$$

$$K_0 = k_2k_3K_w/k_{-2}k_{-3}K_{BH} = k_1k_3/k_{-1}k_{-3}K_{BH}$$

Following established procedures<sup>2,3</sup>, steady-state pseudo-first-order and second order observed rate constants for hydrolysis and formation, respectively, may be written:

$$k_{hydro1} = \frac{k_3}{(a_H + K_{SH})} \left( \frac{k_1a_H + k_2K_w}{k_3 + k_{-2} + k_{-1}a_H} \right) \quad \dots\dots\text{Equ. (3)}$$

$$k_{form} = \frac{k_{-3}K_{BH}}{([H^+] + K_{BH})} \left( \frac{k_{-1}a_H + k_{-2}}{k_3 + k_{-2} + k_{-1}a_H} \right)$$

These are related by the equilibrium constant  $K_{obs} = k_{hydro1}/k_{form}$ , and either formation or hydrolysis data may be used to give equivalent information. We have used both approaches as experimentally convenient. Steady-state data were

analysed according to these rate expressions using non-linear least-squares regression procedures to give  $k_1$ ,  $k_2$  and  $k_{-1}/k_3$ . Detailed balance allows subsequent calculation of  $k_{-3}$  and  $k_{-2}/k_3$ .

$k_3$  is obtained from analysis of the biphasic absorbance kinetics observed in stopped-flow experiments for reactions of this type<sup>2,6</sup>:

$$A(t) = A_0 + A_1 \exp(-r_1 t) + A_2 \exp(-r_2 t) \dots \text{Equ. (4)}$$

where  $r_1$  and  $r_2$  are cumbersome functions of the individual rate constants. It is straightforward, though algebraically tedious, to show that, for the hydrolysis direction in this case:

$$r_1 r_2 = k_3 (k_1 a_H + k_2 K_w) / (a_H + K_{BH})$$

and, with  $k_1$  and  $k_2$  from steady-state data,  $k_3$  is determined.

### Resonance Raman

Concentrated stock solutions of N-retinylidene-n-butylamine were made fresh daily by dissolution of retinal in ethanol containing 10mM n-butylamine. Aliquots of this were subsequently diluted in aqueous 2% (by volume) Ammonyx, also containing 10mM butylamine, to provide the unprotonated Schiff base sample (approx. 0.3mM) for Raman spectroscopy. Other components for the pH-jump experiments consisted again of 2% Ammonyx containing either 0.2M HCl or 0.2M sodium acetate buffer, pH 4-5. Final pH's in the reaction mixtures were measured after each experiment.

Polarized Raman spectra were obtained using an Applied Photophysics Model 36 multichannel instrument incorporating a Tracor Northern TN-1223-I cooled, intensified diode array detector with a TN-1710 mainframe and optical spectrometer module for data display and manipulation. Sample excitation was with the 457.9nm line of a Spectra-Physics Model 171 Argon ion laser with intensity, measured at the sample, of 100mW or less, and a beam diameter approximately 0.2 mm. (488 or 514nm

irradiation gave identical results, but with a higher fluorescent background.) Experiments were carried out at room temperature ( $20 \pm 1^\circ\text{C}$ ). Continuous flow spectra were obtained in a 1cm path-length quartz cell attached to a simple 2-channel T-mixing device constructed of 1mm bore Teflon tubing, with a dead-time under these conditions of about 10 seconds. Sample and pH-jump buffer solutions were pumped continuously at a combined flow rate of about 10 ml/min using separate peristaltic pumps (LKB), giving a sample residence time in the laser beam of less than about 0.15sec. There was no evidence of photoisomerization of samples under these conditions. Trial experiments using the same configuration in a UV-visible spectrophotometer confirmed adequate mixing in this device. Raman spectra of the appropriate solvent mixtures were obtained using the identical flow system and subsequently subtracted from the sample spectra. All spectra consisted of 400 accumulations, with a 0.2sec acquisition time, at an instrumental bandwidth of  $7\text{cm}^{-1}$ , or less. Quoted wavenumbers are accurate to about  $2\text{cm}^{-1}$  (indene calibration).

### Isotopic Labelling

Bovine rod outer segment membranes (ROS) were isolated from the retinas of dark-adapted cattle eyes, obtained fresh locally, by standard techniques<sup>7</sup> and were stored frozen ( $-70^\circ\text{C}$ ) in the dark until use. Oxygen-18 enriched water (20% or 70% enrichment) was from Amersham International, all-trans retinal from Fluka, and all other reagents were of standard analytical grade. N-retinylidene-n-butylamine was prepared as described above.

Retinal was isolated from freeze-dried ROS membranes (equivalent to 5-10 mg. rhodopsin) by repeated extraction with 5-10 ml aliquots of dry methylene chloride (dichloromethane)<sup>8</sup>. Thorough mixing at each stage was obtained by passage through a glass syringe and the supernatant was collected after centrifugation in a bench-top centrifuge (glass tubes). 2-3 extractions were found to be sufficient. Pooled extracts were concentrated in a stream of dry argon gas and purified by elution on preparative silica TLC plates with cyclohexane/ethyl acetate (3:1 by volume). The distinct yellow retinal band was

redissolved in methylene chloride, concentrated under argon gas, and analysed immediately by low resolution mass spectrometry (VG MS-12 linked to a PDP-8 computer, electron ionization 70eV,  $10^{-7}$  torr). Instrumental controls included commercial all-trans retinal and  $^{18}\text{O}$ -labelled retinal obtained by hydrolysis of synthetic N-retinylidene-n-butylamine in the presence of 20% enriched  $\text{H}_2^{18}\text{O}$ .

A typical experimental protocol was as follows: washed, unbleached bovine ROS membranes, containing 5-10 mg of rhodopsin, were freeze dried (liquid nitrogen trap) and then bleached by exposure to 500nm irradiation (100 watt Xe/Hg lamp with interference filter), giving a color change from pink to deep orange indicative of metarhodopsin I formation. 0.5 ml of ice-cold  $\text{H}_2^{18}\text{O}$ , buffered to pH 5.5 with sodium phosphate, was added (immediate color change from orange to pale yellow) and the sample maintained in the dark at  $0^\circ\text{C}$  for various periods between 30 sec. and 15 min. prior to flash-freezing and freeze drying. Retinal was then extracted and analysed as described above. Control experiments following the same protocol included addition of  $\text{H}_2^{18}\text{O}$  buffered to pH 8 to the freeze-dried Meta I-ROS, and the brief bleaching of previously unbleached ROS incubated in  $\text{H}_2^{18}\text{O}$ , at pH 8,  $0^\circ\text{C}$ .

Infra-red spectra (Perkin-Elmer 983) of the carbonyl stretch region were obtained by taking up the extracted retinals in carbon tetrachloride. Solvent backgrounds were subtracted separately.

## RESULTS

Model Studies: Equilibrium & Kinetics

The absorbance spectrum of all-trans retinal ( $\lambda_{max}$  380nm) changes upon Schiff base formation to about 360nm for the unprotonated imine and to 430-445nm, depending on detergent, in the acidic form. This provides a convenient spectral probe for kinetic and equilibrium studies in the optically clear aqueous micelle mixtures. Equilibration of retinal with increasing concentrations of n-butylamine produces a progressive spectral shift with a single isosbestic point characteristic of simple stoichiometric reaction, and with no indication of thermal isomerization of the retinal. The absorbance changes, in most cases, give good linear Benesi-Hildebrand plots and a pH dependence of the apparent dissociation constant ( $K_{obs}$ ) consistent with Equ.2 (Fig.1). These data are consistent with previous estimates in neutral detergent<sup>7</sup> and show that the pH dependence of  $K_{obs}$  is dominated by protonation of the amine. Essentially identical behaviour is observed for neutral and cationic detergents, with only small differences in  $K_0$ , and the same value for  $pK_{BH} = 10.75$ , in agreement with literature values for n-butylamine in dilute aqueous solution<sup>10</sup> and with trial potentiometric titrations in the presence of the detergents (data not shown). A major exception occurs in the case of the strongly cationic SDS where the Benesi-Hildebrand plots are distinctly non-linear and poorly reproducible, indicating a more complex equilibrium process. pH titration of butylamine in the presence of SDS gives anomalous pK's in excess of 11, suggestive of some specific SDS-butylamine interaction or of partitioning of the amine into the SDS micelles. This concentration-dependent effect will clearly affect the apparent equilibrium of the retinal Schiff base reaction, but we have not so far investigated the phenomenon any further. An estimate of  $K_0$  in this case was obtained from comparison of formation and

hydrolysis rates at high pH and does not differ significantly from the other detergents (Table I).

Spectral acid-base titrations of the retinyl Schiff base in different detergents are illustrated in Fig.2, plotted using the procedure described in the experimental section. There are significant differences in apparent pK of the retinyl Schiff base in different micelles, correlating qualitatively with the ionic state of the detergent. The apparent pK in Emulphogene,  $\text{pH}_{\text{mid}} = 6.1$ , is in good agreement with previous estimates under similar conditions in other neutral detergents<sup>11,12</sup>, but somewhat lower values (4.85 and 5.84, respectively) are found for Ammonyx and DTAB, and a dramatically higher value (9.54) in SDS. Similar alterations in apparent pK's in the presence of charged micelles have been reported elsewhere<sup>12</sup> and, bearing in mind that the weakly basic amine oxide detergent, Ammonyx, will itself become protonated below neutral pH, these observations are consistent with simple electrostatic effects on Schiff base protonation and/or hydrogen ion activity in the micellar environment<sup>12,13</sup>. The magnitude of the pK shift in SDS suggests the possibility of specific ionic interaction between the polar sulfonic acid head group and the imine nitrogen, in this case, rather than a delocalized non-specific effect of micellar surface potential. This is reminiscent of the SDS-butylamine interaction postulated above.

Although the titration plots of Fig.2 are all reasonably linear, only in the case of Emulphogene does the slope (n) equal unity. Shallower titrations (n=0.77) are seen for the Schiff base in Ammonyx or DTAB, and sharper (n=1.1) in SDS. We have no general explanation for this phenomenon, though it is consistently observed using various buffers and absorbance wavelengths. In the case of Ammonyx, protonation in a similar pH region and the associated changes in micelle surface potential would attenuate the Schiff base titration, but this would not apply with SDS or DTAB. This non-ideality may possibly reflect changes in micelle potential due to ionic strength changes in the buffer counter-ions during titration. Unfortunately, because of the poor solubility of the detergents at high ionic

strengths, we were unable to test this possibility. However, in some experiments in SDS, in which the buffer also contained 10mM butylamine (in an attempt to suppress hydrolysis, data not shown), the apparent pK was reduced slightly to about 9.3 (compared to 9.54) and the slope closer to 1. Other experiments, mentioned above, on the acid-base titration of butylamine itself in the presence of SDS have shown anomalies suggesting some specific interaction between SDS and the protonated butylamine. This indicates that the anomalous titration behaviour that we have observed is associated with the charge density at the micelle surface and probably involves counterion effects.

The pH dependence of the state of ionization of the retinyl imine is required for quantitative analysis of the reaction kinetics in terms of the carbinolamine intermediate mechanism. In the absence of any appropriate theoretical expression, the data of Fig.2 suggest an empirical equation (Equ. 1, experimental section) which adequately expresses the apparent micellar hydrogen ion activity as a function of measured pH. This, together with experimental parameters given in Table I, is used in the steady-state rate expressions to describe the Schiff base protonation in different detergents. It is worth noting here that this empirical relation is formally equivalent to a non-stoichiometric, or fractional protonation scheme:



with a dissociation constant,  $K = [S][H^+]^n/[SH_n^+]$ . Interestingly, such apparent "fractional protonation" behaviour has been observed on many occasions as a feature of the acid-base equilibrium of the metarhodopsin intermediates of visual pigment photolysis<sup>13</sup>, where it presumably reflects a similar non-ideality in titration behaviour of groups within the protein environment.

Steady-state rate constants for hydrolysis and formation of the model Schiff base as a function of pH in the different detergents, shown in Figs.3 & 4, display all the general features expected of the carbinolamine intermediate mechanism, although there are significant quantitative variations induced by the different micelle environments. Despite these

differences, provided due account is taken of the abnormal Schiff base protonation behaviour, steady-state pH-rate profiles are adequately described by the appropriate rate expressions (Equ.3) and, in most cases, yield the unambiguous sets of rate parameters listed in Table I. Again, however, SDS is an exception where because of the limited pH range over which rate data were accessible, and also possibly because of interference from specific interactions, no stable set of parameters emerged from the least-squares fitting procedures and only rough orders of magnitude estimates are given. Nevertheless, the overall shape of the SDS rate profiles are clearly in line with the general mechanism, though dominated by the large pK shift of the imine in this environment.

Direct evidence for the tetrahedral intermediate comes from rapid-mixing hydrolysis experiments. Transient accumulation of the carbinolamine intermediate during hydrolysis is optimal near the peak of the pH profile. Stopped-flow experiments over a wide range of wavelengths in this pH region, examples of which are given in Fig.5, in all cases showed the biphasic behaviour characteristic of the build-up and decay of the intermediate species, and the kinetic data are well described by the anticipated double-exponential expression (Equ.4). Rate constants for the fast phase ( $r_1$ ) ranged from about 0.02 to 0.3  $\text{sec}^{-1}$ , depending on pH and detergent, whilst the slower phases ( $r_2$ ) were identical to steady-state rates under the same conditions. Analysis of  $r_1$  values in conjunction with the steady-state results gave the additional information required for complete determination of the mechanistic rate constants (Table I). The absorbance spectrum of the intermediate, estimated from the amplitudes of the different kinetic phases in these experiments (not shown), depends on pH and is very similar in form to the parent Schiff base, indicating only changes in extent of protonation, or small variations in extinction coefficient, rather than gross changes in absorbance maxima. Assuming that a red-shift is indicative of protonation of the carbinolamine, as it is with the Schiff base, then the transient spectral changes are consistent with an increase in protonation

at low pH and a decrease at higher pH (in SDS), placing the carbinolamine  $pK_a$  somewhere in the region 7-9, as might be expected<sup>10b</sup>. Estimation of the steady-state accumulation of the intermediate shows that, in most cases, the build-up is no greater than about 5% of the total Schiff base concentration, and usually very much less. In Ammonyx, however, the relatively high value of  $k_1$  (discussed below) favours kinetic accumulation of the intermediate under suitable pH conditions, such that an estimated 50% of the Schiff base may be present as the carbinolamine during the early stages of hydrolysis at pH 4-5. No rapid transients are observable during hydrolysis away from the pH maxima, nor under any accessible conditions during the formation reaction. The latter observation is consistent with the mechanism in which nucleophilic attack by the amine on the aldehyde is rate-limiting in the observable pH range.

Steady-state hydrolysis rates in Emulphogene over the pH range 4-6, where attack of water on the protonated Schiff base is rate limiting, showed variations with buffer type and concentration typical of general base catalysis with a Brønsted coefficient  $\beta$  of about 0.43 (Fig.6), which is reasonable for reactions of this type<sup>14</sup>. However, no such effect was seen in Ammonyx. On examination of the rate parameters of Table I we note that  $k_1$ , the rate constant for the base catalysed step, is significantly higher for Ammonyx than for the other detergents, suggesting that in these micelles the hydrolysis reaction is already experiencing significant base catalysis from the amine oxide head groups of the detergent and that this is sufficient to mask any possible further catalysis from general bases in solution. Support for this comes from the observation that, discounting SDS which seems to be a special case throughout, the ratio  $k_1/k_{-1}$  is reasonably constant over the range of detergents, despite wide variations in the absolute values of the individual rate constants. Thus, any specific micelle interactions seem to have an equal effect on the magnitudes of both the forward and reverse rate constants of this step, in a manner characteristic of a catalytic process rather than a change in thermodynamic equilibrium stability of any of the

reactant species. Similar conclusions may be drawn about the other steps of the mechanism where  $k_2/k_{-2}$  and  $k_3/k_{-3}$  also show little variation, though here the rate constants themselves vary only marginally with detergent.

Hydrolysis in Ammonyx micelles using  $D_2O$ , pD 4.0, as solvent was significantly slower than under identical conditions in  $H_2O$ , giving a solvent isotope effect,  $k^H/k^D$ , of about 2.3. This is close to the value observed in other studies of Schiff base hydrolysis<sup>14</sup> where it has been interpreted mechanistically in terms of a close resemblance of the transition state to the protonated carbinolamine<sup>14,15</sup>.

### Resonance Raman Spectroscopy

Continuous flow Raman data on N-retinylidene-n-butylamine and its hydrolysis products, under various conditions in aqueous Ammonyx dispersions, are summarized in Fig.7. Spectra in 0.1M HCl show intense resonance enhancement, with a strong retinal C=C stretch band at  $1565cm^{-1}$ , a protonated imine C=N stretch at  $1656cm^{-1}$ , and major fingerprint vibrations in the  $1100-1400cm^{-1}$  region characteristic of the protonated all-trans retinal Schiff base<sup>16</sup> (Fig.7A). Hydrolysis is essentially non-existent under these conditions and most of the assigned bands in the high resolution spectra of the crystalline protonated n-butylamine Schiff base<sup>16</sup> can be identified, albeit at lower resolution. Significant changes in this spectrum occur, however, during the early stages of hydrolysis (Fig.7B), approximately 10 seconds after pH jump of the unprotonated imine to the pH 4-5 region (0.1M acetate buffer, final concentration). In particular, there is a marked decrease in intensity of the 1240 and  $1656cm^{-1}$  bands, compared to the protonated Schiff base, together with the appearance of a prominent band at about  $1345cm^{-1}$ . We ascribe these changes to the build-up of the tetrahedral carbinolamine intermediate of imine hydrolysis, which the kinetic studies have shown to be optimal under these conditions. Similar effects are seen using various laser excitation lines and, to a lesser extent, using the detergent Emulphogene instead of Ammonyx. None of these features, especially the  $1345cm^{-1}$  peak, appear in Raman

spectra of the unprotonated Schiff base or retinal hydrolysis products run under identical conditions (Fig.7C,D,E). Such spectra, furthermore, show considerably less resonance enhancement because of the hypsochromic shift of these pigments relative to the exciting line (absorbance maxima: 380 and 360 nm approximately for retinal and the unprotonated Schiff base, respectively, compared to about 440nm for the protonated imine). Moreover, any significant contamination from such sources during the early stages of hydrolysis would give rise to a shift in the  $1565\text{cm}^{-1}$  C=C band. No such shift is observed. In any case, the kinetic studies indicate that the Schiff base is predominantly protonated at pH 4 to 5 and that less than 10% complete hydrolysis occurs within 10 seconds under these conditions.

The Raman spectrum Fig.7B consists, therefore, of a mixture of the tetrahedral carbinolamine intermediate of the imine hydrolysis reaction together with un-reacted protonated Schiff base, in roughly equal proportions as judged from the appropriate rate expressions under these conditions. Subtraction of 50% of the protonated imine spectrum (Fig.7A) yields an estimate of the Raman spectrum of the pure intermediate (Fig.8) and this, to our knowledge, represents the first such spectrum reported for any transient carbinolamine. The spectrum retains many of the major features of the protonated Schiff base, but with the significant loss of the  $1240$  and  $1656\text{cm}^{-1}$  bands and the presence, already noted, of the new band at  $1345\text{cm}^{-1}$ . In the absence of any small-molecule carbinolamine spectra for comparison we can make no firm assignment for this vibration, apart from noting that its frequency is consistent with the alcoholic O-H in-plane deformation that might be expected in the carbinolamine. Though, by analogy with the complex vibrational behaviour of amide groups, we should not necessarily expect the spectrum of this linkage to be simply a superposition of amine and alcoholic characteristic group frequencies because of potential coupling between the modes. (Deuterium labelling experiments, though attempted, were unhelpful here because the kinetic isotope effect in  $\text{D}_2\text{O}$  diminishes the transient levels of the carbinolamine to below detectable limits in these spectra).

The  $1656\text{cm}^{-1}$  band is predominantly due to modes associated with the protonated C=N bond of the imine<sup>16</sup>, and its disappearance is entirely consistent with conversion of this group to a carbinolamine linkage. Assignment of the band at about  $1240\text{cm}^{-1}$  in the protonated Schiff base is not entirely certain, though it seems to be a highly mixed combination of C-C, C=C, C-CH<sub>2</sub> stretch vibrations and CCH in-plane rocks involving several carbons, including C-15<sup>16</sup>. It is not unreasonable, therefore, that alcoholic substitution on C-15 might significantly affect this mode. We note, however, that the intensity of this band appears somewhat greater in our detergent-solubilized spectra than in the solid state<sup>16</sup>, and this might reflect possible conformational differences between the protonated Schiff base in the micelle and the crystal which could affect mode assignment.

But, regardless of the precise mode assignments, the most surprising feature of the carbinolamine spectrum is its remarkable similarity to the published spectrum of the metarhodopsin II photoproduct of bovine rhodopsin<sup>17</sup>, most notably in the presence of the hitherto unexplained  $1345\text{cm}^{-1}$  peak (Fig.8). The ramifications of this observation in relation to the hydrolysis step of rhodopsin photolysis are considered below.

### <sup>18</sup>O Labelling Studies

The starting point for these experiments was the early observation that, in the absence of water, bleaching of rhodopsin does not proceed further than the metarhodopsin I intermediate<sup>18</sup>. In our hands, freeze-dried bovine rod outer segments are pale pink, changing to a stable orange color (Meta I) on exposure to light. This color persists on addition of ice-cold pH 8 buffer, whereas pH 5.5 buffer gives an immediate change to pale yellow (Meta II). Both these intermediates are stable for many minutes at 0°C in water<sup>13b, 17</sup>, and for much longer if immediately freeze dried.

Low-resolution mass spectra of unlabelled retinals, either commercial material or that extracted from fully bleached freeze-dried ROS, show typical fragmentation patterns with a

major parent ion peak at 284 m/z, and a minor peak at 285 arising mainly from natural abundance carbon-13 (Table II; samples A,C,D)<sup>16</sup>. The absence of any higher mass ions together with a constant 285/284 ratio of  $0.24 \pm 0.02$ , confirms the lack of potential interference from retinol or retinoic acid in these preparations. By contrast, in preliminary trials using retinal extracted from RDS fully bleached in aqueous buffers slightly enriched in  $^{18}\text{O}$ , or from hydrolysed synthetic retinal Schiff base in the same medium (Table II; sample B), an additional peak at 286 was observed, consistent with the anticipated hydrolytic incorporation of  $^{18}\text{O}$  in the aldehydic C=O group. This confirmed the feasibility of a more detailed study of the effect of  $\text{H}_2^{18}\text{O}$  specifically at the metarhodopsin stage of bleaching. Data obtained using more highly enriched  $\text{H}_2^{18}\text{O}$  are also shown in Table II.

Bleaching of RDS in isotopically enriched water under conditions favouring Meta I formation (pH 8, 0°C), or addition of  $\text{H}_2^{18}\text{O}$  to dried Meta I-containing RDS under the same conditions, gives molecular ion ratios of the extracted retinals identical to natural abundance spectra (Table II; samples C,D). However, addition of  $\text{H}_2^{18}\text{O}$  to dried Meta I-RDS under conditions favouring transition to Meta II gives rise to a large additional peak at 286 m/z (samples E,F). Previous studies<sup>13,17</sup> have shown that in RDS membranes at 0°C the metarhodopsin photoproducts are relatively stable under appropriate pH conditions (pH 8 for Meta I, pH 5.5 for Meta II). Transformation of Meta II to subsequent intermediates is very slow (minutes - hours) under these conditions, and  $^{18}\text{O}$  incorporation varied little with  $\text{H}_2^{18}\text{O}$  incubation time in our experiments. In fact yields of the 286 parent ion were somewhat lower for the longer incubation times, possibly due to exchange with atmospheric moisture or because subsequent intermediate stages (Meta III, indicator yellow) involve re-formation of retinal-imine linkages. The 285/284 ratios remained constant in all these experiments, ruling out the possibility of artefacts due to retinal oxidation products. Relative yields of m/z 286 ions were always less than expected from the (nominal) 70% enrichment of the labelled water. It is

not clear whether this is due to extraneous retinal from partial bleaching of the starting material, incomplete initial photoreaction of the rhodopsin, differences in the fragmentation ratios of labelled and unlabelled retinals, or isotopic dilution from residual water in the freeze-dried samples. Nevertheless, these experiments clearly demonstrate significant  $^{18}\text{O}$  uptake from  $\text{H}_2^{18}\text{O}$  during the Meta I  $\rightarrow$  Meta II transition, but not earlier.

If  $^{18}\text{O}$  incorporation is indeed due to hydrolysis then, clearly, the expected site of incorporation must be the carbonyl oxygen of the aldehyde, and this is supported by IR spectra of extracted retinals in the carbonyl-stretch region (Fig.9). Unlabelled retinals show the usual strong  $\text{C}=\text{O}$  band at  $1664\text{cm}^{-1}$ , whereas retinal extracted under  $^{18}\text{O}$  labelling conditions gives an additional band at about  $1638\text{cm}^{-1}$ . This shift is consistent with a simple isotope effect on the  $\text{C}=\text{O}$  stretch vibration due to an increased reduced mass of the  $\text{C}=\text{O}$  group, and agrees with published shifts in other  $^{18}\text{O}$ -labelled aldehydes<sup>20</sup>.

## DISCUSSION

Three significant conclusions, bearing on the stability and photolysis of rhodopsins and related proteins, have been established by the experiments reported here. Firstly, although the precise behavior may be modulated by environmental effects, model retinal Schiff base formation and hydrolysis conforms in all respects to the conventional tetrahedral carbinolamine reaction mechanism so that we may, with some confidence, begin to interpret some of the apparently anomalous properties of the rhodopsin chromophore. Secondly, the resonance Raman spectrum of this transient carbinolamine intermediate is virtually identical to the spectrum of the metarhodopsin II intermediate encountered during bleaching of bovine rhodopsin. Finally, retinal extracted from bovine photoreceptor membranes after exposure to  $H_2^{18}O$  solely during the Meta I to Meta II transition shows isotope uptake at the carbonyl oxygen position. Taken together, these last two observations support the hitherto unconventional view<sup>17</sup> that the metarhodopsin transition marks the start of the chromophore hydrolysis step of visual pigment photolysis.

Prior to this work there was considerable circumstantial evidence that chromophore hydrolysis might be involved as early as the metarhodopsin stage. For example: (i) Water is required for the photoreaction to proceed beyond Meta I<sup>18</sup>. (ii) Meta-rhodopsin is the first stage at which the retinyl chromophore becomes accessible to water-soluble reagents such as hydroxylamine and sodium borohydride<sup>21</sup>, and it is not unreasonable to presume similar accessibility to water itself. (iii) The transition from Meta I to Meta II is the only spontaneous endothermic step of the bleaching sequence (+10 kcal/mole)<sup>17,22</sup>, and the energetics are consistent with Schiff base hydrolysis enthalpies in model compounds (8-12 kcal/mole)<sup>17</sup>. (iv) The kinetics and equilibrium of the Meta I  $\rightarrow$  Meta II transition are complex, involving asynchronous and anomalous protonation changes<sup>13,23</sup>, and possible base

catalysis<sup>13a</sup> that are reminiscent of the features observed here in the hydrolysis of model retinal Schiff bases. (v) The 380nm absorbance maximum of Meta II is the same as free retinal. This was first noted in the original work on metarhodopsin tautomerism<sup>13b</sup>, though the authors ruled out hydrolysis at this stage mainly on the basis of rapid reversibility to Meta I and on the photo-reversibility of Meta II to the parent rhodopsin. But this rests on the mistaken assumption that hydrolysis of the chromophore linkage is synonymous with release from the active site. If, as indicated by the present work, the hydrolysed chromophore in Meta II still resides in the specific retinal binding site of opsin then such considerations are no longer a problem.

Our experiments are not necessarily unambiguous. Although control experiments using the same protocol but without Meta II formation give no isotope labelling, it might be argued that the <sup>18</sup>O incorporation results are an artefact of the extraction procedure rather than indicators of in situ attack by water. This seems unlikely in view of the resonance Raman data (Fig.8) showing remarkable similarity between the spectrum of the initial product of Schiff base hydrolysis and that of authentic metarhodopsin II. But even here some caution must be exercised since the Meta II Raman spectrum has itself been the subject of some controversy<sup>17,24</sup>, with Callender's group arguing strongly that it supports the conventional view of metarhodopsin II as the unprotonated retinal Schiff base<sup>17</sup> despite: (a) the lack of any feature corresponding to the C=N stretch<sup>24</sup>, (b) the closer correspondence of the 1569cm<sup>-1</sup> C=C stretch of Meta II with retinal (1574cm<sup>-1</sup>) and, now, the carbinolamine (1564cm<sup>-1</sup>) rather than the unprotonated imine (1582cm<sup>-1</sup>), and (c) without any assignment for the 1345cm<sup>-1</sup> band. There are also some experimental uncertainties involved in correcting for residual Meta I in the sample<sup>17</sup>, and it is conceivable that this spectrum also contains preferentially enhanced features from other unidentified species isochromic with Meta I. Nevertheless, the weight of experimental evidence now indicates that hydrolysis of the retinal Schiff base linkage of rhodopsin starts at the

metarhodopsin stage of bleaching, and that Meta II probably represents, at least in part, a stabilized form of the tetrahedral carbinolamine species in the retinal binding site.

If this is so, then it implies the existence of some unusual specific interactions in the retinal binding site of rhodopsin, some of which may be inferred from the properties of opsin and the unbleached pigment. The model studies have established that under normal circumstances a stable retinal Schiff base forms only with an unprotonated amine group, and the resultant imine bond becomes susceptible to hydrolysis upon protonation<sup>25</sup>. But visual pigment and related chromophores are stable over a wide pH range, and pigment regeneration by recombination of the appropriate retinal isomer with opsin<sup>26</sup> or bacterio-opsin<sup>27</sup> is rapid and spontaneous at physiological pH. We therefore infer that the active site lysine is unprotonated, or only partially protonated, at physiological pH, with an anomalously low  $pK_a$  that allows rapid and thermodynamically stable Schiff base formation. This is in agreement with studies on the energetics and protonation states of bovine rhodopsin<sup>17</sup>, and with the protonation changes during reconstitution of bacteriorhodopsin<sup>28</sup>. There are precedents in other proteins as well: in the Schiff base enzyme acetoacetate decarboxylase<sup>29</sup>, for instance, it has been established by chemical techniques that the active lysine has a similarly low  $pK_a$ . Amongst the various non-covalent interactions within the protein active site, only the Coulombic effects of close proximity with cationic groups (arginine or additional lysine residues, for example) can be reasonably responsible for such dramatic reductions in the  $pK_a$  of the active lysine<sup>17,27</sup>. (Interaction with a histidine residue seems less likely since imidazole is normally a much weaker base and probably would not dominate an electrostatic interaction with an adjacent primary amine.) This is not inconsistent with the possible disposition of several basic amino acid residues within the protein structure, as suggested from analysis of the primary sequence<sup>1\*</sup>. Simple calculations<sup>30</sup>, together with experimental data on diamines<sup>19</sup>, indicate that a single positive charge within a few

Angstroms of an amino group is sufficient to reduce the pK by the required 3-4 units.

Barring any major conformational changes, the same active site contacts should persist in the presence of retinal and should similarly depress the pK of the chromophoric imine. Yet, according to most spectroscopic criteria, the Schiff bases of rhodopsins appear to be protonated<sup>1</sup>, and remain so in the unbleached pigment over a wide pH range. The imine pK<sub>a</sub> in bacteriorhodopsin has been measured<sup>21</sup> at about 13.3 and, although not yet determined, is likely to be similarly high in the visual rhodopsins. This anomalously high pK is opposite to what should be expected from simple electrostatic effects of adjacent cationic groups. While it is tempting at this stage to suppose that there are indeed major conformational differences between opsin and rhodopsin which alter the disposition of charged groups in the active site region (possibly introducing a negatively charged group into the vicinity of the Schiff base, with effects similar to those seen in the SDS model experiments), we have been unable to devise a rational scheme that satisfactorily accounts for the basic observations. An alternative explanation is that the retinal binding site changes relatively little, if at all, during recombination and that the adjacent positively charged group (lysine, arginine, etc.) responsible for depressing the reactive lysine pK in the apo-protein now actively participates in protonating the retinyl Schiff base nitrogen by formation of an (-NH...N)<sup>+</sup> hydrogen bond<sup>17</sup>. This clearly satisfies the requirement for no overall change in protonation during bleaching and regeneration of rhodopsin<sup>17</sup> (or bacteriorhodopsin<sup>20</sup>) at neutral pH, and is given theoretical support by recent ab initio calculations on protonated amine-imine hydrogen bonds<sup>32</sup>. In such circumstances the equilibrium position of the H-bond proton can depend critically on the relative orientations of the donor and acceptor groups and slight reorientations can result in the reversal of the relative pK's of the groups involved, together with proton transfer from one nitrogen to the other. Such a process might form part of the proton translocation mechanism of

bacteriorhodopsin<sup>32</sup>, and also recalls the deuterium isotope effects observed in picosecond kinetic studies of rhodopsin photolysis which indicate proton translocation associated with formation of the primary batho-intermediate<sup>33</sup>. Small changes in relative orientation during the primary cis-trans photoisomerization could result in translocation of the (exchangeable) proton within the NH...N hydrogen bond. The red shift of bathorhodopsin with respect to the parent rhodopsin might indicate that proton transfer is towards the imine nitrogen in this case, implying that the Schiff base is only partially protonated in the unbleached pigment. Recent observations<sup>34</sup> on the effects of lysine methylation may be relevant here. Firstly, permethylation of all rhodopsin lysines, excluding the active lys-296, gives a spectrally identical protein which is fully viable as regards bleaching, regenerability and biochemical activity. This permethylation converts the primary amino groups to tertiary dimethylamines, without loss of charge at physiological pH. If one of these lysines happened to be the putative adjacent group in the retinyl binding site it would still be capable of NH...N bonding and proton donation to the imine nitrogen, even in this modified form. A more interesting modification is that involving the additional monomethylation of lys-296 itself, which produces a bleachable pigment red shifted to about 520nm.<sup>34a</sup> In this case the methylated Schiff base nitrogen must carry the full formal positive charge, and cannot H-bond to any adjacent group. Although there may be other explanations, the further red shift in this already anomalously bathochromic pigment suggests that only partial protonation is necessary to achieve the 500nm  $\lambda_{max}$  of unmodified rhodopsin.

Regardless of the source of the perturbations, this reversal in pK of the active lysine and the chromophoric Schiff base has important consequences for the stability of the pigment under physiological conditions. The thermodynamic stability of model Schiff bases under normal conditions ( $K_{aH} > K_{bH}$ ) falls rapidly below the pK of the amine (see Equ.2 and Fig.1), yet the rhodopsins are stable at neutral pH under conditions where model

Schiff bases would hydrolyse rapidly. This is clearly not a simple kinetic stability due to protonation or inaccessibility to water since formation of the Schiff base (regeneration) is spontaneous under the same conditions. Reversal of the  $pK$ 's ( $K_{BH} < K_{BH}$ ) for whatever reason, however, reverses the situation such that thermodynamic stability is now greatest at low pH (Equ.2). This, incidentally, is always the case for methylated Schiff bases where the permanently protonated imine becomes increasingly susceptible to hydrolysis by  $OH^-$  at high pH, and this may be of significance when considering the effect of such a modification on the metarhodopsin transition<sup>34b</sup>.

Other factors which must be taken into account when considering the possible retinal-opsin interactions include the electrical neutrality of the binding site<sup>35</sup> and the source of the chromophoric shift of rhodopsins. The most plausible explanations for the latter are various forms of the "point-charge" model<sup>36</sup>, which invoke the presence of a negatively charged carboxylate group close to the retinyl moiety in the active site (though positive groups may serve equally well). This is not inconsistent with our hypothesis of an additional positive group interaction with the imine nitrogen, indeed the pair may form a salt-bridge and satisfy the electrical neutrality condition without requiring the presence of counter ions in the retinal binding site. Furthermore, the conjugate base of an aspartic or glutamic acid residue close to the imine may serve an additional role in catalysing hydrolysis of the Schiff base linkage at a later stage in photolysis (see below).

With the foregoing in mind we can now begin to visualize a plausible sequence of events in the bleaching of rhodopsin. We imagine a rhodopsin binding site containing both an anion ( $-COO^-$ ) and a cation ( $-NH^+$ ) in close proximity to the 11-cis retinal imine linkage. This linkage is (partially) protonated by ( $-NH...N-$ )<sup>+</sup> bond formation to the adjacent cation. Initial photon absorption induces a rapid cis-transoid isomerization of the retinyl group, and a slight reorientation in relative positions of the Schiff base and its adjacent H-bond donor

reverses the relative pK's of the two groups and forces translocation of the proton along the hydrogen bond towards the imine nitrogen to produce the red-shifted, more fully protonated bathorhodopsin intermediate. (This, incidentally, destabilises the NH...N bond<sup>22</sup> and may contribute in part to the large energy storage observed in this first step<sup>22</sup>.) On the picosecond scale of this process there is little time for any other major conformational changes, but subsequent structural relaxation in the immediate active site vicinity (to give lumirhodopsin) followed by more global conformational changes (giving metarhodopsin I) can be envisaged as the protein relaxes to accommodate the new retinal configuration. To our minds this exhausts the number of plausible conformational changes that may be invoked without the intervention of additional chemical processes, and by this stage the active site conformation has changed to a sufficient extent to reduce the stabilizing influences on the Schiff base linkage and to allow access to solvent water and the start of hydrolysis. A plausible mechanism for this stage is sketched in Fig.10. Attack of water, base catalysed by the proximal point charge (glutamate or aspartate), forms the carbinolamine species (step 1). The consequent change from trigonal to tetrahedral configuration results in relative reorientation of active site contacts, breaking the -NH...N- hydrogen bond and allowing conventional protonation (from the solvent) of the more basic carbinolamine (step 2). This is the proton uptake characteristic of the Meta I  $\rightarrow$  II transition<sup>13</sup>. Simple deprotonation of the carbinol by proton release to the solvent, required to form the zwitterionic species as the next stage of hydrolysis<sup>2</sup>, is inhibited by the adjacent carboxylate anion but could occur by proton transfer to this group (step 3), consistent with changes in carboxylate protonation revealed by FTIR difference spectra<sup>27</sup>. The linkage now finally breaks (step 4) to give the retinal aldehyde, held in place by non-covalent interactions. This non-covalent complex will be unstable, however, because of the sterically unfavourable trans configuration of the retinal and irreversible retinal dissociation can now take place (step 5), though this is

not necessarily a straightforward process and could involve transimination and transient, non-specific Schiff base formation with adjacent amines along the way, giving a plausible explanation for the later metarhodopsin III and indicator-yellow intermediates.

There remain some paradoxes, however, and it is not clear at this stage which of the various species in Fig.10, following water attack on Meta I, are to be identified with the spectral Meta II state. The model compound stopped-flow experiments indicate that the retinal carbinolamine has spectroscopic properties similar to the parent Schiff base in detergent micelles, rather than the somewhat lower  $\lambda_{max}$  that might be anticipated by comparison with more stable pentaenes. It is difficult to predict the additional effects of point-charge interactions and possible chromophore strain during the metarhodopsin transition, but the 380nm  $\lambda_{max}$  of Meta II is identical to that of free retinal and suggests the presence of the aldehyde at this stage. By contrast, the Raman spectrum of Meta II points more to some form of the carbinolamine. It seems feasible that the spectroscopically identified Meta II state is actually a dynamic mixture of the various chemical species that cannot be resolved in the UV/visible region, or which are sampled to differing extents by the different spectroscopic techniques. But, regardless of these uncertainties about the finer mechanistic details, we note that the significant change from trigonal to tetrahedral configuration at the retinal-opsin linkage during carbinolamine formation could be responsible, either directly or indirectly by inducing protein conformational changes, for triggering the G-protein activation and subsequent biochemical steps thought to be involved in the photoreceptor response and which have been shown to be initiated by the metarhodopsin II intermediate<sup>34,36</sup>.

ACKNOWLEDGEMENTS: We are grateful to Dr.S.W.Provencher for the provision of the DISCRETE program and to Prof.L.D.Barron for advice and use of the Raman instrument. Financial support for equipment and research studentships (S.F.D. and J.L.R.) was from the U.K. Science and Engineering Research Council.

## REFERENCES &amp; NOTES

- (1) For background see: (a) Wald, G. *Science* 1968, 162, 230.  
 (b) Knowles, A.; Dartnall, H. J. A. "The Eye", Vol. 2B, 2nd. edn.; Academic Press: New York, 1977. (c) Honig, B. *Annu. Rev. Phys. Chem.* 1978, 29, 31. (d) Birge, R. R. *Annu. Rev. Biophys. Bioeng.* 1981, 10, 315. (e) Balogh-Nair, V.; Nakanishi, K. in "New Comprehensive Biochemistry, Vol. 3. Stereochemistry" (Ch. Tamm, ed.), p. 283; Elsevier Biomedical Press: Amsterdam, 1982. (f) Findlay, J. B. C.; Pappin, D. J. C. *Biochem. J.* 1986, 238, 625. For reviews of photolysis intermediates, see: (g) Applebury, M. L. *Vision Res.* 1984, 24, 1445. (h) Ostroy, S. E. *Biochim. Biophys. Acta* 1977, 463, 91. (i) Birge, R. R. in "Biological Events Probed by Ultrafast Laser Spectroscopy", p. 299; Academic Press: New York, 1982.
- (2) (a) Jencks, W. P. "Catalysis in Chemistry and Enzymology"; McGraw-Hill: New York, 1969.  
 (b) Cordes, E. H.; Jencks, W. P. *J. Am. Chem. Soc.* 1963, 85, 2843.  
 (c) Jencks, W. P. *J. Am. Chem. Soc.* 1959, 81, 475.
- (3) Benesi, H. A.; Hildebrand, J. H. *J. Am. Chem. Soc.* 1949, 71, 2703.
- (4) (a) Provencher, S. W. *Biophys. J.* 1976, 16, 27.  
 (b) Provencher, S. W.; Vogel, R. H. *Math. Biosci.* 1980, 50, 251.
- (5) Espenson, J. H. "Chemical Kinetics and Reaction Mechanisms"; McGraw-Hill: New York, 1981.
- (6) Fersht, A. R.; Jencks, W. P. *J. Am. Chem. Soc.* 1970, 92, 5432.
- (7) Papermaster, D. S.; Dreyer, W. J. *Biochemistry* 1974, 13, 2438.
- (8) Seltzer, S.; Lin, M. *Meth. Enzymol.* 1982, 88, 542.
- (9) De Pont, J. J. H. H. M.; Daemen, F. J. M.; Bonting, S. L. *Arch. Biochem. Biophys.* 1970, 140, 267.
- (10) (a) Christensen, J. J.; Izatt, R. M.; Wrathall, D. P.; Hansen, L. D. *J. Chem. Soc. (A)*, 1969, 1212. (Adjusted to 20°C.)  
 (b) Perrin, D. D.; Dempsey, B.; Serjeant, E. P. "pK<sub>a</sub> Prediction for Organic Acids and Bases"; Chapman & Hall: London, 1981.
- (11) Blatz, P. E.; Johnson, R. H.; Mohler, J. H.; Al-Dilaimi, S. K.; Dewhurst, S.; Erickson, J. O. *Photochem. Photobiol.* 1971, 13, 237.

- (12) (a) Hartley, G.S.; Roe, J.W. *Trans. Faraday Soc.* 1949, 36, 101.  
(b) Behme, M.T.A.; Cordes, E.H. *J. Am. Chem. Soc.* 1965, 87, 260.  
(c) Kito, Y.; Nashima, K. *Photochem. Photobiol.* 1980, 32, 443.  
(d) Romsted, L.S. *J. Phys. Chem.* 1985, 89, 5107.
- (13) (a) Parkes, J.H.; Liebman, P.A. *Biochemistry* 1984, 23, 5054.  
(b) Matthews, R.G.; Hubbard, R.; Brown, P.K.; Wald, G. *J. Gen. Physiol.* 1963, 47, 215. (c) Abrahamson, E.W.; Wiesenfeld, J.R. in "Handbook of Sensory Physiology" (H.J.A. Dartnall, Ed.) Vol. VII, Part 1, p.69; Springer-Verlag: West Berlin, 1972.  
(d) Abrahamson, E.W.; Fager, R.S. *Curr. Topics Bioenergetics* 1973, 5, 125.
- (14) Brault, M.; Pollack, R.M.; Bevins, C.L. *J. Org. Chem.* 1976, 41, 346.
- (15) Archila, J.; Bull, H.; Langenaur, C.; Cordes, E.H. *J. Org. Chem.* 1971, 36, 1345.
- (16) Smith, S.O.; Myers, A.B.; Mathies, R.A.; Pardoen, J.A.; Winkel, C.; Van den Berg, E.M.M.; Lugtenburg, J. *Biophys. J.* 1985, 47, 653.
- (17) (a) Doukas, A.G.; Aton, B.; Callender, R.H.; Ebrey, T.G. *Biochemistry* 1978, 17, 2430. (b) Pande, J.; Pande, A.; Callender, R.H. *Photochem. Photobiol.* 1982, 36, 107.
- (18) (a) Wald, G.; Durnell, J.; St. George, R.C.C. *Science* 1950, 111, 179.  
(b) Rafferty, C.N.; Shichi, H. *Photochem. Photobiol.* 1981, 33, 229.
- (19) Cooper, A.; Converse, C.A. *Biochemistry* 1976, 15, 2970.
- (20) Pinchas, S.; Laulicht, I. "Infrared Spectra of Labelled Compounds"; Academic Press; London, 1971.
- (21) (a) Bownds, D.; Wald, G. *Nature* 1965, 205, 254. (b) Akhtar, M.; Blossie, P.T.; Dewhurst, P.B. *Biochem. J.* 1968, 110, 693.  
(c) Ratner, V.L.; Bagirov, I.G.; Fesenko, E.E. *Vision Res.* 1981, 21, 251.
- (22) (a) Cooper, A. *Nature* 1979, 282, 531. (b) Cooper, A. *FEBS Lett.* 1981, 123, 324. (c) Cooper, A.; Dixon, S.F.; Tsuda, M. *Eur. Biophys. J.* 1986, 13, 195.
- (23) (a) Bennett, N. *Biochem. Biophys. Res. Comm.* 1978, 83, 457.  
(b) Bennett, N. *Eur. J. Biochem.* 1980, 111, 99.
- (24) Allan, A.E.; Cooper, A. *FEBS Lett.* 1980, 119, 238.

- (25) As also shown by the pioneering work of the Liverpool group: (a) Morton, R.A.; Pitt, G.A.J. *Biochem. J.* 1955, 59, 128. (b) Pitt, G.A.J.; Collins, F.D.; Morton, R.A.; Stok, P. *Biochem. J.* 1955, 59, 122.
- (26) Henselman, R.A.; Cusanovich, M.A. *Biochemistry* 1976, 15, 5321.
- (27) Oesterhelt, D.; Schuhmann, L. *FEBS Lett.* 1974, 44, 262.
- (28) Fischer, U.C.; Oesterhelt, D. *Biophys. J.* 1980, 31, 139. (Though these authors rejected the low-pK<sub>a</sub>-lysine hypothesis on the basis of the paradoxical consequences for Schiff base protonation.)
- (29) Kokesh, F.C.; Westheimer, F.H. *J. Am. Chem. Soc.* 1971, 93, 7270.
- (30) Electrostatic repulsion between two single point charges, with separation R Å in a medium of dielectric constant D, gives  $\Delta pK = -240/DR$ , approximately. The value of D within the protein matrix has recently been estimated to be in the range 2.5 to 4 (Gilson, M.K.; Honig, B.H. *Biopolymers* 1986, 25, 2097). The potentially large pK shifts arising thus from a proximal positive charge will be partially offset by a possible nearby negative group, discussed later.
- (31) (a) Druckmann, S.; Ottolenghi, M.; Pande, A.; Pande, J.; Callender, R.H. *Biochemistry* 1982, 21, 4953. (b) Sheves, M.; Albeck, A.; Friedman, N.; Ottolenghi, M. *Proc. Natl. Acad. Sci. USA* 1986, 83, 3262.
- (32) (a) Hillenbrand, E.A.; Scheiner, S. *J. Am. Chem. Soc.* 1985, 107, 7690. (b) Scheiner, S.; Hillenbrand, E.A. *Proc. Natl. Acad. Sci. USA* 1985, 82, 2741. For similar suggestions concerning non-protonated or H-bonded Schiff bases see, for example: (c) Favrot, J.; Leclerc, J.M.; Roberge, R.; Sandorfy, C.; Vocelle, D. *Chem. Phys. Lett.* 1978, 53, 433. (d) Rafferty, C.N.; Shichi, H. *Photochem. Photobiol.* 1981, 33, 229. (e) Merz, H.; Zundel, G. *Biochem. Biophys. Res. Comm.* 1986, 138, 819.
- (33) Peters, K.; Applebury, M.L.; Rentzepis, P.M. *Proc. Natl. Acad. Sci. USA* 1977, 74, 3119.
- (34) (a) Longstaff, C.; Rando, R.R. *Biochemistry* 1985, 24, 8137. (b) Longstaff, C.; Calhoon, R.D.; Rando, R.R. *Proc. Natl. Acad. Sci.* 1986, 83, 4209.

- (35) Birge, R.R.; Murray, L.P.; Pierce, B.M.; Akita, H.; Balogh-Nair, V.; Findsen, L.A.; Nakanishi, K. *Proc. Natl. Acad. Sci. USA* 1985, 82, 4117.
- (36) (a) Kropf, A.; Hubbard, R. *Ann. N.Y. Acad. Sci.* 1958, 74, 266.  
(b) Honig, B.; Dinur, U.; Nakanishi, K.; Balogh-Nair, V.; Gawinowicz, M.A.; Arnaboldi, M.; Motto, M.G. *J. Am. Chem. Soc.* 1979, 101, 7084.  
(c) Baasov, T.; Sheves, M. *J. Am. Chem. Soc.* 1985, 107, 7524.  
(See also ref. 1e.)
- (37) (a) Siebert, F.; Mantele, W.; Gerwert, K. *Eur. J. Biochem.* 1983, 136, 119. (b) Rothschild, K.J.; Cantore, W.A.; Marrero, H. *Science* 1983, 219, 1333.  
(c) De Grip, W.J.; Gillespie, J.; Rothschild, K.J. *Biochim. Biophys. Acta* 1985, 809, 97.
- (38) (a) Bennett, N.; Michel-Villaz, M.; Kuhn, H. *Eur. J. Biochem.* 1982, 127, 97. (b) Emeis, D.; Kuhn, H.; Reichart, J.; Hofmann, K.P. *FEBS Lett.* 1982, 143, 29.

TABLE I: Kinetic and Equilibrium Parameters for the Retinal/  
n-Butylamine Reaction in Detergent Micelles\*.

	Ammonyx	Emulphogene	DTAB	SDS
$pK_{BH}$	10.75	10.75	10.75	~ 11
$pH_{mic}$	4.85	6.1	5.84	9.54
$n$	0.77	1	0.77	1.1
$p\theta$	-2.37	0	-1.6	4.4
$K_0$ (mM)	0.22	0.13	0.25	~0.25
$k_1$ ( $s^{-1}$ )	0.31	$6.1 \times 10^{-4}$	$7.9 \times 10^{-3}$	~0.01
$k_2$ ( $M^{-1}s^{-1}$ )	$1.2 \times 10^4$	$2.0 \times 10^4$	$2.6 \times 10^4$	~ $3 \times 10^6$
$k_3$ ( $s^{-1}$ )	.028	.026	.025	~.05
$k_{-1}$ ( $M^{-1}s^{-1}$ )	$4.0 \times 10^6$	420	6500	~ $2 \times 10^6$
$k_{-2}$ ( $s^{-1}$ )	$1.1 \times 10^{-4}$	$9.4 \times 10^{-6}$	$1.5 \times 10^{-4}$	~0.05
$k_{-3}$ ( $M^{-1}s^{-1}$ )	124	371	153	~10
$k_1/k_{-1}$	$7.8 \times 10^{-7}$	$1.5 \times 10^{-6}$	$1.2 \times 10^{-6}$	~ $5 \times 10^{-6}$
$k_2/k_{-2}$	$1.1 \times 10^6$	$2.2 \times 10^6$	$1.7 \times 10^6$	~ $6 \times 10^6$
$k_3/k_{-3}$	$2.3 \times 10^{-4}$	$7.0 \times 10^{-6}$	$1.6 \times 10^{-4}$	~ $5 \times 10^{-3}$

\* Except as indicated for SDS, where only order-of-magnitude estimates are available, typical maximum estimated error limits are as follows:  $pK_{BH}$ ,  $pH_{mic}$ ,  $n$ ,  $p\theta$  (+/- 0.05);  $K_0$  (+/- 10%); rate constants (+/- 20%).

TABLE II: Low-resolution mass spectra of retinals. Relative abundances in the molecular ion region, normalized to the m/z 284 peak.

Retinal sample*	m/z		
	284	285	286
A	1	.24	0
B	1	.23	.14
C	1	.23	0
D	1	.25	0
E	1	.24	.69
F	1	.28	.42

- (A) Commercial, natural abundance all-trans retinal.
- (B) Retinal after hydrolysis from N-retinylidene-n-butylamine in 20% enriched  $H_2^{18}O$ .
- (C) Extracted from Meta I-RDS incubated for 10-15 min. in 70% enriched  $H_2^{18}O$  at pH 8, 0°C.
- (D) Extracted from RDS membranes, pre-equilibrated in 70%  $H_2^{18}O$  and bleached to the Meta I stage at pH 8, 0°C.
- (E) Extracted from RDS membranes after a 30 second exposure to 70%  $H_2^{18}O$  during the Meta I  $\rightarrow$  II transition, pH 5.5, 0°C.
- (F) As E, but with a 10 min. exposure to labelled water.

## FIGURE LEGENDS

FIG.1 Observed dissociation constant ( $K_{obs}$ ) as a function of pH for N-retinylidene-n-butylamine in 2% aqueous Emulphogene, determined from equilibrium absorbance changes ( $\Delta A$ ) over a range of butylamine concentrations ( $B_{tot}$ ). Inset: Example of the Benesi-Hildebrand plot of data at two different wavelengths for this system at pH 8.5 .

FIG.2 pH-titrations of N-retinylidene-n-butylamine in Ammonyx (A), Emulphogene (E), DTAB (D), and SDS (S). Determined from the initial absorbances during pH-jump stopped-flow experiments and plotted according to Equ.1 .

FIG.3 Steady-state pH-rate profiles for hydrolysis of N-retinylidene-n-butylamine in aqueous detergent mixtures at 20°C. A = Ammonyx; E = Emulphogene; D = DTAB ; S = SDS. The solid lines are theoretical profiles plotted according to the carbinolamine mechanism using the parameters listed in Table I. Except for SDS, points above pH 8 are obtained from formation rate data.

FIG.4 Steady-state pH-rate profiles for formation of N-retinylidene-n-butylamine in aqueous detergent mixtures at 20°C. A = Ammonyx ; E = Emulphogene; D = DTAB; S = SDS. The solid lines are theoretical profiles for second-order formation rates according to the carbinolamine mechanism using the parameters from Table I. Data below pH 8 are calculated from hydrolysis rates under these conditions. Data points for DTAB and Emulphogene give equally good fits to the theoretical curves, but have been omitted for clarity.

FIG.5 Examples of stopped-flow data showing transient absorbance changes during the initial stages of hydrolysis of N-retinylidene-n-butylamine in SDS (360nm, pH 11), Ammonyx (370nm, pH 5), DTAB(370nm, pH 5.5) and Emulphogene (370nm, pH 6).

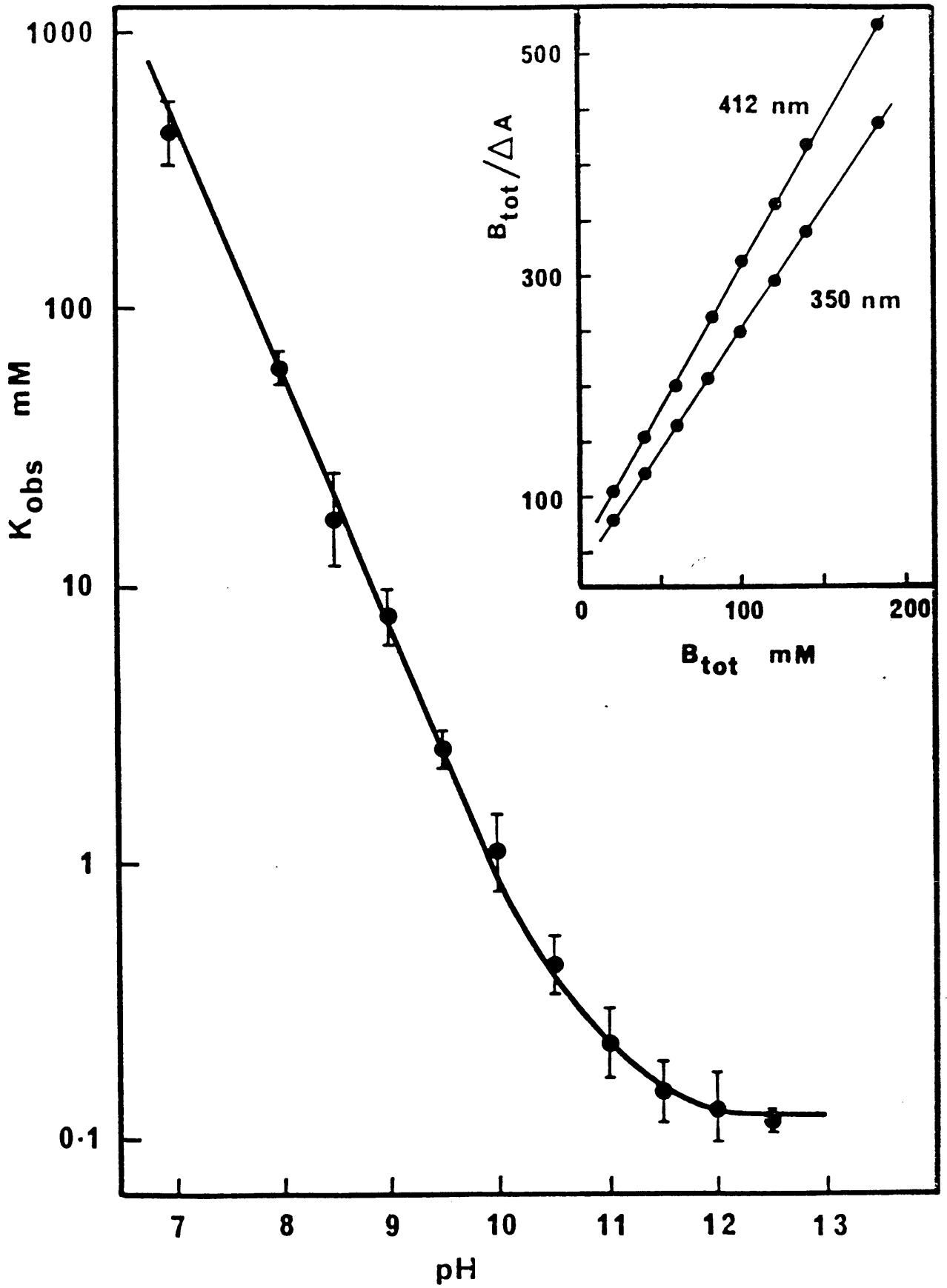
FIG.6 Statistically-corrected Brønsted plot of general base catalysis constants ( $k'_b$ ) as a function of conjugate acid dissociation constants ( $K'_{aH}$ ) for hydrolysis in Emulphogene. General bases used included formate, acetate, succinate, phosphate, pyridine and piperazine, as indicated.

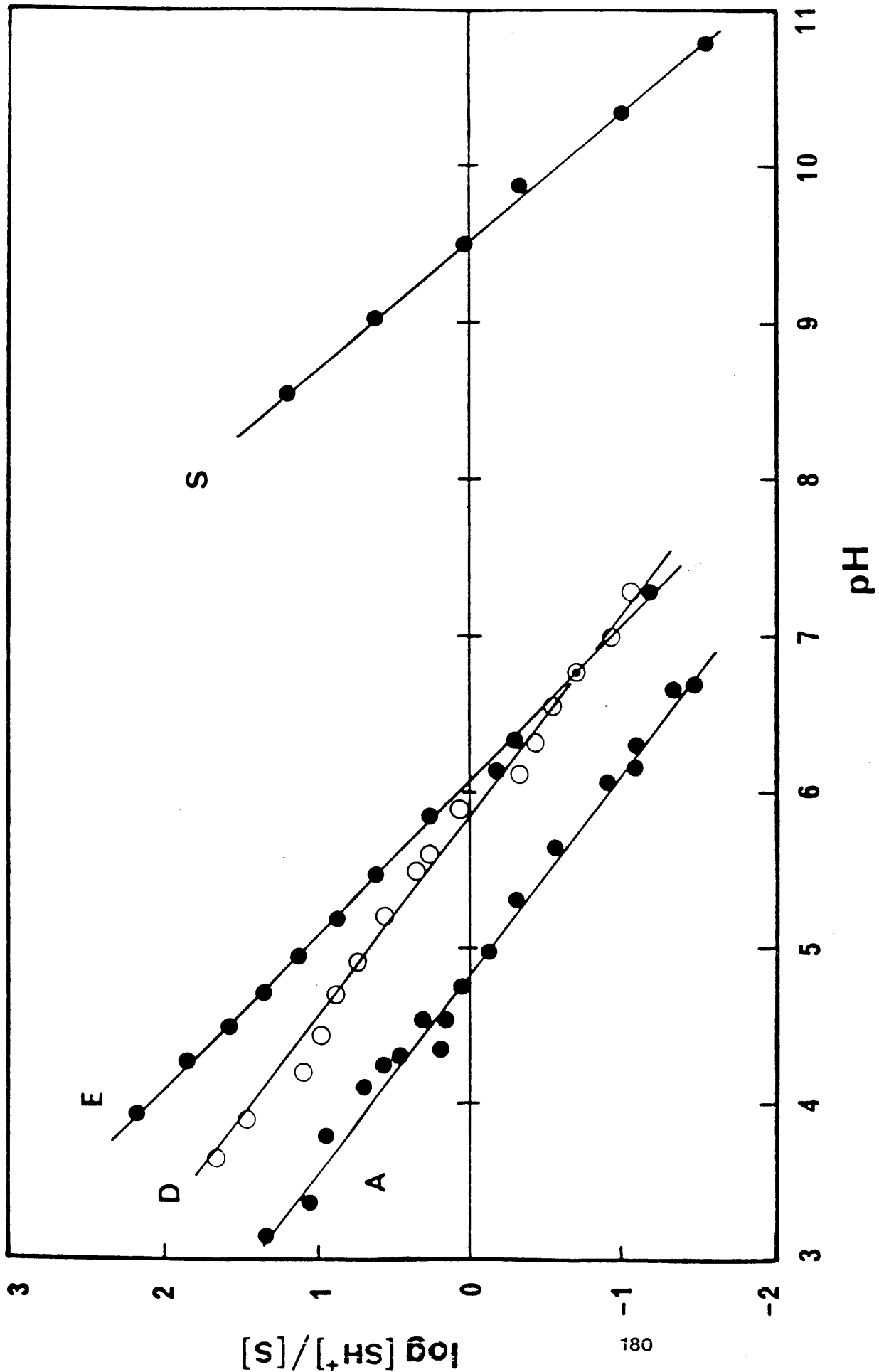
FIG.7: Continuous-flow, pH-jump resonance Raman spectra (100mW, 457.9nm excitation, solvent background subtracted) of N-retinylidene-n-butylamine and its hydrolysis products in 2% aqueous Ammonyx mixtures. (A) Protonated Schiff base in 0.1M HCl. (B) Schiff base approximately 10 seconds after pH-jump to pH 4.2 (C) Unprotonated Schiff base in 10mM butylamine. (D) Schiff base total hydrolysis products, approximately 20 minutes after pH jump to pH 4.2. (E) All-trans retinal in pH 4 buffer. All spectra were run consecutively under identical instrumental conditions with the same total retinal concentration, and are shown to scale (except where indicated) in order to illustrate the different extents of resonance enhancement.

FIG.8: Resonance Raman spectrum of the tetrahedral carbinolamine intermediate (X) of hydrolysis of N-retinylidene-n-butylamine in aqueous Ammonyx micelles, pH 4-5, derived by subtraction of the protonated Schiff base component from continuous-flow spectra during the early stages of hydrolysis. The metarhodopsin II spectrum, for comparison, is re-drawn on the same wavenumber scale from ref.17a. The major peak positions in these spectra are identical within instrumental resolution.

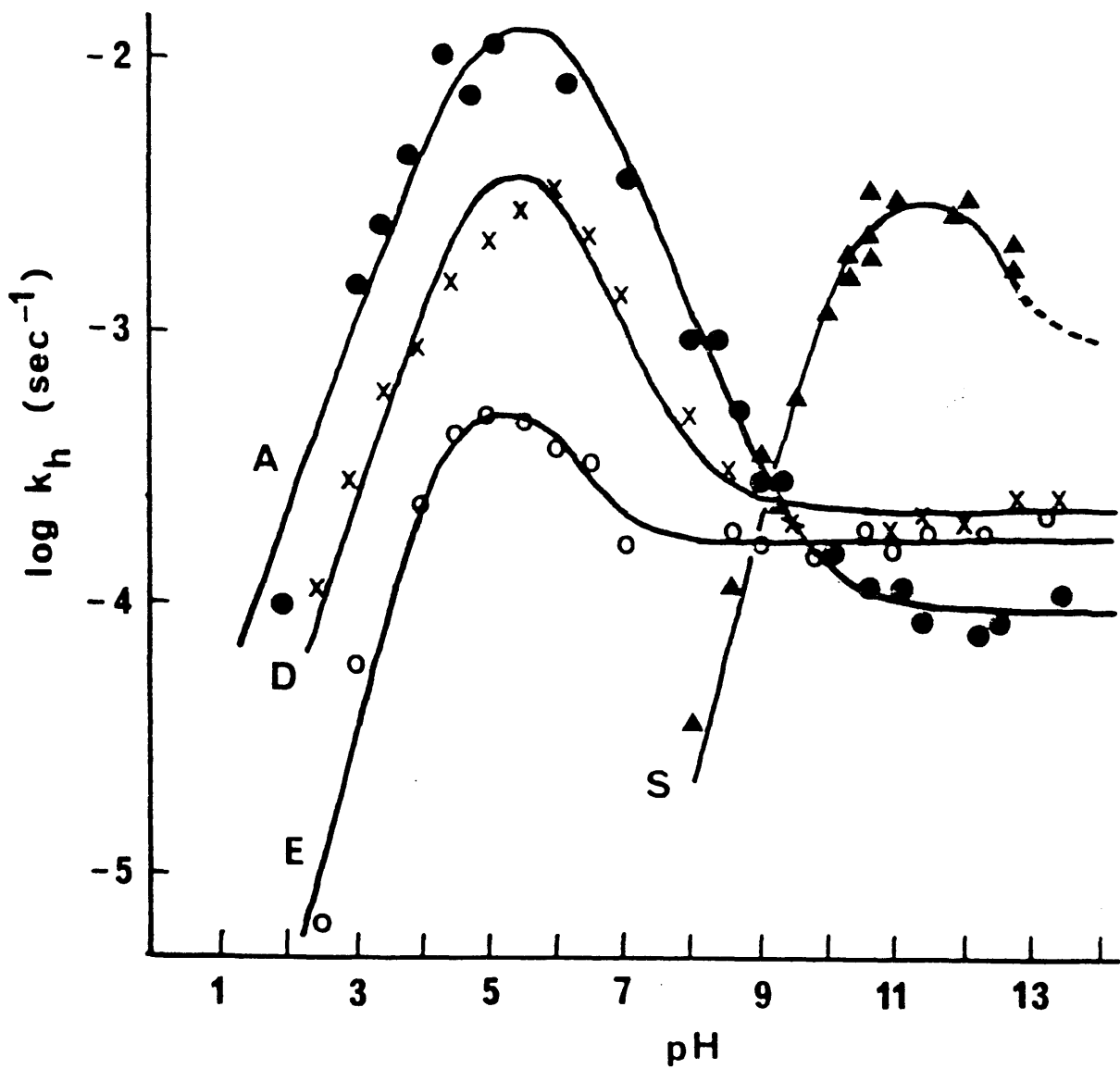
FIGURE 9: Superimposed tracings of infra-red spectra in the carbonyl-stretch region, solvent background ( $CCl_4$ ) subtracted, arbitrary % transmission scale. (A) Commercial all-trans retinal. (B) Retinal extracted from bleached ROS membranes. (C) Retinal extracted from ROS membranes exposed to 70% enriched  $H_2^{18}O$  at the Meta I  $\rightarrow$  Meta II stage.

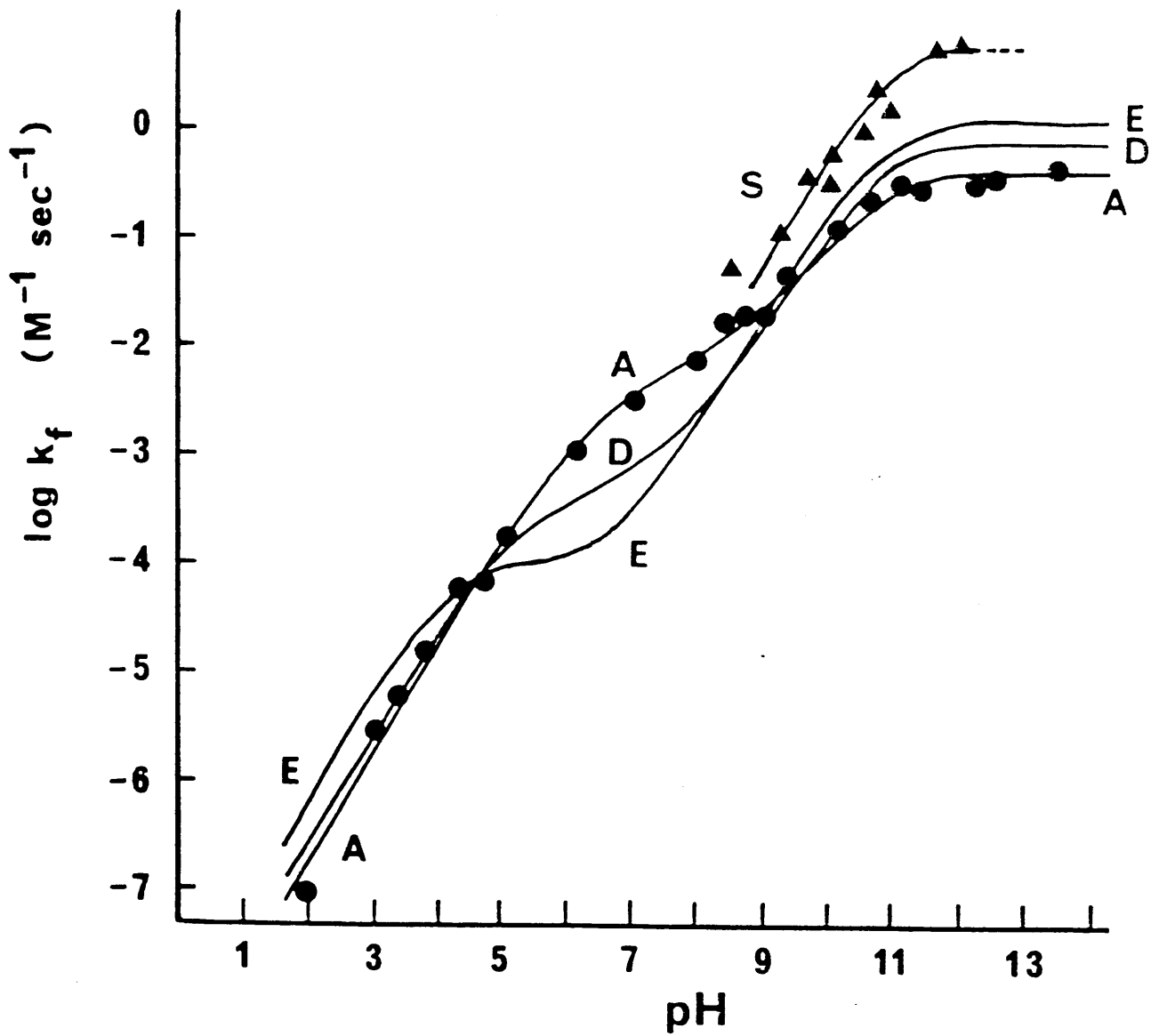
FIG.10: Outline scheme for the hydrolysis of the retinal Schiff base chromophore in the active site of rhodopsin, incorporating the tetrahedral carbinolamine intermediate, as a possible model for the Meta I-II transition (see text for details). Note that prior to release of the all-trans retinal from the binding site (step 5), all steps are potentially reversible.

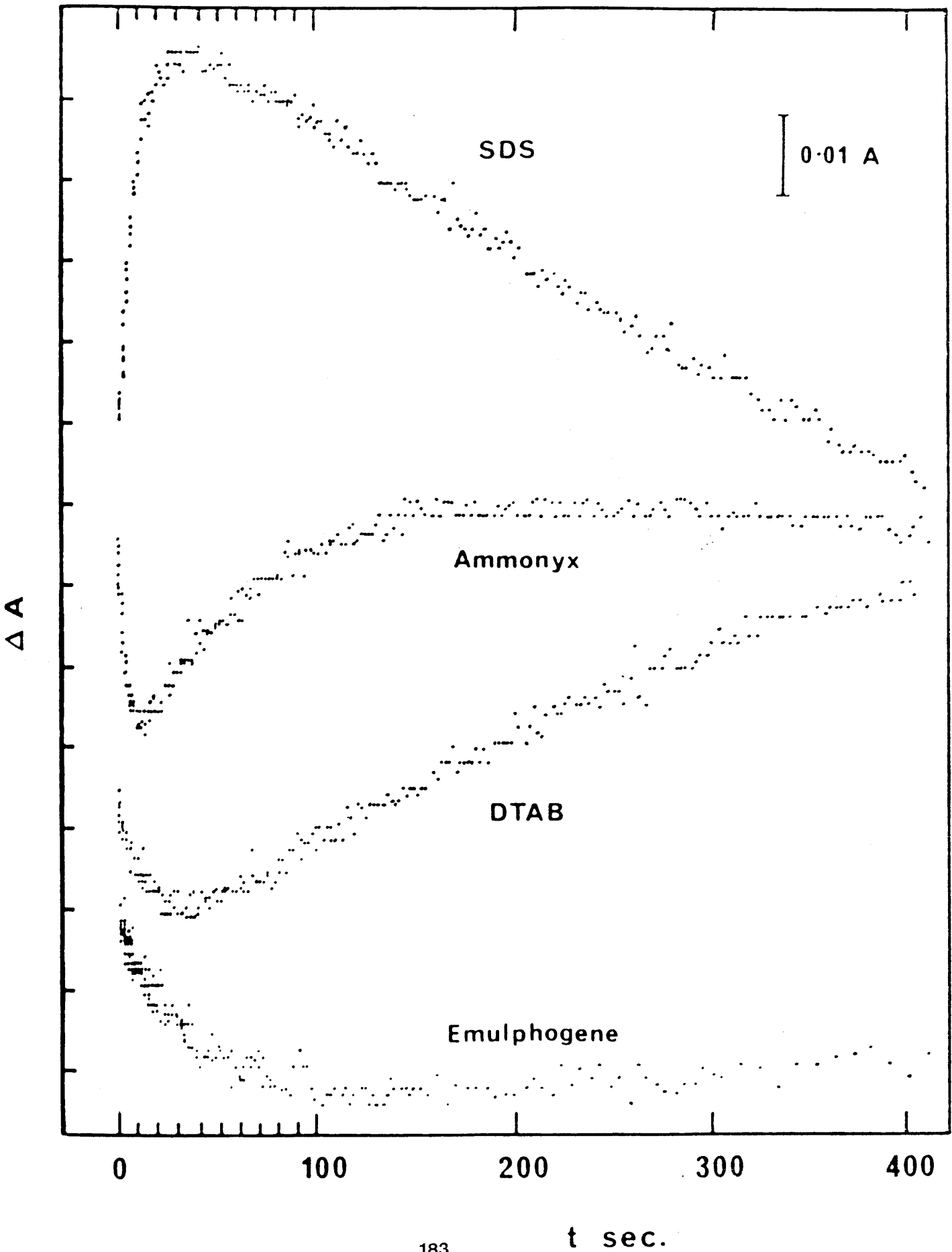


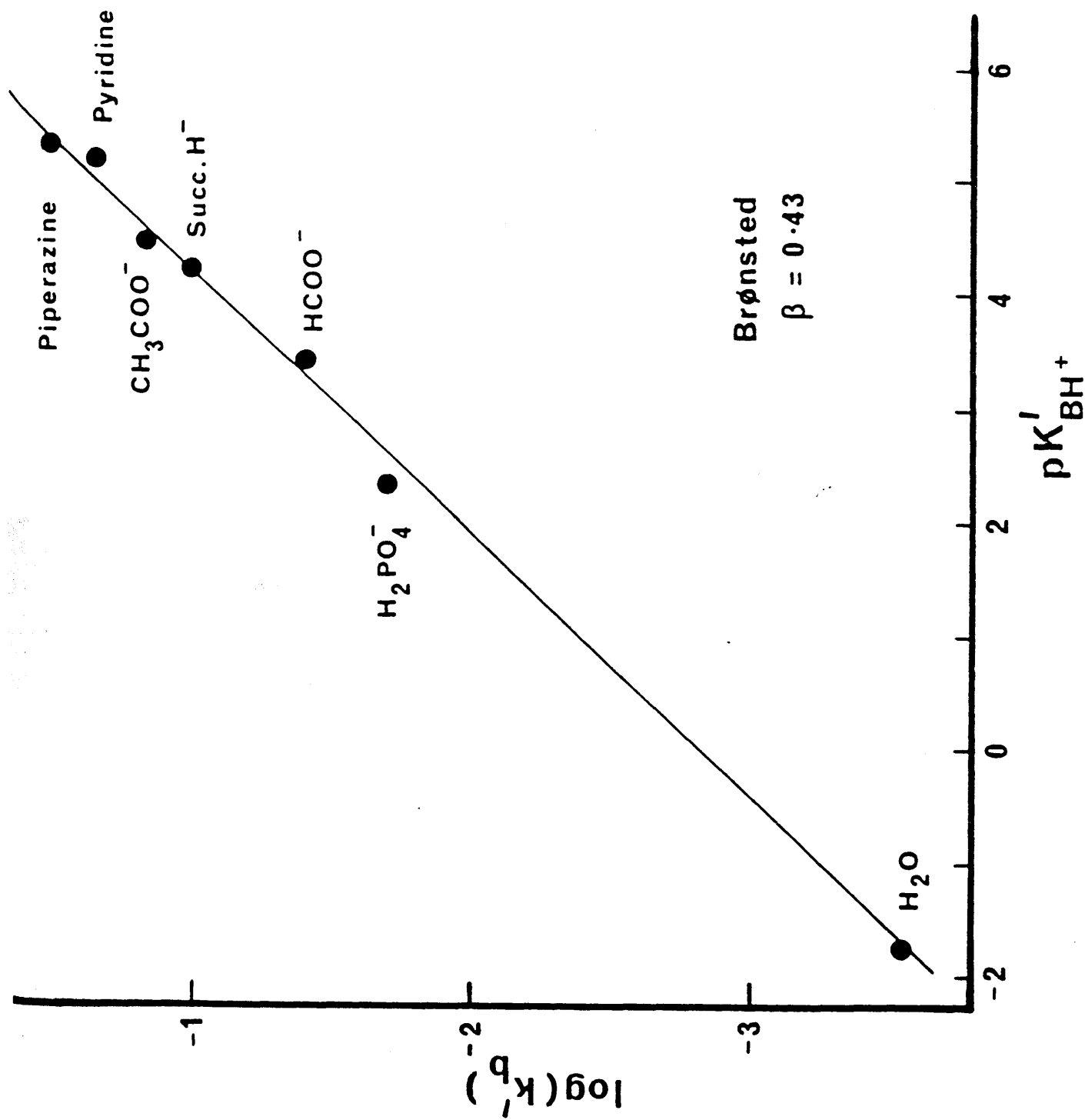


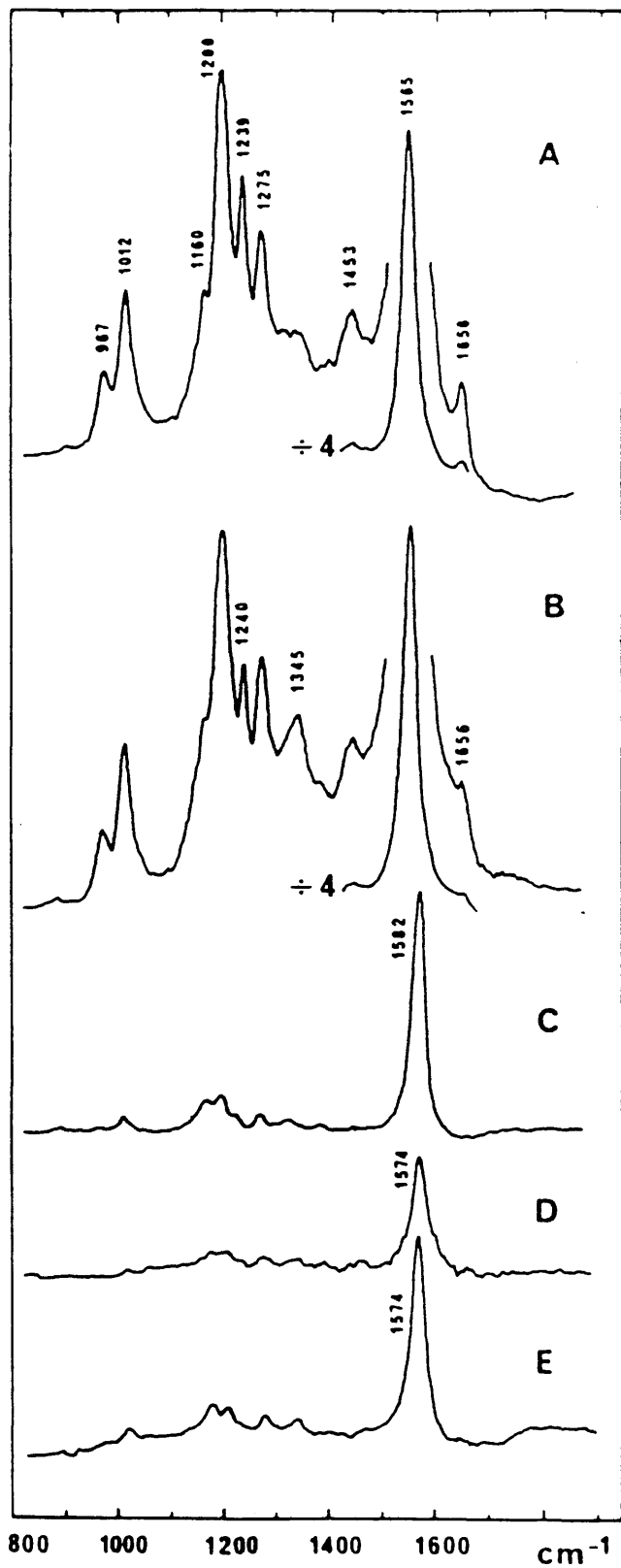
Cooper et al. Fig.2

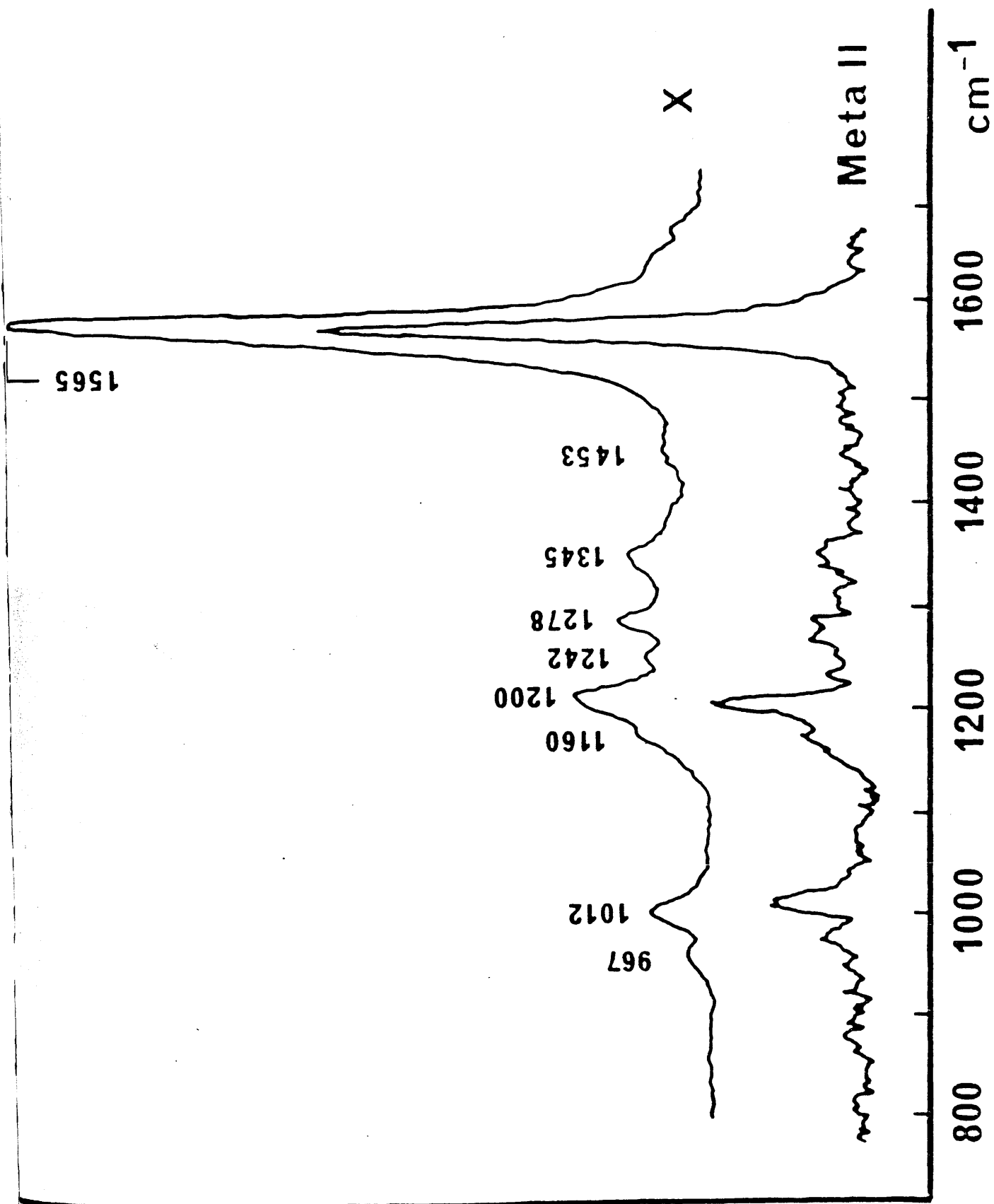


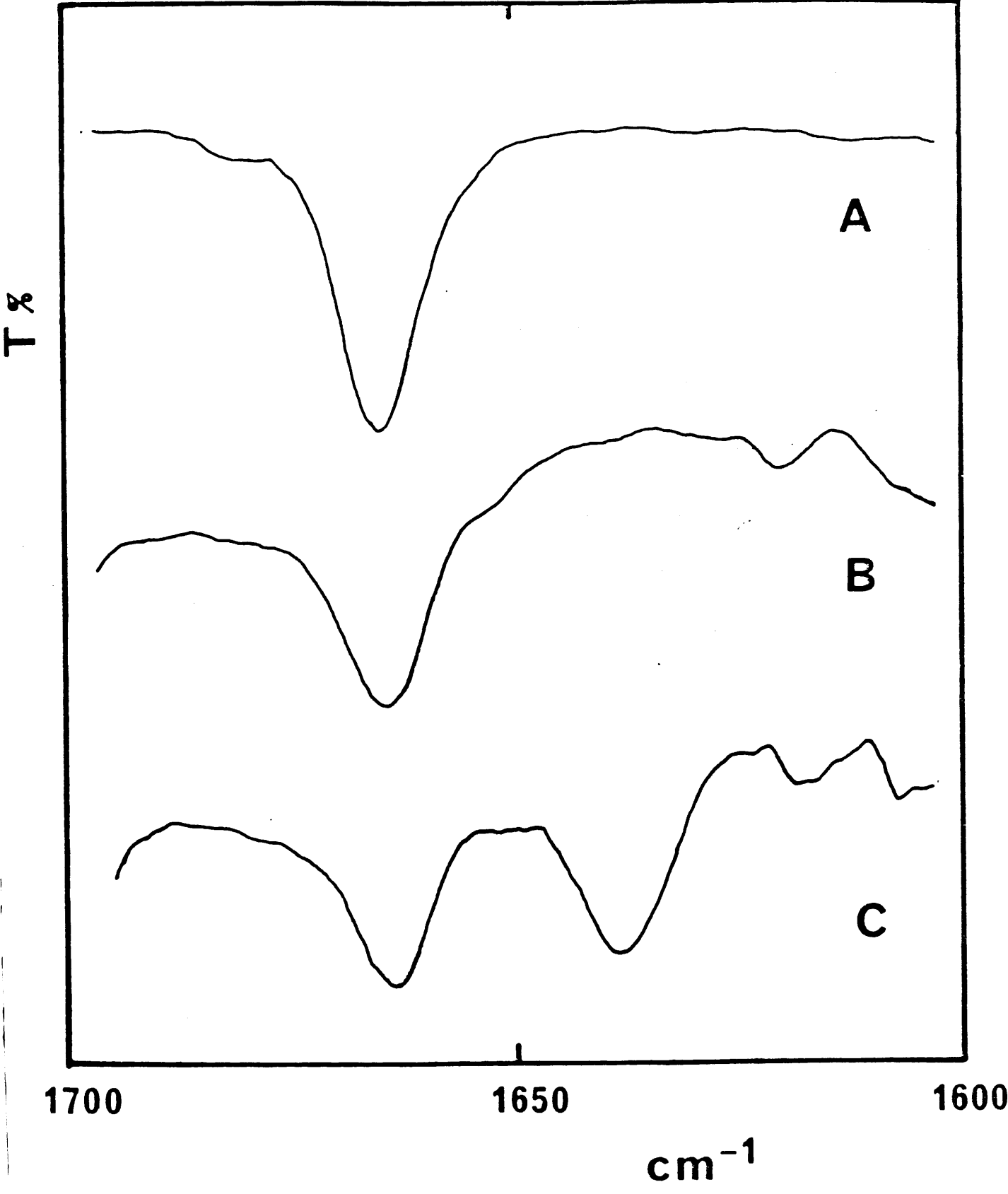


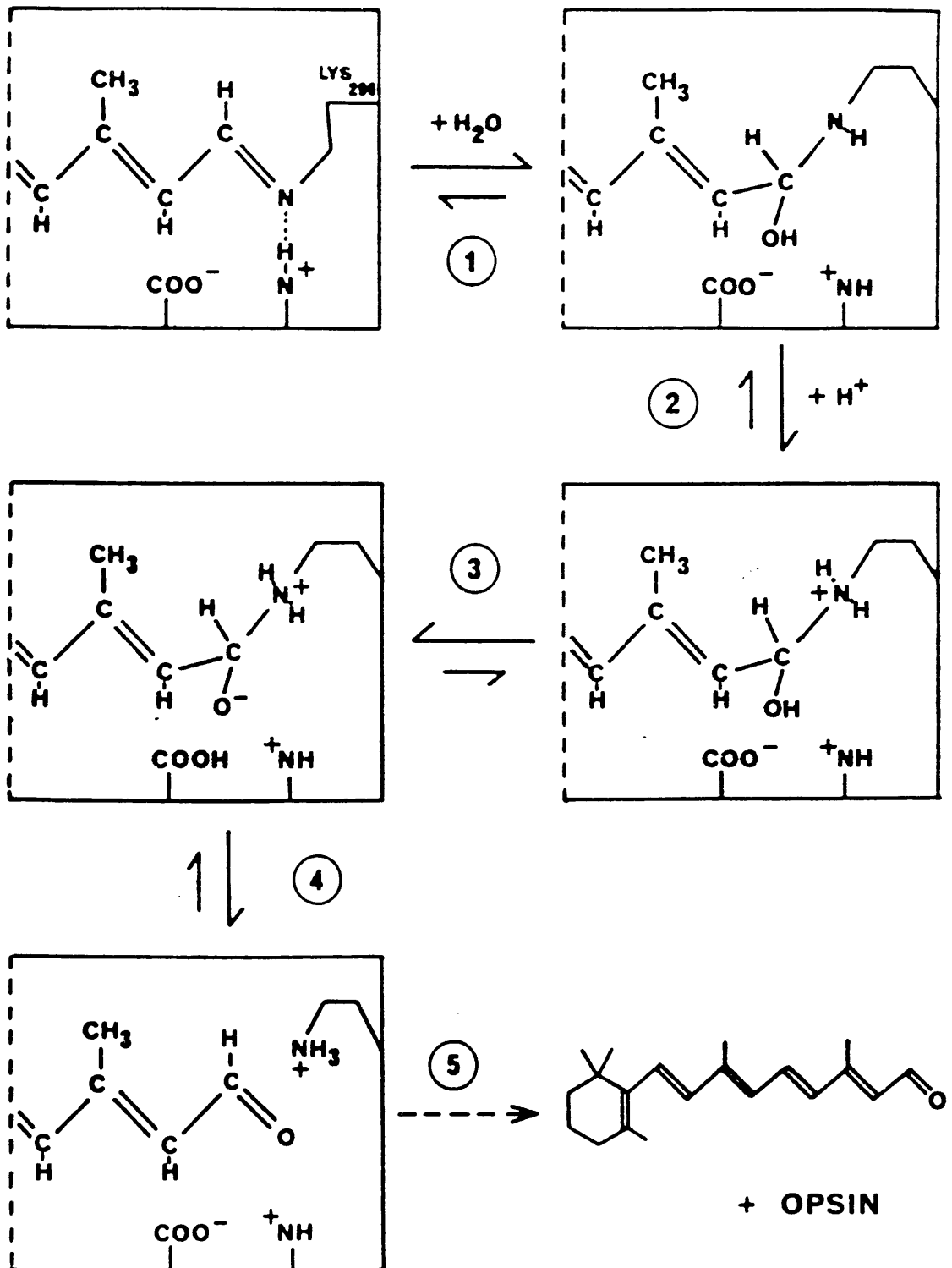












## REFERENCES

## REFERENCES

1. (a) B. Honig, *Ann. Rev. Phys. Chem.*, 1978, 29, 31-57.
- (b) R.R. Birge, *Ann. Rev. Biophys. Bioeng.*, 1981, 10, 315-354.
- (c) V. Balogh-Nair and K. Nakanishi, in "New Comprehensive Biochemistry, Vol.3. Stereochemistry", (Ch. Tamm, Ed.); Elsevier Biomedical Press: Amsterdam, 1982, 283-334.
- (d) J.B.C. Findlay and D.J.C. Pappin, *Biochem. J.*, 1986, 238, 625-642.
- (e) A. Knowles and H.J.A. Dartnall, *The Eye*, Vol.2B, 2nd Edition (H. Davson, editor) Academic Press, London, 1977.
2. R.W. Young, *J. Cell Biology*, 1967, 33, 61-72.
3. F. Boll, *Mber. Berlin. Akad.*, 1876, 41, 783-787 as reported in *Handbook of Sensory Physiology*, Vol.7, Part 1, ed. H.J.A. Dartnall (Springer, Berlin, 1972) p.34.
4. G.Wald, *Nature*, 1933, 132, 316-317.
5. R.Hubbard and G.Wald, *J.Gen. Physiol.*, 1952, 36, 269-315.
6. A. Kropf and R. Hubbard, *Ann. N.Y. Acad. Sci.*, 1958-59, 74, 266-280.
7. Y.A. Ovchinnikov, *FEBS Lett.*, 1982, 148, 179-191.
8. R. Hubbard, *J. Gen. Physiol.*, 1953-54, 37, 381-399.
9. R.J. Lythgoe, *J. Physiol.*, 1937, 89, 331-358.
10. S.Ball, F.D. Collins, P.D. Dalvi and R.A. Morton, *Biochem. J.*, 1949, 45, 304-307.
11. G.A.J. Pitt, F.D.Collins, R.A.Morton and P.Stok, *Biochem. J.*, 1955, 59, 122-127.
12. R.A. Morton and G.A.J. Pitt, *Biochem. J.*, 1955, 59, 128-134.
13. D. Bownds, *Nature*, 1967, 216, 1178-1181.
14. M. Akhtar, P.T. Blosse and P.B. Dewhurst, *Biochem. J.*, 1968, 110, 693-702.

15. R.S. Fager, P. Sejnowski and E.W. Abrahamson, *Biochem. Biophys. Res. Commun.*, 1972, 47, 1244-47.
16. L. Rimai, R.G. Kilponen and D. Gill, *Biochem. Biophys. Res. Commun.*, 1970, 41, 492-497.
17. A. Lewis, R.S. Fager and E.W. Abrahamson, *J. Raman Spect.*, 1973, 1, 465-470.
18. A.R. Oseroff and R.H. Callender, *Biochem.*, 1974, 13, 4243-4248.
19. J. Shriver, G. Mateescu, R. Fager and D. Torchia, *Nature*, 1977, 270, 271-274.
20. A. Cooper and C.A. Converse, *Biochemistry*, 1976, 15, 2970-2978.
21. V.J. Wulff, R.G. Adams, H. Linschitz and E.W. Abrahamson, *Ann. N.Y. Acad. Sci.*, 1958-59, 74, 281-290.
22. G.E. Busch, M.L. Applebury, A.A. Lamola and P.M. Rentzepis, *Proc. Nat. Acad. Sci. USA*, 1972, 69, 2802-2806.
23. R.R. Birge and L.M. Hubbard, *J. Am. Chem. Soc.*, 1980, 102, 2195-2205.
24. G. Eyring and R. Mathies, *Proc. Nat. Acad. Sci. USA*, 1979, 76, 33-37.
25. T. Yoshizawa, in : *Handbook of Sensory Physiology*, Vol. 7, Part 1, ed. H.J.A. Dartnall (Springer, Berlin, 1972) p.146.
26. A. Cooper, *Chem. Phys. Letts.*, 1983, 99, 305-309.
27. R.G. Matthews, R. Hubbard, P.K. Brown and G. Wald, *J. Gen. Physiol.*, 1963, 47, 215-240.
28. A.G. Doukas, B. Aton, R.H. Callender and T.G. Ebrey, *Biochemistry*, 1978, 17, 2430-2435.
29. A.E. Allan and A. Cooper, *FEBS Lett.*, 1980, 119, 238-240.
30. G. Wald, J. Durell and R.C.C. St. George, *Science*, 1950, 111, 179-181.
31. C. Baumann, *J. Physiol.*, 1976, 259, 357-366.
32. C. Baumann, *J. Physiol.*, 1978, 279, 71-80.
33. C. Baumann and W. Zeppenfeld, *J. Physiol.*, 1981, 317, 347-364.

34. N. Bennett, *Biochem. Biophys. Res. Commun.*, 1978, 83, 457-465.
35. N. Bennett, *Eur. J. Biochem.*, 1980, 111, 99-103.
36. J.H. Parkes and P.A. Liebman, *Biochemistry*, 1984, 23, 5054-5061.
37. G. Wald, *Science*, 1968, 162, 230-239.
38. N. Bennett, M. Michel - Villaz and H. Kühn, *Eur. J. Biochem.*, 1982, 127, 97-103.
39. B.K.-K. Fung and L. Stryer, *Proc. Nat. Acad. Sci. USA*, 1980, 77, 2500-2504.
40. B.K.-K. Fung, J.B. Hurley and L. Stryer, *Proc. Nat. Acad. Sci. USA*, 1981, 78, 152-156.
41. E.E. Fesenko, S.S. Kolesnikov and A.L. Lyubarsky, *Nature*, 1985, 313, 310-313.
42. G. Vines, *New Scientist*, 1985, 1467, 40-43.
43. M. Arnaboldi, M.G. Motto, K. Tsujimoto, V. Balogh-Nair and K. Nakanishi, *J. Am. Chem. Soc.*, 1979, 101, 7082-7084.
44. B. Honig, U. Dinur, K. Nakanishi, V. Balogh - Nair, M.A. Gawinowicz, M. Arnaboldi and M.G. Motto, *J. Am. Chem. Soc.*, 1979, 101, 7084-7086.
45. M. Sheves, K. Nakanishi and B. Honig, *J. Am. Chem. Soc.*, 1979, 101, 7086-88.
46. I. Tabushi and K. Shimokawa, *J. Am. Chem. Soc.*, 1980, 102, 5402-5404.
47. C.S. Irving, G.W. Byers and P.A. Leermakers, *Biochemistry*, 1970, 9, 858-864.
48. T. Kakitani and H. Kakitani, *J. Phys. Soc. Japan*, 1975, 38, 1455-1463.
49. R. Hubbard and R.C.C. St. George, *J. Gen. Physiol.*, 1958, 41, 501-528.
50. T. Kitagawa and M. Tsuda, *Biochim. Biophys. Acta*, 1980, 624, 211-217.
51. A. Cooper, S.F. Dixon and M. Tsuda, *Eur. Biophys. J.*, 1986, 13, 195-201.
52. T. Ebrey, M. Tsuda, G. Sassenrath, J.L. West and W.H. Waddell, *FEBS Lett.*, 1980, 116, 217-219.
53. S.F. Dixon and A. Cooper, *Photochem. Photobiol.*, 1987, 44 (in press).

54. R. Henderson, *Ann. Rev. Biophys. Bioeng.*, 1977, 6, 87-109.
55. W. Stoeckenius, *Acc. Chem. Res.*, 1980, 13, 337-344.
56. A. Lewis, J. Spoonhower, R. Bogomolni, R.H. Lozier and W. Stoeckenius, *Proc. Nat. Acad. Sci. USA*, 1974, 71, 4462-4466.
57. K. Nakanishi, V. Balogh-Nair, M. Arnaboldi, K. Tsujimoto and B. Honig, *J. Am. Chem. Soc.*, 1980, 102, 7945-7947.
58. J.L. Spudich, D.A. McCain, K. Nakanishi, M. Okabe, N. Shimizu, H. Rodman, B. Honig and R.A. Bogomolni, *Biophys. J.*, 1986, 49, 479-483.
59. J. Lugtenburg, M. Muradin-Szweykowska, C. Heeremans and J.A. Pardoen, *J. Am. Chem. Soc.*, 1986, 108, 3104-3105.
60. E.H. Cordes and W.P. Jencks, *J. Am. Chem. Soc.*, 1962, 84, 832-837.
61. W.P. Jencks, *J. Am. Chem. Soc.*, 1959, 81, 475-481.
62. G. Lamaty, J.P. Roque, A. Natat and T. Silou, *Tetrahedron*, 1986, 42, 2657-2666.
63. G. Lamaty, J.P. Roque, A. Natat and T. Silou, *Tetrahedron*, 1986, 42, 2667-2676.
64. E.H. Cordes and W.P. Jencks, *J. Am. Chem. Soc.*, 1963, 85, 2843-2848.
65. P.K. Chang and T.L.V. Ulbricht, *J. Am. Chem. Soc.*, 1958, 80, 976-979.
66. E.J. Poziomek, D.N. Kramer, B.W. Fromm and W.A. Mosher, *J. Org. Chem.*, 1961, 26, 423-427.
67. P.A.S. Smith, *Open-chain nitrogen compounds*, Vol.1, 1965 (W.A. Benjamin, Inc.) p.296.
68. A. Terol, S. Alberola, B. Jeanjean, F. Sabon and J.C. Jumas, *Acta. Cryst.*, 1982, B38, 636-638.
69. A. Cooper, S.F. Dixon, M.A. Nutley and J.L. Robb, *J. Am. Chem. Soc.*, 1987, In press.
70. F.J.W. Roughton, *Proc. Roy. Soc. B*, 1934, 115, 473-495.
71. B. Chance, *J. Franklin Inst.*, 1940, 229, 455-476, 613-640 and 737-766.

72. P. Moore, " Stopped-Flow, An Experimental Manual", 1972, Molecular Sciences, University of Warwick, Coventry, p.17.
73. Ref.72, p.24 and P. Moore, S.F.A. Kettle and R.G. Wilkins, Inorg. Chem., 1966, 5, 220-223.
74. P.R. Carey, Biochemical Applications of Raman and Resonance Raman Spectroscopies, 1982, Academic Press.
75. P.K. Glasoe and F.A. Long, J. Phys. Chem., 1960, 64, 188-190.
76. A.K. Covington, M. Paabo, R. A. Robinson and R.G. Bates, Anal. Chem., 1968, 40, 700-706.
77. J.H. Fendler and E.J. Fendler, Catalysis in Micellar and Macromolecular Systems, 1975, Academic Press.
78. B.D. Flockhart, J. Colloid Sci., 1961, 16, 484-492.
79. H.B. Klevens, J. Phys. Colloid Chem., 1948, 52, 130-148.
80. K.W. Herrmann, J. Phys. Chem., 1962, 66, 295-300.
81. T.G. Ebrey, Vis. Res., 1971, 11, 1007-1009.
82. H. Shichi, M.S. Lewis, F. Irreverre and A.L. Stone, J. Biol. Chem., 1969, 244, 529-536.
83. S.W. Provencher, Biophys. J., 1976, 16, 27-41.
84. B. Curry, A. Broek, J. Lugtenburg and R. Mathies, J. Am. Chem. Soc., 1982, 104, 5274-86.
85. S.O. Smith, A.B. Myers, R.A. Mathies, J.A. Pardoen, C.Winkel, E.M.M. Van Den Berg and J. Lugtenburg, Biophys. J., 1985, 47, 653-664.
86. J. Pande, A. Pande and R.H. Callender, Photochem. Photobiol., 1982, 36, 107-109.
87. W.P. Jencks, "Catalysis in Chemistry and Enzymology"; McGraw-Hill: New York, 1969.
88. J.H. Espenson, "Chemical Kinetics and Reaction Mechanisms"; McGraw-Hill : New York, 1981.
89. D.D. Perrin, B. Dempsey and E.P. Serjeant, "pK<sub>a</sub> Prediction for Organic Acids and Bases", Chapman and Hall, London, 1981.

90. P.E. Blatz, R.H. Johnson, J.H. Mohler, S.K. Al-Dilaimi, S. Dewhurst and J.O. Erickson, *Photochem. Photobiol.*, 1971, 13, 237.
91. Y. Kito and K. Nashima, *Photochem. Photobiol.*, 1980, 32, 443-445.
92. M.T.A. Behme and E.H. Cordes, *J. Am. Chem. Soc.*, 1965, 87, 260-265.
93. M. Brault, R.M. Pollack and C.L. Bevins, *J. Org. Chem.*, 1976, 41, 346-350.
94. J. Archila, H. Bull, C. Lagenaur and E.H. Cordes, *J. Org. Chem.*, 1971, 36, 1345-1347.
95. D. Bownds and G. Wald, *Nature*, 1965, 205, 254-257.
96. A. Cooper, *FEBS Lett.*, 1981, 123, 324-326.
97. R.A. Henselman and M.A. Cusanovich, *Biochem.*, 1976, 15, 5321-5325.
98. D. Oesterhelt and L. Schuhmann, *FEBS Lett.*, 1974, 44, 262-265.
99. F.C. Kokesh and F.H. Westheimer, *J. Am. Chem. Soc.*, 1971, 93, 7270-7274.
100. J.J. Christensen, R.M. Izatt, D.P. Wrathall and L.D. Hansen, *J. Chem. Soc. (A)*, 1969, 1212-1223.
101. M. Sheves, A. Albeck, N. Friedman and M. Ottolenghi, *Proc. Natl. Acad. Sci. USA*, 1986, 83, 3262-3266.
102. U.C. Fischer and D. Oesterhelt, *Biophys. J.*, 1980, 31, 139-145.
103. S. Scheiner and E.A. Hillenbrand, *Proc. Natl. Acad. Sci. USA*, 1985, 82, 2741-2745.
104. K. Peters, M.L. Applebury and P.M. Rentzepis, *Proc. Natl. Acad. Sci. USA*, 1977, 74, 3119-3123.
105. C. Longstaff and R.R. Rando, *Biochem.*, 1985, 24, 8137-8145.
106. C. Longstaff, R.D. Calhoon and R.R. Rando, *Proc. Natl. Acad. Sci. USA*, 1986, 83, 4209-4213.
107. R.R. Birge, L.P. Murray, B.M. Pierce, H. Akita, V. Balogh-Nair, L.A. Findsen and K. Nakanishi, *Proc. Natl. Acad. Sci. USA*, 1985, 82, 4117-4121.
108. A. Cooper, *Nature*, 1979, 282, 531-533.

109. K.J. Rothschild, W.A. Cantore and H. Marrero, Science, 1983, 219, 1333-1335.
110. W.J. de Grip, J. Gillespie and K.J. Rothschild, Biochim. Biophys. Acta, 1985, 809, 97-106.
111. B. Honig, A. Warshel and M. Karplus, Acc. Chem. Res., 1975, 8, 92-100.
112. L. Zechmeister and A. Polgar, J. Am. Chem. Soc., 1943, 65, 1522-1528.
113. R.L. Christensen and B.E. Kohler, Photochem. Photobiol., 1973, 18, 293-301.
114. R.R. Birge, K. Schulten and M. Karplus, Chem. Phys. Letts., 1975, 31, 451-454.
115. B. Honig, U. Dinur, R.R. Birge and T.G. Ebrey, J. Am. Chem. Soc., 1980, 102, 488-494.

